DISSERTATION

NEUROINFLAMMATION AND THE TWO-HIT HYPOTHESIS OF PARKINSON'S DISEASE

Submitted by

Collin M. Bantle

Department of Environmental and Radiological Health Sciences

In partial fulfillment of the requirements

For the Degree of Doctor of Philosophy

Colorado State University

Fort Collins, Colorado

Fall 2019

Doctoral Committee:

Advisor: Ronald B. Tjalkens

Mark Zabel
Julie Moreno
Takamitsu Kato
Elissa K. Randall

ABSTRACT

NEUROINFLAMMATORY AND THE TWO-HIT HYPOTHESIS OF PARKINSON'S DISEASE

The ever-increasing prevalence of neurodegenerative diseases, Alzheimer's Disease (AD) and Parkinson's disease (PD), impose one the most significant medical and public health threats throughout the world. Characteristic PD symptoms include loss of voluntary motor control due to α-synuclein protein-aggregation, neuroinflammatory glial activation, mitochondrial dysfunction, oxidative stress, and progressive neuronal loss. There are currently no disease-modifying therapies for the disease nor has the etiology of PD been elucidated. Epidemiologic and experimental evidence suggests that genetic susceptibility, environmental pesticide exposure, and viral infections are possible risk-factors for PD, but a clear understanding of the environmental links to PD and how these factors can act in concert remains extremely limited. Research is beginning to shed light on neuroinflammation as a converging and coalescing pathway in the pathogenesis and pathophysiology of genetic, sporadic, and postencephalitic PD. While it has been appreciated since the late 1980s that brain inflammation is a hallmark of PD and other age-related neurodegenerative diseases, the immunological role of glia and the key trophic and inflammatory factors and pathways responsible for neurotoxicity and neuronal death in PD have not been clearly elucidated. Understanding how these pathways are regulated in glia during genetic, sporadic, and postencephalitic PD, and how they can directly or secondarily affect the onset and progression of PD is of keen interest. Therefore, the subject of this work will be to explore mechanisms by which glial cells modulate neuronal injury in genetic, sporadic, and

postencephalitic cases of PD, with an emphasis on the role of neuroinflammatory activation of glia in single and two-hit models of PD.

DEDICATION AND ACKNOWLEDGEMENTS

I dedicate this dissertation to Laura and Leo. I could not have done it without you two. Your love and support mean the world to me, and I can never thank you enough for the sacrifices made throughout my studies. My family is my compass, and without them, I am forever lost. Additionally, I would like to thank my advisor, Dr. Ron Tjalkens, for his continual support throughout my graduate studies. I would like to extend my gratitude to my committee members, Drs. Mark Zabel, Julie Moreno, Elissa Randall, and Takamitsu Kato. Lastly, I would like to thank Dr. Aaron Phillips for his invaluable guidance throughout the initial stages of my studies.

TABLE OF CONTENTS

ABSTRACT ii

DEDICATION AND ACKNOWLEDGEMENTS.....iv

1. CHAPTER 1- LITERATURE REVIEW.....1

1.1. NEUROINFLAMMATORY ACTIVATION OF GLIA IN PARKINSON'S DISEASE (PD).....1

1.1.1. MICROGLIA.....4

1.1.2. ASTROCYTE.....6

1.2. NEUROINFLAMMATION IN GENETIC VARIANTS OF PD.....9

1.2.1. LRRK2.....11

1.2.2. SNCA.....12

1.2.3. DJ-1.....15

1.2.4. GBA.....17

1.2.5. PINK1 AND PARKIN.....19

1.3. NEUROINFLAMMATION IN SPORADIC PD PD.....21

1.3.1. ROTENONE.....22

1.3.2. MPTP.....24

1.3.3. MANGANESE.....26

1.4. NEUROINFLAMMATION IN POSTENCEPHALITIC PD.....29

1.4.1. INFLUENZA.....31

1.4.2. MOSQUITO-BORNE VIRUSES.....34

1.4.3. HSV-1.....40
1.5. NEUROINFLAMMATION AND THE TWO-HIT HYPOTHESIS OF PD.....41
1.5.1. GENE-GENE INTERACTIONS IN PD.....43
1.5.2. GENE-ENVIRONMENTAL INTERACTIONS IN PD 44
1.5.3. ENVIRONMENTAL-ENVIRONMENTAL INTERACTIONS IN PD.....46
2. CHAPTER 2 – INFECTION WITH MOSQUITO-BORNE ALPHAVIRUS INDUCES SELECTIVE LOSS OF DOPAMINERGIC NEURONS, NEUROINFLAMMATION AND WIDESPREAD PROTEIN AGGREGATION.....50
2.1. INTRODUCTION.....50
2.2. MATERIALS & METHODS.....53
2.3. RESULTS.....61
2.4. DISCUSSION.....70
2.5. FIGURES.....79
3. CHAPTER 3 – ASTROCYTE INFLAMMATORY SIGNALING MEDIATE α-SYNUCLEIN AGGREGATION AND NEURONAL LOSS AFTER ENCEPHALITIC VIRAL INFECTION 91
3.1. INTRODUCTION.....91
3.2. MATERIALS & METHODS.....95
3.3. RESULTS.....103
3.4. DISCUSSION.....108
3.5. FIGURES.....114
4. CHAPTER 4 – JUVENILE MANGANESE EXPOSURE POTENTIATES

NEURODEGENERATION FOLLOWING ENCEPHALITIC INFECTION WITH A NEUROTROPIC VIRUS AND IS DEPENDENT ON NF-κB IN ASTROCYTES.....123
4.1. INTRODUCTION.....123
4.2. MATERIALS & METHODS.....126
4.3. RESULTS.....132
4.4. DISCUSSION.....136
4.5. FIGURES.....142
5. CHAPTER 5 – JUVENILE MANGANESE EXPOSURE INDUCES GLIAL ACTIVATION, HISTONE ACETYLATION, AND A UNIQUE GENE SIGNATURE IN THE BASAL GANGLION FOLLOWING SUBSEQUENT INFECTION WITH H1N1 INFLUENZA IN ADULTHOOD.....146
5.1. INTRODUCTION.....146
5.2. MATERIALS & METHODS.....149
5.3. RESULTS.....158
5.4. DISCUSSION.....163
5.5. FIGURES.....169
6. CHAPTER 6 – JUVENILE EXPOSURE TO MANGANESE EXACERBATES ASTROCYTE-DEPENDENT NEUROINFLAMMATORY INJURY FOLLOWING ADULT CHALLENGE WITH MPTP.....175
6.1. INTRODUCTION.....175
6.2. MATERIALS & METHODS.....178
6.3. RESULTS.....182
6.4. DISCUSSION.....188

6.5. FIGURES.....195

7. CHAPTER 7: DISCUSSION & FINAL CONCLUSIONS.....202

REFERENCES.....211

CHAPTER 1

LITERATURE REVIEW

1.1 NEUROINFLAMMATORY ACTIVATION OF GLIA IN PARKINSON'S DISEASE (PD)

Parkinson's disease (PD) is the second most common neurodegenerative disease after Alzheimer's disease (AD) and the most common movement disorder worldwide (Dauer and Przedborski, 2003). PD affects approximately 1 million Americans alive today, and the US National Institute of Neurological Disorders and Stroke (NINDS) predicts that 50,000 new cases of Parkinson's disease are diagnosed in the US each year (Tanner et al., 2011). With the aging of the Western World, the burden of this disease is set to rise tremendously over the next 35 years. Characteristic symptoms of PD include loss of voluntary motor control due to α-synuclein protein-aggregation, neuroinflammatory glial activation, mitochondrial dysfunction, oxidative stress, and progressive dopaminergic neuronal loss in the substantia nigra par compacta (SNpc). There are currently no disease-modifying therapies for the disease, nor has the etiology of PD been clearly elucidated.

Certain rare genetic mutations are associated with early-onset PD, before the age of 50. These include variants in genes such as *SNCA, DJ-1, PINK1* and *PARKIN, LRRK2* and *GBA*. However, collectively, genetic forms of PD only account for approximately 10% of PD cases, whereas the other 90% of PD cases are thought to be idiopathic or from unknown environmental factors. Interestingly, the vast majority of people with PD-related gene variants and individuals exposed to environmental risk factors rarely develop clinical PD. Research is just beginning to shed light on common pathways and mechanisms of disease pathogenesis and pathophysiology amongst different forms of PD. It is likely that PD is linked to combinatorial interactions

between genetic risk factors, infection with pathogens such as viruses and exposure to environmental neurotoxins. Thus, aging, genetics and environmental stressors each alone are unlikely to initiate PD, but together may be able to induce a clinical disease (Abou-Sleiman et al., 2006; Dauer and Przedborski, 2003; Pang et al., 2019). Importantly, several lines of evidence are beginning converge on neuroinflammatory activation of glia as a common central pathway that could integrate the seemingly disparate pathobiological processes of genetic, sporadic and postencephalitic PD (Duffy et al., 2018; Gerhard et al., 2006; Lindqvist et al., 2013; Mogi et al., 1996).

Furthermore, the majority of PD research over the last two centuries has been primarily focused on the degeneration and malfunction of dopaminergic neurons in the SNpc. However, increasing clinical evidence has suggested a significant role of microglial-derived and astrocyte-derived neuroinflammation in PD, which is supported by clinical observations of increased inflammatory cytokines in cerebral spinal fluid (CFS) and plasma of PD patients and by longitudinal studies showing sustained neuroinflammatory activation of microglia in the midbrain with PET imaging (Nakano et al., 1998; Vermeulen et al., 2002) (Fernandes et al., 2007; Kim et al., 2006). Importantly, neuroinflammation is a common feature of multiple degenerative disorders of the central nervous system (CNS), characterized by augmented numbers of activated microglia and astrocytes, increased level of inflammatory cytokines and decreased levels of anti-inflammatory molecules (Limphaibool et al., 2019). Within the CNS, glia represent over 70% of all cells. While, early descriptions of these cells labeled them as the "glue of the brain" with a primarily passive structural role, contemporary research is elucidating many dynamic functions of glia in the developing and adult brain. Astrocytes and microglia are key mediators of neuroinflammatory responses through activation of innate immune

inflammatory gene programs resulting in production of a large array of inflammatory cytokines, chemokines, neurotrophic factors, and other neuromodulatory factors (Tansey and Goldberg, 2010). Moreover, astrocytes and microglia are essential for neuronal development and neuronal support, regulating synaptic function, brain metabolism and cerebral blood flow (Rohn and Catlin, 2011). Although inflammatory activation of microglia and astrocytes is required during neuronal development and infections, chronic release of inflammatory chemokines and cytokines, along with a reduction of neuronal homeostatic support, can directly and indirectly, induce dopaminergic neuronal loss in the SNpc, contributing significantly to neuronal death in PD (Amor et al., 2010; Limphaibool et al., 2019; Rohn and Catlin, 2011).

Neuroinflammatory activation of glia may be triggered by variety of immunological challenges. These include bacterial or viral infections, neuronal injury, environmental insults, genetic mutations, and α-synuclein protein oligomers and aggregates, which can activate both microglia and astrocytes via Toll-like receptors (TLRs), leading to excessive production of pro-inflammatory cytokines and reactive oxygen species (ROS)(Kim et al., 2013a; Kim et al., 2013b; Rannikko et al., 2015). In addition, the nigro-striatal dopamine pathway is highly sensitive to intracellular and extracellular perturbation due to genetic mutations, neurotoxic insults, and microbial infection, and increasing amounts of data suggest that neuroinflammatory activation of glia may play a critical role in the initiation and progression of dopaminergic loss in genetic, sporadic, and postencephalitic PD (Aloisi, 1999; Block and Hong, 2005; Hirsch et al., 2005; Minghetti et al., 2005; Streit et al., 2004). Glial inflammatory activation is regulated by several pathways including mitogen-activated protein kinases (MAPKs), activator protein-1 (AP-1), Janus kinase (JAK)/signal transducer and activator of transcription (STAT), and interferon regulator factor families, and nuclear factor kappa B (NF-κB)(Glass et al., 2010b; Karin, 2005;

Tjalkens et al., 2017). Reports in literature indicate that chronic neuroinflammation induces dopaminergic degeneration and that anti-inflammatory agents inhibit dopaminergic cell death in animal models of PD. However, whether glial mediated dopaminergic neuronal loss in PD is due to a gain of inflammatory function or loss of physiological function, including trophic and antioxidant support, remains elusive. Both likely contribute to the spontaneous dopaminergic neuronal loss in PD, suggesting that gene-environment interactions likely modulate glial activation and damage to dopaminergic neurons in PD.

Identifying common molecular pathways that modulate tissue injury in PD is critical to understanding disease pathophysiology and to identification of therapeutic targets. Because neuroinflammation is an important component in the pathogenesis of many disease states of the CNS, it is becoming clear that inflammatory activation of glia may also have a causal role in the initiation and progression of PD. Thus, chronic activation of innate immune inflammatory pathways in glia may be a critical link between genetic, sporadic and post-encephalitic PD, as well as in environmentally induced forms of PD. Understanding the mechanisms by which brain inflammation is initiated and sustained in glia will likely help to delineate the key players that contribute to PD pathogenesis, and may be of great importance for the identification of novel therapeutic targets. In addition, the fact that glial activation may act in advance of dopaminergic neuronal cell death and α-synuclein protein aggregation may facilitate early diagnosis and drug targets that can prevent disease development. The following sections of this review discuss the role of inflammatory activation in microglia and astrocyte in PD and their potential protective and detrimental roles in PD pathogenesis.

1.1.1. MICROGLIA

Microglia are the first responders and the resident immune cell in the CNS, making up around 5-10% of the total cells in the brain (Li and Barres, 2018). Microglia localize to specific neuroanatomical regions, including the medulla oblongata, pons, hippocampus and basal ganglia, particularly the SNpc, which are affected regions in AD and PD (Mittelbronn et al., 2001). Under normal physiological conditions, microglia exist in a quiescent and ramified state in the absence of any inflammatory stimuli, which is achieved by immunosuppressant release of immunoregulatory molecules by astrocytes and neurons (Lee et al., 2008). This communication between neurons and glia is critical to prevent unneeded inflammatory activation. In a resting state, microglia release both anti-inflammatory and neurotrophic factors while surveying their respective CNS microenvironments (Streit et al., 2004). However, in the presence of inflammatory stimuli like ATP, environmental toxins, bacteria, viruses, and α-synuclein, microglia become activated and transition into an activated and ameboid phenotype, proliferate, and migrate to the site of insult (Block and Hong, 2005; Di Virgilio et al., 2009; Kim, 2006; Kim et al., 2005; Kim et al., 2006).

Furthermore, once activated, microglia can be both beneficial and deleterious in disease. Microglial activation has been simplified and categorized into M1 and M2 reactions, which represent an inflammatory and activated state, M1, and a quiescent and ramified state M2 (Block and Hong, 2005). M1 activation promotes neuroinflammation and neurotoxicity, while M2 activation mediates anti-inflammatory effects and neurotrophic support (Tang and Le, 2016). Acute activation of microglia is generally believed to be neuroprotective, while chronic activation has been implicated as a potential mechanism in PD and related diseases (Du et al., 2018). Chronic activation of M1 microglia release a diversity of inflammatory factors including cytokines, chemokines, ROS, and nitric oxide (NO) that are toxic to dopaminergic neurons (Kim

et al., 2005). Additionally, pro-inflammatory mediators released by activated astrocytes can act on microglia receptors, increasing microglial activation and inducing a chronic M1 inflammatory state (Troncoso-Escudero et al., 2018).

Taken together, increasing clinical evidence has suggested a significant role for chronic microglial-derived neuroinflammation in PD (Duffy et al., 2018; Gerhard et al., 2006; Lindqvist et al., 2013; Mogi et al., 1996). Accordingly, prevention of M1 microglial activation by pharmacologic or genetic approaches protects against neuroinflammatory pathology and dopaminergic neuronal loss form inflammatory insult in experimental models of neurodegeneration (Benskey et al., 2018) It is becoming clear that microglia activation contributes to loss of DA neurons and our lab has recently shown that microgliosis precedes α-synuclein protein aggregation in a novel neuroinflammatory model of PD, suggesting that glia may play a causal role in PD initiation. Thus, targeting specific inflammatory mediators in microglia may be a valuable approach in PD pathogenesis. However, due to insufficient neuroinflammatory models of PD coupled with complex glial-glial signaling, and interacting inflammatory pathways in PD, identification of anti-inflammatory targets and the creation of successful therapies for PD will be challenging (Tansey and Goldberg, 2010).

1.1.2. ASTROCYTES

Glial cells account for over 70% of the cells in the brain and astrocytes are the most abundant glial cell type in the CNS (Sofroniew and Vinters, 2010). Astrocytes function to support neuronal homeostasis, participate in the maintenance of the blood-brain barrier (BBB) and are dynamic regulators of the neuronal synaptic communication and cerebral blood flow. They also provide continuous trophic support and energy metabolism to neurons by secreting glial-derived neurotrophic factor (GDNF), regulating extracellular ion balances in the CNS, and

shuttling lactate and glutamine to neurons (Sofroniew and Vinters, 2010). Importantly, research is beginning to elucidate the roles of astrocytes in PD pathogenesis. Similar to microglia, astrocytes respond to inflammatory stimuli such as ATP, environmental toxins, bacteria, viruses, and α-synuclein through pattern associated molecular pattern receptors (PAMP)(Glass et al., 2010b; Tanaka et al., 2013). Activation of astrocytes is measured by increased expression of glial-fibular acid protein (GFAP)(Glass et al., 2010b). In addition, astrocytes activation can be neuroprotective through isolation of damaged areas by glial scar formation, production of glutathione, BBB repair and release of neurotrophic factors such as NGF and GDNF. However, astrogliosis and chronic inflammatory activation can also be neurotoxic and promote neurodegeneration (Block and Hong, 2005; Kuno et al., 2006; Sofroniew and Vinters, 2010).

The existence of astrocytes was first documented over 100 years ago, and although astrogliosis is continually observed in PD animal models and human PD patients in the basal ganglia, few studies have interrogated the role of reactive astrocytes in PD. Recent studies have shown that astrocytes release proinflammatory cytokines such as IL-1β, COX-2 and TNF-α after inflammatory activation of extracellular α-synuclein by the TLR4 pathway (McCabe et al., 2017; Rannikko et al., 2015). Additionally, astrocytes are involved in the uptake and clearance of α-synuclein from the CNS (Booth et al., 2017). Overexpression of α-synuclein in astrocytes induces inflammatory activation of astrocytes and microglia with associated degeneration of dopaminergic neurons in mice (Sofroniew and Vinters, 2010). Furthermore, Liddelow et al. have shown that similar to microglia, astrocytes can be A1 neurotoxic astrocytes or A2 neuroprotective astrocytes (Liddelow and Barres, 2017; Liddelow et al., 2017a). A1 reactive astrocytes are activated by microglia secreted IL-1a, TNF and complement component 1q (C1q), which suggest glial-glial communication are necessary for astrocyte inflammatory

activation (Liddelow and Barres, 2017; Liddelow et al., 2017a). Interestingly, A1 neurotoxic astrocytes cause degeneration of co-cultured human iPSC-derived dopaminergic neurons, which suggests that A1 astrocytes release neurotoxic factor and/or also lose trophic capacity to support and maintain neuronal survival (Liddelow and Barres, 2017). Furthermore, human post-mortem tissues from PD patients show an increase in A1 reactive astrocytes in the nigrostriatal pathway (Liddelow and Barres, 2017). PD is due to the selective loss of dopaminergic neurons in the SNpc, however, the mechanistic reasons for selective loss of dopaminergic neurons in the SNpc while other regions are spared is unclear. Recent evidence shows that regional difference in astrocytes modulate the selective vulnerability of SNpc dopaminergic neurons (Kostuk et al., 2019). This suggests that astrocytes in the SNpc may be more sensitive to phenotypic conversion into an A1 neurotoxic phenotype relative to other brain regions.

Although microglia have been previously thought of as the primary inflammatory cell in the CNS, inflammatory activation of astrocyte is often more persistent than microglia and is believed to be important in chronic inflammatory activation associated with PD (Saijo et al., 2009) In addition, astrocytes culture studies have shown that isolated human astrocytes are the primary source for NO production in the brain (Ashley et al., 2016; Lin et al., 1995). Multiple genes that are implicated in PD likely play a role in inflammatory activation of astrocyte in response to inflammatory stimuli, suggesting that astrocytes dysfunction may enhance neuron loss in PD (Booth et al., 2017).

There is increasing evidence glial-derived neuroinflammatory injury in PD. Thus, inhibition of glial inflammatory responses could represent an effective therapeutic approach in PD (Duffy et al., 2018; Gerhard et al., 2006; Lindqvist et al., 2013; Mogi et al., 1996). Under normal physiological conditions, microglia and astrocytes support neurons but upon activation

from inflammatory stressors, glia switch from their neuroprotective role to a pathogenic one, contributing to disease onset and progression. Interestingly, 17 PD gene variants involved in the development of PD are also highly expressed in astrocytes and microglia (Booth et al., 2017). Therefore, glial dysfunction is likely critical to idiopathic and genetic PD. For decades, therapies aimed to attenuate PD have solely targeted neurons. Thus, these previous studies suggest that targeting glial cells may be the next logical step in the development of therapies for the treatment of PD and related neurological diseases (Troncoso-Escudero et al., 2018).

1.2. NEUROINFLAMMATION IN GENETIC VARIANTS OF PD

Approximately 90% of PD cases are sporadic and the disease has long been considered an idiopathic disorder with an age-related increase in incidence. Moreover, the lack of geographic clusters with epidemiological studies go against environmental toxins as being the sole cause of PD (Pang et al., 2019). Over the last 20 years, genome-wide association studies (GWAS) have provided new genetic insights into the disease etiology and pathogenesis, strengthening the possibility of specific gene variants playing a role in PD pathogenesis (Lesage and Brice, 2009; Tanner et al., 2011). To date, there are 26 identified loci known to be associated with an increased susceptibility to PD (Lill, 2016). Both GWAS and candidate gene association studies have shown that the most common variants are in proximity to LRRK2, SNCA, DJ-1, PINK1, Parkin, as well as low-frequency coding variants in GBA (Billingsley et al., 2018). However, similar to other genetically complex diseases, the vast majority of these gene variants rarely manifest clinically, which highlights the likelihood of a combined interaction between genetic susceptibility and environmental factors driving PD initiation.

Given that neuroinflammatory activation of glia may play a significant role in initiation of PD following environmental exposures, increasing amounts of evidence are beginning to shed

light on the expression of these gene variants in nonneuronal cells types, such as microglia and astrocytes (Booth et al., 2017; Chen et al., 2018; Keatinge et al., 2015; Sun et al., 2018; Torres-Odio et al., 2017). How these gene variants, directly and indirectly, drive unique transcription signatures in glia is still unclear, but research is beginning to suggest that genetic and epigenetic modulations in glia may be critical to the spontaneous degeneration of dopaminergic neurons in familial PD (De Jager et al., 2014; Lill and Bertram, 2015; Lunnon et al., 2014).

Neuroinflammation contributes to the neuropathology in toxin-induced models of PD with Rotenone and MPTP, and previous work has also shown that the majority of PD-linked genes such as α-synuclein and LRRK2, promote neuroinflammation through activation of microglia and astrocytes (Daher et al., 2015; Gao et al., 2008; Gillardon et al., 2012; Kim et al., 2013a; Lee et al., 2010; Lopez de Maturana et al., 2014; Moehle et al., 2012; Qin et al., 2016; Russo et al., 2015). Additionally, previous evidence has shown that PINK1, Parkin and DJ-1 are increased in reactive astrocytes in the human PD brain tissue and may be regulated through NF-κB-expression in glia (Tran et al., 2011; van Horssen et al., 2010; Wilhelmus et al., 2011; Witte et al., 2009).

Nevertheless, few studies have interrogated the role of neuroinflammatory activation of glia in genetic PD patients and genetic based models. However, neuroinflammatory activation of glia seems to be a conserved pathogenic mechanism across the major gene variants associated with early onset PD. Therefore, the following chapters discuss the role of inflammatory activation in microglia and astrocyte in LRRK2, SNCA, DJ-1, PINK1, PARKIN, and GBA gene variants, and their potential role in familial PD pathogenesis. Although these studies focus on monogenic mutations, future studies looking at the capacity of multiple gene mutations to act in concert will be of great interest.

1.2.1. LRRK2

The first finding to suggest a familial form of PD was discovered in the early 1990s, after the identification of the rare and recessive forms of gene variants that were associated with early-onset of the disease, which include *PRKN, PINK1,* SNCA, and *DJ-1(Bonifati et al., 2003; Kitada et al., 1998; Polymeropoulos et al., 1997). Shortly after, in* 2004, the leucine-rich kinase 2 (*LRRK2*) was identified as the most common genetic form of PD (Paisan-Ruiz et al., 2004; Zimprich et al., 2004). Collaborative research has shown that the most common pathogenic variant in *LRRK2* is the p.G2019S, and this specific variant is responsible for about 1% of patients with genetically complex PD and 4% of patients with a family history of PD (Billingsley et al., 2018). Variant carriers have an age-dependent chance of developing the disease with a 28% increased risk at 59 years to 51% increased risk at 60 years reaching up to 75% at 80 years of age (Spatola and Wider, 2014). However, the corresponding pathogenic mechanisms of LRRK2 mutants remain largely unknown.

Increasing evidence suggests that LRRK2 is expressed in nonneuronal cell types and could be a modulator of the neuroinflammation, suggesting that neuroinflammation of glia is a converging molecular pathway in LRRK2 mutants and related genetic mutations (Bell et al., 1971; Pang et al., 2019). Moreover, LRRK2 is expressed in multiple immunological cells including B lymphocytes, peripherical macrophages, and astrocytes (Lee et al., 2019). Treatment with a variety of inflammatory cocktails includes, LPS, TNF and α-synuclein fibrils modulate inflammatory cytokine production in LRRK2 knockouts (KO) and overexpression models (Gillardon et al., 2012; Ho et al., 2019; Kozina et al., 2018; Russo et al., 2019). Interestingly, relative levels of LRRK2 expression are low in neurons, and some data has suggested that LRRK2 is most abundantly expressed in microglia and astrocytes in the SNpc (Booth et al.,

2017). Previous studies have shown that LRRK2 KO mice suffer impaired microglia phagocytosis of bacterial and viral particles in the brain (Chen et al., 2018). Additionally, co-culture experiments using induced pluripotent stem cell-derived astrocytes and neurons from familial mutant LRRK2 G2019S PD patients have shown that, upon co-culture on top of LRRK2 G2019S PD astrocytes, LRRK2 G2019S PD neurons display morphological signs of neurodegeneration and astrocyte-derived α-synuclein accumulation, whereas co-culture on top of healthy astrocytes attenuated the pathology (di Domenico et al., 2019).

Therefore, these previous studies suggest that LRRK2 may play a role in neuroinflammation activation of glia. Considering that microglia and astrocytes become inflammatory and neurotoxic during aging and that LRRK2 is significantly expressed in aged microglia and astrocytes, LRRK2 may modulate inflammatory responses in glia that induce disease in aging populations (Clarke et al., 2018; Kim et al., 2012; Marker et al., 2012; Moehle et al., 2012). Together, these previous findings highlight the pathogenic crosstalk between neurons and glial cells and could unveil a crucial non-cell-autonomous contribution of astrocytes and microglia in LRRK2 PD patients.

1.2.2. SNCA

Spontaneous neuronal loss, gliosis, and the formation of insoluble α-synuclein protein plaques is a hallmark of PD, Lewy body dementia and multiple system atrophy (MSA). Alpha-synuclein (SNCA) is a presynaptic terminal protein that is abundantly expressed in the neocortex, hippocampus, thalamus, cerebellum and in the SN. The structure of the protein consists of three distinct regions: the alpha-helical N-terminal amphipathic membrane-bound regions (residues 1- 60), the central hydrophobic amyloid component that is involved in protein

aggregation (residues 61-95), and the highly acidic, proline-rich, C-terminal tail which likely interacts with synaptic vesicles (residues 96-140)(Clayton and George, 1998; Ueda et al., 1993). Although the function of α-synuclein is still elusive, studies have shown a key role for α-synuclein in the regulation of dopamine neurotransmitter release, synaptic function, plasticity of dopaminergic neurons, and neuroinflammatory activation of glia (Bendor et al., 2013; Eisbach and Outeiro, 2013; Lashuel et al., 2013).

At least 30 mutations in the SNCA gene have been found to induce early-onset disease with the most common mutations located in the N-terminal/membrane-bound portion, which include A53T, A30P, E46K, H50Q, and G51D, (Bozi et al., 2014; Flagmeier et al., 2016; Kruger et al., 1998; Polymeropoulos et al., 1997; Zarranz et al., 2004). Research has also shown that duplications and triplications of the SNCA locus can induce early-onset disease (Campelo and Silva, 2017; Chartier-Harlin et al., 2004; Ibanez et al., 2004). It is known that N-terminal point mutations in SNCA and overexpression of SNCA induce accelerated protein aggregation and neuronal loss, but whether neuron loss following accelerated protein aggregation is primarily due to neuronal dysfunction, glia activation, or both is unclear.

Several factors are associated with α-synuclein aggregation, including impairment of neuronal protein degradation and clearance, which may induce the release of undigested α-synuclein from the cell. Extracellular α-synuclein is thought to be the most toxic conformation of the protein and astrocytes and microglia are the primary scavengers of extracellular α-synuclein following release from neurons (Filippini et al., 2019). Interestingly, microglia are thought to be the primary phagocytic cell in the brain, but astrocytes are thought to play a significant role in phagocytosis of α-synuclein as well. Endocytosis of extracellular α-synuclein and inflammatory activation in glia involves receptor recognition by pattern-recognition receptors (PRR): TLR4

and TLR2, and by the purinergic receptor P2X7 (Jiang et al., 2015; Refolo and Stefanova, 2019). While TLR 2 and 4 are thought to be the primary modality of α-synuclein endocytosis, recent evidence has shown that microglial inflammatory response can also occur through FcγR-mediated phagocytosis (Cao et al., 2012). Moreover, astrocytes exposed to α-synuclein undergo activation of the TLR4 pathway with associated increases in IL-1β, COX-2 and TNF-α cytokines (Booth et al., 2017; Filippini et al., 2019; Rannikko et al., 2015). However, whether this inflammatory activation induces a gain of neurotoxic activation or a loss of homeostatic function in glia is unclear (Filippini et al., 2019). Previous studies with genetic-based A53T mice have shown that overexpression of mutated α-synuclein induces astrogliosis, impaired astroglia homeostatic function, with subsequent microgliosis and neurodegeneration (Gu et al., 2010). Additionally, isolated glia culture experiments with different pathogenic forms of α-synuclein results in neuronal α-synuclein aggregation, selective loss of dopaminergic neurons, impaired motor functions, and an increased inflammatory profiles in glia without overt glia death (Olsen and Feany, 2019). This may suggest that extracellular α-synuclein is as neuronal derived microglial and astrocyte inflammatory stress signal.

Interestingly, Lee et al. reported that α-synuclein clearance is reduced in activated microglia and astrocytes, and that phagocytic function of glia is impaired during aging (Filippini et al., 2019; Lee et al., 2008). Considering that aging alone induces inflammatory activation of glia, this may suggest that α-synuclein clearance is decrease in aging populations and could play a role in PD pathogenesis (Clarke et al., 2018; Liddelow and Barres, 2017; Liddelow et al., 2017a) Therefore, dopaminergic neurotoxicity in PD is likely due to a gain of inflammatory activation of glia, a loss protein clearance, and loss of homeostatic trophic support form glia.

Taken together, α-synuclein likely plays a role in the innate immune system and induces reactivity of glial cells in the brain. Neuroinflammation seems to be a common mechanism in genetic variants models of SNCA, KO SNCA models, and overexpression models of SNCA. These previous studies suggest that that α-synuclein uptake in glia contributes to PD and related α-synucleinopathies, and that pathogenic α-synuclein may induce selective toxicity of dopaminergic neurons (Olsen and Feany, 2019). Although the exact mechanisms facilitating endocytosis and inflammatory activation of microglia and astrocytes following treatment with α-synuclein are unclear, research is beginning to identify the molecular mechanisms of α-synuclein uptake and unique transcriptional signatures in glia following treatment with α-synuclein. Future studies elucidating the role of glia crosstalk between microglia and astrocyte inflammatory activation following exposure to α-synuclein may shed light on the pathogenic mechanisms at play (Refolo and Stefanova, 2019).

1.2.3. DJ-1

DJ-1 is expressed in astrocytes and is important for maintaining mitochondrial function. Mutations in DJ-1 result in an early onset form of PD, strongly implicating altered redox balance and dysregulation of mitochondrial function in astrocytes as an important modulator of PD pathogenesis. Although DJ-1 is expressed ubiquitously throughout the body, it is highly expressed in neurons and reactive astrocytes in the CNS (Bandopadhyay et al., 2004; Neumann et al., 2004). DJ□1 is a 189 amino acid protein with multiple functions but is primarily thought to function as a mitochondria oxidative stress sensor and reactive oxygen scavenger (Ashley et al., 2016; Trudler et al., 2014). Additionally, DJ-1 protects against metal-induced neurotoxicity and regulates intracellular antioxidant stress responses through the transcription factor Nrf2 (nuclear factor-like 2) (Bjorkblom et al., 2013).

DJ-1 missense mutations increase the risk of developing early-onset PD, likely due to a loss of function, and increased ROS production. Additionally, DJ-1 can indirectly inhibit aggregation of α-synuclein through its chaperone protein activity, protecting dopaminergic neurons from spontaneous cell death. (Shendelman et al., 2004; Zhou et al., 2006). Conversely, *DJ-1* KO mice fail to recapitulate the critical clinical and neuropathological features of PD, and despite the decades of research on DJ-1 and its involvement in PD pathology, it is still unclear how DJ-1 contributes to PD pathogenesis (Ashley et al., 2016).

Due to the abundant expression of DJ-1 in glia and its role in mediating oxidative stress, increasing evidence suggests that deficiencies in DJ-1 expression or function might induce PD pathology through the loss of physiological function. Chronic oxidative stress in glial cells also induces altered intracellular signaling and mitochondrial perturbations, leading to increased inflammatory activation. Considering that microgliosis and astrogliosis is a significant pathological feature of PD, DJ-1 deficiency induces an increased cell sensitivity to dopamine and increased pro-inflammatory cytokines production of such as IL-1β and IL-6 in microglia and astrocytes (Trudler et al., 2014). Additionally, DJ-1 is thought to be a positive regulator of astrogliosis through STAT3 and Sox9 expression in the SNpc (Choi et al., 2018).

Furthermore, DJ-1-deficient microglia have reduced expression of triggering receptor expressed on myeloid cells 2 (TREM2), which is thought to be a regulator of microglia phagocytosis and key player in multiple neuroinflammatory and neurodegenerative diseases. Moreover, DJ-1-deficient microglia also have increased monoamine oxidase activity, resulting in elevated levels of ROS and NO that cause dopaminergic neurotoxicity in the SNpc. More recent studies found that DJ-1 may regulate the assembly of lipid rafts in astrocytes as well (Kim et al., 2016; Kim et al., 2013b). Lipid rafts are highly organized vesicles that are involved in receptor

trafficking, endocytosis, and signal transduction, and mutations in *DJ-1 leads to a decrease in* lipid raft proteins flotillin-1 and caveolin-1, resulting in a disrupted lipid raft assembly (Simons and Ehehalt, 2002). Additionally, DJ-1 knockout in astrocytes exhibit impaired glutamate uptake and increased excitoneurotoxicity, by decreasing the expression of EAAT2, an astrocyte-specific glutamate transporter that has previously been shown to assemble in lipid rafts (Kim et al., 2016; Kim et al., 2013b). The role of DJ-1 variants in PD is still unclear, but this data suggests that loss of DJ-1 function in glia likely play a significant role in PD disease development. Further studies of DJ-1-mediated cellular pathways in microglia and astrocytes will contribute useful insights into the development of PD and may provide future avenues for novel therapeutic targets.

1.2.4. GBA

Another gene variant that is closely associated with early-onset PD is β-glucocerebrosidase (GBA), which encodes the lysosomal enzyme glucocerebrosidase (GCase), an enzyme involved in sphingolipid metabolism. GCase is a metabolic enzyme that is localized in the lysosomal membrane, that cleaves the beta-glucosidic linkage of glucocerebroside, which is an abundant glycolipid in the cell membrane of neurons (Rijnboutt et al., 1991; Vielhaber et al., 2001). Hetero- and homozygous mutations in GBA cause PD and Gaucher's disease, a lysosomal storage disease characterized by the accumulation of glucocerebrosides in macrophages (Mucci and Rozenfeld, 2015; Stirnemann et al., 2017). Homozygous mutations in GBA causes Gaucher's disease, while heterozygous mutations increase one's risk for PD.

Accordingly, lysosomal dysfunction and accumulation of α□synuclein are thought to play a principal role in PD pathogenesis. Genetic variants in GBA account for at least 10% of all PD cases due to the loss of GCase activity (Gegg and Schapira, 2018). Cellular and animal

models of GCase deficiency result in lysosomal dysfunction, and in particular the autophagy-lysosome pathway, resulting in the CNS accumulation of α□synuclein. Mutant GCase can also induce the unfolded protein response (UPR), which might also contribute to PD pathogenesis (Gegg and Schapira, 2018). Moreover, GCase activity was found to be significantly decreased in postmortem brain tissue from PD brains with heterozygote GBA mutations and in sporadic PD patients as well, with the most significant decrease of 58% in heterozygote GBA mutations and 33% in sporadic PD patients in the substantia nigra. Although calcium dysregulation and α□ synuclein accumulation are likely contributors, markers of the UPR are increased in the SNpc PD patients with heterozygote GBA mutations as well (Keatinge et al., 2015).

Furthermore, mitochondrial dysfunction and neuroinflammation are also associated with GCase deficiency in PD patients with GBA variants, but the mechanism by which the immune response is triggered in PD patients with GBA variants is unknown (Vitner et al., 2016). Interestingly, certain pathological aspects of human Gaucher's disease and PD provide evidence of early microglial activation preceding α-synuclein aggregation and dopaminergic neuronal cell death (Keatinge et al., 2015). This may suggest that inflammatory activation of glia from GCase deficiency could play a causal role in PD development.

Additionally, astrocyte activation is a hallmark of certain neuronopathic lysosomal storage disorders, and it has been suggested to precede neuronal degeneration as well (Di Malta et al., 2012; Pontikis et al., 2004). Studies using co-culture experiments with primary GCase knockout astrocytes demonstrated a decreased mitochondria resting membrane potential and increased mitochondrial fragmentation in astrocytes (Osellame and Duchen, 2013). Additionally, neurons with GCase deficiency can increase the release of extracellular α□synuclein, which can also be a potent inflammatory stressor to astrocytes and microglia in the nigrostriatal pathway

(Bae et al., 2014; Cavaliere et al., 2017; Fernandes et al., 2016; Ginns et al., 2014; Loria et al., 2017; Magalhaes et al., 2016)

Collectively, these studies provide new insights into the pathogenic mechanisms underlying PD with GBA variants, and the physiological impact of abnormal α-synuclein accumulation and neuroinflammation on the nigrostriatal pathway in PD (Ginns et al., 2014). The relationship between lysosomal dysfunction and inflammatory activation of glia is apparent in PD with GBA mutations, but the underlying mechanisms have yet to be fully characterized. We anticipate this will be an area of future research that will shed light on novel pathogenic mechanisms in PD.

1.2.5. PINK1 AND PARKIN

Many lines of evidence suggest that mitochondrial dysfunction plays a central role in Parkinson's disease. Mitochondria are highly dynamic organelles which fulfill a plethora of functions including regulation of calcium homeostasis, energy metabolism, and inflammatory activation. Increasing amounts of research indicate that several PD-associated genes involved in mitochondrial homeostatic may play a critical role in early-onset PD. Therefore, it is not surprising that an impairment of mitochondrial function results in neuronal degeneration. Of interest, PTEN-induced kinase 1 (PINK1) and Parkin are two genes responsible for familial forms of PD, which act together in regulating mitochondrial stress, surveillance, mitophagy, and mitochondrial biogenesis (Truban et al., 2017). PINK1 is a mitochondrial serine/threonine-protein kinase encoded by the PINK1 gene and Parkin is an E3 ubiquitin ligase that is involved in ubiquitin ligation on the outer membrane of the mitochondria in preparation for proteasomes and lysosome degradation. PINK1 and Parkin act together following mitochondrial stress to recycle damaged mitochondria via autophagy (Seirafi et al., 2015). Therefore, mutations in

PINK1 and Parkin are associated with mitochondrial dysfunction, significant astrogliosis and microgliosis, leading to dopaminergic neuronal death and PD pathogenesis.

Humans with PINK1 and Parkin mutations display elevated cytokines, but few studies have investigated the role of PINK1 and Parkin in neuroinflammation (Sliter et al., 2018; Sun et al., 2018). Experimental evidence has shown that lack of PINK1 and Parkin enhances glial innate immune activation and increases, nitric oxide production, suggesting that loss of PINK1 and Parkin in glia likely initiates early neuroinflammation (Sun et al., 2018). *Interestingly, PINK1* is highly expressed by astrocytes, and *PINK1 express*ion increases during embryonic development (Choi et al., 2016). Experimental studies have shown that *PINK1 and Parkin*-KO mice exhibit a reduced number of astrocytes compared with WT mice; however, this was not after inflammatory challenge (Choi et al., 2018; Choi et al., 2016; Choi et al., 2013) (Hayashi et al., 2000). PINK1 and Parkin KO astrocytes have also been found to have decreased neurotrophic capacity, mediated by a reduction in glutathione secretion (Solano et al., 2008). Additionally, PINK1 and Parkin may be directly involved in the glial inflammatory activation, and mutations induce increased expression of IL-1β and TNF-α (Khasnavis and Pahan, 2014).

Interestingly, PD patients with Parkin mutations present with increased α-synuclein aggregates in astrocytes (Koyano and Matsuda, 2015). Loss of functional mitophagy coupled with mitochondrial dysfunction in glia reduces ATP production and causes inflammatory activation in the glia. Furthermore, it is known that mitochondrial stress can lead to the release of damage-associated molecular patterns (DAMPs) that can activate innate immunity in the CNS (Sliter et al., 2018). Previous reports have shown that KO of STING, a central regulator of the type I interferon response to cytosolic DNA, attenuate dopaminergic neurons from the substantia nigra pars compacta in PINK1 and Parkin mutants (Sliter et al., 2018). However, whether PINK1

and Parkin mutations induce inflammatory activation in glia through DAMPs or intracellular mitochondrial perturbations remains elusive.

Together, these previous studies suggest that PINK1 and Parkin mutations likely activate glia, which reduces neuroprotection and initiates PD. Sporadic and familial PD seem to converge at the level of neuroinflammation in PINK1 and Parkin mutations (Moon and Paek, 2015). Similar to all other gene variants associated with PD, the vast majority of PINK1 and Parkin mutants do not manifest PD clinically. Therefore, secondary genetic factors and environmental exposures are likely at play.

1.3 NEUROINFLAMMATION IN SPORADIC PD

The nigrostriatal dopamine system in the basal ganglia is highly sensitive to damage from environmental neurotoxins. Although multiple genetic mutations have been implicated in PD, the majority of cases are sporadic, emphasizing the importance of environmental factors in the development of PD (Abou-Sleiman et al., 2006; Dauer and Przedborski, 2003). Perhaps the most compelling evidence to support glial-derived inflammatory mechanisms driving PD initiation and progression comes from epidemiological studies. Previous studies suggest that rural living, exposure to environmental pesticides and elevated levels of divalent metals are associated with an increased risk of PD, potentially due to their capacity to induce mitochondrial dysfunction and neuroinflammatory glial activation with associated loss of dopaminergic neuronal loss in the SNpc (Brown et al., 2006; Mayeux, 2003). Although neuroinflammatory activation of glia seems to be a conserved pathogenic mechanism following exposure to the majority of environmental neurotoxicants, few studies have focused on the glia-specific molecular mechanisms modulated in sporadic and idiopathic PD. Glial activation may be an important contributor to neuronal

dysfunction and injury during the early prodromal phase of PD prior to the onset of clinical disease.

The following chapters discuss the role of inflammatory activation of microglia and astrocyte in idiopathic forms of PD, with a focus on exposure to the pesticide, rotenone, the synthetic opioid derivative, MPTP, and the essential metal, manganese (Mn). Although the majority of these studies focus on the role of single toxicant and xenobiotic exposures, individuals with PD clinically manifests during aging and it is likely that any PD patient has encountered a number of environmental insults, which alone may be harmless but together may synergize to initiate PD pathogenesis. We hope that this work inspires others to interrogate the toxicological capacitary of these environmental insults to act in concert.

1.3.1. ROTENONE

Rotenone is a broad-spectrum naturally occurring insecticide, piscicide, and pesticide that potently inhibits mitochondrial complex I, inducing neuroinflammatory activation of microglia and astrocytes leading to neurochemical and neuropathological deficits that closely resemble those in idiopathic PD, including loss of dopaminergic neurons in the substantia nigra pars compacta, decreased dopamine levels and aggregation of α–synuclein (Betarbet et al., 2000; Gao et al., 2013; Yuan et al., 2013). For these reasons, rotenone is used as an animal model for environmental pesticide exposure to study how inhibition of mitochondrial function and generation of oxidative stress are associated with pathological mechanisms relevant to PD (Sherer et al., 2007).

According to a USEPA survey, rotenone was used worldwide and was found to be the most common pesticide used around U.S. homes in the 1990s (Caboni et al., 2004). The use of rotenone in the U.S. began to be voluntarily phased out by 2007 because of its association with

PD (Tanner et al., 2011). Although the mechanisms driving selective loss of dopaminergic neurons following treatment is unclear, it is essential to note that the nigrostriatal dopamine system in the basal ganglia is uniquely sensitive to damage from environmental neurotoxins, and exposure to elevated levels of the pesticides induces neuronal injury to this brain region, as well as cortical and subcortical structures. Furthermore, rotenone is among the environmental neurotoxins that induce pronounced neuroinflammation. Rotenone exposure increases microgliosis, astrogliosis, Toll-like receptor (TLR) expression, and causes persistent neuroinflammatory glial changes in PD-relevant brain regions with associated mitochondrial dysfunction (Gao et al., 2013; McCabe et al., 2017). Rotenone treatment in rodent models increases the release of inflammatory mediators such as COX-2, iNOS and NF-κB with associated increases in brain and serum pro-inflammatory cytokines TNF-α, IL-6, and IL-1β. Interestingly, rotenone-induced mitochondrial dysfunction has been primarily interrogated in neurons, but whether mitochondrial dysfunctions or extracellular factors released from neurons initiates neuroinflammation in glia is unclear (Thakur and Nehru, 2015).

Previous studies have shown that inhibiting microglial activation and production of proinflammatory mediators induced by rotenone attenuates neuronal loss (Liang et al., 2017) Although the exact molecular pathways at play following treatment with rotenone are unclear, data suggest that increased oxidative stress from mitochondrial complex I inhibition in glia activates NFκB associated pathways as well as Nrf2/ARE signaling pathway (Liang et al., 2017; Pistollato et al., 2017). Co-culture studies with microglia and neurons have shown that the presence of glia greatly enhances the neurodegenerative ability of rotenone (Gao et al., 2013; Gao et al., 2002; Yuan et al., 2013). These studies suggest that rotenone directly induces

inflammation in glia and that glia are not solely activated from extracellular factors released from necrotic neurons following treatment with rotenone.

Furthermore, astrocytes also play a significant role in rotenone-induced neurotoxicity. Recent experiments show that rotenone treatment induces DJ-1 in astrocytes in the SNpc. Overexpression of DJ-1 in astrocytes prevents oxidative stress, mitochondrial perturbations, and autophagy dysfunction in neurons, while also attenuating microglial activation following treatment with rotenone (Cabezas et al., 2012; Pistollato et al., 2017) (De Miranda et al., 2018). This again highlights the potential importance of glial-glial communications in neurodegeneration.

Together, these studies suggest not only that mitochondrial dysfunction in neurons is a critical factor in environmental models of PD pathogenesis but also that mitochondrial dysfunction may be similarly important to neuroinflammatory activation of glia following treatment with rotenone. It is still unknown whether inflammatory signatures in glia are altered in specific PD gene variants, such as PINK, PARKIN, and DJ-1. However, considering the conserved pathogenetic mechanisms of mitochondrial dysfunction and inflammation, these data suggests that PINK, PARKIN and DJ-1 mutants would likely have a more severe inflammatory response to rotenone.

1.3.2. MPTP

MPTP (1-methyl-4-phenyl-1,2,3,6-tetrahydropyridine) is a neurotoxin which induces selective loss of dopaminergic neurons in the SNpc and with associated motor symptoms that resemble PD. MPTP is a derivative of the synthetic opioid, meperidine, that crosses the blood-brain barrier and causes severe degeneration of dopaminergic neurons in the SNpc in humans and in non-human primates, resulting in parkinsonian motor deficits that can be partly alleviated

with levodopa (L-dopa), as reported by Langston *et al.* (1984). Over the past decades, the use of MPTP in models of PD and have made important contributions to understanding pathogenic mechanisms and to developing better palliative therapies for PD. The MPTP parent molecule is not toxic but requires metabolism by monoamine oxidase B (MAO-B) in astrocytes to the toxic metabolite, 1-methyl-4-phenylpyridinium (MPP+) cation, which is transported into dopaminergic neurons by the dopamine transporter (DAT) (Jackson-Lewis and Przedborski, 2007). Similar to rotenone, MPP+, inhibits complex I of the electron transport chain in mitochondria and induces neuronal toxicity (Jackson-Lewis and Przedborski, 2007).

MPTP is directly toxic to neurons and induces expression of inflammatory cytokines and chemokines in glia prior to overt neurotoxicity, while simultaneously reducing GDNF levels (Kohutnicka et al., 1998; Machado et al., 2016). This suggests that glial activation may be involved in the progression of dopaminergic neuronal damage during MPTP intoxication. Pharmacological inhibition of microglial attenuates the production of Il-1β and nitric oxide synthase (iNOS) and attenuates loss of dopaminergic neurons (Gelb et al., 1999). Interestingly, MPTP induces neuronal toxicity in C57BL/6 mice whereas BALB-C mice are resistant, and Yasuda and colleagues reported that the sensitivity of C57Bl/6 mice to MPTP might be due to the increased propensity of this strain to greater M1 microglia inflammatory reactions and subsequent increases in the inflammatory markers IL-10, IL-12 p40, IFN-γ and MCP-1/Ccl2 (monocyte/macrophage chemoattractant protein) in the cerebrospinal fluid, whereas these inflammatory markers are absent in BALB-C mice following MPTP treatment (Yasuda et al., 2008). Thus, the susceptibility of C57BL/6 mice to MPTP-induced neurodegeneration may be due to their prominent neuroinflammatory response (Sedelis et al., 2000). Also, our lab has shown that lack of functional NFκB in astrocytes also decreases reactive gliosis by suppressing

the expression of NOS2 and TNFα, resulting in protection against MPTP-induced neuronal apoptosis. This demonstrates that inflammatory activation of glial cells is an important determinant of MPTP neurotoxicity (Kirkley et al., 2019b).

Although these previous studies highlight a gain of inflammatory function in glia to initiate PD pathogenesis, other studies suggest that loss of glial support can also promote neurodegeneration. Previous work has shown that depletion of microglia with a CSF1R inhibitor exacerbated the impairment of locomotor activities and the loss of dopaminergic neurons in the SNpc (Episcopo et al., 2013; Hyman et al., 1991; Skaper, 2012; Yang et al., 2018). (Chen et al., 2004).

Collectively, these studies highlight the involvement of microglia and astrocytes in MPTP induced neurotoxicity. The complex interactions between neurons, microglia, and astrocytes will continue to be an area of focus in MPTP induced neurotoxicity. Surprisingly, multiple studies have shown insufficient protection of dopaminergic neurons with glial inflammatory inhibitors, suggesting that inflammatory activation of glia is not the sole cause of MPTP induced neurotoxicity but likely involves direct neurotoxicity and loss of glial trophic support (Di Monte et al., 1992; Machado et al., 2016). Therefore, future neurodegenerative therapies should consider combinational therapies with neuroinflammation inhibitors, coupled with neuronal growth factors.

1.3.3. MANGANESE

Exposure to elevated levels of the essential element manganese (Mn) causes neuronal injury in the basal ganglia, as well as cortical and subcortical structures. The long-term health effects of excessive exposure to Mn are a concern both in children and adults. In adults,

occupational exposure to high levels of inhaled Mn causes an extrapyramidal form of parkinsonism presenting with initial neuropsychiatric symptoms followed by progressive motor dysfunction characterized by dystonia, bradykinesia, rigidity and gait abnormalities (Couper, 1837; Crossgrove and Zheng, 2004; Huang et al., 1989; Perl and Olanow, 2007; Rodier, 1955). Additionally, childhood exposure to Mn is a significant problem due to higher absorption across the blood-brain barrier and decreased biliary excretion compared to adults, which raises concerns over the impact that exposure to Mn early in life could have on neurological function during aging (Aschner et al., 2005; Landrigan et al., 2005). Brain Mn levels are also elevated by chronic iron deficiency, designated by WHO as a major world health problem affecting millions of children (Garcia et al., 2007). In addition, children receiving long-term parenteral nutrition are at risk for Mn-induced neurological damage, as are individuals with inherited deficits in the hepatic metabolism of Mn (Avelino et al., 2014; Fell et al., 1996). Mn exposure not only causes behavioral and learning problems in children but also affects motor function, consistent with alternations in fine motor control reported in both rodent and non-human primate models of Mn neurotoxicity (Beaudin et al., 2015; Bouchard et al., 2007a; Guilarte et al., 2008a; Herrero Hernandez et al., 2003; Rugless et al., 2014; Wasserman et al., 2006; Woolf et al., 2002).

Furthermore, various neurotransmitter systems may be impaired due to Mn overexposure as well, especially dopaminergic, but also cholinergic and GABAergic in the nigrostriatal pathway (Peres et al., 2016) (Sidoryk-Wegrzynowicz and Aschner, 2013). Several proteins have been identified to transport Mn, including divalent metal transporter-1 (DMT-1), SLC30A10, transferrin and ferroportin, which are highly expressed on glial cells (Bjorklund et al., 2018). Therefore, glial cells are the primary target of Mn in the brain, both for sequestration of the

metal, as well as for activating inflammatory signaling pathways that damage neurons through overproduction of numerous reactive oxygen and nitrogen species and inflammatory cytokines.

Exposure to Mn is well known to cause activation of microglia and astrocytes in affected brain regions. Clinically, Mn neurotoxicity is characterized by neuronal loss and reactive gliosis in the striatum, globus pallidus (GP) and substantia nigra pars reticulata (SNpr) (Yamada et al., 1986). These effects were also observed in the pre-frontal cortex of *Cynomolgus* macaques exposed to Mn, as well as the SNpc, where Mn exposure induces increased numbers of inflammatory microglia and astrocytes (Verina et al., 2011) (Guilarte et al., 2008b). Neuroimaging studies in South African mineworkers chronically exposed to low levels of Mn reported lower neuron densities in the striatum (ST) and increased numbers of microglia in the GP (Gonzalez-Cuyar et al., 2014). Also, our lab has reported extensively on the neurotoxic and neuroinflammatory effects of Mn in developing and adult mice, demonstrating that activation of microglia and astrocytes is critical to the detrimental effects of Mn on neurons and susceptibility to secondary environmental exposures and infections (Moreno et al., 2011a; Moreno et al., 2009a; Moreno et al., 2009c; Streifel et al., 2013; Streifel et al., 2012).

Additionally, exposing glial cultures to Mn results in the release of inflammatory factors such as TNFα, IL-1β, and IL-6; however, the exact mechanisms driving microglia and astrocytes activation after Mn exposure is not well understood but likely involves mitochondrial perturbations, increases in intracellular ROS, and activation of inflammatory signaling cascades. ROS production from Mn exposure can also damage neurons directly by increasing lipid peroxidation and mitochondrial dysfunction, causing subsequent energy failure, protein modifications, and DNA damage (Mosley et al., 2006). The formation of peroxynitrite is also thought to be a significant contributor to neurotoxicity through nitration of tyrosine and serine

residues of proteins (McCarthy et al., 2017; Moreno et al., 2008; Moreno et al., 2009b; Moreno et al., 2009c). Also, Mn potently affects glial signaling through P2Y and P2X purinergic ATP receptors, which may suggest pharmacological inhibition of NFκB could reduce neuroinflammation in glia and prevent neuronal loss following Mn induced neurotoxicity (Frank-Cannon et al., 2009; Streifel et al., 2014; Streifel et al., 2013).

Together, these previous studies demonstrate that glial activation promotes neurodegeneration of dopaminergic neurons through the production of reactive nitrogen, oxygen-free radicals, and inflammatory activation of glia following treatment with Mn. However, few studies have elucidated the potential loss of neurotrophic factors in Mn induced neurotoxicity. It is also still not clear how exposures to Mn might act in concert with other environmental and genetic risk factors of PD. Pesticides and gene mutations affecting mitochondrial function and glial inflammatory activation could very well increase toxicity to heavy metals such as Mn and increase one's risk of PD (Zhang et al., 2009). Furthermore, by examining specific glial-derived mechanisms in several genetic and toxin-based PD models, we may better understand the implications of neuroinflammation in PD and discover new targets for therapeutic intervention.

1.4. NEUROINFLAMMATION IN POSTENCEPHALITIC PD

Considerable evidence suggests that viral CNS infections can directly or indirectly influence the onset and progression of neurodegenerative diseases (Mattson, 2004; Sadasivan et al., 2017). Multiple investigators have suspected pathogenic microbes as etiological factors of neurodegeneration, and increasing evidence has suggested that proteins involved in neurodegeneration, such as: α-synuclein, ß-amyloid, tau, and prion protein, are antimicrobial peptides—mediating the neuroinflammatory response and reducing microbial load in the brain (Beatman et al., 2015; Chida et al., 2018; Eimer et al., 2018).

Following the 1918 “Spanish Flu” pandemic, nearly every patient who had an acute episode of encephalitis lethargica from influenza infection went on to develop postencephalitic parkinsonism (Dourmashkin, 1997; Reid et al., 2001). Additionally, many neurotropic mosquito-borne viruses, including the West Nile virus (WNV), Japanese encephalitis virus (JEV), and St. Louis encephalitis virus can cause PD-like symptoms in humans and rodents(Jang et al., 2009b). Older reports indicate that Western Equine Encephalitis Virus (WEEV), also a mosquito-borne virus, may be capable of causing parkinsonism in humans following encephalitic infection (Mulder et al., 1951; Palmer and Finley, 1956). Residual neurological defects can occur long after the WEEV infection has subsided and may include tremor, cognitive deterioration, and cogwheel rigidity. In a more recent report, 6 of 25 patients from a Colorado epidemic of WEEV presented with a ‘parkinsonian syndrome’ in the form of severe, progressive neurological sequelae(Schultz et al., 1977). Interestingly, antibodies against mosquito-borne viruses have been reported in patients with von Economo’s postencephalitic parkinsonism and idiopathic PD, suggesting a viral etiology in some instances.

Moreover, infection of rodents with H5N1 influenza A and WNV resulted in α-synuclein phosphorylation and aggregation (Elizan et al., 1978) (Clarke et al., 2014). Studies have also found an increase in antibody titers to HSV-1 in idiopathic PD patients and recent studies identified homologous cross-reactivity between HSV-I proteins and α-synuclein, where auto-antibodies against HSV-I peptide were cross-reactive with an α-synuclein epitope (Caggiu et al., 2019; Marttila et al., 1981; Olsen and Feany, 2019). This suggests that HSV-I induces an autoimmune response through molecular mimicry in PD.

Although microglia and astrocytes express endogenous pattern recognition receptors (PRRs) that respond to a variety of damage-associated molecular patterns (DAMPs) such as

viruses, few studies have experimentally tested the role of neuroinflammation in postencephalitic PD (Glass et al., 2010b). We have recently demonstrated that intranasal infection with WEEV induced selective loss of dopaminergic neurons in the SNpc, associated with persistent microgliosis, astrogliosis, and the development of proteinase resistant α-synuclein aggregates that spread into the cortex, hippocampus, and midbrain by 8 weeks post-intranasal infection (8WPI) in wild-type CD-1 mice (Bantle et al., 2019). Additionally, the majority of α-synuclein aggregates were located in and amongst dying neurons with surrounding phagocytotic microglia (Bantle et al., 2019). However, whether viral-mediated loss of dopaminergic neurons following acute infection with WEEV or other encephalitic infections is due in part to an increased neuroinflammatory response of microglia and astrocytes remains to be determined. Furthermore, the correlation between viral infection and PD is obvious, but the mechanisms underlying postencephalitic parkinsonism remain unclear (Caggiu et al., 2019). Along with our previous work, the mechanisms are thought to involve increased innate inflammatory signaling in glial cells, resulting in persistent neuroinflammation, but it is still elusive whether neurons benefit from activated microglia and astroglia due to the release of trophic factors or the clearance of damaged cells and insoluble protein aggregates following encephalitic infection. Therefore, in the next sections of this review, we discuss the role of neuroinflammatory activation of glia in postencephalitic PD with a keen focus on influenzas viral infections, mosquito borne-viral infection, and infection with HSV-1.

1.4.1. INFLUENZA

Influenza viruses can infect a wide variety of vertebrate hosts, ranging from birds and pigs to humans. Although influenza viruses are typically known to induce upper-respiratory-tract infections, infection with influenza viruses can also result in encephalitic infection in humans,

with neurological symptoms ranging from headaches to parkinsonism. This range of neurological symptoms manifests following infection with several influenza strains, including the pandemic 1918 H1N1 virus, the more recent A/California/04/2009 (CA/09) H1N1 outbreak, and the outbreak of avian influenza H5N1. The original association between viral exposures and PD stems from the influenza pandemic towards the end of the First World War (1914–1918), which was associated with a dramatic increase in Parkinsonism. This dramatic increase in post-encephalitic parkinsonism after the 1918 H1N1 pandemic is one of the few times in history that the number of cases of PD have increased so rapidly. Furthermore, animals infected by H5N1 viruses suffer an acute neurological sequala characterized by PD like neuromuscular dysfunction (Jang et al., 2012; Jang et al., 2009a). More recently, studies by Smeyne et al. demonstrated that intranasal inoculation of the neurotropic avian influenza virus H5N1 in C57BL/6J mice resulted in rapid propagation of H5N1 into the CNS with associated dopaminergic neuronal loss and α-synuclein phosphorylation and aggregation in the SNpc (Jang et al., 2012; Jang et al., 2009a).

Although the pathology of the influenza encephalitis has been well described, the mechanism of neuropathology is controversial, with some attributing it as a primary response to the physical presence of the virus within the CNS, while others believe that it occurs as a secondary adaptive immune response to systemic infection (Dale et al., 2004; Smeyne et al., 2016). Interestingly, peripheral inflammation resulting from infection with the non-neurotropic H1N1 influenza virus can result in a 'cytokine storm' leading to CNS inflammation and neurodegeneration in the SN as well, suggesting that an encephalitic infection is not needed to induce the neuropathology associated with influenza infections (Deleidi and Isacson, 2012).

Furthermore, infection with H1N1 and H5N1 results in significant gliosis with associated increased pro-inflammatory mediators including IL-6, TNF-α, elevated levels of cytochrome C,

a marker of mitochondrial injury, and ROS production (Fazekas et al., 2005; Sun et al., 2015; Yamamoto et al., 2002; Yamanaka et al., 2006). More specially, infection with H5N1 influenza virus induces chronic innate immune activation in glial cells which causes the degeneration of dopaminergic neurons in the SNpc(Jang et al., 2012; Jang et al., 2009a). Sustained activation of microglia and astrocytes after encephalitic infection has also been reported after H1N1 infections, which suggest that peripheral and encephalitic viruses can induce long lasting inflammatory activation of glia and contribute to protein aggregation and neurodegeneration in the CNS during aging (Sadasivan et al., 2012; Sadasivan et al., 2017).

Moreover, the sustained activation of microglia and astrocytes after infection with influenza may also suggest that H1N1 infections can increase susceptibility to secondary neurotoxic and neuroinflammatory insults. Recent studies have reported infection with H1N1 potentiates the neurotoxic effects of MPTP in a mouse model of PD in which the cumulative effects of exposure to MPTP after infection with H1N1 induced a more significant loss of dopaminergic neurons in the SNpc than either insult alone (Limphaibool et al., 2019; Sadasivan et al., 2017). Also, the synergistic increase in microgliosis and loss of dopaminergic neurons in the SNpc was eliminated through the use of influenza vaccinations or treatment with oseltamivir carboxylate (Sadasivan et al., 2017). This data suggests that people who are more susceptibles to infection and those without appropriate vaccinations or antiviral therapies may have a higher risk of developing PD and related neurological diseases later in life (Harris et al., 2012; Smeyne et al., 2016).

Collectively, these studies highlight the capacity of influenza viruses to initiate CNS proteinopathies and neurodegeneration in PD. Thus, chronic inflammation in the brain following influenza infections likely promotes α-synuclein aggregation and an increased likelihood of

developing early-onset PD. Interestingly, whether individuals with PD related genes variant are more susceptible to developing PD following influenza infections is unknown. Also, few studies have infected transgenic immunosuppressed mice to assess whether the parkinsonian symptoms are attenuated or exacerbated following infection with influenza. However, these previous findings suggest that inhibition of the glial immune response would likely mitigate the neuropathology following infections. Taken together, these studies show that a pandemic influenza pathogen, or other viral pandemics, could initiate CNS disorders of protein aggregation including Parkinson's and Alzheimer's diseases though inflammatory activation in the brain.

1.4.2. MOSQUITO-BORNE VIRUSES

A number of neurotropic mosquito-borne viruses, including the West Nile virus (WNV), Japanese encephalitis virus (JEV), St. Louis encephalitis, and most notably, Western Equine Encephalitis Virus (WEEV), induce many of the pathological features of PD such as protein aggregation, gliosis, mitochondrial dysfunction, and neuronal loss following encephalitic infection (Bantle et al., 2019; Beatman et al., 2015). Our lab has recently shown that CNS infection with WEEV in wildtype mice causes a pattern of neuronal injury, glial activation and protein aggregation that resembles pathological features of PD and related disorders, which could explain the diagnosis of post-encephalitic parkinsonism in humans infected with WEEV(Finley et al., 1955). Encephalitic infection with multiple neurotropic viruses such as coxsackie B4, Epstein-Barr virus, Japanese B encephalitis and HIV can induce broad viral dissemination and gliosis, degeneration of dopaminergic neurons in SNpc (Beatman et al., 2015; Berger and Arendt, 2000; Cree et al., 2003; Dimova et al., 2006; Hersh et al., 2001; Hsieh et al., 2002; Mattos et al., 2002; Murgod et al., 2001; Roselli et al., 2006)(Elizan and Casals, 1991; Ogata et al., 1997). We have recently demonstrated that infection with WEEV induces

expression of inflammatory cytokines and chemokines (MCP-1, IL-12, IFN-γ, and TNF-α) in brain and serum mimicking the profile observed in PD(Logue et al., 2010b) (Dobbs et al., 1999; Logue et al., 2010b; Mogi et al., 2007; Reale et al., 2009).

Furthermore, JEV and WNV are additional arboviruses that can induce parkinsonism following encephalitic infection (Beatman et al., 2015; Clarke et al., 2014; Grubaugh et al., 2016; Gullberg et al., 2015; Jang et al., 2009b; Jang et al., 2009c; Ogata et al., 1997; Yang et al., 2011). JEV and WNV induce a broad spectrum of movement disorders including hypokinesia, tremor, rigidity, and dystonia with associated Parkinsonian neuropathology, including protein aggregation, dopaminergic neurons, and gliosis. Previous work has shown a higher incidence of JEV infections among PD patients, and a JEV-induced PD rat models show decreased dopamine levels and neuropathological changes resembling those with idiopathic PD (Das et al., 2011; Hamaue et al., 2006). Moreover, WNV infected human patients consistently show an increased level of α-syn in brain tissue, and infection of α-synuclein KO mice with WNV causes a 10-fold increase in viral production, increased neuronal injury, and increased mortality (Beatman et al., 2015). This may suggest that α-synuclein plays an antimicrobial role in the brain by inhibiting viral replication (Limphaibool et al., 2019).

Glial activation is a common feature of viral encephalitis, with astrogliosis observed in the frontal and temporal white matter in cases of von Economo's disease and post-encephalitic PD (Silva da Costa et al., 2012),(Ronca et al., 2017),(Elizan and Casals, 1991). Following infection with WEEV, our lab noted persistent glial activation in the SNpc and ST that likely contributed to the increased neuronal loss in surviving host animals(Bantle et al., 2019). Neuronal injury from activation of microglia and astrocytes is consistently described in other

encephalitic models, such as experimental autoimmune encephalomyelitis (EAE), which causes significant astrogliosis and microgliosis and release of glial-derived neurotoxic and inflammatory molecules (Ludlow et al., 2016). However, whether the neuroinflammatory response is driving selective loss of dopaminergic neurons following encephalitic infection with WEEV and other arboviruses in the SNpc is unclear.

Although, arboviral RNA can persist in mouse brains 3-17 months after acute infection and may contribute to the persist inflammatory activation of glial after virus particles have cleared the CNS, it is possible that innate-immune responses in glial cells are primarily responsible for the reactive gliosis observed after infection with mosquito-borne viruses (Sperlagh and Illes, 2007). Recent work has shown that astrocytes and microglial can adopt a long-lasting neurotoxic and proinflammatory phenotype that may help to combat infection but may also worsen neuronal degeneration following infection (Hirsch and Hunot, 2009; Liddelow and Barres, 2017; Liddelow et al., 2017a; Wendeln et al., 2018). Whether encephalitic infections have the capacity to induce persistent phenotypic changes in glia is unclear, but our data along with other supports encephalitic infections inducing chronic activation of glia that facilitates early-onset PD during aging(Levine and Griffin, 1992). Additionally, recent work has shown that glial can mount innate immunological memory following inflammatory insults through epigenetic modulations, suggesting that encephalitic infection may induce lasting inflammatory changes in glia through histone and DNA acetylation and methylation (Wendeln et al., 2018).

In addition to the glial innate immune response in the CNS, a systemic inflammatory response may also contribute to the PD pathogenesis. PD patients have higher serum concentrations of TNF-α and IFN-γ. Importantly, WEEV infection was also shown to induce

higher concentrations of TNF-α and IFN-γ in serum of mice (Elizan et al., 1978; Finley et al., 1955; Hahn et al., 1988; Liu et al., 1970; Logue et al., 2009; Logue et al., 2010a; Logue et al., 2010b; Mossel et al., 2013a; Mossel et al., 2013b; Mulder et al., 1951; Netolitzky et al., 2000; Palmer and Finley, 1956; Phillips et al., 2016; Phillips et al., 2014; Phillips et al., 2013; Rico et al., 2016; Schultz et al., 1977). Because mitochondrial antiviral signaling protein (MAVS) pathways are initiated by activation of cytosolic dsRNA receptors such as retinoic acid-inducible gene 1 (RIG-1), perturbing mitochondrial dynamics through viral infection may also be relevant to the mechanism of neurodegeneration following encephalitic infections with arboviruses. WNV, JEV, and WEEV dsRNA, formed during viral replication, may therefore activate innate immune pathways in the CNS and contribute to the neuropathology following encephalitic infection.

Furthermore, mouse models of virally-induced parkinsonism typically have chronic microglial activation that parallels the spread of α-synuclein aggregation (Jang et al., 2009a; Jang et al., 2009b). Also, synucleinopathy and gliosis have been reported following infection with WNV, JEV, and influenza A (Elizan and Casals, 1991), (Jang et al., 2009a),(Bantle et al., 2019; Clarke et al., 2014). Glial activation is an important feature of encephalitic infections with all arboviruses, with astrogliosis observed in the frontal and temporal white matter in cases of von Economo's disease and postencephalitic PD, however, is still elusive whether glial cells play a protective role to clear and attenuate viral infection or if glia activation worsens the neuronal degeneration following infection (Elizan and Casals, 1991). The removal of damaged neurons by activated microglia is both a homeostatic mechanism but also likely related to broader inflammatory activation of glia that is neurotoxic, as is associated with the pathogenesis of PD

and related disorders (Duffy et al., 2018)[,](Neumann et al., 2009),(Joers et al., 2017),(Sanchez-Guajardo et al., 2013),(Skaper et al., 2018).

Moreover, the capacity of neuroinflammatory activation of glia to modulate the rate of α-synuclein spread over time is poorly understood. Some evidence suggests that α-synuclein aggregation represents a direct or indirect neuroprotective and antimicrobial response (Beatman et al., 2015; Eimer et al., 2018; Stolzenberg et al., 2017). Whether α-synuclein directly induces neuroprotection by restricting viral replication or indirectly regulates gene expression of anti-viral cytokines, chemokines, and neuroprotective signaling molecules in glia is unclear. Alpha-synuclein has also been noted in microglia and astrocytes following infection, and whether these inclusions spread through glia transmission is still unknown. The presence of α-synuclein in glia likely facilitates the clearance of protein inclusions from the CNS, as previously noted, but additional longitudinal studies are needed to confirm this finding (Rey et al., 2018)[,](Bruck et al., 2016).

In 2003, Braak and colleagues conducted a critical study which mapped the progressive spread of α-synuclein pathology in cases of sporadic PD (37), leading to a stage I–VI classification system of PD severity and progression. These findings have led to the hypothesis that α- synuclein pathology spreads in a progressive manner, beginning in the enteric nervous system and olfactory bulb, and may be the result from an unknown pathogen (Braak et al., 2013; Braak et al., 2003a; Braak et al., 2003b). Accordingly, our recent description of WEEV-induced parkinsonism demonstrates a pattern of viral infection that mimics the Braak staging system for mapping the progressive spread of α-synuclein pathology in PD (Braak et al., 2003a). Infection with WEEV results in loss of dopaminergic neurons within the SNpc, with viral-expressed proteins detectable in dopaminergic neurons of the olfactory bulb and substantia nigra and the

formation of α-synuclein pathology (Bantle et al., 2019) . Interestingly, theses parkinsonian symptoms manifest long after the virus has cleared from the brain, suggesting that dopaminergic neuronal loss may due to the subsequent host immune response or α-synuclein plaque formation after an encephalitic infection (Schultz et al., 1977). Similar parkinsonian symptoms have also been noted in over 50% of patients who survive encephalitic infection with WNV, long after WNV has cleared the brain (Vasek et al., 2016). Arboviruses can alter the expression of transcripts associated with interferon signaling and the unfolded protein responses, which may facilitate PD pathogenesis as well (Dobbs et al., 1999; Mogi et al., 2007; Reale et al., 2009). Also, arboviruses inhibit mitochondrial bioenergetics, thereby depressing cellular ATP content and inducing oxidative stress, which are associated with neuronal injury and glial activation in PD and related neurodegenerative disorders (Silva da Costa et al., 2012).

Together, arboviral infections seem to mimic the inflammatory and the spatiotemporal progression of idiopathic PD. Although idiopathic and postencephalitic PD pathology differ, understanding the mechanisms initiating neuronal loss and α-synuclein protein aggregation following infection with arboviruses may help to understand the underlying pathogenic mechanisms in PD. These data suggest that glia play a critical role in initiating PD-like pathology following encephalitic infection with WEEV, JEV, and WNV through innate inflammatory signaling that damages dopaminergic neurons, hinders clearance of α-synuclein aggregate, and modulates other homeostatic cellular processes. Neuroinflammatory activation of glial cells following encephalitic infection could therefore act in concert with neuronal oxidative stress and mitochondrial dysfunction to facilitate protein misfolding and loss of dopaminergic neurons.

1.4.3. HSV-1

The association of herpes simplex virus 1 (HSV-1) and neurodegeneration has been previously focused on AD and neuropsychiatric disorders due to its ability to modulate β-amyloid deposition, tau phosphorylation, and axonal demyelination in AD and multiple sclerosis (MS) (Kobayashi et al., 2013; Wozniak and Itzhaki, 2013). However, recent evidence is beginning to suggest that HSV-1 could also be involved in the initiation of parkinsonism (Limphaibool et al., 2019).

Previous work has shown that increased serological measurements of HSV-1 in PD serum correlates with increased inflammatory cytokine levels and worsened α-synuclein aggregation (Bu et al., 2015). Moreover, the association of HSV-1 and PD has primarily been focused on HSV-1 playing a role in triggering an autoimmune response in PD, leading to dopaminergic neuronal degeneration through adaptive immune mechanisms (Caggiu et al., 2016; Caggiu et al., 2017). Caggiu et al. have also suggested that HSV-1 viral proteins initiate autoimmune activation of α-synuclein protein after phagocytosis by microglia in the brain, through a process called molecular mimicry (Limphaibool et al., 2019). Additional studies have suggested an autoimmune mechanism in PD; however, the mechanism and significance in human idiopathic and hereditary PD are still unclear (Sulzer et al., 2017).

Although few studies have interrogated the role of glia in HSV-1 induced PD, one study has shown that following encephalitic infection with HSV-1, microglia control the synaptic spread of HSV-1 through the neuronal release of ATP and purinergic receptor activation. Interestingly, these studies highlighted that depletion of microglia increased the level of viral replication without worsened neuronal loss, suggesting that microglia could play a role in neuronal loss due to encephalitic infection with HSV-1 through inflammatory activation (Fekete

et al., 2018). Additionally, mounting adaptative immune responses to α-synuclein likely requires presentation on MHC-II molecules on professional antigen-presenting cells, such as microglia.

Future studies looking at KO α-synuclein murine and overexpression models may help to elucidate the connection between HSV-1 and α-synuclein. Additionally, future studies with pharmacological inhibition of T-cell maturation in PD relevant animal models will address whether T-cells are playing a role in dopaminergic neuronal loss following encephalitic infection with HSV-1. A better understanding of the underlying mechanisms of HSV-1 induced neurodegeneration may shed light on novel immunological mechanisms in PD and related neurological disorders.

1.5. NEUROINFLAMMATION AND THE TWO-HIT HYPOTHESIS OF PD

Parkinson's is the second most common movement disorder, and around 60,000 American's are diagnosed with PD each year. Identification of etiological factors is crucial to understanding the etiology of PD and related neurological diseases. Although many genetic mutations and environmental risk factors have been suggested as a cause or risk factors for PD, only one percent of people in the U.S. are currently suffering with PD. Similar to other complex multifactorial diseases, the vast majority of genetic mutants, environmental exposures and encephalitic infections do not manifest in clinical PD, which may suggest that multiple hits are required to manifest clinical PD.

Understanding why genetic mutations, environmental exposures and encephalitic infections induce neurodegeneration in select populations and not others is of great interest. Research is just beginning to interrogate the possible convergence between multiple PD related gene mutations, genetic and environmental interactions, environmental-environmental

interactions, and their respective roles in early-onset PD. Interestingly, only around 20% of LRRK2 carriers develop clinical PD by the age of 80, and twin studies have shown that a very low percentage of twins both exhibit PD (Clark et al., 2006; Wirdefeldt et al., 2004). However, recent genetic studies have shown that individuals with both GBA1 and LRRK2 mutations manifest clinical PD symptoms at a much higher frequency than individuals who carry LRRK2 or GBA1 mutation alone. Additionally, our research, along with collaborating groups, have demonstrated using a two-hit model of PD, that prior exposure to environmental neurotoxins can induce a worsened encephalitic infection and an increased neuroinflammatory response, consisting of microglia activation and more significant neuronal damage resulting from a secondary insult (Sadasivan et al., 2017). Moreover, other reports have shown that chronic inflammation within the CNS can sensitize neuronal tissue to secondary insults that would otherwise not induce significant neurological damage independently (de Pablos et al., 2014; Kanaan et al., 2008; Koprich et al., 2008; Pintado et al., 2012; Tansey, 2010).

Since PD generally manifests later in life, individuals with and without PD genetic risk factors will likely encounter several environmental insults, which alone may be innocuous but together may act in concert to produce early-onset PD. Therefore, neuroinflammation may be in a critical link that makes dopaminergic neurons of the substantia nigra particular targets of multiple genetic and environmental hits (Sulzer, 2007). Lack of this information hinders scientific and medical progress in understanding the pathogenesis of PD, as well as identification of key susceptible populations to neurological disease following exposures to environmental neurotoxins, including pesticides and encephalitic infections. The next sections discuss the role of glial activation in the two-hit hypothesis of PD.

1.5.1. GENE-GENE INTERACTIONS IN PD

Around 10% of PD cases are hereditary, while the other 90% are idiopathic and of any unknown etiology. PD has long been considered an idiopathic disorder, but the lack of geographic clusters with epidemiological studies go against environmental toxins as being the sole cause of PD (Pang et al., 2019). Over the last 20 years, genome-wide association studies GWAS studies have provided new genetic insights into the disease etiology and pathogenesis. However, one of the most puzzling questions in PD research remains as to why such a low percentage of PD gene mutants manifest clinically. Similar to other complex diseases, this suggests that multiple molecular pathways in a diversity of cell types are likely perturbed in PD.

Surprisingly, few studies have assessed the possibility of a two-hit genetic paradigm in animal and in vitro models of PD. A recent study in Ashkenazi Jewish (AJ) patients found a small population of individuals with LRRK2 and GBA gene mutations (Yahalom et al., 2019). Alone, both of the mutations have a low a penetrance and rarely manifest in clinical PD, but this study was able to show that individuals with mutations in both GBA1 and LRRK2 exhibit PD symptoms at an earlier age, suggesting a possible synergistic effect of the two variants in PD pathogenesis. Considering the possible role of GBA1 and LRRK2 in astrocytes and microglia, characterization of the neuroinflammatory response with PET-CT imaging and postmortem analysis in AJ patients will be of great interest. Previous studies have interrogated the possibility of DJ-1 gene mutations coupled with a PARKIN mutation, but they were unfortunately unable able to identify any PD patients with a DJ-1 and PARKIN mutation (Hedrich et al., 2004).

Furthermore, due the rare occurrence of PD patients with mutations in multiple PD related genes, few two-hit genetic studies have been conducted. Although, dual-mutations in PD patients are rare, future in vitro and in vivo studies interrogating the role of multiple PD

mutations will likely identity novel coalescing pathways in PD. Dual-mutations poses a unique paradigm and may help to identify converging therapeutic targets in PD and related diseases. There has been a particular interest in the role of LRRK2, GBA, and α-synuclein mutations in dopaminergic neurons. However, due to previous convincing evidence of LRRK2, GBA, and α-synuclein mutations playing a role in glia, we hope to inspire others to assess the role of glial cell activation in future dual-mutations studies.

1.5.2. GENE-ENVIRONMENT INTERACTIONS IN PD

In most PD cases, disease onset is probably triggered by a complex interplay of many genetic and environmental factors, each of which conveys a minor increase in the risk of disease. However, due to the low penetrance of PD gene variants, it has been postulated that genetic variation in PD risk factors might depend on the co-occurrence of environmental exposures, but convincing evidence is still lacking. Recently, there has been particular interest whether mutations in LRRK2, α-synuclein and GBA mutations renders increased sensitivity to environmentally toxicant and glial activation. Given the vast distribution of LRRK2, α-synuclein and GBA in immune cell and non-neuronal cells types, it is likely that environmental and genetic factors modify PD initiation and progression (Zanon et al., 2018). Both sporadic and familial PD patients, clinically present with increased cytokines level in the brain and CSF, extensive astrocyte and microglial activation, and infiltration of peripheral immune cells into the brain (Kozina et al., 2018). Among the genes implicated in both PD and its inflammatory processes, LRRK2 has received considerable attention (Rudyk et al., 2019). Inflammatory agents, such as LPS, as well as chemical toxicants like MPTP and rotenone, have been shown to influence LRRK2 expression in glia, suggesting that LRRK2 may be a critical general mediator of inflammatory pathology associated with multiple environmental insults (Rudyk et al., 2019).

Previous work has also shown that chronic administration of the LPS induces significant loss of nigral DA neurons in Parkin KO mice but not wild-type mice even though both groups of mice showed similar increases in markers of neuroinflammation compared to control mice treated with saline (Frank-Cannon et al., 2009).

Accordingly, recent studies suggest that LRRK2, which is highly expressed in microglia and astrocytes, may also play a role in Mn-triggered neuroinflammation and neurotoxicity (Chen et al., 2018). Mn exposure may induce LRRK2 expression in glia with associated dopaminergic neuronal damage, and inhibition of LRRK2 decreases the expression of glia-derived inflammatory cytokines (Chen et al., 2018). Moreover, several studies implicate LRRK2 expression in peripheral macrophages and suggest that LRRK2 may play a role in restricting enteric pathogens, and LRRK2 knockout mice show increased susceptibility to systemic infections (Gardet et al., 2010; Herbst and Gutierrez, 2019). Also, α-synuclein is recognized on glial cells by TLR-2 and 4, and LRRK2 localizes to the membrane to regulate TLR 2 and 4 expression. This may suggest that LRRK2 can indirectly modulate inflammatory activation of α-synuclein on glial cells (Kim et al., 2019; Schapansky et al., 2014). Moreover, LRRK2 knockout rats are protected from neurodegeneration induced by α-synuclein overexpression and intra-nigral LPS exposure, suggesting that inhibition of LRRK2 might have a neuroprotective effect in PD (Daher et al., 2014). Previous studies have also shown that LRRK2 can regulate the NLRP3 inflammasome as well as the proinflammatory transcription factors nuclear factor of activated T-cells (NFAT) and nuclear factor kappa-light-chain-enhancer of activated B cells (NF-κB) in glia (Herbst and Gutierrez, 2019). Interestingly, LRRK2 can also regulate the secretion of the anti-inflammatory cytokine, IL-10, in macrophages after infection with *M. tuberculosis (Hartlova et al., 2018; Herbst and Gutierrez, 2019)*

Taken together, it continues to be mutually agreed upon that the majority of PD cases are likely due to different combinations of environmental exposures and genetic susceptibility. A clear understanding of mechanisms common between genetic and environmental factors is essential for early detection and successful translation of potential therapies. Although the majority of previous genetic-environmental interactions studies have been focused on the LRRK2, these data clearly support the idea that LRRK2 contributes to cytokine-mediated inflammatory responses. Given the low penetrance of LRRK2 and related PD mutations, it is likely that inflammatory stressors may be required to initiation and promote PD pathology. Thus, LRRK2 and related mutations may act as the first hit by a modulating and exacerbating neuroinflammatory activation of glia following subsequent environmental exposures during aging. Therefore, aging, genetics and environmental factors each alone may rarely be sufficient to cause PD for most patientsl; however, when these factors act in unison, they likely induce a measurable pathology (Pang et al., 2019).

1.5.3. ENVIRONMENTAL-ENVIRONMENTAL INTERACTIONS IN PD

The hypothesis of an infectious etiology in PD stems from clinical observations of a parkinsonian sequala in individuals infected with the influenza virus who later developed encephalitis lethargica (Limphaibool et al., 2019). These observations then motivated the two-hit hypothesis concerning the pathogenesis of idiopathic PD by Hawkes et al. The original two-hypothesis of PD describes a neurotropic pathogen which enters the nervous system through the olfactory pathway and enteric plexuses and preganglionic vagal fibers, ultimately leading to a cascade of neurodegenerative events in the substantia nigra pars compacta (SNpc) (Hawkes et al., 2007; Limphaibool et al., 2019). While some individuals have hypothesized that misfolded α-synuclein may act as a neurotropic pathogen in this two-hit hypothesis, the exact neurotropic

pathogen remains elusive. Moreover, whether a concurrent exposure must occur in the enteric plexus and olfactory system to induce PD is unclear. Interestingly, our lab has recently shown that intranasal infection with a mosquito-borne virus in wild-type mice accelerated neurodegeneration and α-synuclein protein aggregation, without any peripheral infection or enteric propagation of virus (Bantle et al., 2019). However, similar to the low penetrance of genetic mutations in PD, it remains unclear why encephalitic infections and environmental exposures induce neurodegeneration in select populations and not others.

Research has recently demonstrated using a two-hit model of PD, that prior exposure to environmental risk factors of PD can induce a worsened neuroinflammatory response to subsequent neurotoxins and encephalitic infections, consisting of microglia and astrocyte activation and greater neuronal damage resulting from a secondary insult (Sadasivan et al., 2017). Importantly, neuroinflammatory glial activation precedes protein aggregation and dopaminergic loss in rodent models of PD, and previous studies have shown that persistent glial activation can sensitize neuronal tissue to a secondary insults that would otherwise cause minimal neural injury (de Pablos et al., 2014; Duffy et al., 2018; Kanaan et al., 2008; Koprich et al., 2008; Pintado et al., 2012; Sadasivan et al., 2017; Tansey, 2010). Sadasvian et al. have recently shown that viral exposure to H1N1 can potentiate glial activation and dopaminergic loss following exposure to MPTP in adult mice, and that loss of dopaminergic neurons is eliminated through the use of influenza vaccinations or treatment with oseltamivir carboxylate with associated reduction of microgliosis (Sadasivan et al., 2017). Accordingly, our lab has previously reported using a two-hit environmental model of PD that mice exposed to Mn orally from weaning through puberty were more sensitive to Mn when re-exposed as adults (Moreno et al., 2009a; Moreno et al., 2009c). We were also able to demonstrate that Mn exposure during

juvenile development increases reactive gliosis and neuronal damage in the basal ganglia following exposure to the neurotoxin MPTP (Kirkley et al., 2019a; Kirkley et al., 2019b; Kirkley et al., 2017b; Miller et al., 2014).

Furthermore, considering that neuroinflammation is a central feature of aging as well, mouse studies have shown that susceptibility to MPTP increases with age (Jackson-Lewis and Przedborski, 2007). Viral infections, environmental exposures, and aging seem to perturb mitochondrial bioenergetics in neuronal and glial cells (Silva da Costa et al., 2012). Whether these mitochondrial perturbations induce neurotoxicity through a cell-autonomous neuronal loss or from mitochondrial stress signals and subsequent neuroinflammation in glia is unclear. However, these previous data provide evidence that neuroinflammatory activation of glial cells is critical to the initiation and progression of PD-like pathology following encephalitic infection and neurotoxic insults, shedding light on neuroinflammatory activation of glia as a target for disease intervention in PD and related neurodegenerative diseases. Prior neurotoxic and encephalitic insults may cause lasting neurological deficits through a severe neuroinflammatory response promoting both neuronal injury and protein aggregation in surviving individuals. Recent studies have built upon this ideas revealing that Mn can exacerbate the effects of LPS by increasing the cytokine productions of both microglia and astrocytes that causes dramatic potentiation in production of TNFα, IL-1β, ROS, and NOS2 expression in the SNpc (Barhoumi et al., 2004; Moreno et al., 2011a). In addition, increased levels of these inflammatory factors have also been measured in both rodent and nonhuman primate models of PD, and genetic deletion and pharmacological inhibition of these pathways induces neuroprotection (Streifel et al., 2012; Verina et al., 2011; Zhang et al., 2009; Zhao et al., 2009). Importantly, production of inflammatory mediators in activated glia is highly regulated by innate immune signaling

pathways converging on NF-κB, and may, therefore, be an essential target for modulating the host-immune response for therapeutic intervention in PD (Glass et al., 2010a).

Together, it is becoming clear that neuroinflammation is a central feature of sporadic and postencephalitic PD, with characteristic inflammatory activation of astrocytes and microglia(Moreno et al., 2009c; Perl and Olanow, 2007; Streifel et al., 2012; Verina et al., 2011). These studies have highlighted how microglial and astrocyte activation is a critical initiation step in the development of PD, further emphasizing how neuroinflammatory glial activation likely plays a significant role in the development and progression of PD pathology. Thus, glial activation may exacerbate neurodegeneration, particularly in dopaminergic neurons in two-hit exposure models of PD. Early-life exposures to environmental risk factors may act in concert with subsequent environmental risk factors later in life, causing a more severe neuroinflammatory response, increased protein aggregation and the development of neurodegeneration after a secondary insults. The capacity of environmental toxins to sensitize neural tissue to additional damage from a subsequent toxic insult likely involve persistent inflammatory changes in glial cells. However, few studies have fully assessed this in two-hit PD models, and the current lack of this information hinders scientific and medical progress in understanding the pathogenesis of neurological dysfunction in PD (Brown et al., 2006).Previous findings of synergistic effects from multiple insults supports the two-hit hypothesis of PD, where the combination of toxic and microbial inflammatory stressors lead to spontaneous dopaminergic neuronal death in the SNpc (Limphaibool et al., 2019). Since PD generally manifests during the late years of life, this suggests that any person will encounter any number of environmental insults, which alone may be harmless but together may synergize to produce a measurable PD pathology (Sadasivan et al., 2017).

CHAPTER 2

INFECTION WITH MOSQUITO-BORNE ALPHAVIRUS INDUCES SELECTIVE LOSS OF DOPAMINERGIC NEURONS, NEUROINFLAMMATION AND WIDESPREAD PROTEIN AGGREGATION

2.1 INTRODUCTION

Parkinson's disease (PD) is characterized by loss of voluntary motor control due to the degeneration of dopaminergic neurons of the substantia nigra pars compacta (SNpc), associated with oxidative stress, glial cell activation and α-synuclein protein aggregation. Therapies for PD are limited by an insufficient understanding of both the etiological factors and the pathological mechanisms influencing disease progression. The etiology of PD remains elusive but it is likely linked to interactions between genetic risk-factors, age and environmental stressors, including infectious agents (De Chiara et al., 2012). Viruses, in particular, have been linked to PD and there have been several reports of parkinsonism observed among human survivors of encephalitic viral infection (Jang et al., 2009a). Exposure of the human central nervous system (CNS) to selected viruses have been shown to induce a phenotype that mimics the neuropathology and neurological dysfunction observed in cases of sporadic PD, and increasing evidence implicates viral infection of the CNS as a potentiating factor in multiple neurodegenerative diseases (Eimer et al., 2018; Limongi and Baldelli, 2016; Mattson, 2004). For example, following the 1918 "Spanish Flu" pandemic, nearly every patient who had an acute episode of encephalitis lethargica went on to develop post-encephalitic parkinsonism, a condition with neurological symptoms that closely resemble PD (Jang et al., 2009a),(Dourmashkin, 1997;

Henry et al., 2010a; Reid et al., 2001). Additionally, many neurotropic mosquito-borne viruses, including the West Nile virus (WNV), Japanese encephalitis virus (JEV) and St. Louis encephalitis virus have been shown to induce PD-like symptoms in humans and rodents(Phillips et al., 2016). Recent evidence has suggested that over 50% of patients who survive neuroinvasion with WNV exhibit a neurodegenerative phenotype later in life (Vasek et al., 2016).

Older reports indicate that western equine encephalitis virus (WEEV), another mosquito-borne alphavirus, may be capable of inducing parkinsonism in humans following encephalitic infection and in a more recent report, 6 of 25 patients from a Colorado epidemic of WEEV presented with a "parkinsonian syndrome" with severe, progressive neurological sequelae(Levine and Griffin, 1992; Zhou et al., 2009)·(Schultz et al., 1977). These symptoms included resting tremor, intellectual deterioration and cogwheel rigidity(Schultz et al., 1977), which persist long after resolution of acute infection with WEEV. This may be due to the chronic presence of viral RNA, because alphavirus RNA can persist in mouse brain 3-17 months after acute infection and could therefore induce a sustained neuroinflammatory reaction (Levine and Griffin, 1992). Alphaviruses alter expression of transcripts associated with interferon signaling and unfolded protein responses, and we have previously shown that infection with WEEV induces expression of inflammatory cytokines and chemokines in mouse brain and serum, including MCP-1, IL-12, IFN-γ and TNF-α, that are also associated with PD (Dobbs et al., 1999; Mogi et al., 2007; Reale et al., 2009). Furthermore, alphaviruses inhibit mitochondrial bioenergetics, thereby depressing cellular ATP content and inducing oxidative stress, which are associated with neuronal injury in PD and related neurodegenerative disorders (Silva da Costa et al., 2012). Although these studies suggest that a single encephalitic infection with WEEV can

induce post-encephalitic parkinsonism in the surviving host, the pathogenic mechanisms remain unclear.

To identify mechanisms by which WEEV and related neurotropic alphaviruses cause such persistent neurological deficits following encephalitic infection, we examined the capacity of WEEV to induce progressive neurodegeneration after a single intranasal inoculation in CD-1 mice. We postulated that encephalitic infection WEEV would trigger neuroinflammatory activation of microglia and astrocytes that contributed to neuronal injury and neurobehavioral abnormalities. We demonstrate that intranasal inoculation with recombinant WEEV expressing firefly luciferase ("McFly") induced a consistent and broad encephalitic infection in outbred CD-1 mice and caused robust glial activation and selective loss of dopaminergic neurons in the SNpc. Morbidity and mortality by intranasal infection ocurred within four days but could be attenuated by passive immunotherapy using polyclonal antibodies to the ectodomain of the WEEV E1 glycoprotein to control the extent of infection (Braak et al., 2003a; Braak et al., 2003c). Surviving mice completely cleared the infection by eight weeks and were examined for pathological features associated with neurodegeneration in multiple brain regions, including cortex, hippocampus and the basal midbrain. Following inoculation with McFly and immunotherapy, surviving mice displayed selective loss of dopaminergic neurons in the substantia nigra, as well as behavioral abnormalities and persistent activation of glial cells. In addition, we detected the formation of proteinase K-resistant α-synuclein protein aggregates and a gene expression profile consistent with a progressive neurodegenerative phenotype. In summary, these data indicate that CNS infection with WEEV in wildtype mice causes a pattern of neuronal injury, glial activation and protein aggregation that resembles pathological features

of PD and related disorders, which could explain the diagnosis of post-encephalitic parkinsonism in individuals actually infected with WEEV and similar alphaviruses.

2.2 MATERIALS AND METHODS

Viruses

A full-length infectious clone of the WEEV McMillan strain was derived from an isolate obtained from the Arbovirus Reference Collection at the Center for Disease Control and Prevention in Fort Collins, CO, USA, as previously described (Logue et al., 2009). Detailed descriptions of the molecular cloning methods used to construct recombinant WEEV reporter viruses have been previously reported (Phillips et al., 2016; Phillips et al., 2013). In brief, duplication of the subgenomic promoter (SGP) sequence (nucleotides 7341–7500 of viral genome) of WEEV McMillan strain was used to express of firefly luciferase. The resulting virus we termed "McFly". A separate recombinant WEEV was generated that expressed the fluorescent protein, DsRed, and referred to here as "McRed" virus. The McFly and the McRed plasmids were purified by QIAprep Spin MiniPrep Kit (Qiagen, Valencia, CA USA) and genomic RNA was transcribed *in vitro* using a T7 RNA polymerase (MAXIscript™ kit, Life Technologies, Grand Island, NY USA). BHK-21cells (2×10^7 in 400 µL) were transfected with 20 µL of genomic RNA using an ECM 630 electroporator (BTX Harvard Apparatus, Holliston, MA USA). Two pulses of 450 V, 1200 Ω and 150 µF were administered. The rescued virus was passaged once in BHK-21 cells, collected at 48 hours post-infection (HPI) and stored at −80°C. Stock viruses were quantified using plaque titration in Vero cells before experimental use. Virus titrations were performed in duplicate and plaque assays were performed as described by Liu and colleagues (Liu et al., 1970).

Mouse Infections and In Vivo Imaging

Mouse infections and imaging analysis were adapted from previous studies(Phillips et al., 2016). In brief, all animal protocols used in the current study were approved by the Animal Care and Use Committee at Colorado State University (Permit #11-2605A), and mice were handled in compliance with the PHS Policy and Guide for the Care and Use of Laboratory Animals. All infections were conducted in certified biosafety level 3 (BSL-3) facilities at the Infectious Disease Research Center at Colorado State University in compliance with NIH guidelines under an approved IACUC protocol and were supervised by institutional veterinary staff. Male and Female (6-week-old) CD-1 mice (Charles River Labs, Wilmington, MA USA) were used in this study. Mice were anesthetized with isoflurane (Minrad Inc, Bethlehem, PA USA) through an XGI-8 anesthesia system (Caliper Life Sciences, Waltham, MA USA) connected to the IVIS 200 (Caliper Life Sciences, Waltham, MA USA) imaging camera imaging system. Intranasal infection was conducted at a dose of 1×10^4 PFU in a volume of 20 µL, delivered drop-wise onto the nostrils of lightly anesthetized mice. Mice then received subcutaneous administrations of luciferin substrate (150 mg/kg) to the dorsal cervical spine at 10–15 minutes before imaging. Exposure time was consistent for all animals. Living Image 3.0 software (Caliper Life Sciences, Waltham, MA USA) was used to analyze and process images taken using the IVIS 200 camera. Uninfected mice were used as an imaging control to adjust for background signal, and BLM threshold was established using negative imaging controls at 5×10^3 p/s/cm^2/sr. A standard region of interest was created to measure total light emission for each mouse. Sagittal head images were created by injecting mice subcutaneously with two doses of (150 mg/kg) 10 min apart prior to euthanasia. Animals were then decapitated under isofluorance anesthesia and whole-heads bisected along the medial-sagittal plane, rinsed with PBS and promptly imaged.

CLARITY method of tissue-transmutation and immunostaining

Briefly, brain tissue was processed for CLARITY imaging by incubating formalin-fixed tissue in a solution of acrylamide monomers and a temperature-activated cross-linker for three days (Chung et al., 2013). Tissue was then heated to 40°C, resulting in the formation of a tissue-hydrogel hybrid. Clearing occurs through the gradual removal of endogenous lipid(s) over several days, using multiple changes of sodium dodecasulfate (SDS). Upon completion of the clearing process, the brains were washed three times in 1X TBS, each wash lasting two days. The resultant 'clarified' brain tissue was then amenable to 3D imaging using confocal microscopy. Lipid-cleared tissue-hydrogel was sectioned (coronal or sagittal) and treated with primary antibody (anti-TH 1:200) and incubated for two days at 4°C. Primary antibody was washed with Tris-buffered saline for two days at room temperature, changing the wash buffer three times over the two days. The secondary antibody (anti-rabbit AlexaFluor 488, 1:2000 dilution) was incubated for two days at room temperature. Sections were washed with Tris-buffered saline for two days at room temperature, changing the wash buffer three times over the two days. Slides were counterstained with Hoechst (1:2000) to identify all nuclei. Sections were then washed for 30 minutes and then mounted with a coverslip using 80% glycerol in TBS.

3D-reconstruction of the mouse brain from caudal olfactory to rostral cerebellum

CD-1 mice were infected by intranasal or footpad route with 10^4 PFU WEEV. At first sign of neurological disease, mice were euthanized and processed using the CLARITY method, as described above. Tissue-sections were counterstained with DAPI (1:2000), washed for 30 minutes, mounted using 80% glycerol in tris-buffered saline (TBS), and imaged. The full section montage images resulting from CLARITY imaging were deconvoluted and processed to obtain 3D reconstructions using Imaris software (Bitplane AG, Zurich, Switzerland). Due to the technical constraints of imaging such large volumes of tissue, our imaging was limited to the

region from the caudal olfactory to the rostral cerebellum, the regions most relevant to parkinsonism (Braak et al., 2003a).

Tissue preparation and Immunofluorescent staining

Tissue processing and immunofluorescent staining for dopamine neurons, glial cells and phosphorylated α-synuclein (p129) was performed as reported previously(De Miranda et al., 2013; Hammond et al., 2018; Jang et al., 2009a). In brief, animals were terminally anesthetized with isoflurane and transcardially perfused. After perfusion fixation, the brains were carefully removed from the skull and immersed in the same fixative at 4°C for 3 hours. The brains were then equilibrated in cacodylate-PBS containing 15% sucrose overnight, followed by 30% sucrose. The tissue was then embedded and sectioned at 40 microns on a cryostat microtome producing a mean of 60 sections through the anatomic SN nucleus. Sections were stored at –20°C, free-floating in cryoprotectant (30% w/v sucrose, 30% v/v ethylene glycol; 0.5 M phosphate buffer; pH 7.2) until staining. Free-floating serial sections were washed in PBS and mounted on glass slides for staining followed by antigen-retrieval with 0.01 M sodium citrate buffer (pH 8.45) for 20 min before blocking. All primary antibodies were diluted to their optimized dilutions in 0.1% triton-X containing phosphate buffered saline (PBS): rabbit tyrosine hydroxylase (TH; Millipore; 1:500), mouse Neuronal Nuclei (NeuN; Millipore; 1:250), chicken microtubule-associated protein 2 (MAP2; Abcam 1:100), rabbit glial fibrillary acid protein (GFAP; Dako, 1:500), rabbit Ionized calcium binding adaptor molecule 1 (Iba1; Wako; 1:250), goat ionized calcium binding adaptor molecule 1 (Iba1; Abcam; 1:50), and mouse anti-alpha-synuclein (P129, Wako, 1:100). Sections were stained for DAPI (Sigma) and mounted on glass coverslips in VectaShield mounting medium and stored at 4°C until imaging.

Cell Counting of Neurons and Glia in the Midbrain, Hippocampus and Cortical Brain Regions

Methodologies for imaging and counting of dopamine neurons and glial cells in the SN and nerve terminal in the striatum were adapted from those previously reported (Tapias et al., 2013). Every sixth tissue section was selected and counted, for a total of eight sections per animal for dopaminergic cells and a total of two sections per animal for glia. The studies described here were all performed blinded by a single investigator. Images were captured using an automated Olympus BX51 fluorescence microscope equipped with a Hamamatsu ORCA-flash 4.0 LT CCD camera and collected using Olympus Cellsens software (v 1.15). Quantitative analysis was performed on dual- or triple-labeled fluorescent images generated by montage imaging of an entire coronal brain section compiled from individual images acquired using an Olympus PlanApochromat 10X air objective (0.40 N.A.). One hemisphere of the SN was delineated as an active ROI on the basis of TH immunolabeling and with reference to a coronal atlas of the mouse brain (Allen Brain Atlas). All slides were scanned under the same conditions for magnification, exposure time, lamp intensity and camera gain.

For quantitative assessments, TH+, NeuN+, IBA1+ and GFAP+ soma from the selected ROIs were automatically detected using the CellSens dimension platform. Area of soma, mean intensity values and shape factor threshold-based based quantification filters were manually adjusted to acquire accurate TH+, NeuN+, IBA1+ and GFAP+ cell body counts. Once all eight sections of a single brain were counted for neurons, the total number of TH+ and NeuN+ neurons counted were multiplied by the reciprocal of the volume fraction (18), which is mathematically

derived from three variables; area sampling fraction (1), the height sampling fraction (30 μm/40 μm), and the section sampling fraction (1/6). Mathematical derivations for neuronal counts were adapted from previously cited methods (Tapias et al., 2013). Two sections of each brain were counted for glia and the total number of IBA1+ and GFAP+ glia for each section were divided by the area of the ROI (mm^2) to normalize across all brains. Representative montage images were generated for each treatment group with use of a 10X air PlanApochromat objective (0.40 N.A.). Anatomic landmarks were used to select striatal sections for tyrosine hydroxylase intensity staining in an identical process as we previously reported(Miller et al., 2011), staining all treatment groups simultaneously. Montage images of the striatum were created using a 10X objective and a mask generated to outline the striatum with use of Slidebook software, and mean fluorescence intensity in relative florescence units was obtained. Representative montage images were generated for each treatment group with use of a 10X objective and were displayed using inverted monochrome.

To determine hippocampal and entorhinal cortex total neuronal densities, brains from McRed infected and age-matched CD-1 control mice were serially sectioned at 10 μm. Sections were quantified as previously preformed(Gingras et al., 2015). In brief, 10 μm sections of brain were stained with Cresyl violet to identify Nissl-positive cells. At least 2 sections from the rostral hippocampus containing a fully intact CA1 region (Paxinos and Franklin Bregma -1.70—2.18) as well as entorhinal cortex (Bregma -3.52- -4.04) were identified. For hippocampal densities, the CA1 region medial to the faciola cinereum to CA2 was outlined at 4x using the Neurolucida Neuron Tracing Program. Once the CA1 was outlined, the area of CA1 was empirically determined based on the Neurolucida calibration tool. To determine the cell number, all pyramidal neurons in CA1 were counted at 40x. The number of cells within CA1 were then

divided by area to determine cells/μm^2. At least 2 sections/rostral hippocampus were counted in each brain and an average of these densities was determined. A similar method was used to determine the cellular density of the entorhinal cortex.

Generation of anti-alphavirus E1 immune-serum

For preparation of E1 serum, rabbits were vaccinated with recombinant WEEV McMillan strain E1-ectodomain antigen (10 µg antigen/dose), polyI:C (dsRNA analog) and ODN 1826 (unmethylated CpG DNA) (InVivoGen) to a final concentration of 0.1 mg/mL each, in TiterMax Gold adjuvant (Sigma, St. Louis, MO). Each element was added to the aqueous medium before emulsion with TiterMax Gold prior to injection. This priming dose was followed by an identical boost vaccination, every two weeks, until a total of four doses were administered. Nine weeks following the last boost dose, rabbits were terminated and serum was collected, heat inactivated at 56°C for 30 minutes and stored at -80°C. Naïve serum was collected from control animals. An aliquot of immune serum was tested for titer against E1 antigen-coated titration plates and found to have an antibody titer measurement greater than 26,000 reciprocal value, the cut-off for the assay.

Mouse gait analysis

Mouse gait analysis was performed as previously published (Hammond et al., 2018). Two weeks before initial behavioral testing, all mice were acclimated to the gait analysis equipment and baseline gait measurements were taken. Gait measurements of step size, rate and paw intensity were detected using a custom made real-time video gait analysis system. Video recordings of unrestricted movement down a 1 m glass trackway were conducted measure gait parameters, including stride length, as previously reported (Hammond et al., 2018). All gait testing was performed 8 weeks after inoculation in mock-infected control mice and in mice

infected with WEEV. Values for each parameter were subtracted from initial values at day 0 to obtain measurements representing the change from baseline and all metric were compared back to control/mock-infected mice.

Proteinase K Digestion of frozen tissue sections

For the detection of α-synuclein aggregation in WEEV challenged mice in intact brain sections, free-floating brain sections from infected and non-infected mice were mounted on charged glass slides and probed for phosphorylated α-synuclein (PhosphoSer129/p129) following digestion with proteinase K. Sections were then washed 3 x 5 min with TBS and allowed to adhere onto charged slides for 15 minutes. Sections were then subjected to antigen retrieval by incubating in 0.01M sodium citrate buffer (pH 8.45) for 20 minutes. Proteinase K (pK) (Roche 03-115-887-001) was added to each section at a concentration of 100µg/mL for 30 minutes at 55°C. Sections were again washed 3 x 5 min with TBS and then blocked with either 1% donkey serum or a combination of 1% donkey serum and 1% goat serum. Primary antibodies diluted in 0.1% Triton-X containing TBS are as follows: Rabbit polyclonal anti-tyrosine hydroxylase (1:500; Millipore Cat# AB152), mouse monoclonal anti-p129 (1:100; Wako Cat# 015-25191), and goat polyclonal anti-IBA1 (1:50; Abcam ab5076). Primary antibody was incubated on the sections for 24 hours in 4°C. Secondary antibodies utilized were diluted in TBS along with 1% donkey serum and are as follows: Donkey anti-rabbit Alexa488 (1:500; ThermoFisher A21206), donkey anti-mouse Alexa555 (1:500; ThermoFisher A31570), and donkey anti-goat Alexa647 (1:500; ThermoFisher A21447). Sections were counterstained with DAPI (1:2000) and mounted on glass coverslips in VectaShield mounting medium and stored at 4°C until imaging.

Transcriptional analysis of whole-brain homogenates

Dissected whole brains (*n*=3/group) was homogenized and solubilized using TRIzol® Reagent (Thermo Fisher Scientific) and RNA purified per manufacturer's instructions. The purified total RNA was converted to cDNA using the RT^2 first strand kit (SABiosciences) and analyzed using the following SABiosciences (Qiagen) qPCR arrays: 1) PAMM-098Z Mouse mTOR Signaling PCR Array, 2) PAMM-212Z Mouse Cell Death Pathway Finder PCR Array and 3) PAMM-124Z Mouse Parkinson's Disease PCR Array. All arrays were read using a BioRad iQ5 real-time PCR detection system. The same amount of cDNA was applied to each array for 1) uninfected control animals, 2) infected animals or 3) infected and immunotherapy-treated animals. Gene expression data was normalized to the internal control genes, Beta-2 microglobulin and Glyceraldehyde-3-phosphate dehydrogenase across all arrays for each experimental condition based on the criteria of minimal Ct variance, as reflected by lowest standard deviation, and highest normality of distribution (22). Normality of distribution was determined using JMP Version 8 (SAS Institute) statistical software.

2.3 RESULTS

Infection with recombinant WEEV causes significant neuroinvasion and rapid dissemination from the olfactory bulb throughout the brain.

Recombinant WEEV vectors, McFly and McRed, (Fig. 1A) were constructed to express reporter proteins as markers of infection (firefly luciferase and DsRed), using a duplication of the subgenomic promoter sequence. We have previously imaged the entry and spread of alphavirus into the CNS resulting from intranasal and peripheral infection (Phillips et al., 2016)·(Phillips et al., 2014; Phillips et al., 2013). Although both routes of inoculation lead to mid-brain infection,

we used the intranasal route of infection in the current study due to its efficiency in establishing CNS infection. In a preliminary comparison of different WEEV viral strains, medium-virulence (Montana-64) and high-virulence (McMillan) strains of WEEV, we found that the high-virulence strain resulted in significant loss of dopamine neurons in the SNpc within four days of infection (Figure 7). This strain was therefore used as the basis for constructing McFly and McRed vectors.

To identify the extent and spread of WEEV throughout the neuraxis, six-week-old CD-1 mice were intranasally inoculated with McFly at a concentration of 1×10^4 PFU. Luciferase activity was measured in live, intact animals each day for the duration of the infection (Fig. 1C, 1D). Mice were scored by a clinical scoring system in 12-hour increments to assess the severity of the infection on neurobehavioral function. Healthy mice received a score of zero, mice with ruffled received a score of one, mice with slight lethargy, hunched posture and obvious irritable received a score of two, very irritable mice with obvious motor deficits received a score of three, and moribund mice received a score of four. All mice challenged with McFly showed robust luciferase activity and apparent neurobehavioral and motor deficits by 24 hours post-infection, ranging from slight lethargy and hunched posture to severe hypokinesia and ataxia. Without immunotherapy, mice were unable to survive more than 96 hours because of the severity of the encephalitic infection (Fig. 1B, 1C, 1D).

To further characterize the distribution of McFly following intranasal infection, a second cohort of mice was infected and sectioned along the sagittal axis for *ex vivo* imaging. McFly appeared to propagate from the olfactory bulb to the cortices and dorsal basal ganglia, as well as the basal midbrain encompassing the substantia nigra (SN), by 72 hr post-infection (Fig. 1E).

To better track WEEV at the microscopic level and identify the individual nuclei infected following intranasal infection, we employed the DsRed-expressing McRed virus. Analysis of brain tissue from mice infected with McRed revealed consistent viral dissemination in all animals. Brains processed for CLARITY were sectioned from the rostral olfactory bulb to the caudal cerebellum. At 96 hours, McRed infected multiple nuclei involved in neurodegeneration, the glomerular layer of the olfactory bulb (GL), substantia innominate (SI), hippocampus (HIP), thalamus (TH), entorhinal regions of the cortex (ENT), pons, and most notably, the substantia nigra pars compacta (SNpc) (Fig. 1F). Whole brain 3D reconstructions of McRed-infected brains were also performed following subcutaneous and intranasal infection to identify the global distribution of virus throughout the CNS (Figure 8). Notably, intranasal infection with WEEV/McRed resulted in a pattern of viral spread that largely bypassed the striatum but still infected neuronal soma in the substantia nigra and ventral tegmental area.

Intranasal inoculation with WEEV causes selective dopaminergic neuronal loss and glial activation within four days of infection.

After characterizing the neuroanatomical propagation of WEEV following intranasal infection (Fig. 1F), we next wanted to determine if WEEV infection induced neuronal loss in infected brain regions. Intranasal infection with McRed induced significant infection in the hippocampus (CA1) and entorhinal cortex by 4 DPI (Fig. 1F) but neuronal counts of these brain regions showed no significant neuronal loss when compared to age-matched controls (Fig. 2A-C; hippocampus, 338 ± 6.557 vs. 342.8 ± 9.259, p=0.7142 and entorhinal cortex, 101.3 ± 6.96 vs. 90.4 ± 18.1, p=.6730). To further characterize the neuronal tropism of WEEV, coronal and sagittal sections were stained with anti-tyrosine hydroxylase (TH) and imaged by fluorescence

microscopy for co-localization with McRed, which strongly colocalized with TH+ dopaminergic neurons in the SNpc (Fig. 2E-2N). 3D confocal microscocy of the SNpc revealed widespread expression of dsRed in neurons throughout this nucleus (Fig. 2N). Stereological counts of neurons within the SNpc showed significant loss of TH+ dopaminergic neurons at 4 DPI (29% loss, 8707 ± 202.2 vs. 6180 ± 162.6, $p<0.0001$) when compared to age-matched uninfected controls (Fig. 2O). Additionally, marked activation of microglia and astrocytes was evident in McRed-infected brains, with microglia phagocytosis of dsRed-positive cells by 4DPI (Fig. 2P). Hypertrophy and proliferation of GFAP+ astrocytes was noted proximal to dsRed-positive neurons in the SNpc (Fig. 2Q).

Antiviral immunotherapy attenuates CNS infection with WEEV and facilitates viral clearance by eight weeks post-infection.

Given that intranasal inoculation with WEEV caused a severe encephalitic infection with rapid propagation of virus throughout the CNS, we employed passive immunotherapy to prevent mortality in order to characterize the long-term neurological consequences of infection with this alphavirus. The immunotherapy regimen targeting the E1-glycoprotein of WEEV facilitated viral clearance in infected mice, as we reported in previous studies (Phillips et al., 2014; Rico et al., 2016). We optimized the immunotherapy treatment regimen with McFly virus to generate an inoculation protocol that led to active spread of the virus into the midbrain without necessitating euthanasia (Figure 3). Infection of CD-1 mice with McFly was followed by either one treatment at 12 hrs or two treatments at 12 and 48 hrs with either 0.05 mL or 0.1mL of immune serum, or with naïve control serum (Fig. 3A,B). Photon counts of luciferase activity over the first three days of infection demonstrated that 2X 0.1mL of immune serum resulted in the best overall

profile of luciferase expression without incapacitating the animal (Fig. 3C). Animals with luciferase activity measurements in excess of 10^6 photons/sec became severely ill, were euthanized and not used for analysis. Animals with luciferase activity measurements less than 10^5 photons/sec were considered not to have established a CNS infection and were similarly not used for analysis. Any animals having luciferase activity within the defined acceptable range of photon counts (demarcated by the dotted red lines in Fig. 3C) were kept in the study. Survival curve analysis of the various treatment strategies showed that two doses of 0.1mL treatment yielded the highest survival percentage (Fig. 3D). Optimization of the treatment regimen indicated the presence of luciferase activity in the brain for up to 28 days following inoculation with McFly virus (Fig. 3E), with no luciferase activity detected at 8 week post-infecxtion. In parallel studies with McRed virus, mice were similarly treated with passive immunotherapy and brains imaged following CLARITY to detect the presence of dsRed. By 8 weeks post-infection there was no detectible dsRed signal all virus appeared to be cleared from the brains of infected mice (Fig 3F, 3H). This finding is similar to previous results from our group using *in vitro* neutralization and plaque assays with infected brain homogenates, in which WEEV was neutralized with anti-E1 immunotherapy and completely cleared from infected mouse brain following IP treatment with anti-E1 immunoserum (Phillips et al., 2014; Rico et al., 2016).

Mice rescued from WEEV infection using immunotherapy display loss of dopaminergic neurons with associated motor deficits

After optimizing our infection and treatment regimen with anti-E1 immunotherapy, we next examined the neuropathology, dopaminergic neuron loss and motor deficits following encephalitic infection with McFly at 8 weeks post-infection, after complete clearance of virus

from the brain (Figure 4). Mice were infected intranasally with McFly or mock-infected with saline and treated with immunotherapy at 12 hours and 48 hours. Surviving mice were euthanized at eight weeks post-infection (Fig. 4A). To determine whether infection with McFly induced selective loss of dopamingernic neurons in the SNpc or generalized loss of dopaminergic neurons in the basal midbrain, dopaminergic neuronal loss was assessed in the (SNpc) and ventral trigeminal area (VTA), as well as dopaminergic terminals in the striatum (ST). Analysis of infected mice revealed a significant loss of dopaminergic soma in both medial and lateral aspects of the SNpc, with apparent necrotizing morphology of remaining dopaminergic neurons, coupled with deteriorating projecting fibers to the substantia nigra pars reticulata (SNr) (Fig. 4B-G). Loss of dopaminergic neurons in the VTA was also noted. Quantitative analysis of infected brains revealed a 38% loss of TH+ dopaminergic neurons (9774 ± 494.5 vs. 6009 ± 374.5, $p<0.005$) and a 31% loss of NeuN+ total neurons (13347±365.6 vs. 9141±436.1, $p<0.00005$) in the SNpc. Dopaminergic neurons in the VTA were decreased by 30% following infection (14388 ± 1624 vs. 10002 ± 1026, $p<0.05$), without significant loss of NeuN+ total neurons (33216±2463 vs. 25488±2595, $p<0.0005$) (Fig. 4I, 4L). Dopamine terminal loss was also observed in the ventromedial striatum when compared to age-matched controls receiving only immunotherapy (Fig. 4M), with a 29% decrease in fluorescence staining intensity relative to control animals (442.1± 21.06 vs. 315.8± 22.99 arbitrary fluorescence units).

Surviving mice showed apparent neurobehavioral deficits consistent with deprecations of dopaminergic function that included postural instability, tremors, dyskinesia and rigidity (S3). Additionally, quantitative gait analysis was conducted using a real-time video gait analysis system (Fig. 4N). All measurements where compared back to baseline control measures for each individual mouse. Infected mice exhibited obvious lethargy and an increased run duration when

traveling a fixed distance, along with a decreased duty cycle relative to control mice (0.242 ± 0.1912 vs. -0.2618 ±0.1044 and 0.5509 ± 2.211 vs. 7.383 ± 1.378, *p<0.005). Duty cycle is defined as the percentage of stance over the sum of stance and swing duration, and stance is defined as the time each paw is in contact with the glass trackway(Wang et al., 2012). Increased run duration and decreased duty cycle both indicate hypokinesia in surviving mice 8 weeks post-infection with WEEV.

Encephalitic infection with WEEV causes persistent activation of microglia and astrocytes in surviving host animals.

A well-described clinical feature of post-encephalitic parkinsonism is microgliosis and astrogliosis throughout the CNS, mediated by damage associated molecular patterns (DAMP) and pathogen associated molecular patterns (PAMP) that are primarily expressed on glial cells (Barcia, 2013; Fricke et al., 2016; Rothhammer et al., 2018).

To characterize the extent of glial cell activation following infection with WEEV, we determined the relative number of microglia and astrocytes in the SNpc, ST and VTA in mice at 8 weeks post-infection (Figure 5). We observed gliosis throughout the CNS in mice surviving encephalitic infection with WEEV but considering the selective loss dopaminergic neurons (Figure 2), we decided to quantify gliosis throughout the nigrostriatal pathway solely. There was significant microgliosis in the SNpc, SNr and ST with associated amoeboid/reactive microglial morphology 8 weeks post-infection in surviving mice when compared to age-matched controls (Fig. 5A-5D). Quantitative analysis of infected brains revealed a 46% increase of IBA1+ microglia in the SNpc (499.5 ± 52.37 vs. 270.8± 42.27, p<0.005), a 31% increase IBA1+ microglia in the SNr (486 ± 4 2.55 vs. 337.3 ± 45.19, p<0.05) and a 40% increase of microglia in

the ST (416.6 ± 36.37 vs. 248.6.3 ± 38.87, $p<0.00005$) (Fig. 5E). Astrogliosis was quantified using glial fibrillary acidic protein (GFAP). Infected animals exhibited significantly more GFAP+ astrocytes in the SNpc, SNr and ST with apparent hypertrophic/reactive morphology at eight weeks post-infection (Fig. 5F-5I). Quantitative analysis of infected brains revealed a 69% increase of GFAP+ astrocytes in the SNpc (555.1 ± 57.1 vs. 170 ± 40.84, $p<0.0005$), a 56% increase in GFAP+ astrocytes in the SNr (882.6 ± 94.91.55 vs. 494.8 ± 102.1, $p<0.0005$), and a 79% increase of astrocytes in the ST (189.8 ± 24.29 vs. 40.07 ± 6.859, $p<0.0005$) (Fig. 5J).

Intranasal infection with McFly causes the formation of proteinase K-resistant α-synuclein plaques and a gene expression profile consistent with neurodegeneration.

Previous studies have shown that encephalitic infection can induce the formation of α–synuclein aggregation following infection in humans and mice (Beatman et al., 2015; Caggiu et al., 2019; Jang et al., 2009a; Jang et al., 2009c). To determine how infection with WEEV could modulate the aggregation of α–synuclein in outbred CD-1 mice, we examined brain sections from infected and control mice for expression of α–synuclein phosphorylated at Serine 129 (P129), a marker of the aggregated form of the protein (Anderson et al., 2006). Selected sections were also treated with proteinase K to assess the formation of insoluble α–synuclein plaques. We observed prominent P129+ α–synuclein aggregate formation in the hippocampus, cortex, substania nigra and mammillary body in surviving mice (Fig. 6A-6J). Acutely infected mice that were not treated with immunotherapy did not show P129+ α–synuclein aggregates at 4 DPI in any brain regions examined. Cells positive for P129 immunoreactivity appeared to co-localize primarily with IBA1+ microglia in all P129+ positive nuclei and did not appear to co-localize with TH+ or NeuN+ neurons in the substania nigra (Fig 6K-6N).

We then performed immunostaining in proteinase K-treated sections for TH and P129 to assess the formation of proteinase K-resistant aggregates in mice following intranasal infection with WEEV at 8 weeks post-infection. Proteinase K treatment caused complete degradation of TH in both control and infected sections with no loss of DAPI nuclear staining. Immunostaining for P129 in treated sections revealed the presence of proteinase K-resistant α–synuclein aggregates in the hippocampus, cortex, substania nigra and mammillary body only in infected sections (Fig. 6O-6X).

Considering the extensive distribution of α–synuclein aggregates throughout the CNS following infection with WEEV and since neurodegenerative mechanisms are likely to be common despite the sensitivity of the substantia nigra, we determined the transcriptional profiles using quantitative PCR arrays (qPCR arrays) on whole-brain homogenates to examine the expression of genes associated with a neurodegenerative phenotype (Figure 9). Transcriptional analysis was performed on mice having received one of the following treatments: animals receiving McFly virus and anti-E1 immunotherapy collected at three days post inoculation, control animals receiving mock infection (media only) collected at three days, animals receiving McFly virus and anti-E1 immunotherapy collected at four weeks post-inoculation and control animals receiving mock infection and anti-E1 immunotherapy (as immunotherapy control) collected at four weeks post mock infection (Figure 9A). All results were normalized to mock-infected/IgG treated mice. The following RT² Profiler PCR Arrays were used for cDNA quantification: Mouse mTOR Signaling (Figure 9B), Mouse Parkinson's Disease Array (Supplemental Figure 3C), and Mouse Cell Death PathwayFinder (Figure 9D). Genes with statistically significant differences in fold-regulation, when compared to the mock-infected control animals, were graphed in ascending order. The gene expression profile at 3 DPI was

consistent with previously characterized profiles following acute encephalitic infection with a mosquito-borne virus and appeared to be involved with innate antiviral immune activation (Yang et al., 2011). When comparing the gene profiles at 3 DPI and 28 DPI, a shift in the pattern of gene expression was observed. At 28 DPI, genes more closely related to neurodegeneration were upregulated on the Cell Death array, including *Htt, Bcl2, Irgm1* and *Akt1*, whereas and *Park7* and *Aldh1a1* were upregulated on the mouse PD array (Figure 9C, 9D). *Phospholipase D1(Pld1), Phospholipase D2(Pld2)* and *Pten* were 4-6 fold upregulated in surviving host at, 28 DPI, and have been implicated in neurodegenerative diseases and downstream signaling of ß-amyloid and *amyloid precursor protein (APP)* (Figure 9A) *(Ihle and Abraham, 2017; Oliveira and Di Paolo, 2010)* . The PD array revealed 6-fold upregulation of *Immune-related GTPase M (Irgm1),* which is associated with neuronal autophagy (Figure 9C) (He et al., 2012). *DJ-1 protein (Park7)* was upregulated 4-fold in surviving host mice as well. Additionally, multiple genes involved in neurodegeneration, including *Huntington protein (Htt)* and *Amyloid precursor protein (APP)*, were also found to be upregulated 4-fold in surviving host mice when compared to controls and acutely infected mice at 3 DPI. Additional genes that were uniquely upregulated in the 28 DPI group on the Cell Death and PD gene arrays appeared to be involved with calcium homeostasis and mitochondrial dysfunction.

2.4 DISCUSSION

Increasing epidemiologic and experimental evidence suggests that viral infection is a possible risk-factor for neurodegenerative diseases such as Parkinson's disease (PD) and Alzheimer's disease (AD) (Lewy, 1932) (Beatman et al., 2015; Eimer et al., 2018). In the present study, we found that encephalitic infection with WEEV in outbred CD-1 mice by intranasal inoculation resulted in viral spread from the olfactory tracts to the basal midbrain. We did not

detect infection within peripheral neurons of mice, based on *in vivo* imaging of mice infected with McFly, which suggests that WEEV infection in outbred CD-1 mice is highly specific to the brain. This finding is similar to previous studies that have shown Sindbis virus, another neurotropic mosquito borne virus, can infect the spinal cord of mice but is unable to infect the peripheral nerves (Cook and Griffin, 2003). This specificity to the CNS is likely due to the fact that peripheral neurons lack the amount of ER, polyribosomes, mitochondria and oxidative environment observed in CNS neurons to facilitate alphavirus replication (Darnell and Richter, 2012; Du and Richter, 2005; Huang et al., 2003; Richter, 2007; Wu et al., 1998). Additionally, the Braak staging system of human Parkinson's disease demonstrates that α-synuclein pathology spreads in a stereotyped manner beginning in the enteric nervous system and olfactory bulb; and may be the result of an unknown pathogen (Braak et al., 2003a; Braak et al., 2003c). Notably, 7–8.3% of PD brains show Lewy body pathology in the SN without any dorsal motor nucleus of vagus (DMV) pathology indicating that olfactory spread may be independent of DMV involvement (Attems and Jellinger, 2008; Kalaitzakis et al., 2008). Although the dorsal motor nucleus and gastrointestinal tract were completely void of pathology, we show that following intranasal inoculation, McFly rapidly disseminates from the olfactory bulb to the basal ganglia, similar to the progressive spread of α-synuclein pathology cases in sporadic PD (Fig. 1).

WEEV is a non-promoter driven virus and simple intranasal inoculation facilitates consistent viral propagation from the olfactory bulb to the entorhinal cortex, hippocampus and basal ganglia by 4 DPI (Fig. 1F). The mechanisms underlying the tropism of WEEV for these brain regions remains to be elucidated but the initial route of exposure and the neuroanatomical architecture certainly influence this regional specificity(Phillips et al., 2016). McRed likely propagates transneuronally from the olfactory bulb through the entorhinal region and

hippocampus and then replicates to the SNpc, in this respective order (Fig. 1F). We previously reported the entry and spread of alphavirus into the CNS resulting from intranasal and peripheral infection and demonstrated that both routes of inoculation lead to mid-brain infection with differing distribution patterns (S2)(Phillips et al., 2016)·(Phillips et al., 2014; Phillips et al., 2013)·(Elizan and Casals, 1991). Neuronal surface adhesion molecules like glycosaminoglycan heparan sulfate, as well as the unique oxidative intracellular environment of select neuronal populations have been cited as possible tropic factors (Ronca et al., 2017; Wyrsch et al., 2012). Previous studies have shown that the replicative protein of WEEV, nsP1 (non-structural protein 1), is sensitive to oxidative changes and needs a highly oxidative intracellular environment for viral replication, suggesting that RNA viruses may utilize oxidative stress induced during infection to control genome RNA capping and viral replication (Gullberg et al., 2015). The high oxidative environment of select brain regions such as the thalamus, entorhinal cortex, hippocampus and substania nigra likely contributes to the consistent dissemination of WEEV to these regions (Fig. 1) (Wang et al., 2009; Wang et al., 2005; Wilde et al., 1997; Wong et al., 2007).

Similar to encephalitic infection with other neurotropic viruses such as coxsackie B4, Epstein-Barr virus, Japanese B encephalitis and HIV, WEEV induced broad viral dissemination and gliosis but caused selective degeneration of neurons largely within the SNpc following acute infection at 4 DPI (Figure 2)(Beatman et al., 2015; Berger and Arendt, 2000; Cree et al., 2003; Dimova et al., 2006; Hersh et al., 2001; Hsieh et al., 2002; Mattos et al., 2002; Murgod et al., 2001; Roselli et al., 2006)·(Elizan and Casals, 1991; Ogata et al., 1997). Although we did not observe α-synuclein aggregation at 4 DPI, the association seen between α-synuclein aggregation in the entorhinal cortex and hippocampus in surviving mice at eight weeks post-infection

supports the assertion made in other studies that α-synuclein aggregation represents a direct or indirect neuroprotective and antimicrobial response (Beatman et al., 2015; Eimer et al., 2018; Stolzenberg et al., 2017). Whether α-synuclein directly induces neuroprotection by restricting viral replication or indirectly regulates gene expression of anti-viral cytokines, chemokines, and neuroprotective signaling molecules is unclear. It is also unknown whether viral-mediated loss of dopaminergic neurons following acute infection with WEEV is due in part to an increased neuroinflammatory response of microglia and astrocytes remains to be determined but we noted significant microglial phagocytosis of DsRed+ SNpc neurons at 4 DPI (Fig. 2P). The removal of these damaged neurons by activated microglia is both a homeostatic mechanism but also likely related to broader inflammatory activation of glia that is neurotoxic, as is associated with the pathogenesis of PD and related disorders (Duffy et al., 2018),(Neumann et al., 2009),(Joers et al., 2017),(Sanchez-Guajardo et al., 2013),(Skaper et al., 2018).

To further characterize the long-term neurological consequences of encephalitic infection with WEEV, we optimized an anti-E1 immunotherapy regimen that facilitated viral clearance and host survival. Although viral RNA can act as a continued source of inflammation, imaging of luciferase and dsRed at 8 weeks post-infection indicated that WEEV was completely cleared at this time point (Fig. 3F). Surviving animals showed motor deficits, loss of TH+ dopaminergic neurons (38% loss) and NeuN+ total neurons (31% loss), as well as significant loss of dorsomedial dopamine terminals in the striatum (29% loss) when compared to acutely infected mice without immunotherapy (Figure 4). Interestingly, we observed equal levels of viral replication in the SNpc and VTA, although the dopaminergic neurons in the VTA appeared to be less affected, demonstrating the selective vulnerability of SNpc dopaminergic neurons (Brichta and Greengard, 2014).

Considering that WEEV is completely cleared from the brain at eight weeks post-infection, the pathological features noted at this time point are likely due to chronic inflammatory activation of glial cells following infection (Figure 5). Glial activation is a common feature of viral encephalitis, with astrogliosis observed in the frontal and temporal white matter in cases of von Economo's disease and in post-encephalitic PD (Elizan and Casals, 1991; Ronca et al., 2017; Silva da Costa et al., 2012). Neuroinflammation is associated with all neurodegenerative diseases, characterized by inflammatory activation of both astrocytes and microglia(Hirsch and Hunot, 2009). Here we saw persistent glial activation in the SNpc, SNr and ST following encephalitic infection with McFly that likely contributes to the increased neuronal loss in surviving host animals. Neuronal injury from activation of microglia and astrocytes is consistent with that described in other encephalitis models, such as experimental autoimmune encephalomyelitis (EAE), that causes severe glial reactions and release of glial-derived neurotoxic factors (Ludlow et al., 2016). Similar to such models of encephalitis, we propose that innate immune inflammatory responses in glial cells are primarily responsible for the reactive gliosis observed after infection with WEEV(Sperlagh and Illes, 2007). Following viral infection, astrocytes and microglia can adopt a long-lasting neurotoxic and proinflammatory phenotype that may help to combat infection but may also worsen neuronal degeneration(Hirsch and Hunot, 2009). Consistent with this idea, it was previously reported that infection with WEEV in CD-1 mice resulted in increased cytokine and chemokine expression (CCL2, CXCL10) in surviving animals (Phillips et al., 2013). Neuroinflammatory activation of glial cells following encephalitic infection could therefore act in concert with neuronal oxidative stress and mitochondrial dysfunction to facilitate protein misfolding and loss of dopaminergic neurons.

Synucleinopathy and gliosis has been reported following infection with WNV and H5N1 influenza A (Elizan and Casals, 1991), (Jang et al., 2009a),(Clarke et al., 2014). It has been suggested that α–synuclein can restricts replication of RNA viruses in the brain following encephalitic infection.(Beatman et al., 2015) However, whether aggregation of α–synuclein is a pathological consequence of encephalitic infection or a protective mechanism to restrict replication of viral RNA is still unclear. In the current study, we observed the formation of large endogenous proteinase K-resistant α–synuclein aggregates in the hippocampus and entorhinal cortex, with smaller P129-immunopositive inclusions in the SNpc in mice surviving intranasal infection with WEEV (Figure 6). We contribute the lack of P129+ in the SNpc likely due to the low expressional levels of SNCA in wild-type mice. Interestingly, we did not detect α–synuclein protein aggregates at 4 DPI, suggesting that development of these pathological protein aggregates was secondary to other sequela of viral infection, such as oxidative stress and inflammatory activation of glial cells. P129+ inclusions appeared to overlap the same neuroanatomical regions that were positive for DsRed following intranasal infection (Figure 2). Recent studies have shown a very similar distribution of α–synuclein protein aggregates following stereotactic administration of preformed α–synuclein fibrils (PFFs)(Rey et al., 2016). Following stereotactic administration of PFF into the olfactory bulb, pK-resistant protein plaques were detected in the hippocampus, cortical regions and substantia nigra at six months post-injection (Rey et al., 2018; Rey et al., 2016). Here, we show that the majority of P129+ inclusions did not appear to co-localize with neurons or astrocytes but seemed to be primarily co-localized with IBA1+ microglia. The P129+ cells appeared to be dying neurons which likely no longer express TH and NeuN, explaining the lack of NeuN in P129+ cells. Additionally, phagocytosis of dying neuronal populations likely explains the localization of P129+ in

microglia, which is consistent with other findings (Bruck et al., 2016). Additional studies examining the timecourse of glial activation and protein aggregation will be required to more precisely determine how activation of astrocytes and microglia is linked to aggregation of α–synuclein during infection with WEEV. Reports using stereotactic administration of PFFs into the olfactory bulb did not determine if α-synuclein aggregates in the midbrain spread through direct transneuronal propagation of the originally injected PFFs or from a seeding event that caused the formation of new endogenous α-synuclein aggregates (Rey et al., 2016). Considering that McFly solely expresses firefly luciferase and that no exogenous α-synuclein was introduced during inoculation, our data suggest that seeding of α-synuclein aggregation following infection with WEEV facilitates the pathological conversion of native α-synuclein into the formation of proteinase-K resistant aggregates in select brain regions. Whether these inclusions spread through a transneuronal mechanism or from glia transmission is still unknown. The presence of α-synuclein in IBA1+ cells is likely facilitating the clearance of protein inclusions from the CNS, as previously noted, but additional longitudinal studies are needed to confirm this finding (Rey et al., 2018), (Bruck et al., 2016).

Common features of neurodegenerative diseases include neuronal loss, neuroinflammation, gliosis, ER-stress, mitochondrial perturbations, autophagy dysfunction and activation of cell death pathways. We observed significant differences in gene profiles from whole brain homogenates between surviving host at 3 DPI and 28 DPI. The most significant differences between gene families were involved in lipid metabolism, calcium signaling, inflammation and proteins involved in neurodegeneration. Upregulation of innate immune and cell death modulators was observed at 3 DPI, consistent with a gene profile following acute encephalitic infection. Conversely, we observed a drastic gene profile shift at 28 DPI that

produced a pattern of gene expression consistent with a neurodegenerative phenotype: App (Amyloid precursor protein), Htt (Huntington) and Park7 (DJ1), which is linked to preservation of mitochondrial function in Parkinson's disease(Antipova and Bandopadhyay, 2017). Recent evidence has suggested that Phospholipase D1/D2 *(Pld1, Pld2)* significantly modify autophagy during nutrient deprivation and are direct downstream targets of Amyloid Precursor Protein (APP), possibly explaining the significant upregulation of these genes (Figure 9) (Oliveira and Di Paolo, 2010). Activation of surrounding glia is likely a key contributor as well, similar to that described in other encephalitic infections causing severe glial activation and release of glial-derived neurotoxic mediators (Ludlow et al., 2016). Aldh1a1, an astrocytic differentiation marker, was significantly increased in the 28 DPI group. Moreover, NF-κB-dependent release of astrocyte-specific complement proteins has been shown to produce neuronal ER-stress and intracellular neuronal calcium perturbations (Hirsch and Hunot, 2009; Ludlow et al., 2016). Intracellular calcium perturbations and glial activation therefore likely influence the specificity of neuronal injury in the SNpc following infection with WEEV (Lian et al., 2016).

In accordance with previous clinical findings, these data demonstrate that encephalitic infection with WEEV in outbred CD-1 mice targets multiple brain regions affected in neurodegenerative diseases such as PD(Schultz et al., 1977). To replicate human cases of encephalitic infection with WEEV and to interrogate the long-term neurological consequences ensuing from such infections, immunotherapy treatment was used to establish a cohort of mice that consistently survive CNS infection with WEEV and completely clear virus. The onset, progression and clearance of the infection was demonstrated by *in vivo* bioluminescence and fluorescent imaging of virally expressed firefly luciferase and dsRed. Examination of surviving mice revealed significant gait abnormalities, loss of dopaminergic neurons in the SNpc and

VTA, loss of TH-positive terminals in the striatum, long-lasting glia activation, the formation of proteinase-K resistant α-synuclein inclusions and a gene expression profile consistent with neurodegeneration. The selective and rapid loss of TH+ dopamine neurons and development of proteinase K-resistant α-synuclein aggregates from a single inoculation with WEEV, coupled with high specificity for the SNpc, may help to explain why encephalitic infection with mosquito-borne alphavirus can cause parkinsonism in humans. Further work is required to determine how dopaminergic neurons in the SNpc appear to be selectively vulnerable to infection with WEEV. Consistent with clinical cases of encephalitic infection with this virus, the experimental results presented here indicate that the pattern of neuropathological injury and progression of neurodegeneration following infection with WEEV resembles certain features of parkinsonism. It is particularly striking that infection with WEEV caused the development of α–synuclein aggregates within eight weeks of infection in wild-type mice. This finding, combined with rapid progression, glial activation and selective loss of dopaminergic neurons within the SNpc suggest that recombinant WEEV, when used in conjunction with immunotherapy, could be a robust animal model for studying neurodegenerative mechanisms relevant to PD.

2.5 FIGURES

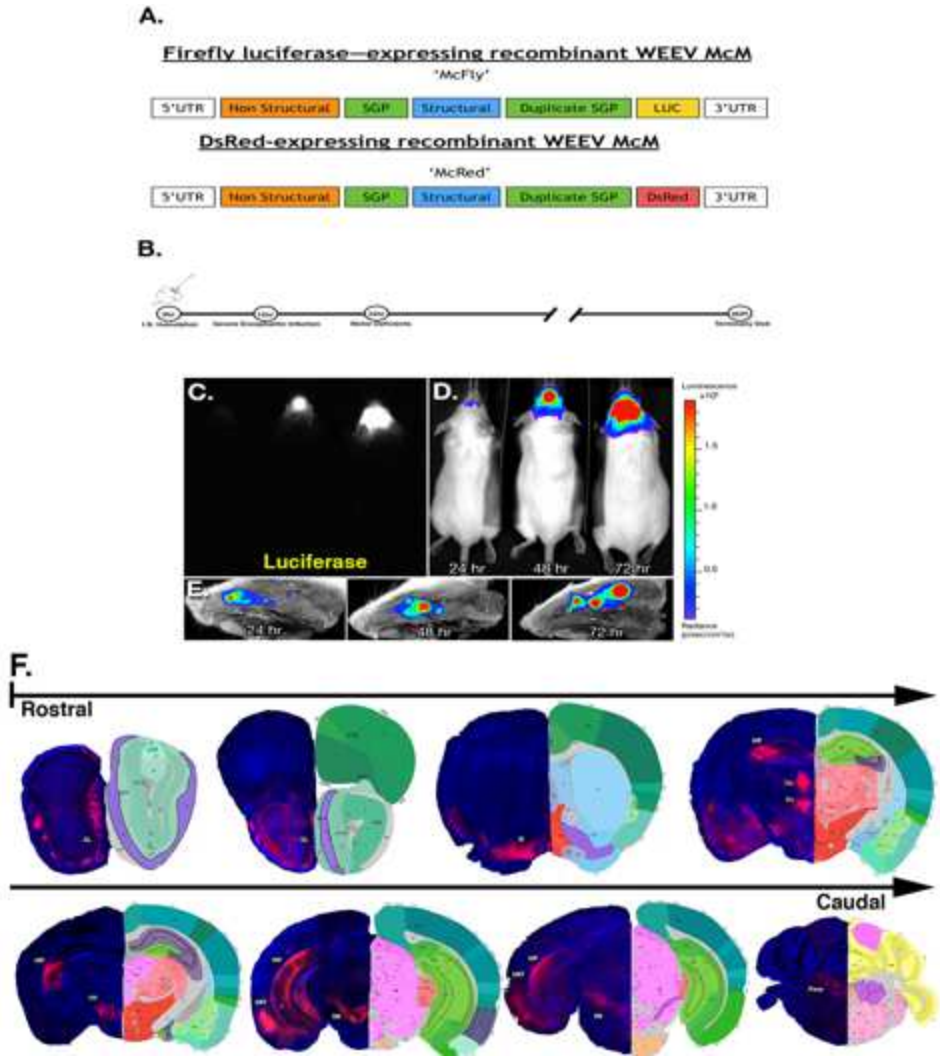

Figure 2.1. Regional specificity of recombinant Western Equine Encephalitis Virus following intranasal infection. (A) Schematic diagram illustrating the structure of vectors for each recombinant virus used in these studies. Subgenomic promoter (SPG), untranslated region (UTR). **(B)** Schematic diagram illustrating treatment regimen with WEEV. **(C)** Raw image of luciferase-activity in McFly-infected mice (left-24 HPI, middle-48 HPI, right-72 HPI). **(D)** Pseudo-colored image of luciferase-activity overlaid onto whole body images during the timecourse of infection. **(E)** *Ex vivo* sagittal hemispheric images of luciferase activity at specific times post-infection demonstrating progressive spread of WEEV from the olfactory bulb to caudal brain regions. **(F)** Six-week old CD-1 mice were administered 1×10^4 PFU of DsRed producing WEEV (McRed) via intranasal inoculation and euthanized four days post-infection. Brains were cryosectioned coronally and dsRed+ infected nuclei were labeled (purple) with reference to the allen brain atlas. Individual nuclei with presence of Dsred were labeled: GL (glomerular layer), SI (substantia innominate), MB (mammillary hippocampus (HIP), thalamus (TH), entorhinal regions of the cortex (ENT), and pons.

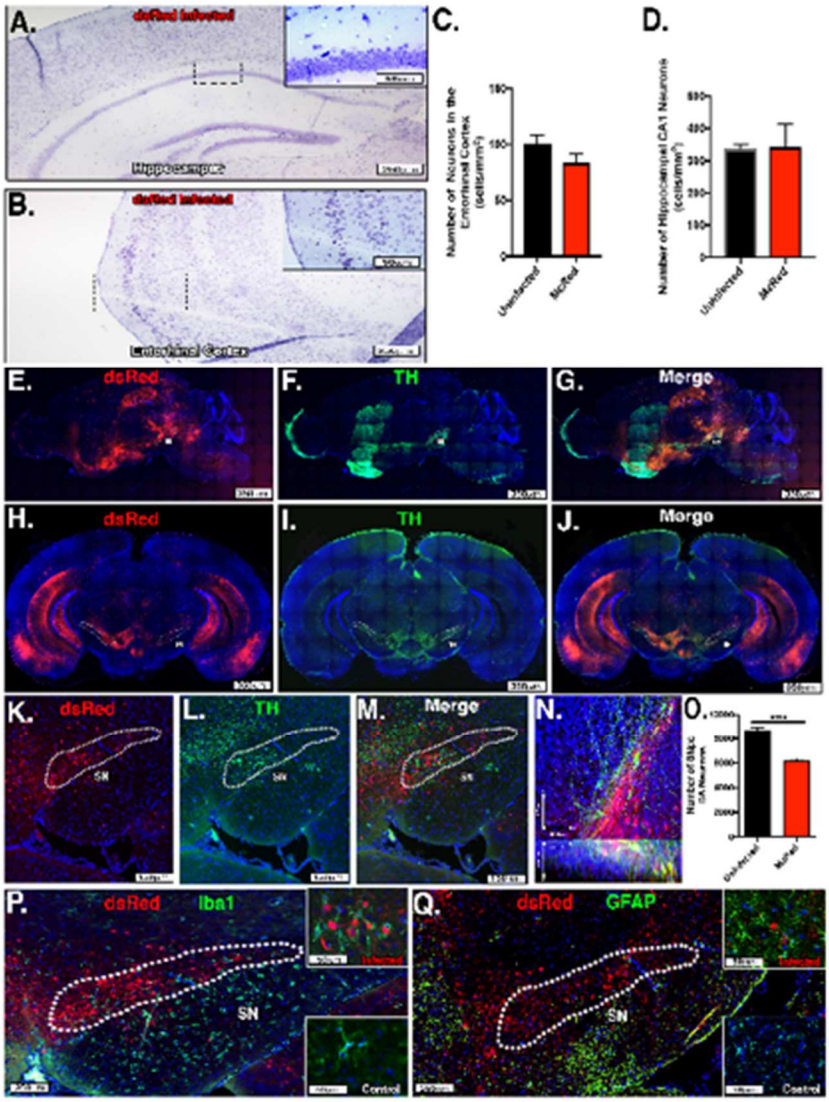

Figure 2.2. dsRed-expressing WEEV (McRed) shows strong tropism for dopaminergic neurons and causes selective dopaminergic neuronal loss and glial activation following intranasal inoculation. (A-D) Neuronal densities in hippocampus and entorhinal cortex were examined at 4 DPI following intranasal infection with McRed. No significant neuronal loss was detected in the hippocampus (CA1) or the entorhinal cortex (338 ± 6.557 vs. 342.8 ± 9.259, p=0.7142 and 101.3 ± 6.96 vs. 90.4 ± 18.1, p=.6730) (N=4/group). **(E-G)** Sagittal and coronal sections from CLARITY processed brains **(H-J)** were immunostained for TH+ dopaminergic neurons.High magnification confocal images **(K-N)** demonstrate co-localization of DsRed (red) and TH+ DA neurons (green). White dotted regions delineate the substania nigra pars compacta (SN). **(N)** X and Y coordinates in top panel with X and Z coordinates in lower panel. **(O)** Number of DA neurons in SNpc were examined with 3D design-based stereology 4 DPI. A 29% loss of DA was observed between treatment groups. (29% loss, 8707 ± 202.2 vs. 6180 ± 162.6). Intense staining for IBA1-positive microglia (green) **(P)** and GFAP-positive astrocytes (**Q)** was noted at 4 DPI in the SN following infection with McRed when compared to aged matched controls (bottom right of panels). White dotted region delineates the substania nigra pars compacta (SN). (N=3/group). ****p<0.0001.

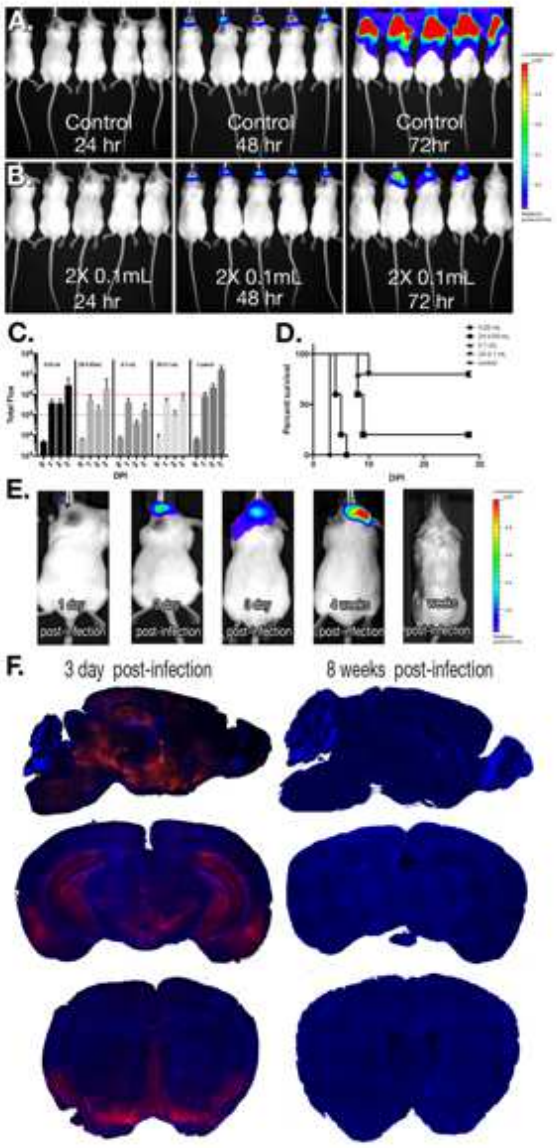

Figure 2.3. Anti-E1 immunotherapy in WEEV-infected CD-1 mice rescues from lethal infection and facilitates clearance of virus by 8 weeks post-infection. (A, B) Mice were infected with McFly and received either a mock treatment (naïve pre-immune serum) or anti-E1 immunotherapy (anti-E1 polyclonal rabbit immune serum). Bioluminescence measurements were acquired every 24 hours following inoculation. **(C)** Immunotherapy treatment was optimized to achieve consistent CNS infection without mortality, demarcated by red lines indicating the upper and lower range of acceptable luciferase-activity. For each treatment regimen, the measured luciferase activity is shown for the head region. Volumes indicate amount of immunized rabbit serum administered. 2X means the animals in that group received doses of immune serum at both 12 and 48 hrs post-infection. **(D)** Survival curves for the different treatment regimens employed. **(E-F)** Following treatment with immune serum at 12 and 48 hrs post-infection, regimen after intranasal infection with McFly and McRed, animals completely cleared virus by 8 weeks post-infection.

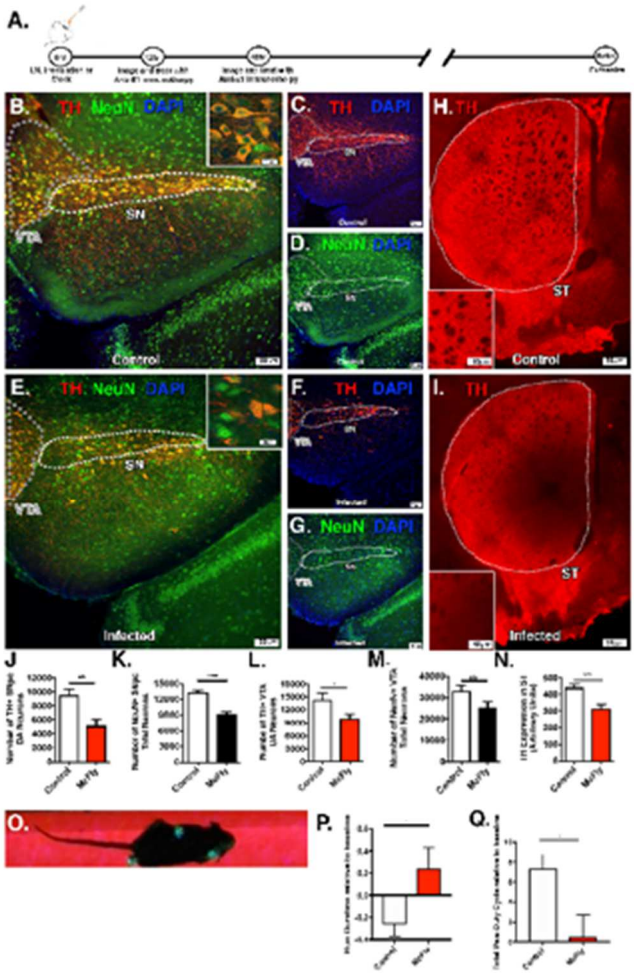

Figure 2.4. Following intranasal infection with WEEV and immunotherapy, surviving mice develop progressive dopaminergic neuronal loss and motor deficits. (A) Six-week-old CD-1 mice were intranasally (I.N.) inoculated with luciferase-expressing WEEV (McFly) or saline vehicle control and treated with anti-E1 polyclonal antiserum at 12hr and 48hr post-infection and euthanized eight weeks later. Outlined regions indicating the VTA and SN were used for quantification. **(B-G)** Immunofluorescence of DA neurons (red) and total neurons (green) of control or infected. **(H, I)** DA terminals from the striatum of control and infected mice with representative high-magnification images. White dotted line indicates the region used for quantification. **(J-N)** Quantitative assessment of DA neurons and total-neurons in the SNpc and revealed a 38% loss of TH+ dopaminergic neurons (9774 ± 494.5 vs. 6009 ± 374.5) and a 31% loss of NeuN+ total neurons (13347±365.6 vs. 9141±436.1) in the SNpc. Dopaminergic neurons in the VTA were decreased by 30% following infection (14,388±1,624 vs. 10,002 ± 1,026), without significant loss of NeuN+ total neurons (33,216±2,463 vs. 25,488±2,595). **(N)** DA terminal mean intensity reduction of 29% when compared to control. **(O-Q)** Infected mice exhibited an increased run duration when traveling a fixed distance, along with a decreased duty cycle relative to control mice (0.242 ± 0.1912 vs. -0.2618 ±0.1044 and 0.5509 ± 2.211 vs. 7.383 ± 1.378) when measured with a quantitative gait analysis system. All measurements were compared to baseline control values for each individual mouse. (N=6/group). * $p<0.05$ ** $p<0.005$, ***$p<0.0005$, ****$p<0.00005$.

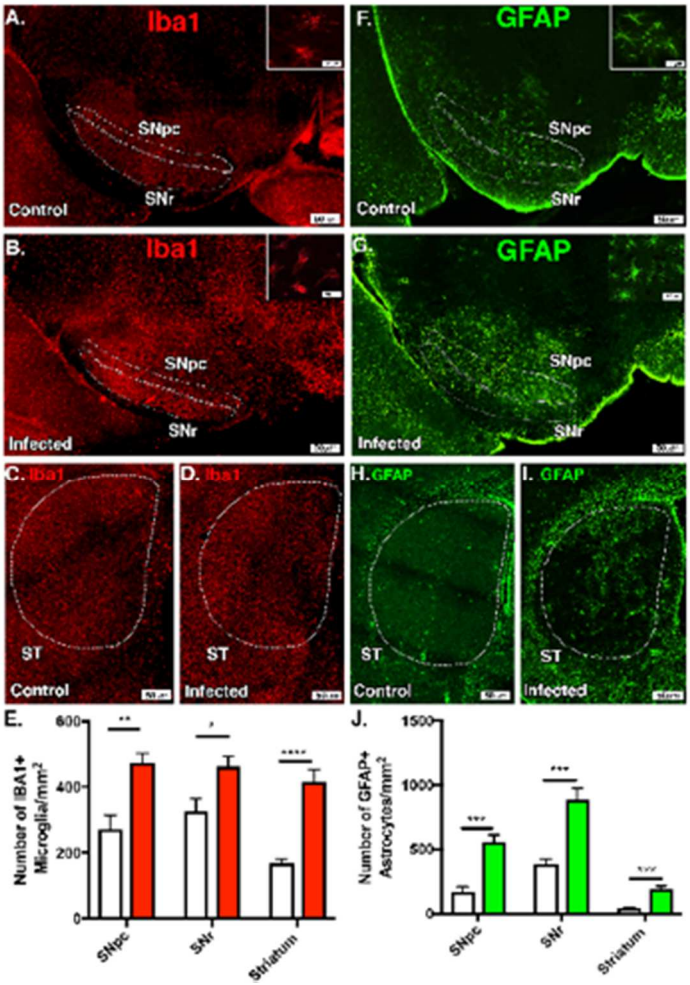

Figure 2.5. Persistent microgliosis and astrogliosis is present following encephalitic infection with WEEV. Six-week-old CD-1 mice were intranasally (I.N.) inoculated with luciferase-producing McFly virus or saline and intraperitoneally treated with anti-E1 polyclonal antibody at 12hr and 48hr post-infection and euthanized eight weeks later. **(A, B)** White dotted region and grey dotted regions delineate the substania nigra pars compacta (SNpc) and substania nigra reticulate (SNr) used for microglia (IBA1, red) quantification. **(C, D)** Iba1-positive microglia were detected by immunofluorescence microscopy in control (A) and infected (B) CD-1 mice I weeks post-infection. White dotted region indicates the striatum of control and infected animals. **(E)** Quantitative analysis of each respective brain region in control (white) and infected brains (red) revealed a 46% increase of IBA1+ microglia in the SNpc (499.5 ± 52.37 vs. 270.8± 42.27), a 31% increase IBA1+ microglia in the SNr (486±42.55 vs. 337.3±45.19), and a 40% increase of microglia in the ST (416.6±36.37 vs. 248.6.3±38.87). **(F, G)** White dotted region and grey dotted regions delineate the substania nigra pars compacta (SNpc) and substania nigra reticulata (SNr) used for astrocyte (GFAP, green) quantification. **(C, D)** White dotted region indicates the striatum of control and infected animals. **(J)** Quantitative analysis of infected brains revealed a 69% increase of GFAP+ astrocytes in the SNpc (555.1 ± 57.1 vs. 170± 40.84), a 56% increase in GFAP+ astrocytes in the SNr (882.6±94.91.55 vs. 494.8±102.1), and a 79% increase of astrocytes in the ST (189.8±24.29 vs. 40.07±6.859). (N=6/group). * $p<0.05$ ** $p<0.005$, *** $p<0.0005$, **** $p<0.00005$.

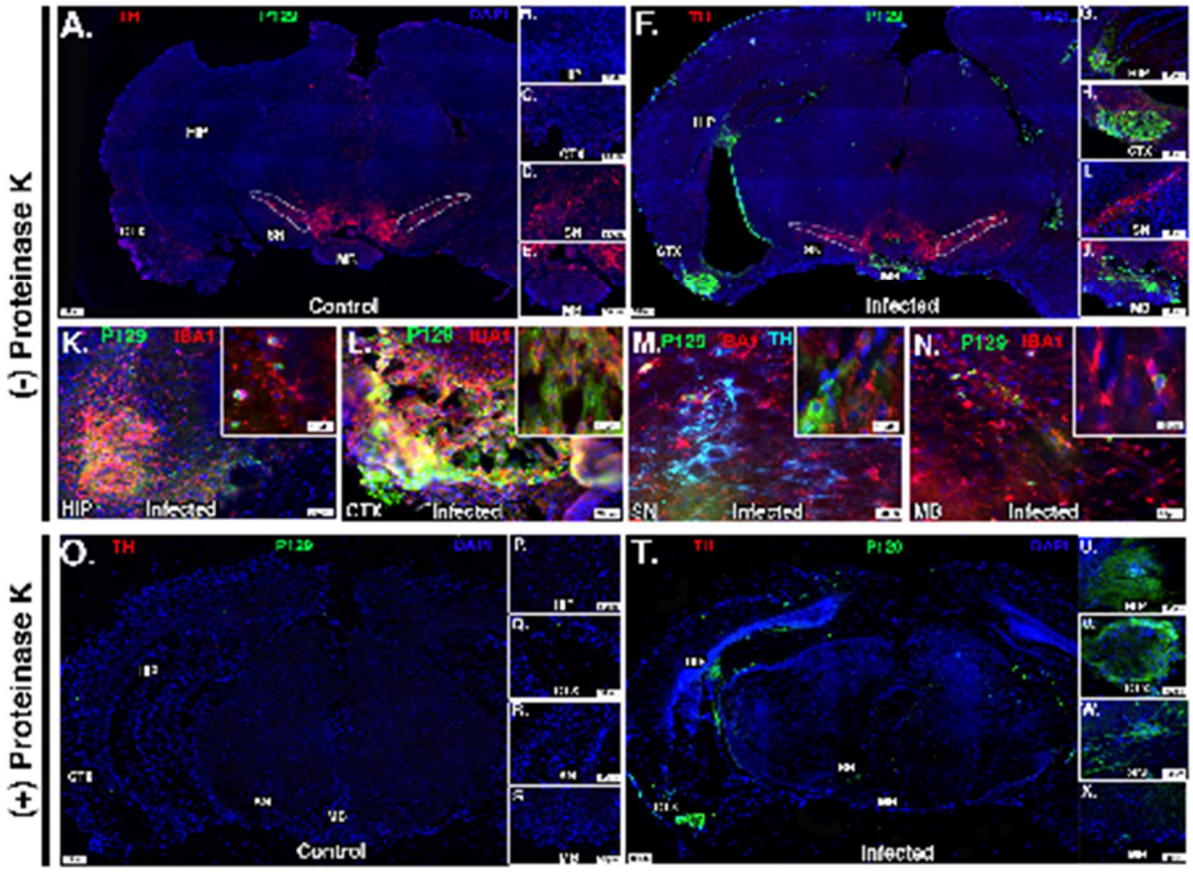

Figure 2.6. Surviving mice show formation of proteinase K resistant α–synuclein aggregates in multiple brain regions. CD-1 mice were infected with McFly virus and treated with immunotherapy regimen and euthanized 8-weeks post-inoculation. **(A-J)** Infected and control sections were stained with TH (tyrosine-hydroxylase, Red), P129 (phosphorylated α–synuclein 129, Green), and DAPI 8 weeks post-inoculation with McFly. **(B-E)** High-magnification images of uninfected control mice and **(G-J)** infected brain mice. White dotted region delineates the substania nigra pars compacta (SN). Individual nuclei positive for P129 staining were labeled as follows: HIP (hippocampus), CTX (cortex) and MB (mammillary body). **(K-N)** High-magnification images, 20x magnification, showing P129+ plaques and co-localization with IBA1+ microglia in select nuclei. **(O, X)** Proteinase K treated brain sections with complete degradation of TH depicting proteinase K-resistant α–synuclein aggregates (green). Also depicted are high-magnification images showing the presence of P129+ proteinase K-resistant plaques in infected mice **(U-X)** and the absence of P129+ plaques in uninfected control mice **(P-S)**.

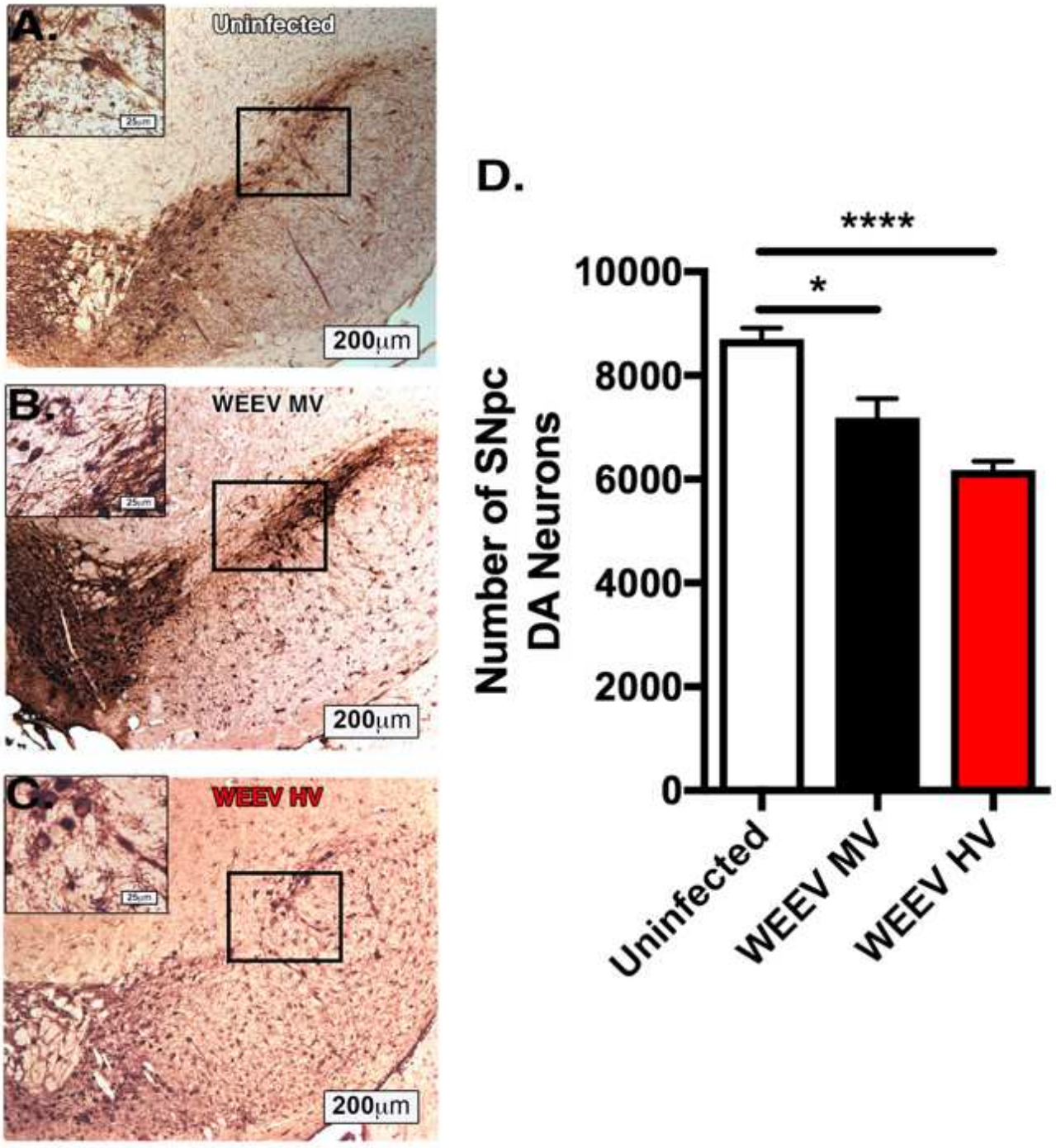

Figure 2.7. High-virulence (McMillan strain) causes more significant dopaminergic neuronal in loss in the SNpc than medium-virulence (Montana-64 strain) within 4 days of infection. (A-C) Six-week old CD-1 mice were administered 1×10^4 PFU medium virulent wEEV/Montana-64 strain (MV) or high virulent WEEV/McMillan (HV) or mock infected via intranasal inoculation and euthanized four days post-infection. (**D)** Brains were cryosectioned and the number of DA neurons in SNpc were examined with 3D design-based stereology 4 DPI. (N=3/group). * $p<.05$ and **** $p<0.0001$.

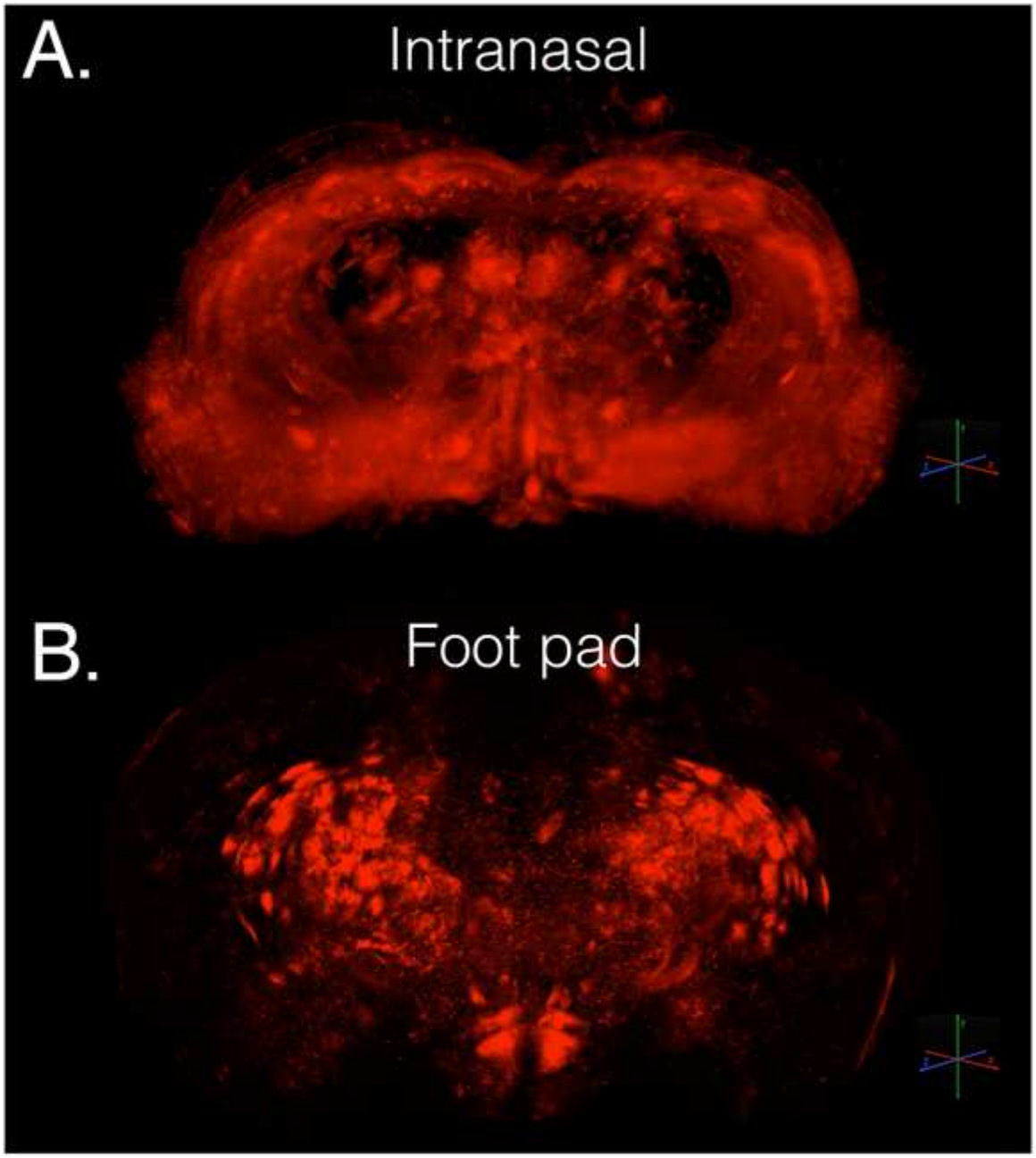

Figure 2.8 Infection with McRed by intranasal and subcutaneous foot pad inoculation result in dramatically different patterns of viral dissemination in the CNS. (See Videos 2.1 and 2.2) 3D reconstructions of dsRed-expressing WEEV in brain following intranasal (**A**) or foot pad (**B**) routes of inoculation. Six-week old CD-1 mice were administered 1×10^4 PFU of McRed (McMillan-DsRed) via intranasal inoculation and euthanized four days post-infection. Brains were perfused, embedded in hydrogel and sectioned at 200 μM. Sections were then cleared, removing all lipids, and montages at 10x magnification. 3D-reconstructions were built using Imaris software.

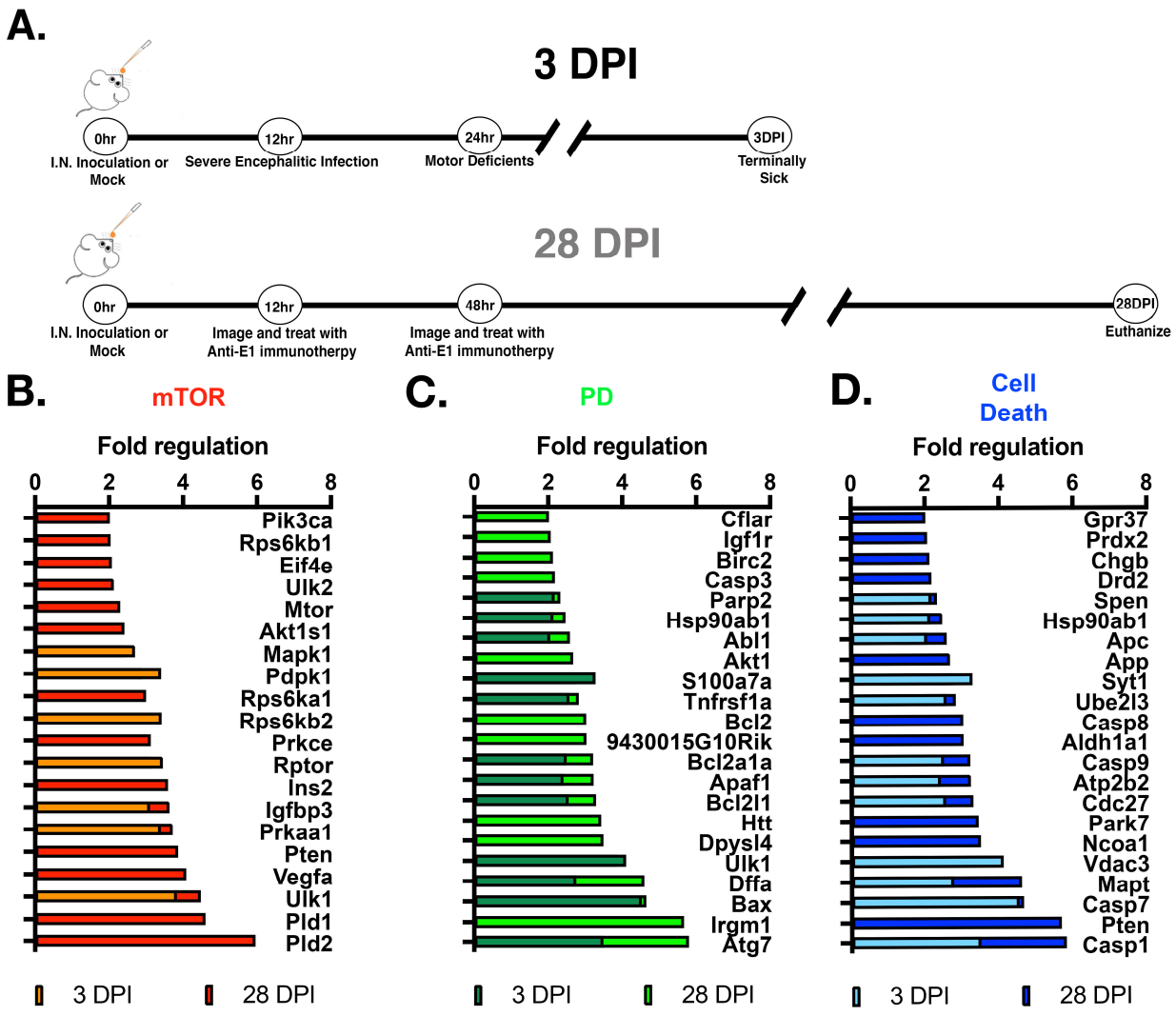

Figure 2.9. Infection with WEEV causes a gene expression profile consistent with neurodegeneration. (A) Treatment schematic. RNA was extracted from whole brain homogenate and assayed using three separate pathway-specific RT² Profiler PCR Array plates: **(B)** mTOR pathway, **(C)** PD-specific genes, and **(D)** Cell Death Pathway Finder. WEEV-infected mice were normalized to mock-infected/IgG-treated control mice. (N=4/group).

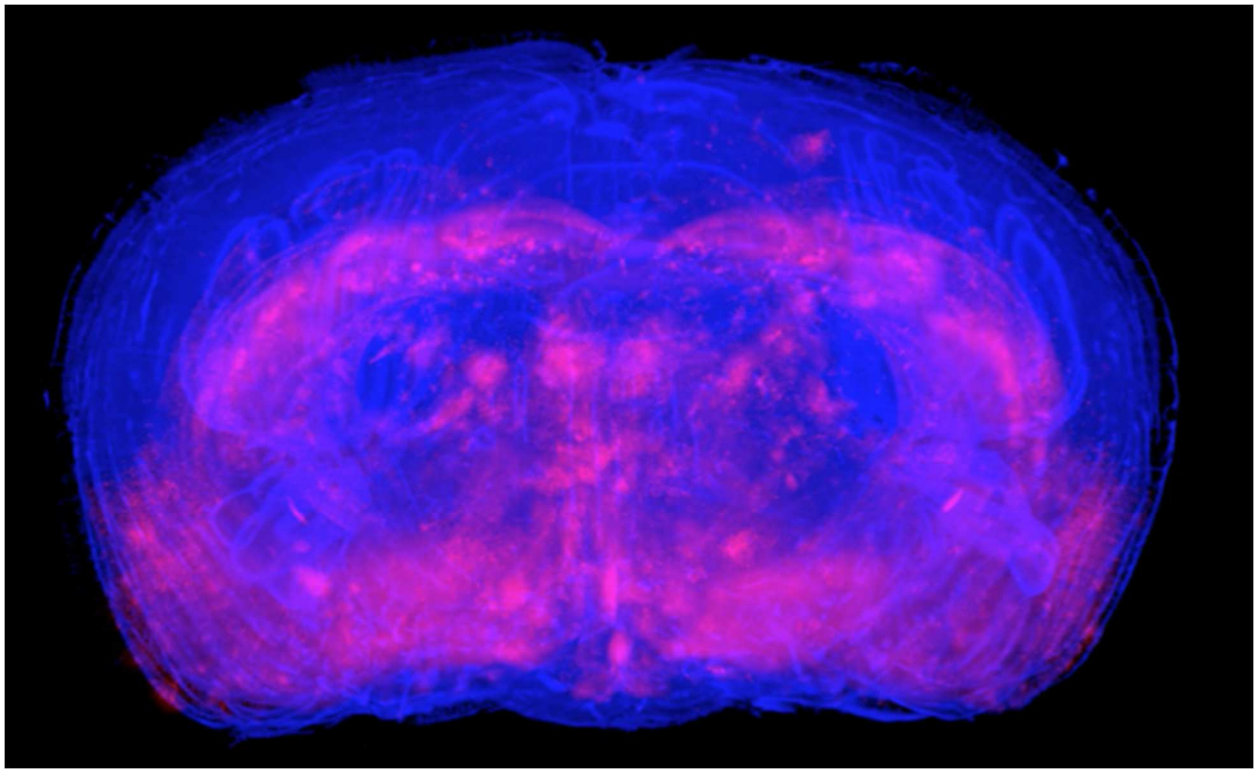

VIDEO 2.1. Viral dissemination throughout the CNS following infection with McRed by intranasal inoculation. 3D reconstruction of dsRed-expressing WEEV in brain following intranasal inoculation was based on montage images of CLARITY brain sections (200 um) collected rostral – caudal throughout the entire mouse brain at 4 days post-infection. Reconstruction and rendering was performed using Bitplane software (IMARIS).

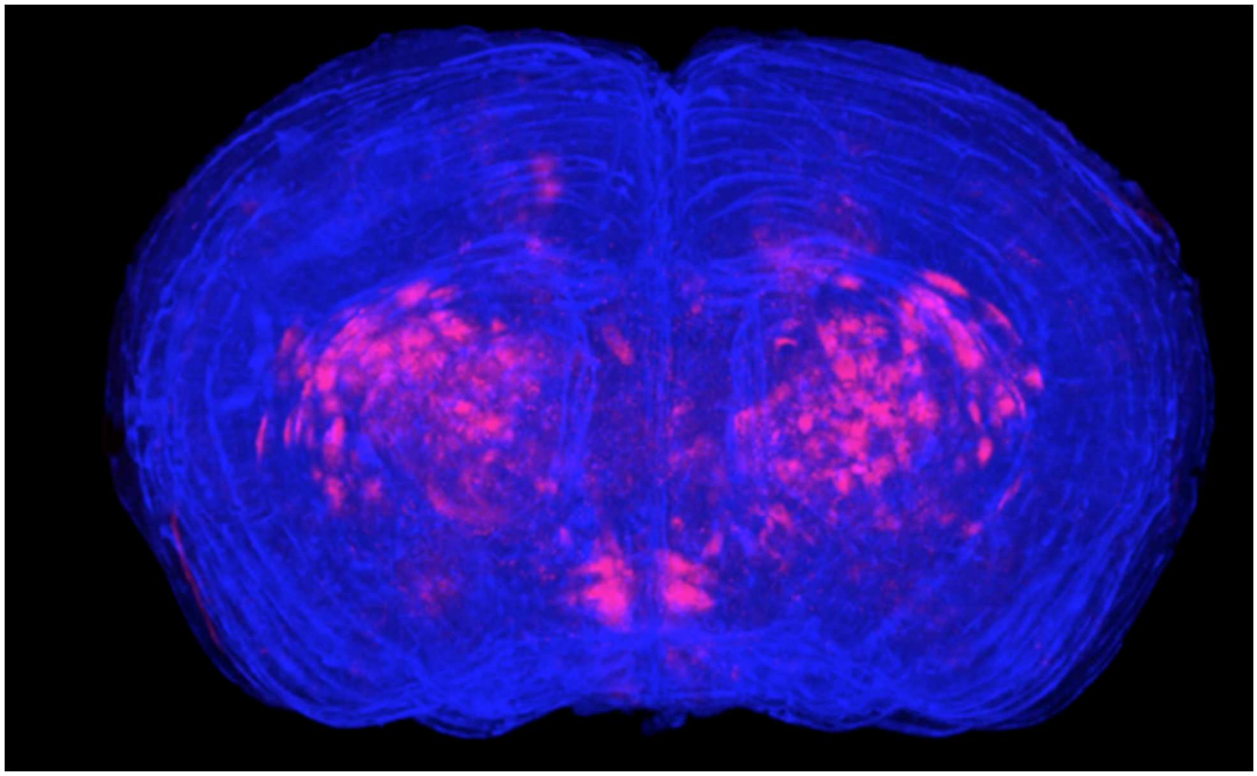

VIDEO 2.2. Viral dissemination throughout the CNS following infection with McRed by foot pad inoculation. 3D reconstruction of dsRed-expressing WEEV in brain following foot pad inoculation was based on montage images of CLARITY brain sections (200 um) collected rostral – caudal throughout the entire mouse brain at 4 days post-infection. Reconstruction and rendering was performed using Bitplane software (IMARIS).

VIDEO 2.3. LOCOMOTOR DEFICITS IN CD-1 MICE FOLLOWING INFECTION WITH WEEV (MCRED) AT 4 DAYS POST-INFECTION.

CHAPTER 3

ASTROCYTE INFLAMMATORY SIGNALING MEDIATE α-SYNUCLEIN AGGREGATION AND NEURONAL LOSS AFTER ENCEPHALITIC VIRAL INFECTION

3.1 INTRODUCTION

The increasing prevalence of neurodegenerative diseases, including Alzheimer's disease (AD) and Parkinson's disease (PD), imposes one of the greatest medical and public health challenges worldwide (Dorsey et al., 2018; Matthews et al., 2019). Although PD affects both the central and peripheral nervous systems, it is primarily characterized by the loss of voluntary motor function due to the degeneration of dopaminergic neurons in the substantia nigra pars compacta (SNpc). There are currently no disease-modifying therapies for the disease, nor has the etiology of PD been fully elucidated. Epidemiological and experimental evidence suggests that genetic susceptibility and exposure to environmental agents such as pesticides and viruses are possible risk factors for PD and related neurodegenerative diseases. There have been multiple reports of parkinsonism observed among human survivors of encephalitic viral infection (Jang et al., 2009a). Following the 1918 Spanish Flu pandemic, nearly every patient who suffered encephalitis lethargica (EL) from an influenza infection went on to develop postencephalitic parkinsonism (Dourmashkin, 1997; Reid et al., 2001). Additionally, many neurotropic viruses, such as West Nile virus (WNV), Japanese encephalitis virus (JEV), H5N1 influenza A and St. Louis encephalitis virus can cause PD-like pathology in humans, including α-synuclein aggregation, neuronal loss and inflammatory activation of microglia and astrocytes (Clarke et al., 2014; Elizan et al., 1978; Jang et al., 2009a). Previous studies have reported that Western Equine Encephalitis Virus (WEEV) also causes parkinsonism in humans following

encephalitic infection (Mulder et al., 1951; Palmer and Finley, 1956; Schultz et al., 1977). This was more recently highlighted by an outbreak where multiple patients from a Colorado epidemic of WEEV presented with PD-like symptoms following encephalitic infection, including tremor, cognitive deterioration and cogwheel rigidity (Schultz et al., 1977). Antibodies against mosquito-borne viruses have been reported in patients with von Economo's postencephalitic parkinsonism and in idiopathic PD, suggesting a viral etiology in some instances (Mulder et al., 1951; Palmer and Finley, 1956). Both virally-induced parkinsonism and PD present with inflammatory activation of microglia and astrocytes, suggesting that neuroinflammatory responses to encephalitic infection may share common mechanisms with those in idiopathic PD (Barcia, 2013). Although the cause of postencephalitic parkinsonism is not fully understood, these studies and others suggest that neuroinflammatory activation of glial cells following viral infection could be a critical initiating factor (Lesteberg and Beckham, 2019).

Reactive gliosis has been increasingly studied as part of the pathophysiology of PD. Neuroinflammation could therefore be a key factor connecting viral encephalitis and the development of parkinsonian neurological symptoms (Caggiu et al., 2019). Clinical evidence suggests a significant role for microglial-derived inflammatory mediators in PD, including the presence of inflammatory cytokines in cerebral spinal fluid (CFS), plasma and in PET imaging studies showing sustained neuroinflammatory activation of microglia in the midbrain of PD patients (Duffy et al., 2018; Gerhard et al., 2006; Lindqvist et al., 2013; Mogi et al., 1996). However, it is still unclear whether neurons benefit from activated microglia and astroglia due to the release of trophic factors or the clearance of damaged cells and insoluble protein plaques. Astrocytes serve critical homeostatic functions that maintain neuronal health and survival, including the release of trophic factors, maintenance of synapses, potassium buffering and

regulation of the blood-brain-barrier (BBB)(Liddelow and Barres, 2017). In contrast, inflammatory activation of astrocytes is associated with initiation and progression of neurodegeneration through increased release of inflammatory mediators that damage associated neurons (Martinez et al., 2017). These reactive "A1" astrocytes release multiple factors that modulate neuronal morphology and synaptic function, as well as the function of microglia. Among the factors released by reactive astrocytes, complement C3 protein modulates microglial activity through the C3/C3aR axis, thereby regulating phagocytic activity and protein aggregation dynamics in the brain (Clarke et al., 2018; Lian et al., 2016; Liddelow and Barres, 2017; Liddelow et al., 2017b; Zhang et al., 2014; Zhang et al., 2010). C3 is transcriptionally regulated in astrocytes by NFκB and has differing effects on microglial activity depending on whether it is expressed acutely or chronically. Acute expression induces microglia phagocytosis and clearance of protein aggregates, whereas chronic expression of C3 suppresses microglial clearance of aggregated proteins (Lian et al., 2016). Thus, chronic phenotypic activation of key A1 genes in astrocytes such as C3 during encephalitic viral infection could directly alter both the inflammatory and phagocytic activity of microglia and promote the formation of neurotoxic of α-synuclein aggregates.

We recently demonstrated that intranasal infection with WEEV induced selective loss of dopaminergic neurons in the SNpc, associated with persistent microgliosis, astrogliosis, and the development of proteinase resistant α-synuclein aggregates that spread into the cortex, hippocampus, and midbrain by 8 weeks post-intranasal infection (8WPI) in wild-type CD-1 mice (Bantle et al., 2019). The majority α-synuclein aggregates were located amongst dying neurons and surrounded with surrounding phagocytotic microglia . However, whether viral-mediated loss

of dopaminergic neurons following acute infection with WEEV is due in part to an increased neuroinflammatory response of microglia and astrocytes remains to be determined.

In the current study, we examined whether neuroinflammatory activation of glia is an initiating event in selective loss of dopaminergic neurons and α-synuclein protein aggregation following encephalitic infection with WEEV. To address this question, we infected C57BL/6J mice with WEEV and examined the time-course of glial activation and protein aggregation sequentially over 8 weeks relative to the loss of dopaminergic neurons in the SNpc. Recognition of viral RNA in endosomes by TLR3 and TLR7 potently triggers the activation of NFκB (Popichak et al., 2018b). We therefore infected astrocyte-specific NF*κ*B KO mice generated in our laboratory in order to interrogate the role of NFκB-regulated gene expression in astrocytes in neuronal injury from WEEV infection. These data demonstrate that microglia rapidly activate in the first stages of encephalitic infection with WEEV, which subsequently induces chronic astrocyte activation and α-synuclein protein aggregation, followed by the maximal extent of dopaminergic neuronal loss. Astrocyte-specific KO of NF*κ*B drastically reduced loss of dopaminergic neurons and α-synuclein aggregation following infection with WEEV, suggesting that innate immune inflammatory signaling in astrocytes is a critical regulator of both neuroinflammation and protein aggregation that precedes neuronal injury. This study highlights how glial cells may play an essential role in the initiation and progression of PD-like pathology following infection with WEEV due to inflammatory activation that directly modulates the dynamics of protein aggregation in the brain. Microglia and astroglia can respond to an array of neuroinflammatory insults that promote chronic production of detrimental complement proteins, pro-inflammatory cytokines and chemokines, and reactive oxygen species (ROS). These data

suggest that chronic glial inflammation contributes to neurodegeneration in post-encephalitic parkinsonism.

3.2 MATERIALS AND METHODS

DsRed and Firefly Luciferase Expressing WEEV Viral Constructs.

The molecular cloning methods used to construct these recombinant WEEV reporter vectors have been previously described (Logue et al., 2009; Phillips et al., 2016; Phillips et al., 2013). In brief, a duplication of the subgenomic promoter (SGP) sequence (nucleotides 7341–7500 of viral genome) of the WEEV McMillan strain was used to express firefly luciferase or DsRed. Plasmids were purified by QIAprep Spin MiniPrep Kit (Qiagen, Valencia, CA USA) and RNA was transcribed *in vitro* using a T7 RNA polymerase (MAXIscript™ kit, Life Technologies, Grand Island, NY USA). BHK-21cells (2×10^7 in 400 μL) were transfected with 20 μL of total RNA using an ECM 630 electroporator (BTX Harvard Apparatus, Holliston, MA USA). The rescued virus was stored at −80°C before plaquing. All plaque titration assays were run in duplicate in Vero cells before experimental use as described by Liu et al. (Liu et al., 1970).

Viral infections in wildtype and astrocyte Specific NFκB knock-out mice.

All animals were housed on a 12 hr light/dark cycle in a temperature-controlled room (maintained at 22-24°C) and had access to standard chow/water ad libitum. Astrocyte-specific NFκB knockout mice were generated as we previously described by crossing mice expressing the human *Gfap -Cre*$^{+/-}$ mice with *Ikk2-loxP*$^{+/+}$ mice(Kirkley et al., 2019a). Progeny were backcrossed four generations to produce *Gfap-Cre*$^{+/-}$/Ikk2$^{F/F}$ (KO) or *Gfap-Cre*$^{+/-}$/Ikk2$^{F/F}$ (WT) animals for the study(Bantle et al., 2019). Infections with recombinant WEEV were performed as previously described (Bantle et al., 2019). Six-week-old male and female C57BL/J6 mice (Charles River Labs, Wilmington, MA USA) or astrocyte-specific NFκB knockout mice were

housed in a biosafety level 3 (BSL-3) facility at the Infectious Disease Research Center on the campus of Colorado State University. Mice were anesthetized with isoflurane (Minrad Inc, Bethlehem, PA USA) through an XGI-8 anesthesia system (Caliper Life Sciences, Waltham, MA USA) connected to the IVIS 200 (Caliper Life Sciences, Waltham, MA USA) bioluminescence imaging system. Following induction of anesthesia, mice were intranasally administered 20 μL of either DsRed-expressing or luciferase-expressing WEEV at a concentration of 1×10^4 PFU/ml. All mice infected with DsRed-expressing WEEV were euthanized at four days-post-infection and used to characterize the viral spread of WEEV, while mice infected with the luciferase-expressing WEEV received a subcutaneous administration of luciferin at a dose of 150 mg/kg and were imaged on an IVIS imager 10–15 minutes later. Uninfected mice were used as an imaging control to adjust for background signal. The exposure time was 2 min under standard settings for the camera, and the Living Image 3.0 software (Caliper Life Sciences, Waltham, MA USA) was used to analyze and process images taken using the IVIS 200 camera. A threshold for significant BLM was established using negative imaging controls at 5×10^3 p/s/cm^2/sr. Total light emission from each mouse was determined by creating a region of interest (ROI) of standard size for each mouse and collecting light emission data. All mice were handled in compliance with the PHS Policy and Guide for the Care and Use of Laboratory Animals, and all animal protocols used in the study were reviewed and approved by the Animal Care and Use Committee at Colorado State University (Permit #11-2605A).

Anti-Alphavirus E1 Treatment Serum.

To generate the anti-alphavirus E1 rabbit serum, rabbits were vaccinated with recombinant WEEV McMillan strain E1-ectodomain antigen (10 μg antigen/dose), which was diluted in an immunological adjuvant comprised of polyI:C (dsRNA analog), ODN 1826

(unmethylated CpG DNA) (InVivoGen), and TiterMax Gold to a final concentration of 0.1 mg/mL. A total of four doses were administered every two weeks before rabbits were terminally bled for serum collection. After collection, serum was heat inactivated at 56°C for 30 minutes and stored at -80°C. Naïve serum was also collected from control animals. All anti-E1 serum was tested against E1 antigen on coated titration plates before its use in the study and was found to have an antibody titer measurement greater than 26,000 reciprocal value. A more thorough description of this protocol can be viewed in our previous publication (Bantle et al., 2019).

Tissue Processing and Sectioning.

One, two, four, and eight weeks after infection with luciferase-expressing WEEV, animals were terminally anesthetized with isoflurane and transcardially perfused. The brains were then extracted, fixed in 3% paraformaldehyde at 4°C and later processed for paraffin embedding and sectioned at 10 microns on a microtome through the anatomic midbrain and mounted on polyionic slides (Superfrost-plus, Fisher Scientific) (Miller et al., 2011; Smeyne et al., 2016).

Immunofluorescent Staining and Imaging.

Coronal and sagittal sections were deparaffinized and immunostained using anti-tyrosine hydroxylase (TH; 1:500; Millipore AB152) to identify dopaminergic neurons, anti-glial fibrillary acidic protein (GFAP; 1:500; DAKO Z0334) to identify astrocytes and anti-calcium adaptor binding protein 1 (Iba-1; 1:250; WAKO 016-20001) to label microglia, per our previously published methods (Hammond et al., 2017; Miller et al., 2011). Sections were visualized by automated montage imaging of individual 10X frames of

each immunostained section using a Hammatsu Flash4.0 digital CMOS camera, ProScan III stage controller (Prior, Rockland, MA USA) and CellSens Dimension software (version 1.12, Olympus, Center Valley, PA, USA). Regions of interest representing distinct anatomical nuclei were analyzed on each composite montage image.

Stereological Assessment of neurons and glial cells.

Methodologies for imaging and counting dopaminergic and total neurons in the substantia nigra, as well as microglia and astrocytes, were adapted from our previously reported studies (Baquet et al., 2009; Tapias et al., 2013). To determine the number of dopaminergic neurons and microglia in the SNpc, deparaffinized sections were double-immunostained for TH and Iba-1 (mouse monoclonal anti-tyrosine hydroxylase and rabbit polyclonal Iba-1 (Wako Chemicals; 1:500)), using secondary antibodies including biotinylated mouse IgG (for TH, 1:1000) or biotinylated rabbit IgG (for Iba-1, 1:1000). Diaminobenzindine (DAB) or a VIP kit (Vector labs) reaction was used to yield a brown (TH) or a purple (IBA-1) chromogen, respectively. All tissue sections were counterstained with Nissl substance and Neutral Red to identify anatomical landmarks. Stereological analysis of dopaminergic neurons and microglia in the SNpc was performed as detailed in Baquet et al. (2009)(Baquet et al., 2009). To determine the number of resting and activated microglia, Iba-1-positive microglia in the SNpc were analyzed using our previously published morphological criteria to distinguish resting and activated microglia from infiltrating macrophages (Graeber and Streit, 2010; Sadasivan et al., 2015; Smeyne et al., 2016; Tansey, 2010). The number of microglia in the right and left SNpc were summed to provide an estimate of the total number of resting and active microglia in the SNpc (Bantle et al., 2019). The investigator was blinded to the individual treatment groups when counting cells.

Neurochemical Detection of Catecholamines.

Samples were prepared and analyzed as we have previously performed (De Miranda et al., 2015). In brief, striatal brain samples were prepared for high performance liquid chromatography (HPLC) coupled with electrochemical detection to quantitate levels of DA, 3, 4-dihydroxyphenylacetic acid (DOPAC), homovanillic acid (HVA), serotonin (5-HT) and metabolite 5-hydroxindoleacetic acid (5-HIAA). All the tissue samples from each experimental group were coded and blinded for unbiased analysis.

Behavioral Analysis.

All mice were acclimated to handling two weeks prior to infection and habituated to the video trackway with repeated runs prior to baseline measurements the day before infections with WEEV (Gouveia and Hurst, 2013; Stuart and Robinson, 2015). Multiple neurobehavioral parameters, including stride length, run duration, step cycle, cadence, duty cycle and stop time were measured using a custom-made real-time video gait analysis system, as previously described (Hammond et al., 2018). All behavioral testing was performed on uninfected and infected mice on days 0, 14, 28, and 56. All parameter values were subtracted from the baseline measurements obtained on day 0 to normalize across all time points and treatment groups.

Immunohistochemical Staining and Pathological Scoring of Phospho-serine 129+ Alpha-Synuclein Protein Aggregates.

Sections were immunohistochemically stained on a Leica Bond-III IHC automated stainer using Bond Epitope Retrieval Solution 2 for 20 minutes. Reactive synuclein cell/cell aggregates were stained using monoclonal antibody, mouse anti-phospho Ser129 (P129) antibody (1:1000, clone pSYN#64, WAKO) (Jang et al., 2009a). Labeling was performed on an

automated staining platform. Fast Red (Bond Polymer Refine Red Detection # DS9390 (Anti-mouse IgG Fast Red Substrate System) was used as chromogen and slides were counterstained with hematoxylin. In all cases, normal and reactive mouse brain sections incubated with primary antibodies was used as a positive immunohistochemical control. Negative controls were incubated in diluent consisting of Tris-buffered saline with carrier protein and homologous nonimmune sera. All sequential steps of the immunostaining procedure were performed on negative controls following incubation. Immunoreactions and neuropathological scoring of P129+ protein aggregates were conducted in the cortex, hippocampus and midbrain on infected and uninfected brain sections by a veterinary pathologist blinded to the treatment groups. Pathological scoring methodology was adapted from previous reports (Rey et al., 2018; Rey et al., 2016). We assessed the presence of P129+ inclusions on two coronal sections per animal that were 20 µm in thickness, spaced at 100 µm intervals within the SNpc, with an *N*=6-8 mice at each timepoint for each treatment group. Each section was analyzed at a 20× magnification using an Olympus IX71 microscope (Center Valley, PA) with Retiga 2000R (Qimaging, Surrey, BC, Canada) and Qcolor3 (Olympus) camera and slidebook software (v6.0, Intelligent Imaging Innovations, Inc., Denver, CO) for image acquisition and analysis. A score of 1 to 5 was assigned to each brain region from a single coronal brain section and scored as follows: 1 = no aggregates, 2 = very sparse and one to two P129+ cells, 3 = mild with less than ten P129+ cells, 4 = dense with more than ten P129+ cells, 5 = very dense with more than 20 P129+ cells involved. The two scores obtained for each individual section were averaged for each mouse.

Quantification of C3 and P129+ Alpha-Synuclein aggregates.

Formalin-fixed, paraffin embedded (FFPE) mouse brain sections from the SNpc of infected mice were mounted on glasses slides and immunofluorescently labaled on a Leica Bond RXM automated robotic staining system using Bond Epitope Retrieval Solution 2 for 20 minutes. Sections were then incubated with primary antibodies for mouse anti-phosphorylated Ser129 (P129) antibody (1:1000, clone pSYN#64, WAKO) and rat anti-C3/C3b (1:500; Abcam 11871). Secondary antibodies included anti-mouse IgG 488 and anti-rat IgG 555. Whole brain immunofluorescent montage images of labeled tissue sections were imaged using a 20x objective and an automated Olympus BX51 fluorescence microscope equipped with a Hamamatsu ORCA-flash 4.0 LT CCD camera and collected using Olympus Cellsens software (v 1.15). Quantitative analysis was performed on dual- or triple-labeled fluorescent images generated by montage imaging of an entire coronal brain section compiled from individual images acquired using an Olympus Plan Apochromat 10X air objective (0.40 N.A.). The cortex, hippocampus and midbrain were delineated by anatomical landmarks and referenced to the Allen brain atlas. A region of interest (ROI) was generated around all P129+ cell aggregates in each neuroanatomical region of interest and the mean fluorescence intensity of C3/C3b was then obtained within each P129+ ROI. Duplicate tissue sections were stained and averaged for each mouse (*N*=6-8 mice at each time point for each treatment group). The investigator was blinded from all experimental groups for data acquisition. All slides were scanned under the same conditions for magnification, exposure time, lamp intensity and camera gain.

Image analysis of reactive astrocytes.

Formalin-fixed, paraffin embedded 8 μm brain sections were immunofluorescently labeled as described above using on a Leica Bond automated stainer using Leica Bond RXM

automated robotic staining system. Sections were then incubated with primary antibodies for anti-rabbit S100β (1:500; Abcam 212816) and rat anti-C3 (1:50; Abcam 11871). Secondary antibodies included anti-rabbit IgG 647 and anti-rat IgG 555. To detect C3+ cells co-localizing with S100β+ astrocytes, individual ROIs were created around all S100β+ astrocytes within the SNpc and the mean C3 intensity was measured within each S100β+ astrocyte. Each brain was analyzed in duplicate and a total *N*=6-8 was utilize for each time point and treatment group. All slides were scanned under the same conditions for magnification, exposure time, lamp intensity and camera gain.

Generation of Normalized Pathological Overlays.

To generate the representative overlays at each time point, the total number of dopaminergic neurons, microglia, macrophages, astrocytes cellular counts and P129 pathological scores from infected mice were normalized to controls. The highest cell count or score from each cell type was used as the denominator to generate a representative ratio. This was preformed to normalize changes in each parameter under investigation across different cells types and for different P129 pathological scores. The respective ratios at each time point (1 week, 2 weeks, and 8 weeks) were then normalized to 100% and presented using GraphPad software (version 6.0; Graph Pad Software, San Diego, CA).

Statistical Analysis.

All data was presented as mean +/- SEM, unless otherwise noted. Experimental values from each mean were analyzed with a Grubb's (α=0.05) test for exclusion of significant outliers. Differences between each experimental group were analyzed using an unpaired t-test or a one-way ANOVA following a Tukey post hoc multiple comparisons test. Significance was identified

as *$P < 0.05$, **$P < 0.01$, ***$P < 0.001$, ****$P < 0.0001$. All statistical analysis was conducted using Prism (version 6.0; Graph Pad Software, San Diego, CA).

3.3 RESULTS

WEEV selectively infects neurons throughout the brain and induces persistent microgliosis and dopaminergic neuronal loss in the substantia nigra pars compacta, with associated neurochemical and neurobehavioral abnormalities.

To determine the viral dissemination of WEEV following intranasal infection, we infected six-week-old C57BL/J6 mice with WEEV-DsRed. Following infection, 100% of mice developed severe locomoter abnormalities and became terminally ill by 4 DPI. Histopathological analysis of brain tissue from infected mice revealed that WEEV showed selective tropism for neuronal cell populations in the entorhinal cortex and hippocampus, as well as dopaminergic neurons in the nigrostriatal pathway, with associated widespread astrogliosis and microgliosis. All microglia and astrocytes were devoid of WEEV-DsRed (Fig. 6 A-C).

We next wanted to interrogate the longer term neuroinflammatory and neurodegenerative consequences of encephalitic infection with WEEV. To achieve this, we utilized a previously established passive immunotherapy treatment regimen coupled with WEEV-LUC that allows for a consistent encephalitic infection without incapacitating the mice (Fig. 6 D-G) (Bantle et al., 2019). We recently demonstrated that WEEV induces selective loss of dopaminergic neurons in the SNpc with widespread gliosis and α-synuclein aggregation in wild-type CD-1 mice by 8 weeks post-infection, but the temporal sequence of neuroinflammation, protein aggregation and neuronal loss remained to be determined (Bantle et al., 2019). To elucidate the order of these pathological events following infection with WEEV, we characterized neuropathological changes in the SNpc at 1, 2, 4 and 8WPI. Stereological assessment of dopaminergic neurons,

microglia and peripheral macrophages in the substantia nigra indicated a significant loss of dopaminergic neurons in the SNpc at all time points with associated microgliosis and peripheral macrophage infiltration following intranasal infection with WEEV (Fig.1 A-J). We also observed ameboid and activated microglial cells from 1WPI persisting to 8WPI, after the inflammatory stimulus had subsided and virus was completely cleared from the brain (Fig 1 K-M) (Bantle et al., 2019). Microgliosis and macrophage infiltration followed the same time course, peaking at 1WPI and decreasing from 4 to 8WPI, when actively replicating virus was no longer detectable in the brain (Fig. 1 N-Q).

These pathological findings correlated with alterations in catecholamine content in the nigrostriatal pathway and with locomotor dysfunction consistent with parkinsonian neurobehavioral abnormalities. We observed a significant decrease of dopamine (DA) and its metabolites, 3,4-Dihydroxyphenylacetic acid (DOPAC) and Homovanillic acid (HVA) at 8WPI in the SN, as well as a significant decrease of DOPAC at 4 and 8WPI in the striatum (Fig. 7 A-L). Neurochemical analysis of mice at 1WPI was not obtainable because of the BSL-3 regulations. We also observed persistent locomotor and gait abnormalities following encephalitic infection with WEEV. Video-based analysis of freely moving gait along a trackway indicated decreased stride length at 1WPI with an increased cadence; surviving mice also developed generalized bradykinesia when compared to age-matched, vehicle-infected control mice (Fig. 7 M-S).

WEEV induces α-synuclein protein plaques in the cortex, hippocampus, and midbrain of surviving wild-type mice.

One of the hallmarks of PD is the formation of α-synuclein protein aggregates and we previously reported the formation of proteinase K-resistant α-synuclein aggregates in the

entorhinal cortex, hippocampus and midbrain of outbred CD-1 mice following intranasal infection with WEEV by 8WPI (Bantle et al., 2019; Jellinger, 2008). To better characterize the development of protein aggregates, we examined levels of phosphorylated α-synuclein (serine 129) in brain tissue of C57BL/J6 mice at distinct timepoints following infection with WEEV using a pathological scoring system to quantify the severity of protein aggregation (Anderson et al., 2006; Rey et al., 2016). The most prominent P129+ α-synuclein protein aggregates were observed in the entorhinal cortex, which was the same neuroanatomical region that had the highest-level of viral replication at 4 DPI (Fig. 6 B-C). Strikingly, we saw P129+ α-synuclein protein aggregates as early as 2 WPI in wild-type mice in the entorhinal cortex, hippocampus and midbrain (Fig. 2A-L). The extent of P129+ α-synuclein protein aggregation was greatest at 2WPI and began to decrease by 8WPI (Fig. 2 A-L).

Encephalitic infection with WEEV induces microgliosis and macrophage infiltration before neuroinflammatory activation of astrocytes and opsonization of α-synuclein protein plaques with complement C3 protein.

Astrogliosis is another well described clinical feature of PD and other related synucleinopathies (Elizan and Casals, 1991; Silva da Costa et al., 2012). Previous research has shown that encephalitic viral infection can cause a phenotypic switch in astrocytes and induce a long-lasting neurotoxic and proinflammatory phenotype, termed A1(Liddelow et al., 2017b). A1 inflammatory astrocytes may help to combat a recurrent encephalitic infection but can also magnify neuronal injury (Hirsch and Hunot, 2009). Notably, A1 astrocytes uniquely express a number of NFκB-regulated proteins, including complement C3 (Lian et al., 2016; Lian et al., 2015). To further characterize the inflammatory state of astrocytes following encephalitic infection with WEEV, we quantified the number of astrocytes and the expression of C3

complement in Sl00β+ astrocytes in the SNpc at 1, 2, 4 and 8WPI. Following intranasal infection, we noted increased numbers of S100β + astrocytes in the SNpc at 1, 2, 4 and 8WPI (Fig. 8 A-I). We also observed an increase in C3 expression in Sl00β+ astrocytes following intranasal infection, with the greatest increases at 4 and 8WPI (Fig. 8 J, K).

To determine how microgliosis, macrophage infiltration, dopaminergic neuronal loss, astrogliosis and α-synuclein protein aggregates were temporally related in the SNpc following encephalitic infection with WEEV, we generated a normalized overlay of these pathological findings (Fig. 3 A). From this overlay, we were able to determine that microgliosis and macrophage infiltration preceded α-synuclein protein aggregation and maximal astrogliosis, and that the peak of astrogliosis and α-synuclein protein plaque load in the SNpc coincided. Microgliosis and macrophage infiltration were the first pathological findings following encephalitic infection with WEEV, highlighting activation of these cell types as a potential cause of dopaminergic neuronal loss and P129+ α-synuclein protein aggregation following encephalitic infection with WEEV.

The NFκB-dependent release of astrocyte-specific complement proteins have been shown to produce neuronal ER-stress, intracellular neuronal calcium perturbation and opsonization of P129+ α-synuclein protein aggregates (Loeffler et al., 2006)(66). Interestingly, there was a slight clearance of P129+ protein aggregates from the brain of infected mice at 8WPI, with the majority of staining located in perivascular regions of the hippocampus and cortex (Fig. 2 K). We next investigated whether C3 could bind to and potentially opsonize P129+ α-synuclein protein aggregates for clearance in the cortex, hippocampus and midbrain following infection with WEEV. Using co-immunofluorescence labeling, we observed that P129+ α-synuclein protein aggregates stained positively with C3b in all brain regions, with highest levels noted in the

midbrain at 8WPI (Fig. 3). No P129+ α-synuclein protein aggregates were detected at 1WPI. Whether C3b binding to α-synuclein protein plaques is a protective mechanism to facilitate clearance or a pathological consequence of the A1 astrocyte phenotype remains to be determined.

Genetic knockout of NF-κB in astrocytes reduces α-synuclein plaque load and decreases neuronal loss and gliosis.

Previous reports have shown that reactive A1 astrocytes are the source of C3 in the brain and that NF-κB-dependent C3 expression in astrocytes regulates amyloid-beta, microgliosis, and neuronal loss (Lian et al., 2016; Loeffler et al., 2006; Shi et al., 2017; Vasek et al., 2016). We therefore determined the effect of selective genetic ablation of NFκB in astrocytes on microgliosis, neuronal loss and P129+ α-synuclein immunoreactivity in *hGfap-cre*$^{+/-}$*/Ikk2*$^{F/F}$ (NFκB KO) transgenic mice following infection with WEEV at 8WPI (Fig. 5A) (Kirkley et al., 2019a). We evaluated 8WPI because C3 expression and colocalization with P129+ plaques was most extensive at this timepoint (Fig. 4 and Fig. 8 K). There was a significant reduction of P129+ α-synuclein plaque load following intranasal infection with WEEV in *hGfap-cre*$^{+/-}$*/Ikk2*$^{F/F}$ KO mice in the cortex, hippocampus and midbrain compared to WT *Ikk2*$^{F/F}$ controls (Fig. 4). Immunohistochemical analysis indicated that residual P129+ α-synuclein plaques in infected KO mice appeared to be entirely void of C3. Additionally, there was reduced microgliosis in the cortex and hippocampus (Fig. 9 B-C) and an overall reduction in astroglial counts in the midbrain of infected KO mice when compared to infected WT mice (Fig. 9 G). These data provides additional support for the importance of cell-cell signaling between microglia and astrocytes in modulating the neuroinflammatory response following encephalitic infection (Liddelow and Barres, 2017).

3.4 DISCUSSION

Considerable evidence suggests that viral infection of the CNS can directly or indirectly influence the onset and progression of neurodegenerative diseases (Mattson, 2004; Sadasivan et al., 2017). An association between viral encephalitis and parkinsonism has been noted for nearly a century but the underlying mechanisms have remained surprisingly obscure (Lewy, 1932). Multiple reports posit that pathogenic microbes could be etiological factors in neurodegenerative disease and increasing evidence suggests that proteins involved in neurodegeneration, such as α-synuclein, ß-amyloid, tau and prion protein, are antimicrobial peptides that modulate the neuroinflammatory response to reduce the microbial load in the brain (Beatman et al., 2015; Chida et al., 2018; Eimer et al., 2018). In the present study, we found that encephalitic infection with WEEV in C57BL/6J mice by intranasal inoculation resulted in rapid neuronal dissemination from the olfactory bulb to the entorhinal cortex, hippocampus and basal ganglia by 4 DPI, while other regions of the nigrostriatal pathway, such as the striatum, were absent of virus (Fig. 6). Why only select neurons are infected is unclear but a similar pattern has been observed by stereotactic administration of α-synuclein preformed fibrils (PFFs) into the olfactory bulb of mice (Rey et al., 2016). WEEV is non-promoter driven virus and, similar to PFF-based mouse models, the selectivity for these regions is likely driven by the neuroanatomical architecture and the unique neuronal and glial environment in these brain regions. However, it has also been suggested that specific neuroanatomical areas of the brain exhibit an innate ability to restrict viral infection (Gullberg et al., 2015; Kostuk et al., 2019; Phillips et al., 2016).

We previously reported that WEEV selectively induces degeneration of dopaminergic neurons in the SNpc with widespread gliosis and α-synuclein plaque formation by 8WPI in outbred CD-1 mice but how neuroinflammatory activation of glial cells was linked to α-

synuclein plaque formation and dopamine neuron loss remained to be determined (Bantle et al., 2019). In the current study, we infected recombinant inbred C57BL/6J mice with WEEV and evaluated the progression of neurological injury over 8 weeks following immunotherapy to rescue animals from lethal infection (Fig. 6). Following inoculation with WEEV, we observed progressive loss of dopaminergic neurons, altered dopamine metabolism and neuromuscular gait abnormalities consistent with a parkinsonian phenotype (Fig. 1, Fig. 7). The overall loss of neurons in the SNpc, the histopathological acellularity of infected brain regions and the persistent neurobehavioral deficits observed at 8WPI support a progressive neurodegenerative lesion in the basal midbrain rather than merely decreased expression tyrosine hydroxylase without overt neuronal loss (Alam et al., 2017).

Viruses potently stimulate neuroinflammatory activation of glia through activation of innate immune signaling emanating from pattern recognition receptors, which likely initiates a lingering inflammatory state in infected brain regions even after WEEV is completely cleared from the brain at 8WPI (Bantle et al., 2019). Determination of the number of microglia and astrocytes supports this assertion, indicating that neuroinflammatory activation of glia persisted at 8WPI after the virus was cleared from brain (Fig 1, Fig. 8). Whether this is a form of innate immunological memory in the brain to prevent recurrent microbial infection or a response to α-synuclein aggregation is unclear. The role of α-synuclein in the brain is still unknown, although α-synuclein KO rodent models suggest an immunomodulatory function, which can promote disease pathogenicity but can also offer protection from proinflammatory responses in other scenarios (Beatman et al., 2015). Other data demonstrate that α-synuclein expression increases following infection with RNA viruses which can directly or indirectly restrict viral replication by directly binding to RNA viruses or by inducing an inflammatory response in glia (Beatman et

al., 2015; Clarke et al., 2014; Lesteberg and Beckham, 2019). Interestingly, α-synuclein expression in enteric neurons increases with viral infection and stimulates innate immune activation of dendritic cells, which parallels our findings in mice infected with WEEV (Stolzenberg et al., 2017). Although we focused on the neuropathogical sequela of WEEV following intranasal infection, subsequent studies will assess whether neuroinvasion from peripheral exposure can also cause PD-like pathology.

In this study, we demonstrated that astrocyte-specific knockout of NFκB KO lowered α-synuclein plaque formation and subsequently reduced microgliosis and dopaminergic neuronal loss (Fig. 5, Fig. 9). This strongly suggests that glial inflammatory processes modulate the neurotoxicity of α-synuclein and that astrocyte-derived signaling molecules are critical to the development of an microgliosis following infection with WEEV, as we previously reported for the astrocyte-derived chemokine, CCL2, in a model of environmentally induced neuroinflammation (Liddelow and Barres, 2017; Popichak et al., 2018a).

Previous reports have suggested that α-synuclein is a catalyst of PD pathogenesis and it has been proposed that α-synuclein activates microglia and astroglia prior to loss of dopaminergic neurons (Bruck et al., 2016). Our data contradicts this, where we found α-synuclein aggregation occurred secondary to microgliosis in the SNpc following infection with WEEV (Fig. 3). Additionally, prevention of microgliosis in astrocyte-specific NFκB KO mice model drastically reduced α-synuclein protein aggregation and dopaminergic neurol loss (Fig. 5, Fig. 9) (Halliday and Stevens, 2011). Accordingly, these data suggest that neuroinflammatory activation of glia may play a causal role in the onset and progression of virally induced parkinsonism. Moreover, considering that the peak of microgliosis preceded α-synuclein plaque formation in wildtype mice and that NFκB KO in astrocytes mitigated both microgliosis and α-

synuclein aggregation, it is possible that inflammatory activation of microglia represents a critical threshold for initiating protein aggregation and neurodegeneration.

We have previously analyzed gene expression in the brains of mice following encephalitic infection with WEEV. Interestingly, we observed a significant increase in astrocytic differentiation markers such as ALDH1a1 at 4WPI. (Bantle et al., 2019). In the current study, we further characterized the inflammatory response of astrocytes in the brain following infection with WEEV by co-localizing the expression of C3 in S100β+ astrocytes to identify inflammatory A1 astrocytes (Fig. 8). Previous studies have shown that inflammatory and neurotoxic A1 astrocytes express the complement protein C3, whereas neuroprotective A2 astrocytes do not (Liddelow et al., 2017b). We found that expression of complement C3 in astrocytes began at 2WPI and persisted to 8WPI, with the highest levels of expression in the midbrain (Fig. 8). Considering that WEEV induces selective loss of dopaminergic neurons in the SNpc, this data supports previous studies showing that the selective vulnerability of dopaminergic neurons in SNpc could be modulated by activated glial cells (Kostuk et al., 2019).

Complement C3 proteins undergo proteolytic cleavage to generate chemoattractant anaphylatoxin C3a and opsins, C3b, that promote microglial migration and phagocytosis (Gutzmer et al., 2006; Zwirner et al., 1998). While assessing C3 expression in astrocytes, we noted significant C3+ P129 α-synuclein plaques in the cortex, hippocampus, and midbrain (Fig. 4). Given that phagocytic cells recognize and engulf targeted particles through complement-mediated opsonization and our previous finding that WEEV induced the P129+ microglia surrounding necrotic neurons in the SNpc, couple with a decrease of P129+ plaques at 8WPI that were C3+ (Fig. 3, Fig. 4), this suggests NFκB-dependent overproduction of C3 by astrocytes is a

mechanism to promote targeting of P129+ plaques for microglial phagocytosis (Bodea et al., 2014; Linnartz and Neumann, 2013; Schafer et al., 2012).

Although it is assumed that microglia phagocytize C3+ α-synuclein plaques for CNS clearance as a homeostatic mechanism, previous work has shown drastic differences between acute and chronic NFκB-mediated C3 in the brain, where chronically increased C3/C3aR signaling in the brain suppresses microglial phagocytosis (Lian et al., 2016). Since Complement C3 is exclusively expressed by astrocytes in the brain, we infected KO *hGfap-cre*$^{+/-}$/*Ikk2-loxP*$^{F/F}$ mice with WEEV to see whether genetic suppression of C3 would worsen or reduce α-synuclein aggregation (Fig. 5) (Kirkley et al., 2019a). Following infection with WEEV in astrocyte-specific NFκB KO mice, we noted a drastic reduction in α-synuclein aggregate formation that appeared to be devoid of C3 in all brain regions (Fig. 5). Whether these transgenic mice undergo rapid clearance of α-synuclein or if they experience a reduced inflammatory response, hindering the onset of the disease, is unclear but this will be an area of focus in future investigations. Moreover, it is continually debated whether neurons benefit from activated microglia and astroglia due to the release of trophic factors or the clearance of damaged cells and insoluble protein plaques by microglia (Bruck et al., 2016; Hall et al., 1999; Liberto et al., 2004; Nimmerjahn et al., 2005; van Rossum and Hanisch, 2004). The precise mechanism by which NFκB KO in astrocytes protects dopaminergic neurons from the neuroinflammatory effects of WEEV is not yet entirely clear but likely favors a neurotrophic A2 phenotype while suppressing an A1 phenotype, thereby mitigating the damaging effects of inflammatory cytokine and chemokine release and facilitating trophic support to surrounding neurons (Kostuk et al., 2019; Liddelow et al., 2017b).

This model of WEEV-induced neurodegeneration has the potential to elucidate novel molecular mechanisms relevant to PD and related diseases, particularly with respect to the role of glial activation as an initiating factor in neuronal injury. This study demonstrates how encephalitic infection with WEEV induces loss of dopaminergic neurons, persistent glial activation and widespread aggregation of α-synuclein in wildtype C57Bl/6 mice. We also discovered that neuroinflammatory activation of glia is critical to the initiation and progression of neuronal loss and α-synuclein aggregation following infection with WEEV. Microgliosis precedes α-synuclein aggregation in this model and NFκB KO in astrocytes drastically ameliorated α-synuclein plaque formation and reduced the number of microglia in the SNpc. This data, along with others, supports chronic neuroinflammation from glia as a detrimental and possible initiating event in the development of parkinsonian deficits following encephalitic viral infection and may be more broadly applicable to the progression of neurodegenerative diseases such as PD. This also highlights the possibility of inhibiting neuroinflammatory activation of glia through NFκB as a potential therapy. The specific inflammatory signaling molecules produced by microglia and astrocytes that modulate neuronal loss and α-synuclein protein dynamics remains to be determined but will be a focus of future studies. These results, along with our previous studies, indicate that WEEV causes lasting neurodegenerative effects through inflammatory activation of glial cells (Bantle et al., 2019).

3.5 FIGURES

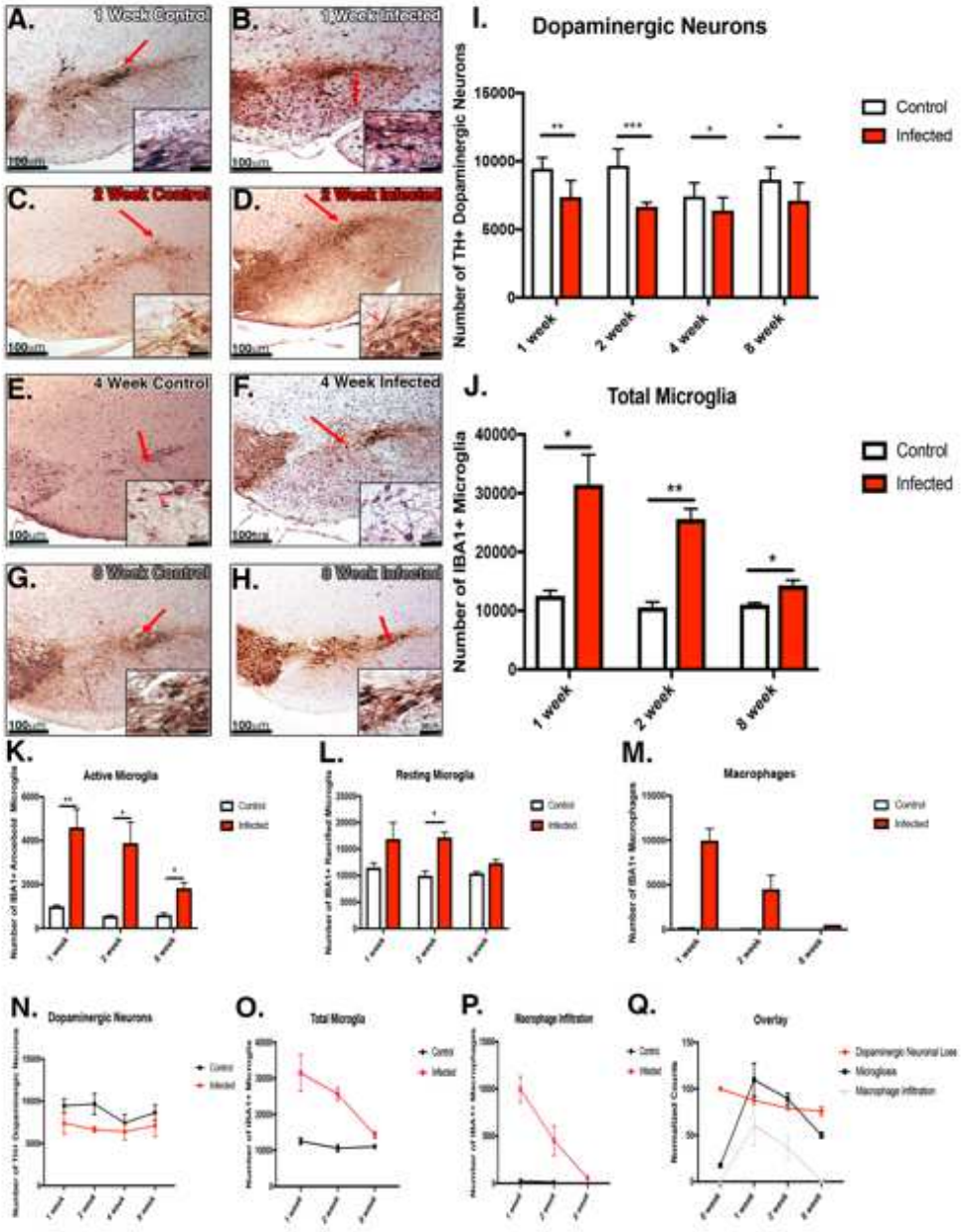

Figure 3.1. Stereological determination of dopaminergic neurons, microglia and peripheral macrophages in the SNpc. (A-H) Representative IHC images of the SNpc from mice infected or mock-infected with saline at 1,2,4, and 8WPI. (I) Stereological assessment of dopaminergic neurons in the SNpc. (J) Stereological assessment of microglia in the SN. (K-M) Quantification of resting and active microglia and infiltrating peripheral macrophages. (N-P) Linear representation of cell counts following encephalitic infection with WEEV at 1,2,4, and 8WPI. (Q) Normalized cell count overlay of dopaminergic neurons (red), microgliosis (black), and macrophage infiltration (dotted grey) at 1, 2, and 8WPI. (*$p<0.05$, ** $p<0.005$, ***$p<0.0005$, n=6-8 per group)

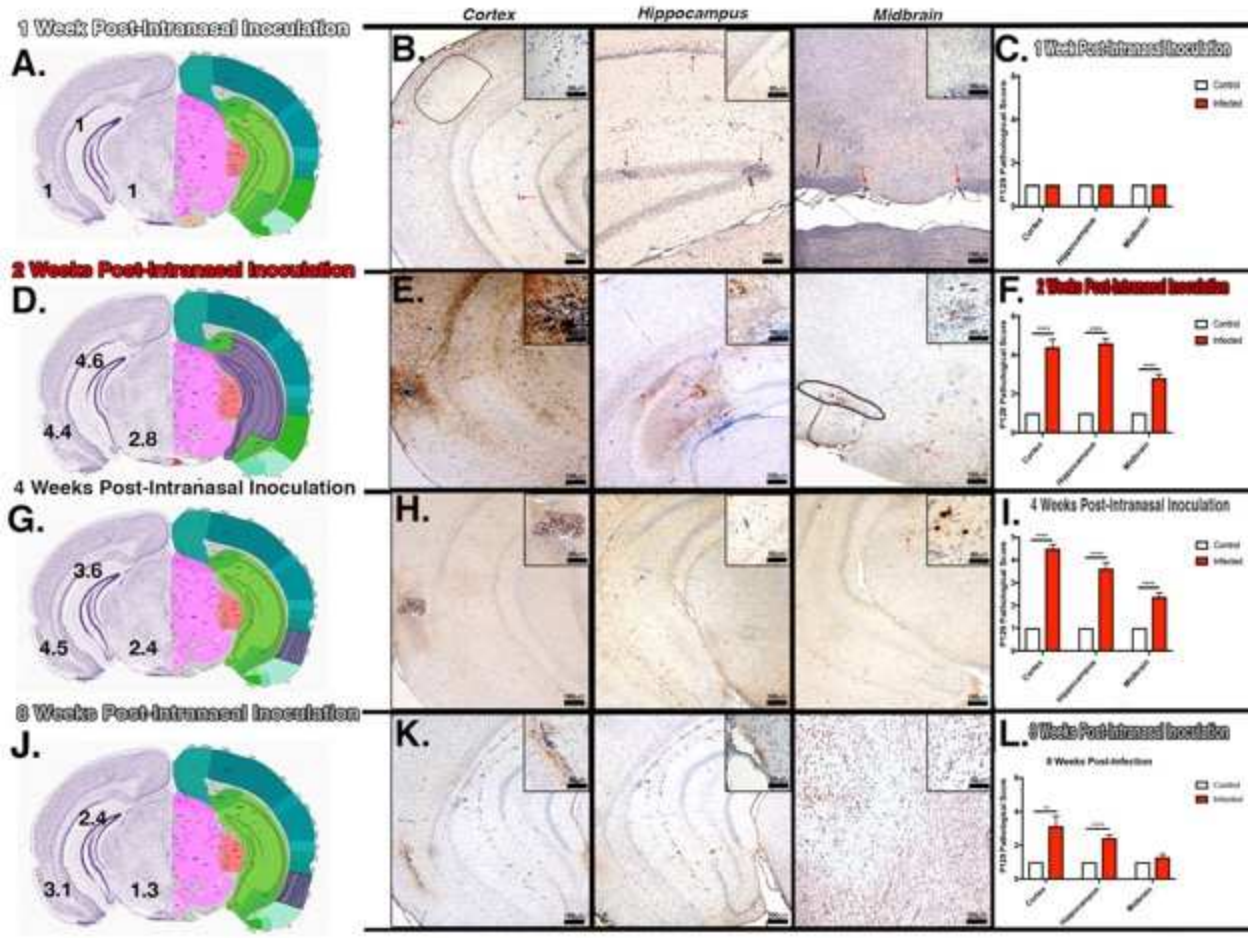

Figure 3.2. WEEV induces rapid formation of α-synuclein protein plaques in the cortex, hippocampus and midbrain of surviving wild-type mice. Representative IHC images and pathological scoring of the P129+ staining from mice infected at 1WPI (A-C), 2WPI (D-F), 4WPI (G-I), and 8WPI (J-L) with representative high magnification 60x images. Red arrow delineates regions of interest and black dotted lines represent regions of hypocellularity and P129+ staining in the SNpc. The average pathological score in the cortex, hippocampus, and midbrain at each time-point is shown is black, and the region with the most significant α-synuclein plaque load is represented in purple on the contralateral side (A, D, G, J). P129+ α-synuclein protein plaques were most significant at 2- and 4-weeks post-infection, while a slight reduction of P129+ α-synuclein protein plaque was observed at 8WPI. (*$p<0.05$, ** $p<0.005$, ***$p<0.0005$, n=6-8 per group)

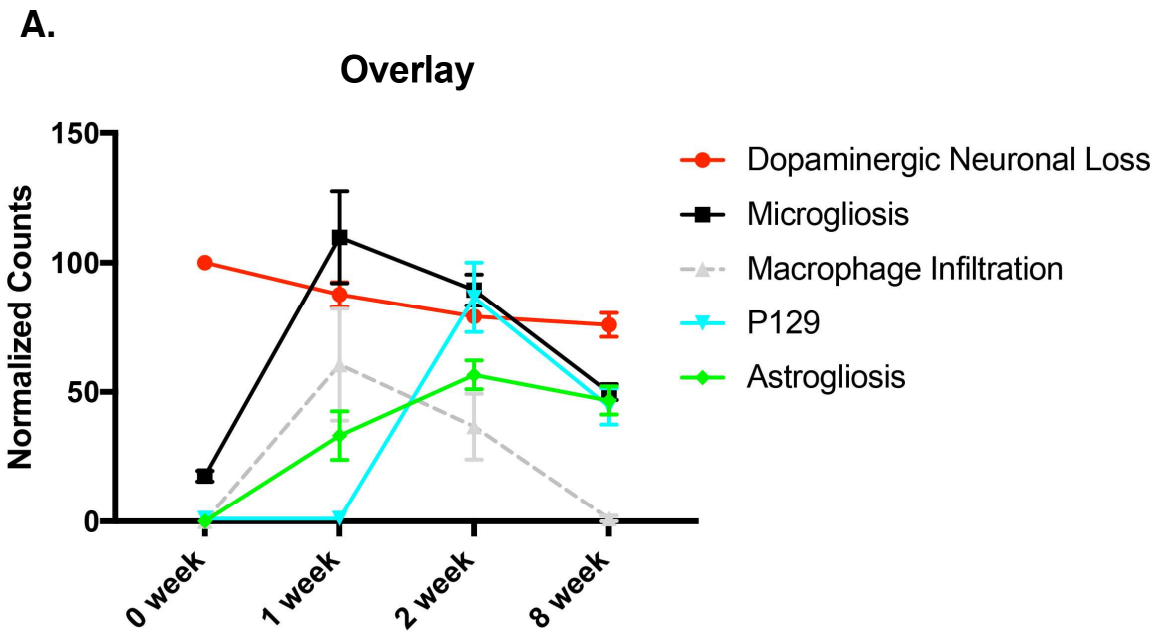

Figure 3.3. Microgliosis and peripheral macrophage infiltration precede astrogliosis and P129+ protein aggregation following intranasal infection with WEEV. (A) Representative overlay of P129+ pathological scoring (turquoise) in the SNpc with dopaminergic neuronal loss (red), astrogliosis (green), microgliosis (black), and macrophage infiltration (dottted grey) at 1, 2, and 8 WPI. Microgliosis and peripheral macrophage infiltration precede astrogliosis and P129+ protein aggregation, and astrogliosis and P129+ pathological scoring both reach their respective maximums at 2 WPI following intranasal infection with WEEV. Astrocytes numbers seem to persistent to 8WPI in comparison to the microglial curve (black). Error bars represent SEM (n=6-8 per group)

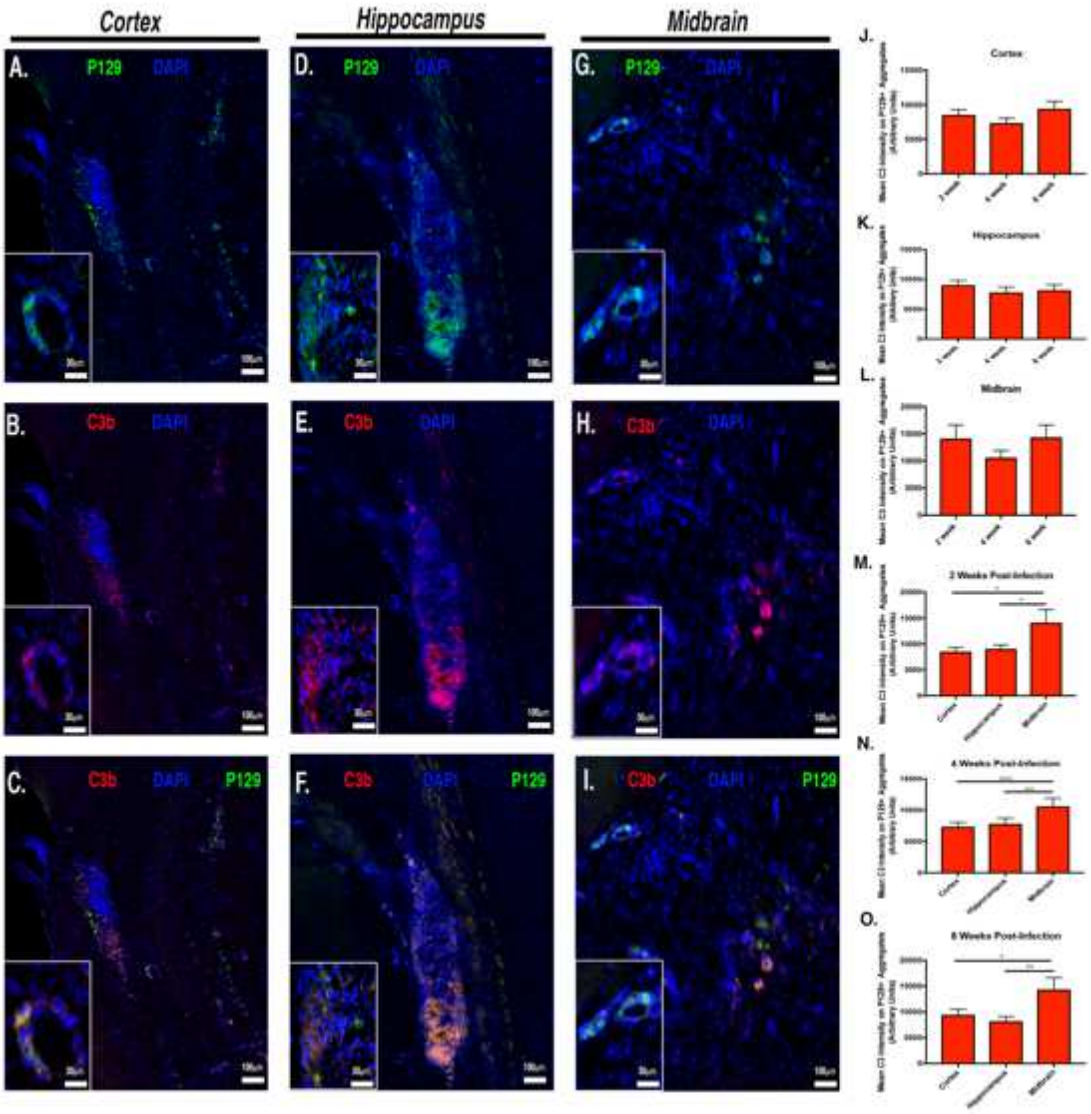

Figure 3.4. Encephalitic infection with WEEV induces opsonization of α-synuclein protein plaques in the cortex, hippocampus, and midbrain with astrocyte-derived complement C3 protein. (A-I) Representative 10x IF images of mice infected at 2,4, and 8WPI with co-immunostained brain sections. P129 (green), anti-C3b (red), and dapi (blue) in the Cortex (A-C), Hippocampus (D-F), and Midbrain (G-I). Insets are 40x high magnification representative images. Each P129+ protein plaque was treated as an individual ROI, and the level of C3b was measured on each plaque in the cortex, hippocampus, and midbrain, at 2 WPI (M), 4 WPI (N), and 8 WPI (O). Encephalitic infection with WEEV induces C3b deposition on P129+ protein plaque most significantly in the midbrain. (*$p<0.05$, ** $p<0.005$, ***$p<0.0005$, n=6-8 per group)

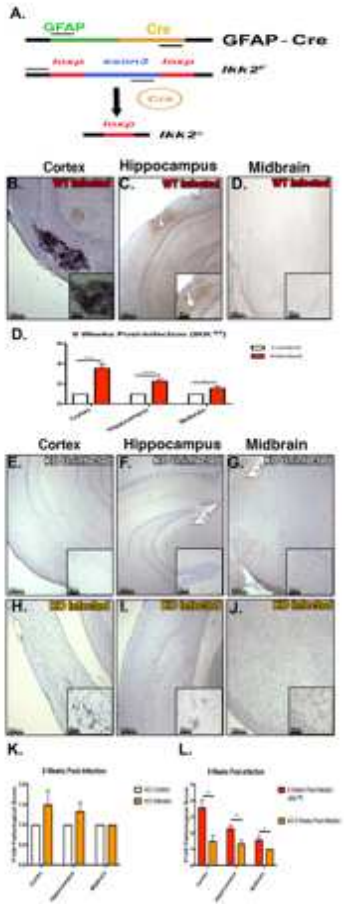

Figure 3.5. Genetic knockout of NF-κB in astrocytes reduces gliosis and α-synuclein aggregation throughout the brain. (A) Schematic illustration of the Cre recombinase under control of the human glial fibrillary acidic protein promoter (hGFAP). Hemizygous GFAP-Cre mice were crossed with I kappa B kinase 2 (Ikk2)-*lox*P mice, which facilitated selective deletion of IKK2 in astrocytes and provided a cell-specific knockout of NF-κB in astrocytes. (B-L) hGFAP-cre$^{+/-}$/IKK2$^{fl/fl}$ (KO) or hGFAP-cre$^{-/-}$/IKK2$^{fl/fl}$ (WT) animals were intranasally infected with WEEV or mock-infected (control) with saline and treated with anti-E1immunotherapy. (B-D) Representative IHC images with representative high magnification 60x inset images of the P129+ staining from hGFAP-cre$^{-/-}$/IKK2$^{fl/fl}$ mice (WT Infected). (D) Pathological scoring of the P129+ staining from hGFAP-cre$^{-/-}$/IKK2$^{fl/fl}$ mice (WT Infected). WT infected mice exhibited significant P129+ α-synuclein protein plaques in the cortex, hippocampus, and midbrain when compared to hGFAP-cre$^{-/-}$/IKK2$^{fl/fl}$ control mice. (E-J) Representative IHC images and pathological scoring of the P129+ staining from hGFAP-cre$^{+/-}$/IKK2$^{fl/fl}$ (KO infected) intranasally infected of mock-infection with saline and treated with anti-E1 immunotherapy (KO uninfected). Insets are high magnification 60x images. (K, L) KO infected mice exhibited significantly less P129+ α-synuclein protein plaques in the cortex, hippocampus, and midbrain, when compared to hGFAP-cre$^{-/-}$/IKK2$^{fl/fl}$ infected mice. There was no significant difference between KO control and KO infected mice in P129+ α-synuclein pathological scoring in the cortex, hippocampus, and midbrain (*$p<0.05$, ** $p<0.005$, n=6-8 per group).

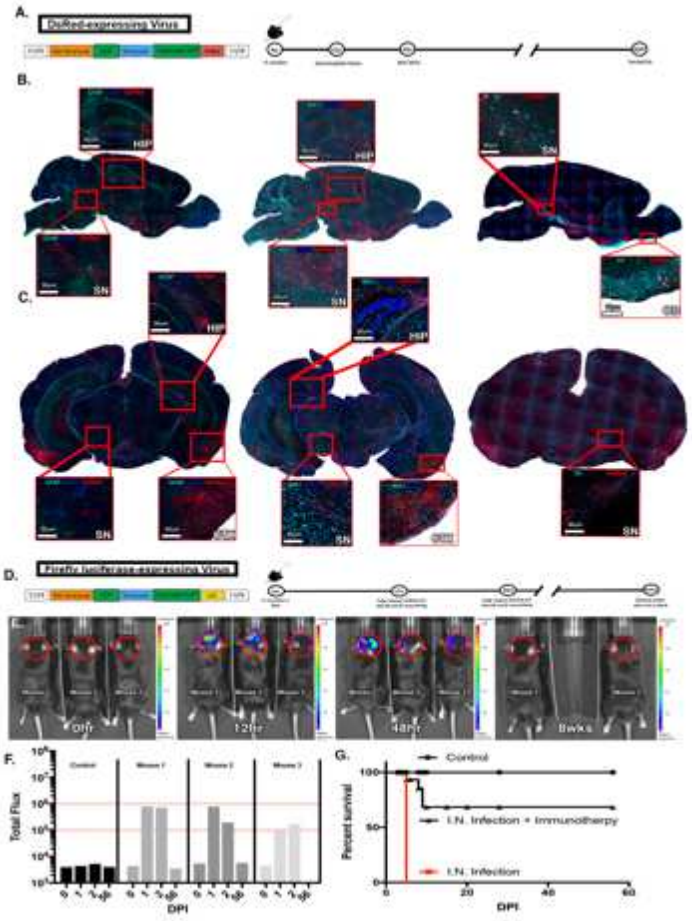

Figure 3.6. Infection with recombinant WEEV constructs coupled with immunotherapy facilitates tracking of the viral propagation and induces a persistent CNS infection without incapacitating the mice. (A, D) Schematic illustration of each recombinant viral sequence used in these studies with their associated treatment regimens. Subgenomic promoter (SPG), untranslated region (UTR). (B, C) Sagittal and coronal sections of mouse brains following intranasal inoculation with DsRed-expressing WEEV (1×10^4 PFU/ml). Intranasal inoculation results in a persistent CNS infection. WEEV exclusively replicates in neurons and not glia in the CNS. Astrocyte marker (GFAP), Microglia marker (IBA1), Dopaminergic neuronal marker (TH). (E) Pseudo-colored image of luciferase-activity on a photograph of the animals at 0hr, 12hr, 48hr, and 8WPI with WEEV-Luc. Following intranasal infection with WEEV-Luc, mice were treated with anti-E1 passive immunotherapy at 12hr and 48hr post-infection. Control mice were mock-infected with saline and treated at 12hr and 48hr post-infection with anti-E1 passive immunotherapy (anti-E1 polyclonal rabbit immune serum). Mice that did not have a sufficient encephalitic infection were removed from the study (mouse 2). (F) The anti-E1 passive immunotherapy regimen was optimized to deliver a consistent level of viral encephalitis (red lines indicate our identified range of acceptable luciferase-activity). (G) 80% of mice receiving anti-E1 passive immunotherapy treatment at 12hr and 48hr survived following intranasal infection with WEEV-Luc, while mice intranasally infected, without immunotherapy treatment, died at 4 DPI. This treatment regimen was used for every mouse throughout the entire study.

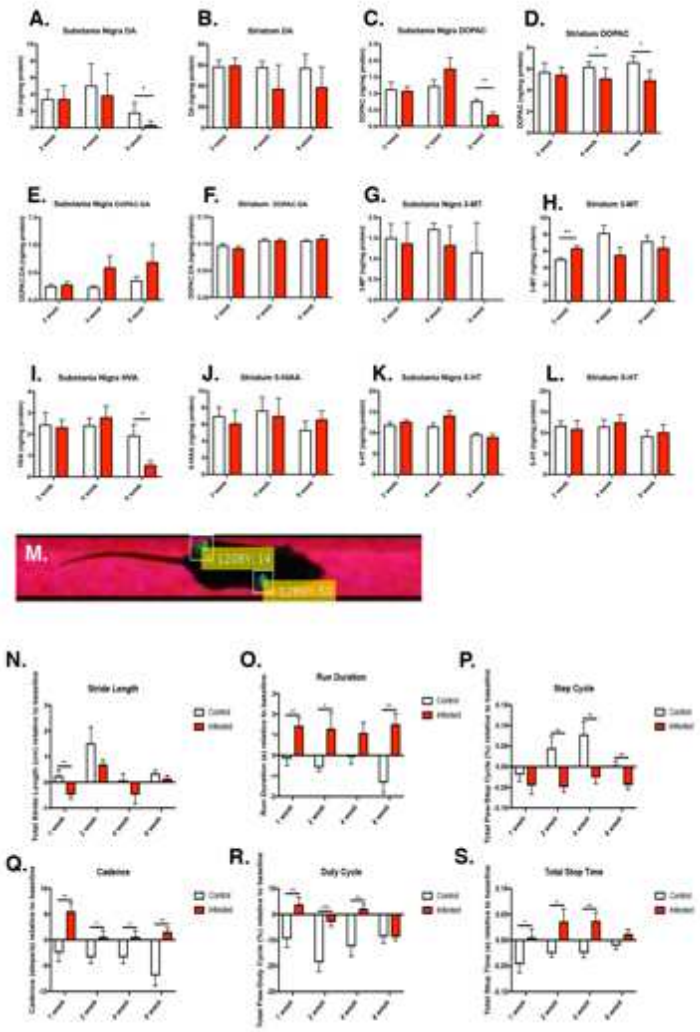

Figure 3.7. Encephalitic infection with WEEV alters catecholamine homeostasis in the brain with associated neurobehavioral abnormalities in wild-type mice. Following infection, brains were rapidly extracted and sectioned to separate the neuroanatomical regions of interest. Levels of nigral and striatal catecholamines and associated metabolites were detected by HPLC analysis with electrochemical detection. (A) Nigral Dopamine *DA* (B) Striatal Dopamine *DA* (C) Nigral metabolite 3,4-Dihydroxyphenyl-acetic acid *DOPAC*. (D) Striatal metabolite 3,4-Dihydroxyphenyl-acetic acid *DOPAC*. (E) Nigral DOPAC/DA ratio. (F) Striatal DOPAC/DA ratio. (G) Nigral metabolite 3-Methoxytyramine *3-MT*. (H) Striatal metabolite 3-Methoxytyramine *3-MT*. (I) Nigral homovanillic acid *HVA*. (J) Striatal serotonin metabolite 5-HIAA. (K) Nigral serotonin *5-HT*. (L) Striatal serotonin *5-HT*. (**P* < 0.05, ***P* < 0.005, ****P* < 0.005; *N*=4-8 animals/group). Neurochemical analysis of mice at 1WPI was not obtainable because of the BSL-3 regulations. (M) Gait measurements of stride length (N), run duration (O), step cycle (P), cadence (Q), duty cycle (R), and total stop time (S) were detected by our custom-made in-house real-time video gait analysis system. Mice infected with WEEV exhibited apparent and persistent bradykinesia when compared to control mice. (*p<0.05, ** p<0.005, ***p<0.0005, n=6-8 per group)

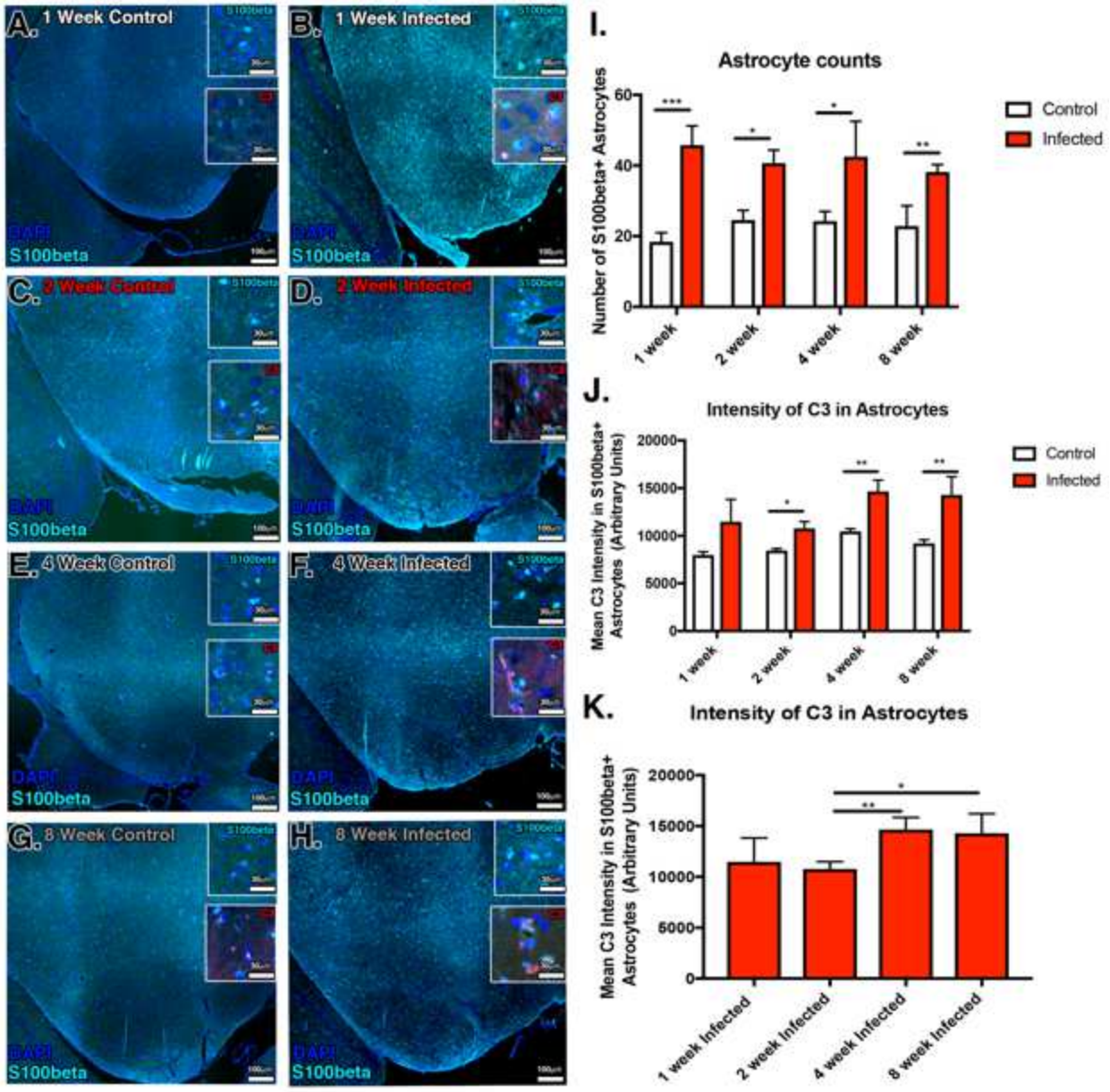

Figure 3.8. Encephalitic infection with WEEV induces astrogliosis and neuroinflammatory activation of astrocytes in the SNpc. Representative 10x montage IF images of mice infected or mock-infected with saline (control) at 1,2,4, and 8 WPI. (A-H) Sections co-immunostained with S100β (turquoise), anti-C3 (red), and dapi (blue) with 40x high magnification insets of the SNpc. (I) Quantification of S100β + astrocytes in the SNpc at 1,2,4, and 8 WPI. (J,K) Each astrocyte in the SNpc was treated as an ROI, and the level of C3 was measured in each cell. Encephalitic infection with WEEV induces an increase in C3 in S100β + astrocytes and is most significant at 4 and 8 WPI. (*p<0.05, ** p<0.005, ***p<0.0005, n=6-8 per group)

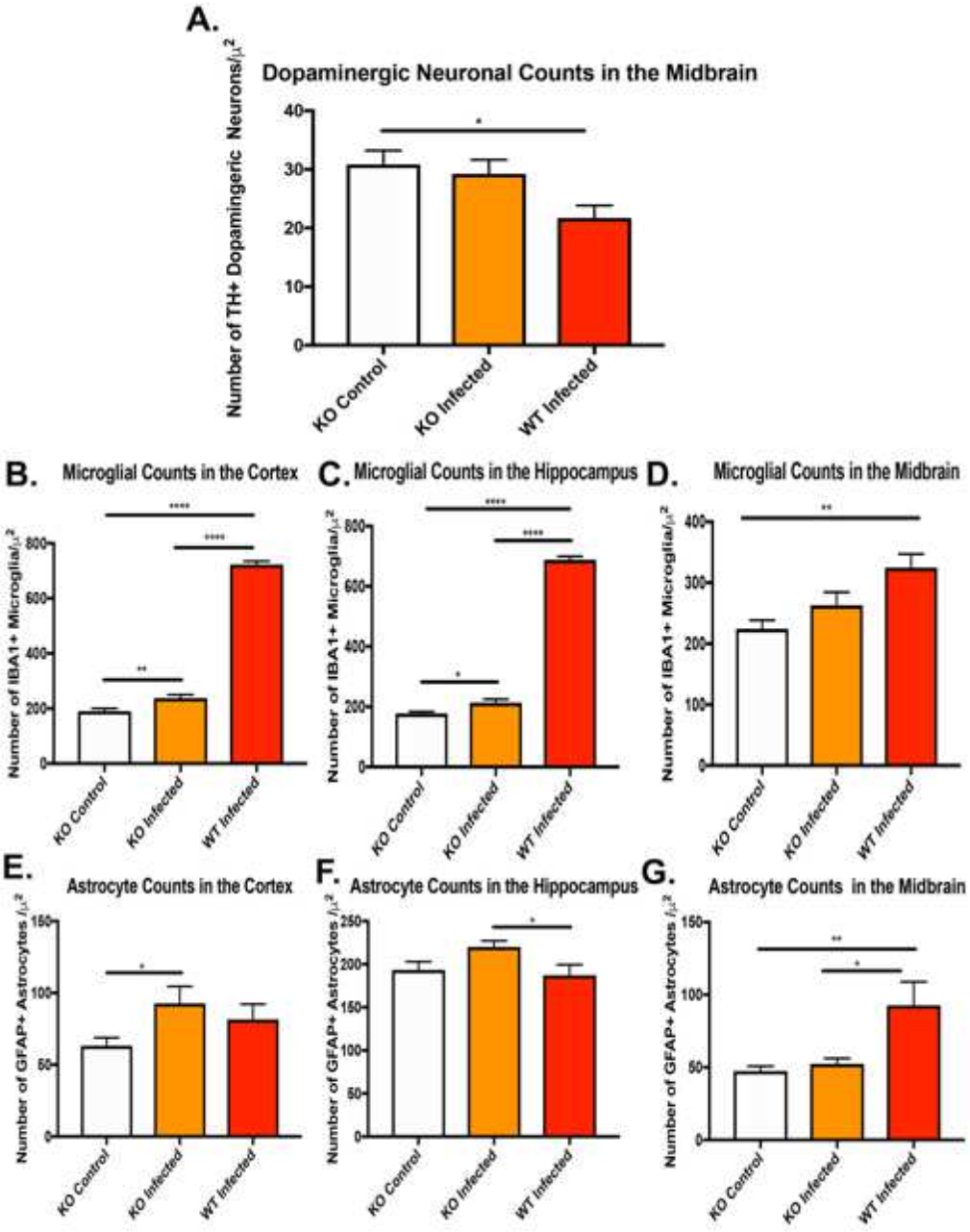

Figure 3.9. Genetic knockout of NF-κB in astrocytes reduces gliosis globally and dopaminergic neuronal loss in the SNpc. hGFAP-cre$^{+/-}$/IKK2$^{fl/fl}$ (KO) or hGFAP-cre$^{-/-}$/IKK2$^{fl/fl}$ (WT) animals were intranasal infected with WEEV or mock-infected with saline (KO control) and aged to 8 WPI. (A) Dopaminergic neurons were quantified in the SNpc, and microgliosis and astrogliosis were quantified in the cortex (B, E), hippocampus (C, F), and midbrain (D, G). (*p<0.05, ** p<0.005, ***p<0.0005, n=6-8 per group)

CHAPTER 4

JUVENILE MANGANESE EXPOSURE POTENTIATES NEURODEGENERATION FOLLOWING ENCEPHALITIC INFECTION WITH A NEUROTROPIC VIRUS AND IS DEPENDENT ON NF-κB IN ASTROCYTES

4.1 INTRODUCTION

Parkinson's disease (PD) is clinically characterized by global dysfunction of voluntary motor control, which includes bradykinesia, gait abnormalities, and resting tremors in the distal extremities(Di Rocco et al., 1996). The motor symptoms manifest when approximately 60% of the SNpc dopaminergic neurons have died, which poses a significant challenge for the development of neuroprotective therapies after diagnosis. For this reason, there is still no disease-modifying therapies for PD nor has the pathogenesis or etiology been elucidated. With the exponential increase in the number of PD cases over the last decade, the identification of etiological factors, prophylactic therapies, and common pathways underlying PD pathogenesis are urgently needed.

PD is due to the spontaneous and progressive degeneration of dopaminergic neurons in the SNpc with accompanied neuroinflammatory activation of glia and α-synuclein protein aggregation (German et al., 1989; Jang et al., 2009c). Epidemiological and experimental evidence suggest that genetic susceptibility, environmental exposures, and viral infection are possible risk factors for PD, but less focus has been placed on how these factors can act in concert. Recent evidence suggests that exposures to environmental toxins can increase neuronal susceptibility and injury from subsequent viral immune challenges (Sadasivan et al., 2017). Moreover, considerable evidence implicates microbial CNS infections as a co-factor in

neurodegenerative diseases, including PD (Bantle et al., 2019; Henry et al., 2010a; Henry et al., 2010b; Jang et al., 2012; Jang et al., 2009c; Sadasivan et al., 2012; Sadasivan et al., 2017). During the "Spanish Flu" pandemic of 1918, nearly every patient who had an acute episode of encephalitis lethargica (EL) from influenza infection went on to develop post-encephalitic parkinsonism (Hayase and Tobita, 1997). We have previously shown that intranasal infection with Western Equine Encephalitis virus (WEEV) causes significant microglial and astrocyte activation before the aggregates of proteinase-K resistant alpha-synuclein and development of parkinsonian motor impairments, which may suggest that astrocytes and microglia play a role in the initiation and progression of PD-like pathology following encephalitic infection with WEEV (Bantle et al., 2019). Additionally, multiple neurotropic viruses, including the Influenza virus H5N1, West Nile virus (WNV), Japanese encephalitis virus (JEV), and Herpes simplex virus (HSV) can induce many of the pathological features of PD such as protein aggregation, gliosis, mitochondrial dysfunction, and neuronal loss following encephalitic infection (Jang et al., 2012; Jang et al., 2009a; Jang et al., 2009b; Sadasivan et al., 2015). Although considerable evidence suggests that neuroinflammatory activation of astrocytes and microglia following viral infection may act as a critical factor in the progression of dopaminergic neuronal loss of the SNpc, whether an increased neuroinflammatory response from environmental neurotoxicant exposure could mediate an encephalitic viral infection and worsen the PD-like pathology is unknown (Bantle et al., 2019; Lesteberg and Beckham, 2019).

It is known that chronic inflammation within the CNS can sensitize neuronal tissue to secondary insults that would otherwise not induce significant neurological damage independently (de Pablos et al., 2014; Kanaan et al., 2008; Koprich et al., 2008; Pintado et al., 2012; Tansey, 2010). However, the role of astrocytes and the specific molecular pathways involved in these

two-hit models are unclear (Tjalkens et al., 2017). Among neurotoxins that could have a pronounced interaction with neurotropic viruses, Manganese ($MnCl_2$) is of interest because excessive exposure early in life can cause lasting effects on neurological function and may enhance neuroinflammation activation of microglia and astrocytes during a secondary viral infection(Doan et al., 1999; Guo et al., 2012; Koschinski et al., 2005; Lin et al., 1995; Seth et al., 2003). Although Mn is an essential dietary nutrient, excessive exposure during juvenile development can induce long-term neurological defects, termed manganism, which is due to the overproduction of free radicals, mitochondrial perturbations, inflammatory activation of glia, and depletion of antioxidant stores (Bouchard et al., 2007b; Gunter et al., 2006; Kessler et al., 2003; Liu et al., 2005; Perl and Olanow, 2007; Racette et al., 2012; Tjalkens et al., 2008). Therefore, exposure to Mn early in life may, therefore, increase susceptibility to neurodegeneration following encephalitic viral infections with WEEV.

There is a strong scientific rationale for studying the combined pathogenic effect of encephalitic infection and environment exposures on neurological outcomes, and we proposed that using a two-hit model of PD would allow a better understanding of disease etiology and enable the identification of individuals who are more susceptible to PD and related neurodegenerative diseases following encephalitic infection. Microglia are known to be the first responders to encephalitic infections and Mn in the brain, but less is known about the immunological response of astrocytes to these environmental insults. To examine whether reactive astrocyte activation contributes to neuroinflammation and disease-like progression following infection with WEEV, we used a two-hit model of environmental toxin induced neurodegeneration with juvenile exposure to Mn followed by adult infection with WEEV. These exposures were conducted in both wildtype mice and in astrocyte-specific knockout mice lacking

nuclear factor Ikappa-B kinase subunit beta knockout (KO). Dual treatment with $MnCl_2$ and WEEV in wild-type mice induced an exacerbated encephalitic infection, astrogliosis, and p129+ positive α-synuclein plaque formation in the SNpc, hippocampus, and cortex. Strikingly, KO mice dual treated with $MnCl_2$ and WEEV were protected against this exacerbated encephalitic infection, astrogliosis and α-synuclein plaque development. Collectively, this data shows that chronic neuroinflammatory of activation of astrocytes caused by excessive juvenile exposure to the environmental toxin manganese can increase neuronal susceptibility and injury following a subsequent viral immune challenge with WEEV. These observations have important implications in public health and identify key signaling pathways in astrocytes that render individuals more susceptible to neurological disease following exposures to environmental neurotoxins and viral infections.

4.2 MATERIALS AND METHODS

DsRed and firefly Luciferase recombinant WEEV constructs.

The subgenomic promoter (SGP) sequence (nucleotides 7341–7500 of viral genome) of WEEV McMillan strain was duplicated to express DsRed and Firefly luciferase. Plasmids were purified by QIAprep Spin MiniPrep Kit (Qiagen, Valencia, CA USA) and RNA was transcribed using a T7 RNA polymerase (MAXIscript™ kit, Life Technologies, Grand Island, NY USA). Recombinant plasmids were then transfected with 20 μL of total RNA using an ECM 630 electroporator (BTX Harvard Apparatus, Holliston, MA USA) in BHK-21cells (2×10^7 in 400 μL). After transfection, virus was collected and stored at −80°C before quantification of viral concentration with plaque assays. All plaque assays were run in duplicate in Vero cells before experimental use as described by Liu et al. (Liu et al., 1970). A more detailed describing of the

methods used to build these DsRed and Firefly luciferase WEEV reporter viruses can be found in previous publications (Logue et al., 2009; Phillips et al., 2016; Phillips et al., 2013).

Generation of astrocyte-specific knockout mice.

Astrocyte-specific knockout mice for IKK2 were generated as previously described (Kirkley et al., 2019b). Briefly, *hGfap-cre*$^{+/-}$ (Cat#: 004600; Jackson Laboratories) mice were backcrossed on a C57/BlJ6 background for twelve generations before crossbreeding with *Ikk2-loxP*$^{+/+}$mice. Four generations of crossbreeding were conducted to acquire *hGfap-cre*$^{+/-}$/*Ikk2-loxP*$^{+/+}$ (KO). Littermates lacking Cre recombinase (*hGfap-cre*$^{-/-}$/*Ikk2-loxP*$^{+/+}$) were used as genotype controls for the study.

Viral infections and manganese chloride treatment regimen in control and transgenic mice.

Procedures were approved by Colorado State University Institutional Animal Care and Use Committee (IACUC) and were conducted in compliance of National Institute of Health guidelines. Infected mice were housed in a biosafety level 3 (BSL-3) facility at the Infectious Disease Research Center on the campus of Colorado State University. C57BL/6 astrocyte-specific knockout mice (*Gfap -Cre*$^{+/-}$ mice with *Ikk2-loxP*$^{+/+}$) and control mice (*Gfap -Cre*$^{-/-}$ mice with *Ikk2-loxP*$^{+/+}$) were housed on a 12 hr light/dark cycle in a temperature-controlled room (maintained at 22-24°C). At day P21, mice were administered $MnCl_2$ (50mg/kg/day) or normal drinking water by monitoring water intake and weight gain for 30 days. At P51 mice were placed back on regular drinking water and intranasally administered WEEV-DsRed, WEEV-Luc, or saline. Infections with recombinant WEEV were performed as previously described (Bantle et al., 2019). Mice were anesthetized with isoflurane (Minrad Inc, Bethlehem, PA USA) through an XGI-8 anesthesia system (Caliper Life Sciences, Waltham, MA USA) connected to the IVIS 200 (Caliper Life Sciences, Waltham, MA USA) bioluminescence imaging system. Lightly

anesthetized mice were then administered 20 μL dropwise on the nostrils of either DsRed-WEEV or Luc-WEEV at a concentration of 1×10^4 PFU/ml. Mice infected with DsRed-WEEV were euthanized at four days-post-infection and used to characterize the viral spread of WEEV in $MnCl_2$ treated and control mice. All mice infected with Luc-WEEV received a subcutaneous administration of luciferin at a dose of 150 mg/kg, 10-15 minutes prior to imaging on an IVIS imager. For background subtractions, uninfected mice were used as image controls. All mice were imaged on the same exposure time at 2 minutes, under standard settings for the IVIS 200 camera. Image analysis was performed on Living Image 3.0 software (Caliper Life Sciences, Waltham, MA USA). Total light emission from each mouse was determined by creating a region of interest (ROI) of standard size for each mouse and collecting light emission data. All mice received the same level of encephalitic infection by creating a threshold for significant BLM of 5×10^3 p/s/cm^2/sr, and to prevent mortality, infected mice and control mice received an anti-E1 immunotherapy intraperitoneally at 12 and 48hrs post-infection. After infection, mice were aged an additional eight weeks before euthanasia and brain tissue extraction.

Generation of anti-alphavirus E1 for passive immunotherapy.

The details of this method can be viewed in our previous publication (Bantle et al., 2019). Rabbits were vaccinated with four doses, in two increments of recombinant WEEV McMillan strain E1-ectodomain antigen (10 μg antigen/dose) in an immunological adjuvant comprised of polyI:C (dsRNA analog), ODN 1826 (unmethylated CpG DNA) (InVivoGen), and TiterMax Gold to a final concentration of 0.1 mg/mL. After eight weeks of dosing, rabbits were terminally bled for serum collection. Before treatment in mice, rabbit serum was heat-inactivated at 56°C for 30 minutes and stored at -80°C. ELISA assays were run on anti-E1 serum against E1 antigen on coated titration plates before use in the mice. Naïve serum was also collected from

control animals for ELISA controls. Only serum with an antibody titer measurement greater than 26,000 reciprocal value was used in the study.

Tissue preparation and sectioning.

Ten-day and eight-week post-infection with Luc-WEEV, animals were terminally anesthetized with isoflurane and transcardially perfused. The brains were then extracted, fixed in 3% paraformaldehyde at 4°C and later processed for paraffin embedding and sectioned at 8 microns on a microtome through the anatomic midbrain and mounted on polyionic slides (Superfrost-plus, Fisher Scientific) (Miller et al., 2011; Smeyne et al., 2016).

Immunofluorescent Staining and Imaging.

Coronal sections were deparaffinized and immunostained using formalin-fixed, paraffin-embedded 8 μm brain sections using a Leica Bond RXM automated robotic staining system. Sections were immunohistochemically stained on a Leica Bond-III IHC automated stainer using Bond Epitope Retrieval Solution 2 for 20 minutes and then incubated in primary antibody with anti-tyrosine hydroxylase (TH; 1:500; Millipore AB152)to identify dopaminergic neurons, anti-Neuronal Nuclei (NeuN; 1:250, Millipore; MAB377) to identify total neurons, anti-glial fibrillary acidic protein (GFAP; 1:500; DAKO Z0334) to identify astrocytes, anti-calcium adaptor binding protein 1 (Iba-1; 1:250; WAKO 016-20001), and anti-serine phosphorylated 129 (p129; 1:100; WAKO pSYN#64) to label α-synuclein plaques, per our previously published methods (Hammond et al., 2017; Miller et al., 2011). Immunofluorescent secondary antibodies were diluted in TBS at a 1:500 dilution. Immunofluorescent secondary antibodies included anti-rabbit, anti-mouse, and anti-goat in 488, 555, and 647. Immunostained sections were imaged by creating a montage imaging of individual 10X images using a Hammatsu Flash4.0 digital CMOS

camera, ProScan III stage controller (Prior, Rockland, MA USA) and CellSens Dimension software (version 1.12, Olympus, Center Valley, PA, USA). Each region of interest representing distinct anatomical nuclei (SNpc, Hippocampus, and Cortex) were analyzed on each composite montage image.

Quantification of infected neurons.

Dsred-WEEV infected coronal sections were deparaffinized and montage imaged with a 10X objective with a Hammatsu Flash4.0 digital CMOS camera, ProScan III stage controller (Prior, Rockland, MA USA) and CellSens Dimension software (version 1.12, Olympus, Center Valley, PA, USA). Each region of interest (ROI) was delineated with reference to the Allen brain atlas. Two brain sections per animal were selected from the same anatomical regions. DsRed-WEEV infected cells were quantified after imaging with the use of an adaptive threshold with shape factor and area (um^2) object filters for semi-automatic cell detection (Tapias et al., 2013). Infected (DsRed+ cells) in selected brain regions, cell number was divided over the area (μm^2) of the region. The sum of the two sections was averaged. The investigator was blinded from all experimental groups during imaging and infected cell quantification. (N=6-8 per group)

Glial cell quantification.

Formalin-fixed, paraffin embedded 8 μm brain sections were immunofluorescently labeled as described above using on a Leica Bond automated stainer using Leica Bond RXM automated robotic staining system. $GFAP^+$ and $Iba\text{-}1^+$ cells were costained with anti-TH (Abcam 76442) to demarcate the SN. A total of two sections/animal were selected that the same anatomical regions of SN, Hippocampus, and Cortex and imaged with a 10X objective with a Hammatsu Flash4.0 digital CMOS camera, ProScan III stage controller (Prior, Rockland, MA

USA) and CellSens Dimension software (version 1.12, Olympus, Center Valley, PA, USA). ROIs were created with reference to the Allen Brain Atlas. Following semiautomated quantification of $GFAP^+$ and Iba-1^+ cells an adaptive threshold with shape factor and area (um^2) object filters for automatic cell detection, based on previously published algorithms (Tapias et al., 2013). Detected cell number was divided over the area (μm^2) of the region. The sum of the two sections was averaged. The investigator was blinded from all experimental groups during imaging and cell quantification. (N=6-8 per group)

Pathological scoring of phospho-serine 129+ α-Synuclein plaques.

Formalin-fixed, paraffin embedded 8 μm brain sections were immunofluorescently labeled as described above using on a Leica Bond automated stainer using Leica Bond RXM automated robotic staining system. Anti-phospho Ser129 (P129) antibody (1:1000, clone pSYN#64, WAKO) labeling plaques underwent neuropathological scoring in the cortex, hippocampus, and midbrain on infected and uninfected brain sections by a blinded investigator (Jang et al., 2009a). The pathological scoring method was adapted from previous reports (Rey et al., 2018; Rey et al., 2016). The presence of P129+ plaques was assessed on two coronal sections per animal with an *N*=6-8 mice per group. Each section was analyzed at a 10× magnification, and a score of 1 to 5 was assigned to each brain region from a single coronal brain section and scored as follows: 1 = no aggregates, 2 = very sparse and one to two P129+ cells, 3 = mild with less than ten P129+ cells, 4 = dense with more than ten P129+ cells, 5 = very dense with more than 20 P129+ cells involved. The two scores for each individual section were averaged for each mouse.

Statistical Analysis

All data proved in this manuscript was presented as mean +/- SEM, unless otherwise noted. The experimental values from each mean were analyzed with a Grubb's (α=0.05) test for exclusion of significant outliers, and the differences between each experimental group were analyzed by a one-way ANOVA following a Tukey *post hoc* multiple comparisons test. Significance was identified as $^{++}P < 0.01$, $*P < 0.05$, $**P < 0.01$, $***P < 0.001$, $****P < 0.0001$. The N=6-8 per group for the entirety of this study, unless stated otherwise. All statistical analysis was conducted using Prism (version 6.0; Graph Pad Software, San Diego, CA).

4.3 RESULTS

Juvenile manganese chloride exposure induces an exacerbated encephalitic infection with WEEV in adulthood.

At normal physiological levels, $MnCl_2$ is not toxic to neurons; however, when susceptible populations—such as juveniles—are exposed to elevated levels of $MnCl_2$, neurotoxic effects are observed in the globus pallidus (Gp), striatum (caudate-putamen, Cp), substania nigra (SN), and hippocampus. This neurotoxicity stems from the overproduction of numerous reactive oxygen and nitrogen species, and increased production and release of pro-inflammatory cytokines from reactive glia (Moreno et al., 2011b; Zhang et al., 2003). Additionally, our lab has previously established that intranasal infection with WEEV-DsRed propagates along the neuronal axis from the olfactory bulb to the entorhinal cortex, hippocampus, and nigrostriatal pathway by 4 days post-infection (DPI). Furthermore, previous reports have shown that elevated levels of essential metals can modulate the severity and distribution of infection (Guo et al., 2012). However, whether $MnCl_2$ has the capacity to modulate the infectivity of WEEV in PD relevant brain

regions is unknown. In order to evaluate the level of WEEV in PD relevant brain regions of mice pretreated with $MnCl_2$ during juvenile development, mice were treated with $MnCl_2$ or water followed by intranasal infection with WEEV-Dsred (**Fig 1 A, B).** The PD relevant brain regions were delineated with reference to the Allen Brain Atlas, and infected cells were quantified in the globus pallidus (Gp), striatum (caudate-putamen, Cp), substantia nigra (SN), and hippocampus (**Fig 1 C-J).** Representative montage images are depicted in (**Fig 1 C-J).** Based on quantitation of DsRed+ cells, pretreatment with $MnCl_2$ during juvenile development significantly increased the severity of encephalitic infection with WEEV in the globus pallidus (Gp), striatum (caudate-putamen, Cp), substantia nigra (SN), and hippocampus relative to control mice that were pretreated with water (**Fig 1 C-J).**

Astrocyte specific NF-κB knockout reduces the infectivity of WEEV following juvenile exposure to $MnCl_2$.

Both manganese and viral induced parkinsonism can induce lasting effects on the neuroinflammatory status of astrocytes and microglia into adulthood, which could play a fundamental role in $MnCl_2$ induced potentiation of WEEV infection severity in PD relevant brain regions (**Fig 1**). We have previously shown that infection with WEEV causes activation of microglia and astrocytes, selective loss of dopaminergic neurons, and the formation of insoluble α-synuclein protein plaques that is attenuated with astrocyte-specific NFκB KO mice, suggesting that glia play a critical role in initiating PD-like pathology following encephalitic infection with WEEV(Bantle et al., 2019). Whether juvenile $MnCl_2$ could induce a worsened pathology to WEEV through neuroinflammatory activation of astrocytes was unclear. To assess this question, we pretreated astrocyte-specific NFκB KO mice and control mice with $MnCl_2$ or water,

respectively, during juvenile development and infected with WEEV-Luc or vehicle (**Fig 2A,B**) in adulthood. Mice were then aged for eight weeks post-infection, at which point viral load is undetectable in the CNS (Bantle et al., 2019). The aforementioned treatment groups are illustrated in Figure 2B. Wild-type mice pretreated with $MnCl_2$ showed a significant increase in luciferase activity at 72 hours postinfection (72 HPI) following infection with WEEV-Luc when compared to wild-type mice only receiving water. Genetic inhibition of astrocyte-specific NFκB inflammatory activation attenuated this finding (**Fig 2G**). Strikingly, due to the severity of the infection, 70% of mice pretreated with $MnCl_2$ died at ten days post-infection with WEEV; this effect was reduced in astrocyte-specific NFκB KO mice (**Fig 2 G,H).** Together, these data suggest that juvenile exposure to $MnCl_2$ for 30 days from postnatal days 21 – 51 modulates the severity of encephalitic infection of WEEV through NFκB transcriptional activation in astrocytes.

Encephalitic infection with WEEV induces astrogliosis in the substantia nigra and cortex that is reduced with astrocyte specific NF-κB KO.

Due to the severity of encephalitic infection with WEEV and unforeseen death in the dual treatment group, the wild-type $MnCl_2$ + WEEV treatment group could not be continued for the rest of the study. To accommodate this unforeseen complication and assess whether juvenile Manganese exposure could potentiate encephalitic infection with WEEV, the study was repeated, and tissue was collected at ten-days post-infection. Given that A1/M1 reactive glial cells primarily express damage associated molecular patterns (DAMP) and pathogen associated molecular patterns (PAMP) in the brain , and that astrogliosis is a well-described clinical feature of magnesium and post-encephalitic parkinsonism, we next assessed the relative number of reactive astrocytes in PD relevant brain regions at 8 weeks post-infection in each treatment

group(Clarke et al., 2014). Using immunofluorescent based GFAP+ astrocyte quantification, we characterized the relative number of reactive astrocytes in the SN, hippocampus, and cortex of wild-type and KO mice treated with either $MnCl_2$ alone, WEEV alone, or dual treated with $MnCl_2$ and WEEV. A significant increase in the relative number of GFAP+ astrocytes was noted in the SN and Cortex, but not in the hippocampus following infection with WEEV alone in wild-type mice. Additionally, astrogliosis was reduced in KO animals following infection with WEEV in the SN and Cortex as well (**Fig 3A-H).**

Juvenile manganese chloride exposure solely potentiates α-synuclein plaques in the substantia nigra.

Our lab has previously shown that microgliosis and macrophage infiltration into the brain occurs before activation of astrocytes and α-synuclein protein plaques in the cortex, hippocampus, and midbrain—and that astrocyte-specific NFκB KO reduced α-synuclein plaque load, dopaminergic neuron loss, and gliosis in the SNpc (Bantle et al., 2019). Given that juvenile manganese chloride exposure induced an exacerbated encephalitic infection with WEEV in adulthood and was attenuated with astrocyte-specific NF-κB knockout, we then questioned whether this increased infectivity of WEEV correlated with potentiation of α-synuclein plaque formation in infected brain regions. Using a previously established pathological scoring system, the severity of α-synuclein plaques were scored in SN, hippocampus, and cortex of wild-type and KO mice treated with $MnCl_2$ or water and infected with WEEV or mock-infected with saline (**Fig 4**). Infection with WEEV alone in wild-type mice induced significant α-synuclein plaque formation in the substantia nigra, hippocampus, and cortex (**Fig 4 A-H**). KO mice infected with WEEV alone had a significant reduction of α-synuclein aggregates in the substantia nigra, hippocampus, and cortex. Interestingly, dual treated KO mice experienced a potentiation of α-

synuclein aggregate formation when compared to KO mice that were infected with WEEV alone (**Fig 4 F**).

4.4 DISCUSSION

Considerable evidence suggests that viral CNS infections directly or indirectly influence the onset and progression of sporadic and postencephalitic PD through neuroinflammatory activation of glia in the basal ganglia (Mattson, 2004; Sadasivan et al., 2017). Our previous work has shown that $MnCl_2$ does not typically induce overt neurotoxicity, but that elevated levels of $MnCl_2$ during juvenile development can cause motor disturbances and persistent inflammatory activation in glia that is associated with neuronal injury in the cortex and basal midbrain in adulthood (Gunter et al., 2006; Moreno et al., 2009a). However, whether $MnCl_2$ exposure could potentiate neurodegeneration through neuroinflammatory activation of glia in a model of postencephalitic parkinsonism was unknown (Moreno et al., 2009a). In the current study, we used a two-hit model of environmental neurodegeneration with juvenile exposure to manganese, followed by adult infection with WEEV. To assess the role of inflammatory activation in astrocytes, these exposures were conducted in both wildtype mice and in astrocyte-specific knockout mice lacking nuclear factor Ikappa-B kinase subunit beta knockout (IKK2-KO).

WEEV and other neurotropic viruses can induce many of the pathological features of PD, such as protein aggregation, oxidative stress, autophagy/mitophagy defects, neuroinflammation, and neuronal loss in the substantia nigra par compacta, but whether exposure to $MnCl_2$ early in life could increase the severity of an encephalitic infection and accelerate the development of post-encephalitic parkinsonism was unknown. To assess if juvenile treatment with $MnCl_2$ could modulate the infectivity and distribution of WEEV, juvenile mice were pretreated with $MnCl_2$ in drinking water or water alone and infected with WEEV-DsRed (**Fig 1**). Strikingly, exposure to

the Mn increased the level of viral replication in the multiple PD relevant brain regions. The mechanisms underlying the tropism of WEEV for these brain regions are still unclear. Although the neuroanatomical architecture likely influences WEEV's infectious path after intranasal inoculation, WEEV replication is also dependent on the intracellular oxidative environment in cells (Gullberg et al., 2015). The replicative protein of WEEV, nsP1 (non-structural protein 1), is sensitive to oxidative changes and needs a highly oxidative intracellular environment for viral replication. Given that overexposure to Mn in susceptible populations can induce mitochondrial perturbation and increase production of free radicals in caudate-putamen, globus pallidus, SN, and hippocampus, WEEV—along with other RNA viruses—may utilize the increased oxidative environment to enhance viral replication (Gunter et al., 2006; Ronca et al., 2017; Wong et al., 2007; Wyrsch et al., 2012).

Additionally, after uptake in the brain, Mn primarily accumulates in the mitochondria of astrocytes and neurons, which can induce oxidative changes and neuroinflammatory activation of glia through NF-kB activation in the brain (Gavin et al., 1999; Lai et al., 1999; Liccione and Maines, 1988; Morello et al., 2008; Tjalkens et al., 2017). NF-kB is ubiquitously expressed throughout the CNS and when activated, positively regulates neuroinflammatory genes in glia and induces prosurvival/synaptic plasticity genes in neurons. Considering that NF-κB regulates the expression of multiple neuroinflammatory cytokines and chemokines in activated glial cells and prosurvival genes in neurons, we used an astrocyte-specific NF-κB knock mice to assess the role of inflammatory activation in astrocytes in this two-hit exposure model (**Fig 2**). Interestingly, despite receiving immunotherapy concurrent with viral infection, survival rates in the dual treated wildtype mice were extremely low (n=1), while selective NF-κB KO in astrocytes significantly reduced the level of viral replication and morality (**Fig 2 B-G**). These

data likely highlight how astrocyte-based neuroinflammatory responses following encephalitic infection can act in concert with Mn induced oxidative stress and mitochondrial dysfunction.

Depending on the severity of the inflammatory response, astrocytes and microglia can adopt long-lasting neurotoxic and proinflammatory phenotypes that help to combat infection; however, these phenotypic shifts may also contribute to neuronal degeneration (Hirsch and Hunot, 2009). We have shown that WEEV selectively infects the SNpc, hippocampus, and cortex following intranasal inoculation, but only induces dopaminergic cell loss in the SNpc (Bantle et al., 2019). The mechanisms driving this selective vulnerability of dopaminergic neurons as still unclear. Accordingly, evidence has suggested that the selective vulnerability of dopaminergic neurons in SNpc could be due to phenotypic differences in astrocytes and microglia (Kostuk et al., 2019). Given that WEEV induced selective astrogliosis in this SNpc (**Fig 3A**), and selective loss of dopaminergic neurons in the SNpc, this may provide additional support for glial driven selective vulnerability in postencephalitic PD. Additionally, astrogliosis was attenuated in KO mice and absent in the hippocampus (**Fig 3G**).

Unfortunately, due to the unforeseen death in the wild-type dual treatment group, we could not fully assess astrogliosis in wild-type mice dual treated with $MnCl_2$ and WEEV (**Fig. 2G**). To accommodate this complication, the study was repeated at ten-days post-infection. Additionally, we did no observe potentiation of astrogliosis in KO mice infected with WEEV when compared to KO mice pretreated with $MnCl_2$ and infected with WEEV (**Fig 3F-H**), which could explain how $MnCl_2$ induced potentiation of WEEV is mediated through neuroinflammatory activation of astrocytes.

The mechanisms driving this increased susceptibility are unclear, but considering previous reports, these data suggest that Mn exposure during juvenile development likely induces chronic neuroinflammatory activation of glia that produces oxidative stress and depletion of antioxidant stores. This increased oxidative environment may facilitate WEEV's increased replication in the caudate, globus pallidus, SN, and hippocampus. Additionally, WEEV induces the formation of proteinase-K resistant α-synuclein plaques in the SN, hippocampus, and cortex by eight weeks post infection (Bantle et al., 2019). Given the increased level of viral replication in the dual treatment group (**Fig 1,2**), we questioned whether this correlated with a potentiation of α-synuclein plaques as well. Unfortunately, we were unable to make this assessment in wild-type mice, but we did note an increase of α-synuclein protein aggregation exclusively in SN of KO mice dual treated with $MnCl_2$ and WEEV when compared to KO mice infected with WEEV alone (**Fig 4**). Interestingly, the potentiation of α-synuclein protein aggregation was exclusive to the SN. Previous reports have shown that Mn can directly bind α-synuclein to facilitate its misfolding, but whether this potentiation is due to the increased accumulation of Mn in the SN or an increased glial response in the SN is unclear (Harischandra et al., 2019). The functional role of synuclein and related amyloid proteins are still debated, and increasing evidence is beginning to suggest that α-synuclein and related proteins could have an immunological role, mediating the neuroinflammatory response to microbes in the brain (Benskey et al., 2018; Eimer et al., 2018). We found that KO animals were protected from α-synuclein protein aggregation, supporting a possible connection between astrocyte NF-kB activation in protein misfolding. Collectively, these data suggest that the induction of α-synuclein protein aggregation following infection with WEEV is mediated by the production of astrocyte-derived pro-inflammatory cytokines. The specific transcriptional profile and

inflammatory molecules involved in the α-synuclein protein aggregation following infection with WEEV will be a focus of future studies.

In summary, a better understanding of the potential neuroinflammatory mechanisms driving postencephalitic PD would enable identification of susceptible populations, and although the pathogenesis of postencephalitic parkinsonism is still unclear, this study suggest that juvenile environmental exposures with $MnCl_2$ can causing lasting neuroinflammatory effects in glia that could be a critical initiating and potentiating factor in post-encephalitic PD (Lesteberg and Beckham, 2019). Together, these data show that overexposure to $MnCl_2$ may cause lasting neuroinflammatory effects from chronic activation of NF-κB in astrocytes. Therefore, astrocyte-based neuroinflammatory response following encephalitic infection could act in concert with oxidative stress and mitochondrial dysfunction induced by $MnCl_2$, to facilitate neuroinflammatory activation and protein misfolding.

Although the molecular pathways and specific signaling molecules connecting these pathological findings are unclear, we hope that these data inspire future studies using two-hit exposure models of PD. Correlating with our previous studies, these data also suggest that glia may play a critical role in initiating PD-like pathology following encephalitic infection with WEEV (Bantle et al., 2019). We show that KO animals were protected from WEEV-induced PD pathology and associated astrogliosis, which supports the importance of astrocyte NF-kB activation in post-encephalitic parkinsonism, and therefore, inhibition of NF-κB signaling in glial cells could be a promising therapeutic strategy for the prevention of neuroinflammatory induced neurodegeneration. Furthermore, excessive juvenile exposure to environmental neurotoxicants may increase neuronal susceptibility and injury following a subsequent viral immune challenge. These observations could have important implications in public health and facilitate the

identification of individuals more susceptible to neurological disease following exposures to environmental neurotoxins and viral infections.

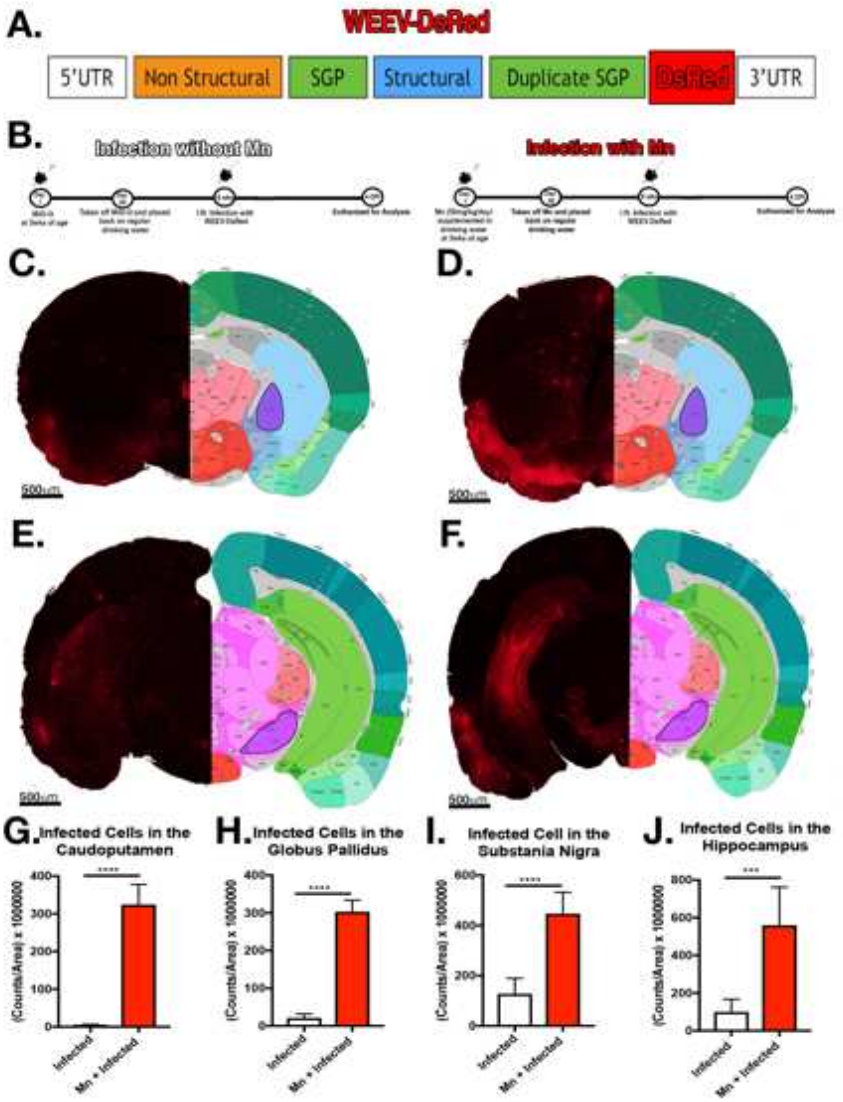

Figure 4.1. Pretreatment with $MnCl_2$ induces a worsened encephalitic infection with WEEV in multiple PD relevant brain regions. (A) Structure of vectors for each recombinant virus used in the study. Subgenomic promoter (SPG), untranslated region (UTR). Wild-type mice were infected with WEEV-DsRed to track the cellular infectivity. **(B)** To assess if juvenile treatment with $MnCl_2$ modulated the infectivity and distribution of WEEV, mice were either treated $MnCl_2$ in drinking water or water alone and either infected with WEEV-DsRed. **(C-D)** Representative striatal sections of mice pretreated with Mn or water and infected with DsRed producing virus. **(E-F)** Representative nigral sections of mice pretreated with $MnCl_2$ or water and infected with WEEV-DsRed. **(G-J)** Quantification of infected neurons in the caudate-putamen, globus pallidus, substantia nigra, and hippocampus (left – right). Mice pretreated with Mn (Red) or water (white). (*$p<0.05$, ** $p<0.005$, ***$p<0.0005$, n=6-8 per group)

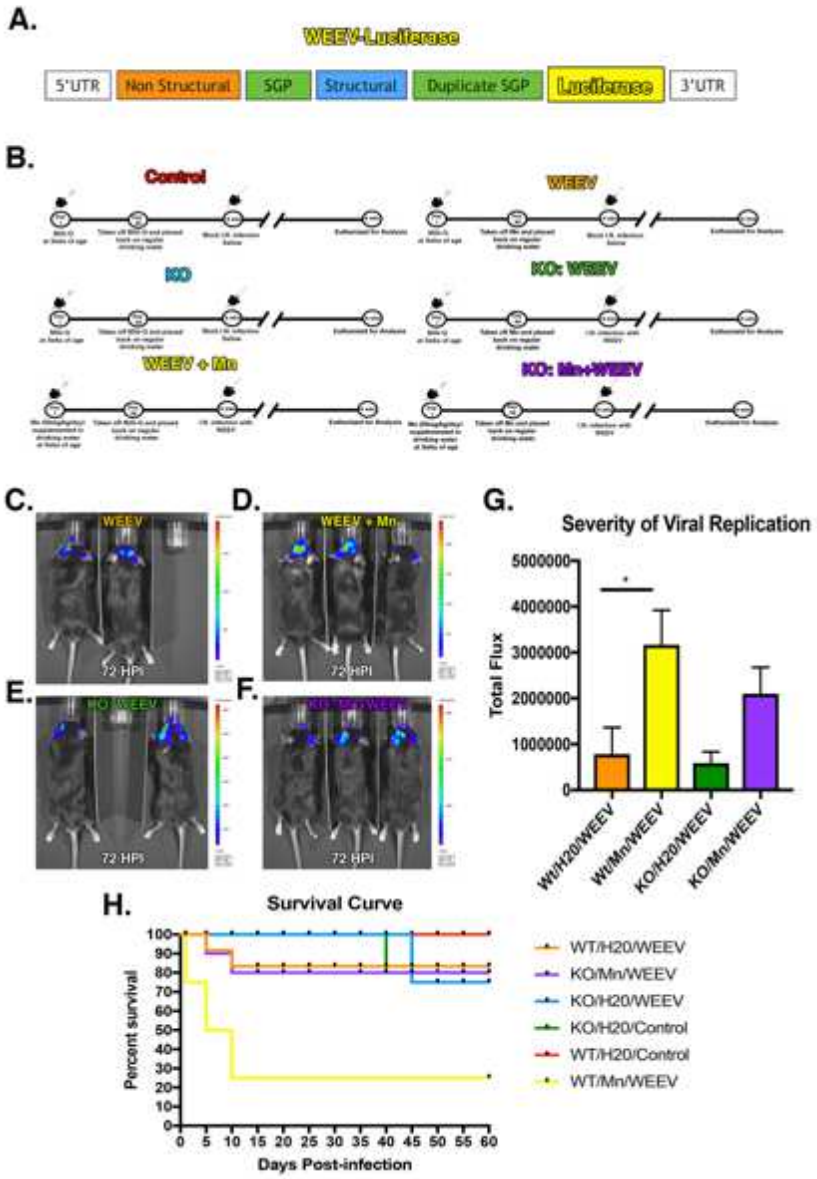

Figure 4.2. Astrocyte NF-κB KO reduces mortality following juvenile exposure to $MnCl_2$ and subsequent encephalitic infection with WEEV. (A) Structure of vectors for each recombinant virus used in the study. Subgenomic promoter (SPG), untranslated region (UTR). Wild-type mice were infected with WEEV-Luc to the track infectivity of WEEV in the live mouse. **(B)** Schematic diagram illustrating the six treatment groups with control and astrocyte-specific NFκB KO mice. Pseudo-colored image of luciferase-activity overlaid onto a photograph of **(C)** wild-type animals infected with WEEV**, (D)** wild-type animals pretreated with $MnCl_2$ infected with WEEV, **(E)** KO animals infected with WEEV**,** and **(E)** KO animals pretreated with $MnCl_2$ infected with WEEV. **(G)** Total Flux was measured in the head of each mouse for each treatment group. **(H)** Survival curve showing the percent survival of each group after the eight-week treatment regimen. (*p<0.05, ** p<0.005, ***p<0.0005, n=6-8 per group)

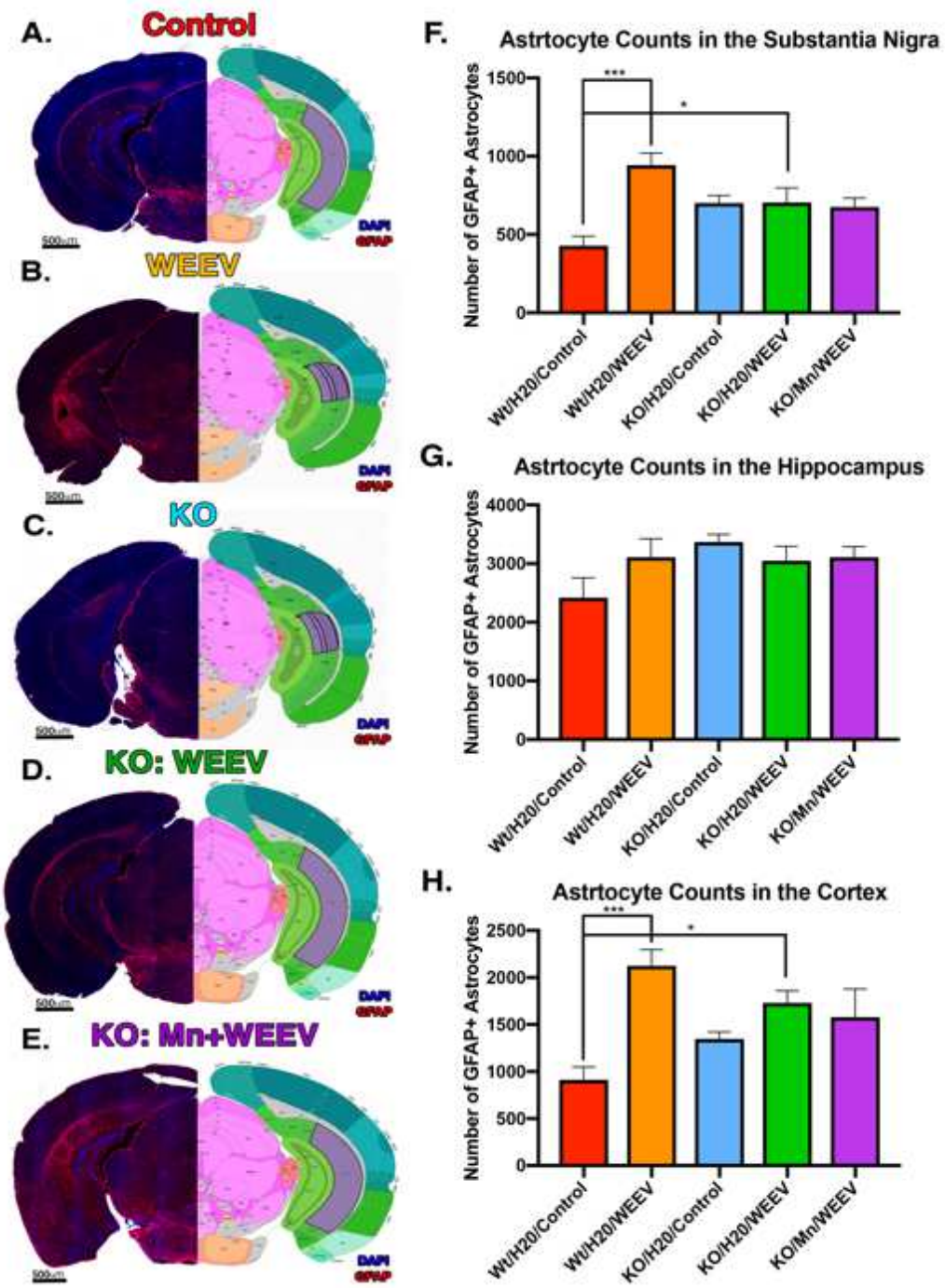

Figure 4.3. WEEV induces astrogliosis in the substantia nigra and cortex that is attenuated with astrocyte-specific NF-*κ*B KO. Representative montaged 10x images of (**A**) a control mouse, (**B**) a mouse infected with WEEV, (**C**) a astrocyte specific KO mouse, (**D**) a astrocytes-specific KO mouse infected with WEEV, and (**E**) a astrocytes specific KO mouse pretreated with $MnCl_2$ and infected with WEEV with a control lateral reference to the Allen brain atlas. Using immunofluorescent based GFAP+ astrocyte quantification, the relative number of astrocytes were quantified in the (**F**)substantia nigra, (**G**) hippocampus, and (**H**) cortex in all five treatment groups at eight weeks post-infection (*p<0.05, ** p<0.005, ***p<0.0005, n=6-8 per group)

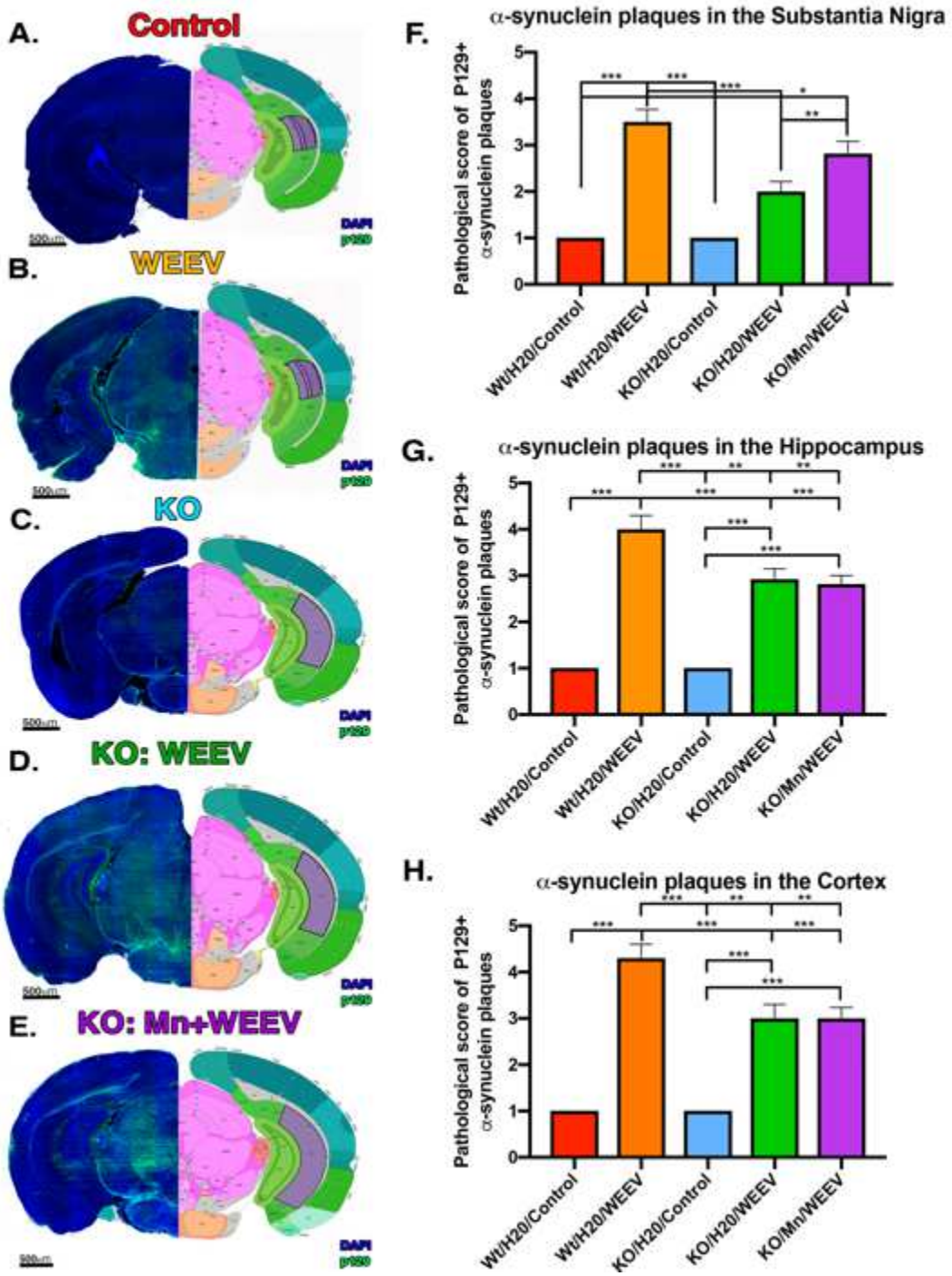

Figure 4.4. Juvenile manganese chloride exposure potentiates α-synuclein plaques in the substantia nigra. Representative montaged 10x images of (**A**) a control mouse, (**B**) a mouse infected with WEEV, (**C**) a astrocyte specific KO mouse, (**D**) a astrocytes-specific KO mouse infected with WEEV, and (**E**) a astrocytes specific KO mouse pretreated with $MnCl_2$ and infected with WEEV with a control lateral reference to the allen brain atlas. Using immunofluorescent based P129+ α-synuclein plaques were scored in the (F)substantia nigra, (G) hippocampus, and (H) cortex in all five treatment groups at eight weeks post-infection (*$p<0.05$, ** $p<0.005$, ***$p<0.0005$, n=6-8 per group)

CHAPTER 5

JUVENILE MANGANESE EXPOSURE INDUCES GLIAL ACTIVATION, HISTONE ACETYLATION, AND A UNIQUE GENE SIGNATURE IN THE BASAL GANGLION FOLLOWING SUBSEQUENT INFECTION WITH H1N1 INFLUENZA IN ADULTHOOD

7.1. INTRODUCTION

With the aging of the western world and no disease-modifying therapies, Parkinson's disease (PD) imposes one of the greatest public health threats worldwide. PD is characterized by the loss of voluntary motor control due to the spontaneous degeneration of dopaminergic neurons in the substantia nigra pars compacta (SNpc) with associated α-synuclein protein-aggregation, neuroinflammatory glial activation, mitochondrial dysfunction, and oxidative stress (Beal, 2010). Genome-wide association studies (GWAS) are beginning to identify gene variants in familial forms of the disease, but the majority of PD cases are thought to be sporadic or of an unknown etiology. Epidemiological and experimental evidence suggests that environmental neurotoxin exposure and viral infections are possible risk factors for sporadic PD. Following the 1918 "Spanish Flu" pandemic, nearly every patient who had an acute episode of encephalitis lethargica (EL) from the H1N1 infection went on to develop postencephalitic parkinsonism; individuals who were born between 1888 and 1924 had a two to three-fold higher risk of developing Parkinson's disease later in life than those born outside of that range (Dourmashkin, 1997; Elizan et al., 1978; Reid et al., 2001) (Clarke et al., 2014).

Our lab and others have recently shown that exposure to certain classes of enveloped RNA viruses, Western equine encephalitis virus (WEEV), experimental autoimmune

encephalomyelitis (EAE), and H5N1 via intranasal infection can induce a parkinsonian pathology in the SNpc (Bantle et al., 2019; Jang et al., 2012). Recent research highlights the neurovirulence of the 1918 H1N1 flu, but it remains unclear why encephalitic infections with the non-neurotropic Influenza, A/California/04/2009 (CA/09) H1N1 induces neurological dysfunction and neurodegeneration in select populations and whether viral CNS infections can directly or indirectly influence the onset and progression of neurodegenerative diseases (Hayase and Tobita, 1997) (Bantle et al., 2019; Henry et al., 2010a; Henry et al., 2010b; Jang et al., 2012; Jang et al., 2009b; Jang et al., 2009c; Mattson, 2004; Sadasivan et al., 2012; Sadasivan et al., 2017).

Furthermore, answers to these questions are aided by investigations into the cellular mechanisms by which viruses exert damage. Importantly, H5N1 avian influenza virus, WEEV, and EAE likely induce neuronal loss through the activation of microglia and astrocytes and subsequent release of glial-derived neurotoxic mediators (Bantle et al., 2019; Jang et al., 2012; Ludlow et al., 2016). Microglia and astrocytes express a variety of damage-associated molecular patterns (DAMPs) that promote inflammation and disease progression in postencephalitic parkinsonism (Tjalkens et al., 2017). Recently, reactive microglia and astrocytes have increasingly become the foci of study when examining the pathophysiology of PD. Therefore, neuroinflammation may be a key factor connecting viral encephalitis and the development of parkinsonian neurological symptoms (Caggiu et al., 2019). Additionally, astrocytes and microglia have innate immunological memory in the brain to facilitate a rapid inflammatory response to recurrent inflammatory stressors, and it has been postulated that this acute and exacerbated inflammatory response from glia may have the capacity to induce neuronal toxicity following secondary insults (Wendeln et al., 2018).

A clear understanding of the environmental links to PD and how these factors can act in unison remains extremely limited. Along with several collaborating labs, our research has demonstrated that elevated levels of $MnCl_2$ during juvenile development can exacerbate neuroinflammatory activation of glia and elevate the production of numerous reactive oxygen species, reactive nitrogen species, and inflammatory cytokines following subsequent exposure to LPS (Moreno et al., 2011a; Moreno et al., 2008; Streifel et al., 2012; Tjalkens et al., 2017; Zhang et al., 2003) (Elizan and Casals, 1991; Liddelow et al., 2017b; Sadasivan et al., 2017). At relevant environmental exposures during juvenile development, $MnCl_2$ is not directly toxic to neurons but can induce chronic neuroinflammation, mitochondrial respiration, and oxidative stress (Zhang et al., 2003). Importantly, the fact that both $MnCl_2$ and viral infection can individually induce parkinsonism with inflammatory activation of microglia and astrocytes in PD relevant brain regions suggest that neuroinflammatory responses to $MnCl_2$ and encephalitic infections may share coalescing mechanisms with those in idiopathic PD (Barcia, 2013; Kim et al., 2019; Moreno et al., 2009a).

Furthermore, previous work suggests that glial inflammatory responses to Mn can exacerbate neuronal injury following secondary neurotoxic insults, but whether Mn can also enhance the severity of neurological damage from encephalitic viral infections with H1N1 is unknown. In the current study we investigated whether elevated levels of an $MnCl_2$ during juvenile development could enhance neuroinflammatory damage to dopaminergic neurons after infection with H1N1 influenza virus and increase one's risk of developing neurological disease later in life. We, therefore, tested this hypothesis by exposing juvenile C57Bl/J6 mice to Mn in drinking water (50 mg/kg/day) for 30 days from days 21 – 51 PN, followed by intranasal infection with H1N1 three weeks later. Control mice received only drinking water followed by

either mock infection or infection with H1N1. Stereological counts of dopaminergic neurons and microglia in the substantia nigra pars compacta were performed. We noted pronounced microglia activation following dual-treatment with $MnCl_2$ and H1N1 relative to either treatment alone. Activated microglial displayed a reactive, amoeboid phenotype and could be seen phagocytizing damaged dopaminergic neurons. Immunofluorescent based analysis of astrocytes revealed that dual treatment induced astrogliosis and a reactive astrocyte phenotype. Additionally, this data suggests that the exacerbated neuroinflammatory response to H1N1 may be modulated through epigenetic changes in glia.

To identify different transcription profiles between treatment groups, total RNA was isolated from the SNpc. Active transcripts were examined by RNA sequencing (RNAseq), and analyzed using the GO Consortium and PANTHER Classification System pathway and overrepresentation platforms and STRING analysis to identify potential unique transcripts and molecular pathways expressed or lost in each treatment group. These analyses revealed the unique activation and loss of multiple stress response pathways involved in antioxidant activity, mitophagy activation, anti-viral activation, and neurodegeneration when dual treated with Mn and H1N1. In summary, these findings suggest that juvenile exposure to elevated levels of $MnCl_2$ during juvenile development may modulate multiple pathways involved in neuroinflammatory activation of glia and downstream neurodegeneration following encephalitic infection with H1N1 influenza virus later in life.

5.2 MATERIALS AND METHODS

Animal treatment regimen

All procedures were approved by Colorado State University Institutional Animal Care

and Use Committee (IACUC) and were conducted in compliance of the National Institute of Health guidelines. Dosing was performed as previously published (al, 2019). Mice were housed in a temperature-controlled room (maintained at 22-24°C on a 12 hr light/dark cycle) and had access to standard chow as needed. At day P21, male and female C57BL/6 mice were administered $MnCl_2$ (50mg/kg/day; Sigma) or normal drinking water. $MnCl_2$ was dosed by monitoring water intake and weight gain for thirty days. At P51, $MnCl_2$ treated mice were placed back on regular drinking water for a period of one month. Mice were then intranasally infected with A/California/04/2009 (CA/09) H1N1 or mock-infected with saline. Mouse infection procedures were adopted from a previous study (Sadasivan et al., 2015). Briefly, for infections, mice were lightly anesthetized with isofluorane and intranasally inoculated with either 10^3 $TCID_{50}$ of CA/09 in 25µl of phosphate-buffered saline (PBS) or PBS alone and monitored daily for 21 days post-infection by assessing any possible neurobehavioral abnormalities or clinical signs of illness. After 21 days, infectioned or mock-infectioned mice were euthanized for tissue collection.

Preparation of A/California/04/2009 (CA/09) H1N1 inoculum

A detailed description of inoculum preparation and administration have been previously reported (Sadasivan et al., 2015). In brief, A/California/04/2009 (CA/09) H1N1 virus was passaged in the allantoic cavity of 10-day-old specific pathogen-free embryonated chicken eggs. At 48 to 72 hours post-infection, allantoic fluid was harvested, clarified by centrifugation, and stored at −70°C. Tissue culture infectious dose 50% ($TCID_{50}$) titers were determined using Madin-Darby canine kidney (MDCK) cells and evaluated by the method of Reed and Muench (Ramakrishnan, 2016).

Tissue processing for Immunohistochemistry and Immunofluorescence based analysis

Mice were anesthetized with isoflurane and transcardially perfused with 3% paraformaldehyde in PBS. Brains were dissected and processed for paraffin embedding. Brains were then sectioned on the microtome at 10μm thickness and mounted on polyionic slides (Superfrost-plus, Fisher Scientific). Deparaffinized SN sections were incubated with primary antibody for identification of dopaminergic neurons [mouse monoclonal anti-tyrosine hydroxylase (TH; Sigma-Aldrich; 1:500), microglia [rabbit polyclonal anti-Iba-1 (Wako Chemicals; 1:500), astrocytes [rabbit polyclonal anti-s100beta (Abcam; 1:500)], complement C3 [rat monoclonal anti-C3(Abcam; 1:100)], serpinA3 [mouse monoclonal anti-serpinA3 (thermos; 1:250)], IP-10 [mouse monoclonal anti-IP-10 (Santa Cruz; 1:500)], IP-10/Cxcl10 [mouse monoclonal anti-cxcl10 (Santa Cruz; 1:250)], Ccl2 [mouse monoclonal anti-Ccl2 (Millipore; 1:500)], and acetylated Lysine residues [rabbit polyclonal anti-acetylated lysine (Cell Signaling; 1:500)]. For immunohistochemical analysis, the secondary antibodies included biotinylated mouse IgG (for TH, 1:1000) or biotinylated rabbit IgG (for Iba-1, 1:1000). Diaminobenzidine (DAB) or a VIP kit (Vector labs) reaction was used to yield a brown (TH) or a purple (Iba-1) color, respectively. For immunofluorescence, anti-mouse, anti-rabbit or anti-rat IgG alexa flour 555, alexa flour 488, or alexa flour 647 were diluted in TBS (2% Triton) at 1:500. Sections were washed 5X (5mins) and stained with DAPI in the final wash after an hour incubation period in the secondary antibody. Sections were then mounted with medium, coverslipped and stored at 4°C until imaged.

Quantification of TH+ dopaminergic neurons and Iba1+ microglia in the substantia nigra pars compacta

Method was performed as previously reported (Sadasivan et al., 2015). In brief, TH+ dopaminergic neurons and Iba-1+ microglia in the SNpc were estimated using standard model-based stereological methods (Baquet et al., 2009; Sadasivan et al., 2012). Counts of total dopaminergic neurons and activated microglia were estimated using Microbrightfield StereoInvestigator (MBF Biosciences, Williston, VT) and the optical fractionator method using an Olympus BX-51 microscope and 100X objective(Graeber and Streit, 2010; West et al., 1991). Additionally, resting or activated microglial were based on morphological differences, as previously reported (Graeber and Streit, 2010; Sadasivan et al., 2012). Resting microglia were defined as having a small oval Iba1+ cell body that averaged 3 microns in diameter with long slender processes, while microglia were classified as activated when the cell body was slightly increased in size compared to resting microglia and had an irregular shape, with shorter and thickener processes. The investigator was blinded from all experimental groups during imaging and cell quantitation.

Quantification of S100beta+ astrocytes and colocalization with astrocyte-specific inflammatory markers in the substantia nigra pars compacta

Formalin-fixed, paraffin-embedded 10 μm brain sections were immunofluorescently labeled using a Leica Bond RXM automated robotic staining system. Sections were immunohistochemically stained on a Leica Bond-III IHC automated stainer using Bond Epitope Retrieval Solution 2 for 20 minutes. Sections were then incubated with primary antibodies for s100β+ [rabbit anti-s100β Abcam; 1:500)], complement C3 [rat monoclonal anti-C3(Abcam;

1:100)], SerpinA3 [mouse monoclonal anti-serpinA3 (thermos; 1:250)], IP-10/Cxcl10 [mouse monoclonal anti-cxcl10 (Santa Cruz; 1:250)], and Ccl2 [mouse monoclonal anti-Ccl2 (Millipore; 1:500)]. Secondary antibodies included anti-rabbit IgG-488, anti-rat IgG 555, and anti-mouse 647. Whole-brain immunofluorescent montage images of labeled tissue sections were imaged using a 20x objective and an automated Olympus BX51 fluorescence microscope equipped with a Hamamatsu ORCA-flash 4.0 LT CCD camera and collected using Olympus Cellsens software (v 1.15). Quantitative analysis was performed on dual- or triple-labeled fluorescent images generated by montage imaging of an entire coronal mouse brain section compiled from individual images acquired using an Olympus Plan Apochromat 20X air objective (0.40 N.A.). All slides were scanned under the same conditions for acquisition time post-staining, magnification, exposure time, lamp intensity, and camera gain. The substantia nigra was delineated by neuroanatomical landmarks and referenced to the Allen brain atlas, following application of an adaptive threshold with shape factor and area (m^2) object filters for automatic s100β+ astrocyte cell detection. Detected cell number was divided over the area (μm^2) of the region. To measure inflammatory proteins within s100β+ astrocytes, mean intensities of $C3^+$ complement C3 [rat monoclonal anti-C3(Abcam; 1:100)], serpinA3 [mouse monoclonal anti-serpinA3 (thermos; 1:250)], IP-10/Cxcl10 [mouse monoclonal anti-cxcl10 (Santa Cruz; 1:250)], and Ccl2 [mouse monoclonal anti-Ccl2 (Millipore; 1:500)] were measured by creating individual ROIs around all S100β+ astrocytes within the SNpc. We assessed the presence of the inflammatory molecules on two coronal sections per animal that were 10 μm in thickness, spaced at 200 μm intervals within the SNpc, with an *N*=6-8 mice for each treatment group. The investigator was blinded from all experimental groups during imaging and cell quantitation.

Quantification of histone acetylation in dopaminergic neurons, microglia, and astrocytes in the substantia nigra par compacta

Formalin-fixed, paraffin-embedded 10 μm brain sections were immunofluorescently labeled as described above using a Leica Bond RXM automated robotic staining system. Sections were then incubated with primary antibodies for TH+ dopaminergic neurons [goat anti-tyrosine hydroxylase (WAKO; 1:500)], s100β+ astrocytes [mouse monoclonal anti-s100 s100β (Abcam; 1:500)], Iba1+ microglia [goat anti-Iba1 (Abcam; 1:100)], and acetylated lysine residues [rabbit polyclonal anti-acetylated lysine (Cell Signaling; 1:500)]. Secondary antibodies included anti-goat IgG 647, anti-mouse IgG 488, and anti-rabbit IgG 555. To measure total lysine acetylation in dopaminergic neurons, astrocytes and microglia in the SNpc, labeled tissue sections were imaged using a 20x objective and an automated Olympus BX51 fluorescence microscope equipped with a Hamamatsu ORCA-flash 4.0 LT CCD camera and collected using Olympus Cellsens software (v 1.15). Quantitative analysis was performed as described above; we generated triple-labeled fluorescent images montage images of an entire coronal mouse brain section compiled from individual images acquired using an Olympus Plan Apochromat 20X air objective (0.40 N.A.). All slides were scanned under the same conditions for acquisition time post-staining, magnification, exposure time, lamp intensity, and camera gain. The substantia nigra was delineated by neuroanatomical landmarks and referenced to the Allen brain atlas, following application of an adaptive threshold with shape factor and area (um^2) object filters for automatic TH+ dopaminergic neurons, Iba1+ microglia, and s100β+ astrocyte cell detection. Mean intensities of acetylated lysine residues [rabbit polyclonal anti-acetylated lysine (Cell Signaling; 1:500)] were measured within TH+ dopaminergic neurons, Iba1+ microglia, and s100β+ astrocyte in the SNpc by creating individual ROIs around each cell type. We assessed

total lysine histone acetylation in dopaminergic neurons, astrocytes, and microglia in two coronal sections per animal that were 10 μm in thickness, spaced at 200 μm intervals within the SNpc, with an *N*=6-8 mice for each treatment group. The investigator was blinded from all experimental groups during imaging and cell quantitation.

RNA sequencing of the substantia nigra

Method was adapted from a previous protocol (Cummings and Slayden, 2017). A systems-based transcriptional analysis of substantia nigra brain tissues from each treatment group was performed, and the treatment groups included control, $MnCl_2$, and H1N1+$MnCl_2$ treated mice. Isolated substantia nigra brain tissues were thawed, homogenized in Trizol reagent (Thermo Fisher), and nucleic acid was isolated by organic partition. Samples were then treated with DNAse (Fermentas, Burlington, Ontario) for 30 minutes and purified by phenol/chloroform/isoamyl alcohol (25:24:1) (Fisher Scientific, Pitts- burgh, PA) extraction and ammonium acetate precipitation. Quality and integrity of total RNA was assessed using the 4200 Agilent Tapestation, and samples were confirmed to have RIN scores of >7. RNA [transcripts & non-coding RNA] was isolated from total host RNA followed by library construction and template preparation with the Ion Total RNA-Seq kit and Ion Chef system kit. Sample libraries were prepared using the Ion Total RNA-Seq kit v2 (Life Technologies) and multiplexed on a P1 chip using Ionxpress RNA-Seq 1–16 kit (Life Technologies). Whole mouse transcriptome sequencing was then performed using the Ion Proton Next Generation Sequencer (Life Technologies) through the core facility at the Infectious Disease Research Complex (IDRC) at Colorado State University. Following Next Generation RNA-seq, we used read count coverage (RPKM or FPKM values) to compare the differential gene expression between groups. Advanced RNA-seq analysis was done using the Tuxedo package in Linux command line,

including alignments using Bowtie2 and differential gene expression analysis using Cufflinks. Local realignment and base quality score recalibration (BQSR) methods were used as needed to reduce false-positive base calls and improve alignments.

Analysis of next-generation sequencing data

Data analysis was performed as previously published (Cummings and Slayden, 2017). In brief, FASTQ files were analyzed using Galaxy for quality trimming, with minimum PHRED quality threshold set at 20 and all read length greater than 20bp. Trimmed reads were then aligned to Mus musculus mm9 using Bowtie2 and gene expression determined using Cufflinks. Expression output was normalized in FPKM format (fragments per kilobase of exon per million reads). Replicate mean values were calculated, and the data was further reduced to FPKM values greater than two. Venn diagrams and Pie chats were generated by comparing the reduced FPKM transcript totals for each treatment group. PANTHER (Protein Analysis Through Evolutionary Relations) Classification System (*http://pantherdb.org/publications.jsp#HowToCitePANTHER)* was used to ascertain functional pathways driving differences in gene expression by analyzing the complete gene lists within each treatment group for their corresponding annotations, accessed from the Gene Ontology (GO) Consortium. Secondarily, the PANTHER statistical overrepresentation test enabled a comparison of those GO annotations across each treatment group to identify functionally related genes relevant to neurodegeneration. The PANTHER gene list analysis was used to perform a functional classification of all the GO-annotated transcripts within each treatment group. This process employed the GO Term of Molecular Function and GO-slim annotation data sets to analyze the expression profiles of each gene list. We charted any differences between treatment groups as the number of gene hits (the % of gene hits for a

GO term /total # annotated gene in that category). The only GO Term categories shown are those with demonstrable differences in the number of gene hits between the treatment groups. The exact genes returned within each GO classification were analyzed in Excel using MATCH function and dual comparisons to find the specific transcripts unique to each treatment category. To further classify RNAseq transcripts according to function, gene lists were analyzed using the PANTHER overrepresentation test. This yielded statistically over or under-represented annotations among gene lists relative to the GO Biological Process and Molecular Function *Mus musculus* datasets. Complete gene lists for each treatment group were imported into the analysis tool. Fisher's Exact test for significance was used with FDR multiple test correction. Resulting GO Terms with an enrichment score >1.5 and a FDR<0.05 were considered significant. Genes relevant to neurodegeneration were selected from significant GO Term gene lists. The Search Tool for the Retrieval of Interacting Genes database (STRING) was used to create a network diagram of functional associations between protein products of unique genes within the H1N1+Mn treatment group. Each protein-protein association is weighted according to evidence channels delineated by differing colors. The confidence cutoff was set to 0.4.

Statistical Analysis

All data was presented as mean +/- SEM, unless otherwise noted. Experimental values from each mean were analyzed with a Grubb's (α=0.05) test for exclusion of significant outliers. Differences between each experimental group were analyzed by a one-way ANOVA following a Tukey *post hoc* multiple comparisons test. Significance was identified as $^{++}P < 0.01$, $^{*}P < 0.05$, $^{**}P < 0.01$, $^{***}P < 0.001$, $^{****}P < 0.0001$. All statistical analysis was conducted using Prism (version 6.0; Graph Pad Software, San Diego, CA).

5.3 RESULTS

Juvenile Manganese exposure increases activated microglial following encephalitic infection with H1N1 in the SNpc.

To assess if Mn exposure during juvenile development would enhance the neurological effects following infection with H1N1 in the substania nigra, three week old C57BL/6J mice were administered $MnCl_2$ (50mg/kg/day) or normal drinking water for a total of 30 days and either intranasally infected with H1N1 or mock-infected with saline at 3 months of age (**Fig. 1A**). Stereological determination of TH+ dopaminergic neurons and morphological analysis of Iba1+ microglia at 21 DPI revealed that pretreatment with $MnCl_2$ induced persistent morphological changes in microglial and increased their reactivity to a subsequent infection with H1N1 (**Fig. 1H, 1I).** We did not observe significant changes in dopaminergic neuronal loss, α-synuclein protein aggregation, or the total number of resting microglia in the SNpc at 21 DPI (**Fig. 1F, 1G**).

Juvenile Manganese exposure increases neuroinflammatory activation of astrocytes following encephalitic infection with H1N1 in the SNpc.

Given the increased number of reactive microglia in the substantia nigra and previous work showing that astrocytes play a significant role in microglial activation through glial-glial communication, we next examined the number and level of astrocyte activation in the basal ganglia following treatment with $MnCl_2$ (50mg/kg/day) and intranasal infection with H1N1 at 21 DPI (**Fig. 2**) (Bantle et al., 2019; Kirkley et al., 2017a; Kirkley et al., 2019b; Popichak et al., 2018a; Tanuma et al., 2006). To determine if dual treatment with $MnCl_2$ enhanced the

inflammatory response of astrocytes and an A1 neurotoxic phenotype in the SNpc, we measured the level of astrogliosis (**Fig. 2 A-E)** and the level of astrocyte specific inflammatory molecules (C3, SerpinA3, IP10, CCL2) in s100β+ astrocytes with immunofluorescence based colocalization (**Fig 2. E).** At 21 DPI, there was a significant increase in SNpc s100β+ astrocytes with dual treatment compared to control and $MnCl_2$ treatment alone (**Fig 2. E).** Additionally, complement C3 and SerpinA3 were significantly increased with pretreatment of Mn and H1N1 infection when compared to control, MnCl2, and H1N1 treatment alone (**Fig 2. J-Y).** Dual treatment did not induce any differences in Interferon gamma-induced protein 10 (IP-10) or monocyte chemotactic protein (Ccl2) (**Fig 2 P-Y).**

Dual treatment with $MnCl_2$ and H1N1 alters of histone acetylation in the SNpc.

The capacity of environmental exposure to sensitize neural tissue to additional damage from subsequent H1N1 encephalitic infection may involve persistent inflammatory changes in glial cells(Sadasivan et al., 2017). Previous work has highlighted how manganese can induce histone acetylation and alter gene expression, chromatin remodeling, cell cycle progression, DNA repair, and apoptosis in neurons and glia(McCarthy et al., 2017; Wendeln et al., 2018). Additionally, histone acetylation is altered in PD, likely due to the effects of dopaminergic neurodegeneration and microglial infiltration in the SNpc (Harrison et al., 2018; Song et al., 2010; Song et al., 2011). Since the mechanisms driving the exacerbated neuroinflammatory response from a two-hit exposure model with juvenile $MnCl_2$ and H1N1 were unclear, we assessed whether juvenile $MnCl_2$ treatment modulates neuroinflammatory activation to a subsequent encephalitic infection with H1N1 through histone acetylation in glia and neurons. To quantitate the level of in histone acetylation in the SNpc, brain sections were stained for total

acetylated lysine in TH+ dopaminergic neurons (**Fig. 3A-E**), s100β^{+} astrocytes (**Fig. 3F-J**), and Iba1+ microglia in the SNpc (**Fig. 3K-O**). Infection with H1N1 alone and dual treatment significantly decreased lysine acetylation in dopaminergic neurons (**Fig. 3A-E**) in the SNpc. Minimal differences were noted in histone acetylation, while treatment with H1N1 alone and dual treatment significantly increased acetylation in Iba1+ microglia in the SNpc (**Fig. 3F-O)**, which corroborates previous findings in human PD brains (Harrison et al., 2018).

Dual treatment with $MnCl_2$ and H1N1 induces a unique transcriptional signature in the SNpc.

Considering the differences in histone acetylation in the SNpc following single and dual treatment with $MnCl_2$ and H1N1, we took an unbiased approach to assess the global transcriptional similarities and differences between control, H1N1, and H1N1+$MnCl_2$-treated mice using Next Generation RNA-sequencing (RNAseq) of SNpc brain sections (**Fig. 3**). Additionally, given the focus of the study and our previous findings showing minimal neuropathology with $MnCl_2$ treatment alone , we did not include a $MnCl_2$-only treatment group in our RNA-seq analysis (Moreno et al., 2011a; Moreno et al., 2009a; Moreno et al., 2008).

To sequence RNA from the substantia nigra, mouse brains were extracted and the substantia nigra was isolated and flash-frozen at PN77. RNA was isolated from each nigral brain sample and sequenced. The resulting FASTQ files were analyzed using Galaxy for quality trimming, with minimum PHRED quality threshold set at 20 and all read length greater than 20bp. Trimmed reads were then aligned to the *mouse* genome using Bowtie2 and gene expression determined using Cufflinks. Local realignment and base quality score recalibration (BQSR) methods were used as needed to reduce false-positive base calls and improve

alignments. The expression output was normalized in FPKM format. The replicate mean values were calculated, and the data was further reduced to FPKM values greater than two

This unbiased and global analysis of the transcriptional profile between Control, H1N1, and H1N1+$MnCl_2$ treated mice revealed that of the 13,168 transcripts annotated from the SN, 351 where unique to control, 290 were unique to H1N1, and 951 transcripts were unique to dual treatment (**Fig. 4A**). A full list of annotated transcripts is provided below (**S. 1**). To assess whether the increased inflammatory phenotype of microglia and astrocytes in the dual treatment group was a gain of function or loss of function, we next determined the major biological pathways that were altered in each treatment group by using the Gene Ontology (GO) Consortium and PANTHER Classification System pathway and overrepresentation analyses. Resulting transcript annotations were quantitatively different between treatment groups in the following four Molecular Function GO Term categories: antioxidant activity (GO:0016209) (**Fig. 4B. A**), catalytic hydrolase activity (GO:0016788,GO:0016462,GO:0003924)(**Fig. 4C**), catalytic transferase activity (GO:0008168,GO:0016757,GO:0016301)(**Fig. 4D**), and G-protein coupled receptor activity (GO:0004930) (**Fig. 4E**). The exact genes returned within each GO Term classification were further analyzed to find the specific transcripts unique to each treatment type. Unique transcripts are listed in ig 4.B-E. Of note, the dual-treatment group active transcript list includes Interferon-inducible GTPase1, Dynein heavy chain, homeobox protein, mitochondrial hydrodoxymethylglutaryl-CoA synthase (**Fig 4. B-E**), as well as DJ-1/Park 7, other interferon regulatory proteins, autophagy related proteins (Atg), amyloid-beta precursor bindings proteins, NFκB related inflammatory proteins, and histone acetyltransferases (**S. 1**). Additionally, control and H1N1 treated mice uniquely expressed glutathione peroxidase 8, Oasl3, Deoxyuridine triphosphate (**Fig. 4 B-E**) and glutathione-s-transferase, thioredoxin, and

colony-stimulating factor receptor 1 (CSF1R), suggesting that specific stress response pathways are activated and protective mechanism are lost following dual treatment with $MnCl_2$ and H1N1 when compared to Control and H1N1 treatment alone.

Dual treatment with $MnCl_2$ and H1N1 induces a unique transcriptional signature and highlights a possible association with PD.

GO PANTHER analyses were used to classify and compare transcript lists according to functional pathways , but to attain a system-level understanding of cellular processes, we next interrogated the protein–protein interaction networks in the dual treatment group using the Search Tool for the Retrieval of Interacting Genes database (STRING) (**Fig. 5A**)(Szklarczyk et al., 2019; Szklarczyk et al., 2017). Network nodes represent proteins and lines represent functional associations between those proteins. The color of each line represents the origin and/or type of evidence supporting that protein-protein interaction and the weights of each line correspond to a confidence score for that evidence type. (**Fig. 5A**). From a functional perspective, an association can mean direct physical binding, but STRING evaluates each protein-protein interaction according to the supporting evidence, and these evidence types are divided into seven different channels: neighborhood, cooccurrence, coexpression, experiments, textmining, database, and fusion. The *neighborhood* category are related by conserved and co-transcribed operons; the *coocrruence* category are related by phylogenetic distribution of orthologs of all proteins in a given organism; the *coexpression* category are related by predicted association between genes based on observed patterns of simultaneous expression of genes; the *experiments* category are related by known experimental interactions; the *textmining* category conducts statistical co-citation analysis across a large number of scientific texts, including all

PubMed abstracts and OMIM; the database category is expertly curated and imported from pathway databases; and the *fusion* category is related by proteins that are fused in some genomes and are most likely to be functionally linked (Amberger et al., 2015; Szklarczyk et al., 2019; Szklarczyk et al., 2017). The more lines shown between each protein-protein interaction represents a more likely biological interaction, and the most highly represented interaction were centralized around Lingo 2, Pak6, Tbpl1, and Ctnnb1 (**Fig. 5A**). Additionally, by drawing on several of the RNAseq analyses mentioned, we were able to generate a list of H1N1+Mn unique proteins relevant to neurodegeneration (**Table 1**).Table 1 includes the gene name, protein product description and the pathway of interest to which the genes are annotated. Notable pathways are represented, including those contributing to multiple stress responses and several involved in neuroinflammation, oxidation, and neurodegeneration.

5.4 DISCUSSION

The majority of PD cases are sporadic and of unknown etiology. Previous work highlights how environmental exposures and encephalitic infections can increase susceptibility to neurodegeneration later in life (Dourmashkin, 1997; Hahn et al., 1988; Miner et al., 2016). While chronic inflammatory activation of glia in the nigrostriatal pathway is a well-characterized feature in sporadic PD and post-encephalitic parkinsonism, it is unclear whether previous environmental insult during juvenile development can potentiate secondary insults through chronic inflammatory activation of glia. Using a two-hit model with H1N1 and MPTP, previous work has shown that influenza infections can modulate the CNS immune system in the SNpc following exposure to the known parkinsonian agent, MPTP (Sadasivan et al., 2012). However, it is unknown whether other environmental insults can induce similar effects. To test if juvenile exposure to $MnCl_2$ could prime glia to a worsened neuroinflammatory response following

encephalitic infection with H1N1 in the SNpc, we utilized a two-hit exposure model, coupled with Next Generation RNA-sequencing to search for unique transcriptional signatures.

In conjunction with previous findings, our results suggest that juvenile $MnCl_2$ induces lasting neuroinflammatory and epigenetic alterations in glia that exacerbate the neuroinflammatory response to H1N1 than either treatment alone. Although, dopaminergic neuronal loss or protein aggregation of α-synuclein was not observed at 21 DPI in any treatment group, PD manifest during aging(**Fig. 1**), and given the downward trend of dopaminergic neurons (**Fig.1 F**) and significant increase in reactive microglia in the SNpc with dual treatment (**Fig. 1G**), we anticipate that dual treatment would significantly accelerate dopaminergic neuronal loss and possibly induce protein aggregation during aging in this model. Therefore, these pathological findings may represent a prodromal stage of the PD and highlight the transitional profile of prodromal PD.

Chronic neuroinflammatory activation of microglia and astrocytes is a unifying feature of aging, viral encephalitis, and neurodegenerative disease. Mounting evidence continues to elucidate the importance of microglia-astrocyte signaling in neurodegeneration and neuroinflammation (Elizan and Casals, 1991; Hirsch and Hunot, 2009; Ronca et al., 2017; Silva da Costa et al., 2012). Our lab, along with others, has previously shown that microgliosis precedes astrogliosis and neuronal loss in models of PD (Clarke et al., 2018; Kirkley et al., 2017a; Liddelow et al., 2017a). These previous studies provide evidence that cytokine and chemokine signaling from neuroinflammatory activation of microglia play a critical role in inflammatory activation of astrocytes in the SNpc. Given that dual treatment with $MnCl_2$ and H1N1 potentiated inflammatory activation of astrocyte inflammatory molecules SerpinA3 and C3 (**Fig. 2**), and that $MnCl_2$ and H1N1 dual treatment increased the number of reactive microglia

(**Fig. 1**), these results provide additional evidence that signaling in activated microglia plays a critical role in inflammatory activation of astrocytes. Although there was no detailed molecular interrogation or genetic manipulation with gene knockdowns in this study, we hope to investigate the specific chemokines and cytokines involved in these glia-glia communications with $MnCl_2$ and H1N1 dual treatment in future studies. However, the present work raises additional questions. Interestingly, only SerpinA3 and C3 were increased with dual treatment, and not IP10 and Ccl2 (**Fig. 3**). Whether this finding is unique to this model is unknown. We hope to address this in further studies, and we anticipate that this study will inspire others to interrogate the inflammatory signatures of astrocytes in other two-hit models of PD.

Previous work has shown that $MnCl_2$ is not directly toxic to neurons, but MnCl2 neurotoxicity primarily occurs through activation of inflammatory signaling pathways which damage neurons through overproduction of reactive oxygen and nitrogen species and inflammatory cytokines (Zhang et al., 2003). It has previously been shown that juvenile $MnCl_2$ exposure can induce lasting effects on the neuroinflammatory status of astrocytes and microglia which continues into adulthood and this likely play a fundamental role in an increased susceptibility to secondary infections and environmental insults(Moreno et al., 2011a; Moreno et al., 2009a; Moreno et al., 2008; Popichak et al., 2018b; Streifel et al., 2012). However, the mechanisms regulating this sustained inflammatory state after environmental insults in microglia and astrocytes are unclear. Previous work has shown that glia can have innate immune memory to environmental stimuli through histone acetylation that alters subsequent immune responses (Wendeln et al., 2018). Additionally, decreased acetylation in TH neurons has been noted in clinical PD cases, and histone acetylation is thought to be modulated in glia following exposure to other PD related environmental insults (Guo et al., 2018; Harrison et al., 2018; Song et al.,

2010; Song et al., 2011). Here we demonstrate that juvenile $MnCl_2$ and adult infection with H1N1 causes changes in histone acetylation in dopaminergic neurons, microglia, and astrocytes in SNpc (**Fig. 3**). Also, dual treatment with $MnCl_2$ and H1N1 decreases histone acetylation in dopaminergic neurons, corresponding with previous clinical cases of PD (Guo et al., 2018; Harrison et al., 2018; Song et al., 2010; Song et al., 2011). We postulate that these epigenetic changes in glia likely play a role in their increase inflammatory activation to subsequent infection with H1N1. However, whether these epigenetic changes are lasting or temporary and change during aging is unknown.

Although this study has been primarily focused on the role of inflammatory activation of glia in neurodegeneration, glial cells also play a significant role in homeostatic support of neurons in the SNpc. It is still unclear whether neuroinflammatory activation of glia increases susceptibility to neurotoxicity through a decreased release of neurotropic factors or from the release of neurotoxic inflammatory factors in neurodegeneration (Kostuk et al., 2019; Liddelow et al., 2017b). Inflammatory activation of glia is regulated through multiple pathways including mitogen- activated protein kinases (MAPKs), activator protein-1 (AP-1), Janus kinase (JAK)/signal transducer and activator of transcription (STAT), interferon regulatory factor families (IFN), and the nuclear factor kappa B (NF-κB) pathway. To take an unbiased and global look at the impact of these various treatments in the multiple PD disease relevant pathways, we performed Next Generation RNA-sequencing of SNpc brain sections. We found that dual treatment with $MnCl_2$ and H1N1 induced an increase in the number of unique transcripts and significantly altered the transcriptional profile when compared to H1N1 treatment alone (**Fig. 4**). Dual treatment induced an overrepresentation of Interferon-inducible GTPase1, Dynein heavy chain, homeobox protein, mitochondrial hydrodoxymethylglutaryl-CoA synthase (**Fig 4. B-E**),

as well as DJ-1/Park 7, other interferon regulatory proteins, autophagy-related proteins (Atg), amyloid-beta precursor bindings proteins, NFκB related inflammatory proteins, and histone acetyltransferases (**S. 1**), and an underrepresenting of genes involved in antioxidant activity, such as glutathione peroxidase (**Fig 4. A**). Park7 (DJ1) is linked to the preservation of mitochondrial function in PD, and the unique activation of DJ-1, Atg, and interferon regulatory protein in the dual treatment group likely represents the activation of the antioxidant activation and autophagy stress response pathways (Antipova and Bandopadhyay, 2017). Moreover, given that viral infections can inhibit mitochondrial bioenergetics by depressing cellular ATP content and induce oxidative stress in neurons and glia, these data suggest that juvenile $MnCl_2$ exposure reduces glutathione recycling through a reduction of glutathione peroxidase and exacerbates the oxidative stress in neurons and glia to a subsequent infection with H1N1 (Silva da Costa et al., 2012).

Furthermore, RNA sequencing allows us to identify expression patterns of unique gene within each treatment group. Not only were these genes annotated to specific molecular function and biological processes (**Fig. 4**), but we also created a network summarizing predicted associations between gene products to attain a systems-level understanding of cellular processes in the dual treatment group (**Fig. 5**). DJ-1/*Park7, Lingo2, Keap1, Eif2c1,* and *Pak6* were all unique genes identified using the overrepresentation analysis (**Table. 1**). Interestingly, LINGO2 is a member of LRR gene family, which has been linked to Essential tremor (ET) and PD, and it has even become a promising therapeutic target in multiple sclerosis (MS) and PD (Ranger et al., 2018; Vilarino-Guell et al., 2010; Wu et al., 2011). Together, these findings lend further credence to the involvement of distinct proteins and pathways in the neurologically deleterious effects caused by successive treatment of two insults. Although we did not see significant

dopaminergic neuronal loss, we believe that these unique protein-protein interactions from dual treatment could represent earlier prodromal and initiating stages of neurodegeneration

In summary, a better understanding of PD disease etiology and how environmental insults and microbial infection can act in concert may help identify individuals more susceptible to PD and related neurodegenerative diseases. In this study exposure to 50 mg/Kg $MnCl_2$ from PN 21 – 51 did not result in loss of SNpc dopaminergic neurons; however, a trend toward loss of DA neurons was noted in the dual treatment group, suggesting an increased susceptibility to injury following a systemic viral infection, and my represent a prodromal stage of pathogenesis. Juvenile exposure to Mn resulted in increased neuroinflammatory activation of microglia and astrocytes and a pattern of gene expression consistent with a neurodegenerative phenotype, particularly for genes related to oxidative stress, mitophagy, protein processing, and immune function. The unique expression of specific gene sets (**Fig. 4A, Table 1**) with combinatorial exposure of $MnCl_2$ and H1N1 are suggestive of the mechanism by which environmental exposures and microbial interactions may underlie the more severe neuroinflammatory pathology seen in certain cases of sporadic and post-encephalitic PD. While there are still many knowledge gaps to fill and questions to be answered, this data provides support to how any individual will encounter any number of environmental insults, which alone may be harmless but together may synergize to produce a measurable pathology.

5.5 FIGURES

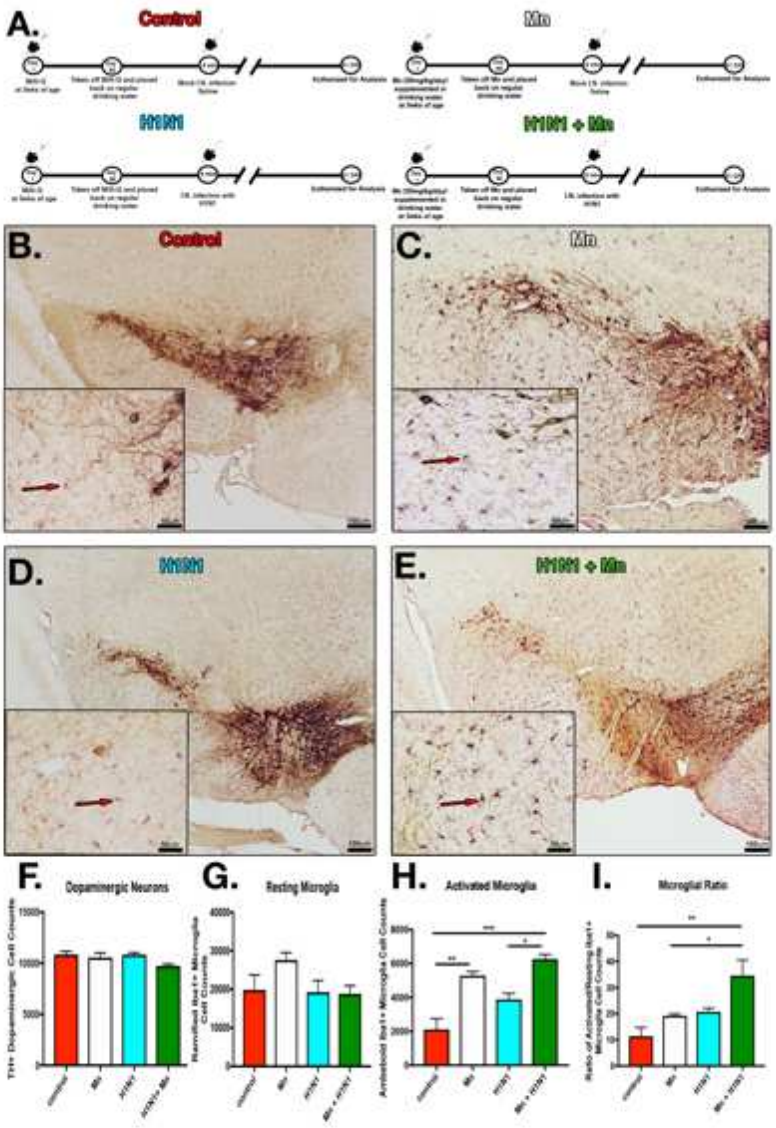

Figure 5.1. Pre-treatment with manganese increases microglial activation in the substantia nigra following infection with H1N1. (A) C57Bl/6 mice were divided into groups with and without Mn in drinking water (50 mg/Kg) from day 21 – 51 PN and then exposed to H1N1 influenza virus three weeks later. Groups: Control, Mn, H1N1, H1N1+$MnCl_2$. (B-E) IHC labeling of dopamine neurons (TH) and microglia (IBA1). (F) Stereological determination of the number of TH+ neurons in the substantia nigra pars compacta (SNpc). (G) Resting microglia in the SNpc. (H) Activated microglia in the SNpc. (I) Ration of activated/resting microglia in the SNpc. **P*<0.05 ***P*<0.01 ****P*<0.001****P<0.0001. *n*=6 mice/group

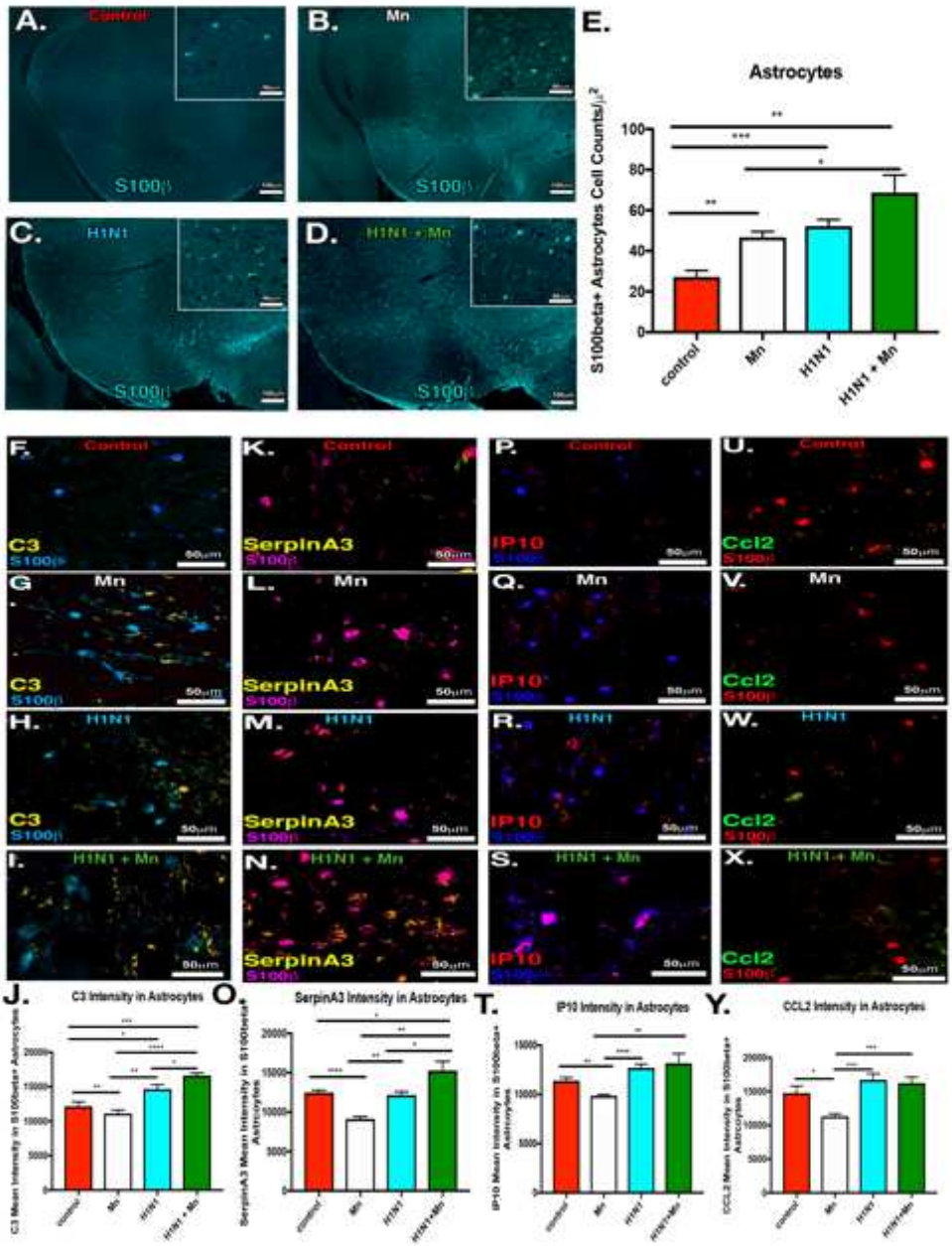

Figure 5.2. Pre-treatment with manganese induces proliferation and inflammatory activation in astrocytes in the substantia nigra following infection with H1N1. (A-D) IF labeling of astrocytes (s100β). Groups: Control, Mn, H1N1, H1N1+ $MnCl_2$. (E) Cell counts of the s100β+ astrocytes in the substantia nigra pars compacta (SNpc). (F-I) IF colocalization of astrocytes (s100β) with complement C3 (C3). (J) C3 mean intensity measurements in s100β+ astrocytes in the SNpc. (K-N) IF colocalization of astrocytes (s100β) with SerpinA3. (O) SerpinA3 mean intensity measurements in s100β+ astrocytes in the SNpc. (P-S) IF colocalization of astrocytes (s100β) with complement IP-10/Cxcl10 (IP-10). (T) IP-10 mean intensity measurements in s100β+ astrocytes in the SNpc. (U-X) IF colocalization of astrocytes (s100β) with complement Ccl2. (J) Ccl2 mean intensity measurements in s100β+ astrocytes in the SNpc. **P*<0.05 ***P*<0.01 ****P*<0.001****P<0.0001. *n*=6 mice/group

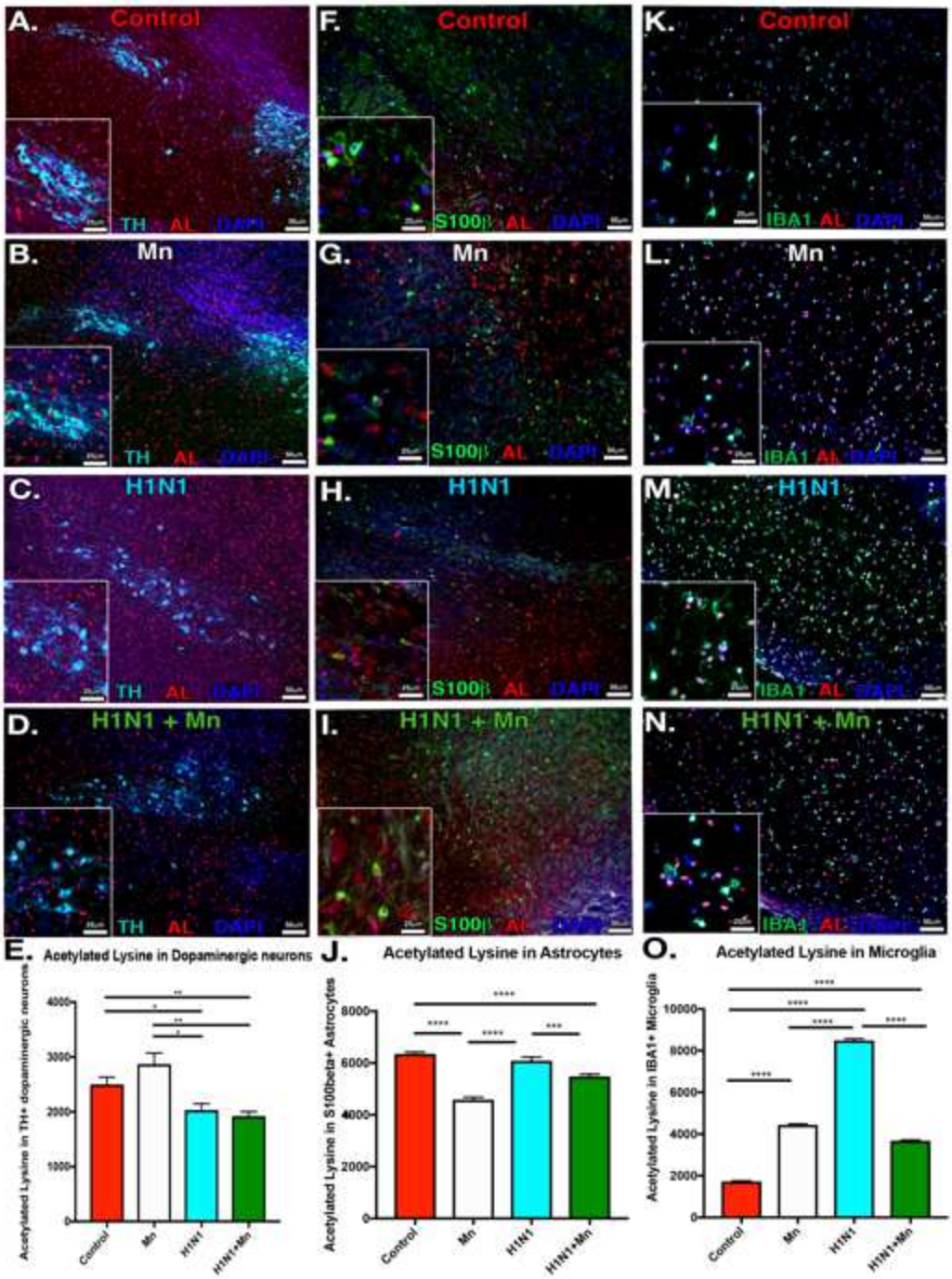

Figure 5.3. **Dual treatment with $MnCl_2$ and H1N1 alters histone acetylation in dopaminergic neurons, microglia, and astrocytes in the SNpc.** (A-D) IF colocalization of dopaminergic neurons (TH) and total acetylated lysine residues (AL). Groups: Control, Mn, H1N1, H1N1+ $MnCl_2$. (E) AL mean intensity measurements in TH+ dopaminergic neurons in the substantia nigra pars compacta (SNpc). (F-G) IF colocalization of astrocytes (s100β) with AL. (J) AL mean intensity measurements in s100β+ astrocytes in SNpc. (K-N) IF colocalization of microglia (Iba1) with AL. (O) AL mean intensity measurements in Iba1+ microglia in the SNpc. **P*<0.05 ***P*<0.01 ****P*<0.001****P<0.0001. *n*=6 mice/group.

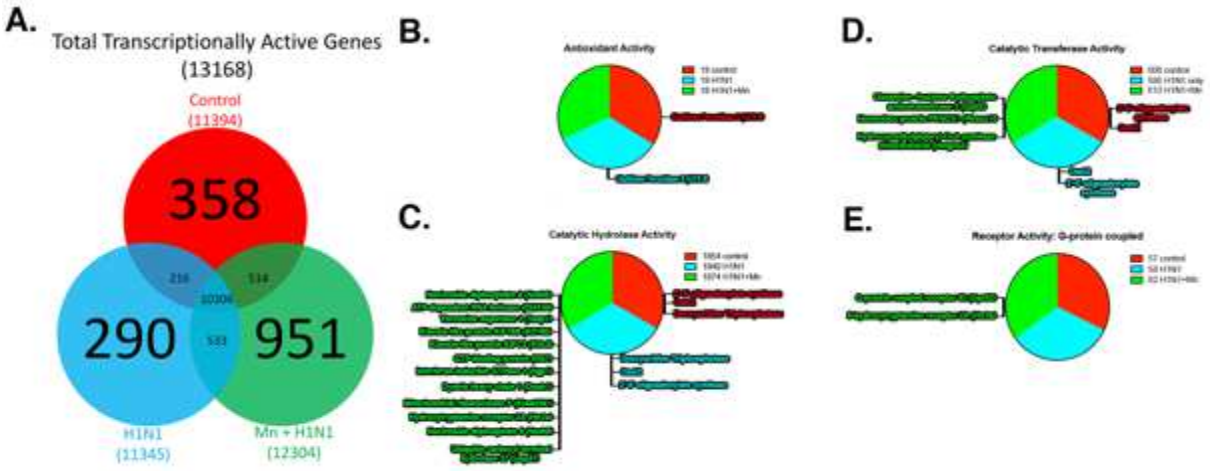

Figure 5.4. RNA sequencing of the H1N1+$MnCl_2$ treatment group highlights uniquely transcribed genes annotated to functionally relevant biological processes. (A) Venn diagram depicting unique and overlapping transcripts. (B-E) GO Consortium & PANTHER Classification System pathway analysis: Pie charts describe the relative proportions of RNAseq transcripts annotated to each GO Term within the *molecular function* Gene Ontology. The exact gene lists unique or uniquely absent from the H1N1+ $MnCl_2$ treatment group are listed for each category. Genes classified according to molecular function and biological process with Panther overrepresentation analysis Functional Enrichment Analyses. Groups: Control, H1N1, H1N1+ $MnCl_2$.

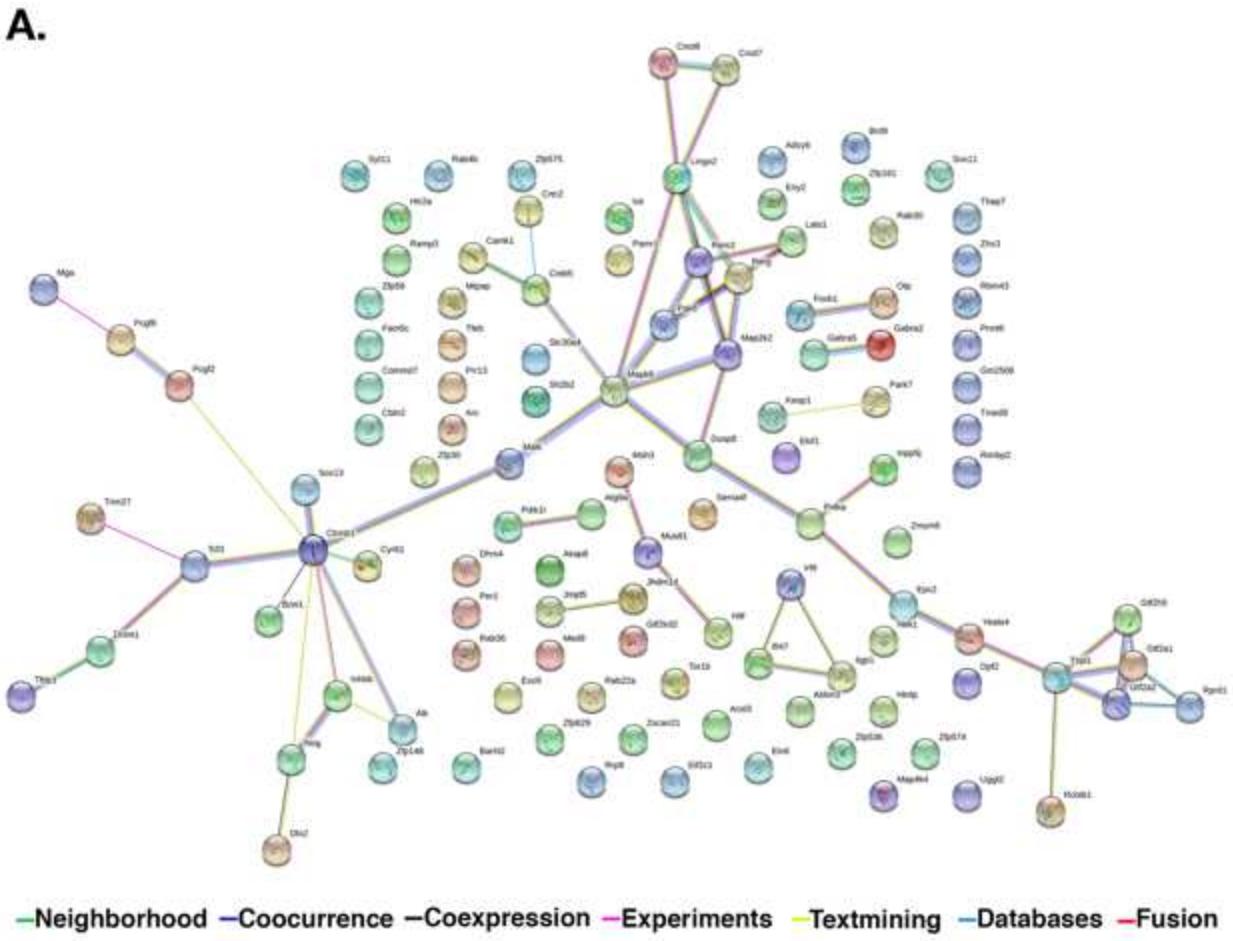

Figure 5.5. Transcriptional connectome of dual treatment group with associated gene products. (A) Search Tool for the Retrieval of Interacting Genes database (STRING) diagram of functional associations between protein products of unique genes within the H1N1+Mn treatment group. Nodes represent proteins and edges correspond to functional interactions. Edge colors differ according to a scored confidence scale based on the extent and type of evidence supporting that particular association. Evidence channels: Green Line: Neighborhood, Navy Line: Coovvurence, Black line: Coexpression, Pink line: Experiments, Yellow line: Textmining, Light blue line: Databases, Red line: Fusion.

Table 5.1. H1N1+Mn unique genes relevant to neurodegeneration. PANTHER overrepresentation analysis was used to more narrowly identify unique genes relevant to neurodegeneration. Results with FDR<0.05 and an enrichment score >1.5 were considered significant. From among statistically significant GO Terms, genes annotated to those categories were selected according to relevance to neurodegeneration. Gene names (leftmost column), protein product description (left middle column), and the related pathway of interest (right middle column).

Genes	Protein Product description	Pathway of Interest
Park7	Parkinson disease (autosomal recessive, early onset) 7; Protein deglycase that repairs methylglyoxal- and glyoxal-glycated amino acids and proteins, and releases repaired proteins and lactate or glycolate, respectively.	SUMOylation of transcription cofactors
Lingo2	Leucine rich repeat and Ig domain containing 2. Genetic polymorphisms in LINGO1 and LINGO2 associated with increased risk of developing essential tremor and Parkinson Disease (PD). Lingo (1,2) is an axonal inhibitor.	Axonal growth inhibition (RHOA activation)
Pak6	Serine/threonine protein kinase that plays a role in the regulation of gene transcription. The kinase activity is induced by various effectors including AR or MAP2K6/MAPKK6. May protect cells from apoptosis through phosphorylation of BAD.	Activation of RAC1
Eif2c1	Eukaryotic translation initiation factor 2C, 1; Required for RNA-mediated gene silencing (RNAi). Binds to short RNAs such as microRNAs (miRNAs) or short interfering RNAs (siRNAs), and represses the translation of mRNAs which are complementary to them. Recent evidence indicates that small RNAs participate in transcriptional regulation in addition to post-transcriptional silencing and damage repair.	Regulation of pTEN mRNA translation
Keap1	Kelch-like ECH-associated protein 1; Acts as a substrate adapter protein for the E3 ubiquitin ligase complex formed by CUL3 and RBX1 and targets NFE2L2/NRF2 for ubiquitination and degradation by the proteasome, resulting in the suppression of its transcriptional activity and the repression of antioxidant response element-mediated detoxifying enzyme gene expression. Retains NFE2L2/NRF2 and may also retain BPTF in the cytosol. Targets PGAM5 for ubiquitination and degradation by the proteasome.	Ub-specific processing proteases
Sox11	Transcriptional factor involved in the embryonic neurogenesis. May also have a role in tissue modeling during development.	Binding of chemokine receptors
Sox13	Member of SOX family of transcription factors.	Binding of chemokine receptors
Arc	Activity regulated cytoskeletal-associated protein; Plays a role in the regulation of cell morphology and cytoskeletal organization. Required in the stress fiber dynamics, cell migration, consolidation of synaptic plasticity and formation of long-term memory.	Trafficking of AMPA receptors
Iigp1	GTPase with low activity. Has higher affinity for GDP than for GTP. Plays a role in resistance to intracellular pathogens. Mediates resistance to infection by targeting bacterial inclusions to autophagosomes for subsequent lysosomal destruction.	Resistance to infection.
Camk1	Calcium/calmodulin-dependent protein kinase that operates in the calcium-triggered CaMKK-CaMK1 signaling cascade and, upon calcium influx, regulates transcription activators activity, cell cycle, hormone production, cell differentiation, actin filament organization and neurite outgrowth.	Transcriptional activation of mitochondrial biogenesis.
Slc30a4	Probably involved in zinc transport out of the cytoplasm, may be by sequestration into an intracellular compartment.	Zinc efflux
Atg9a	Involved in autophagy and cytoplasm to vacuole transport (Cvt) vesicle formation. Plays a key role in the organization of the preautophagosomal structure/phagophore assembly site (PAS), the nucleating site for formation of the sequestering vesicle.	Macroautophagy
Per1	Transcriptional repressor that forms a core component of the circadian clock.	Circadian clock
Gabra2	Gamma-aminobutyric acid (GABA) A receptor, subunit alpha 2; GABA, the major inhibitory neurotransmitter in the vertebrate brain, mediates neuronal inhibition by binding to the GABA/benzodiazepine receptor and opening an integral chloride channel.	Neurotransmitter receptors and postsynaptic signal transmission
Gabra5	Gamma-aminobutyric acid (GABA) A receptor, subunit alpha 5; GABA, the major inhibitory neurotransmitter in the vertebrate brain, mediates neuronal inhibition by binding to the GABA/benzodiazepine receptor and opening an integral chloride channel.	Neurotransmitter receptors and postsynaptic signal transmission
Ildr2	Immunoglobulin-like domain containing receptor 2; May be involved in ER stress and lipid homeostasis.	ER stress pathway
Tcf3	Transcription factor 3; Transcriptional regulator. Involved in the initiation of neuronal differentiation. Heterodimers between TCF3 and tissue- specific basic helix-loop-helix (bHLH) proteins play major roles in determining tissue-specific cell fate during embryogenesis, like muscle or early B-cell differentiation.	CDO (cell-adhesion-molecule/downregulated by oncogenes) in myogenesis
Map4k4	Serine/threonine kinase that may play a role in the response to environmental stress and cytokines such as TNF-alpha. Appears to act upstream of the JUN N-terminal pathway. Phosphorylates SMAD1 on Thr-322.	Oxidative stress induced senescence

CHAPTER 6

JUVENILE EXPOSURE TO MANGANESE EXACERBATES ASTROCYTE-DEPENDENT NEUROINFLAMMATORY INJURY FOLLOWING ADULT CHALLENGE WITH MPTP

6.1.INTRODUCTION

Manganese (Mn) is an essential trace element necessary for multiple enzymatic processes in the central nervous system (CNS) that also accumulates in astrocytes during overexposure. Transport of Mn into astrocytes occurs predominately through divalent metal transporters such as DMT1, ZIP and SLC39A3, where it is a required co-factor for glutamine synthetase (GS), the key enzyme regulating glutamate-glutamine metabolic shuttling between astrocytes and neurons (Erikson and Aschner, 2003; 2006). Mn is also a critical cofactor for superoxide dismutase (Mn-SOD), which protects neurons from the damaging effects of oxidative stress (Zidenberg-Cherr 1983).

However, abnormally high exposure to Mn can be neurotoxic. Epidemiology studies correlate elevated levels of Mn in the brain to cognitive and behavioral impairment, to which children appear to be particularly sensitive (Rugless *et al.*, 2014; Takser 2003; He 1994). In more severe cases, Mn exposure in occupational settings (e.g. mining, welding) can cause ‘manganism' (RODIER, 1955; Wang *et al.*, 1989; Racette *et al.*, 2017), a neurodegenerative disorder with cognitive and motor deficits resembling Parkinson’s disease (PD). These include bradykinesia, dystonia, rigidity and depression (RODIER, 1955; Wang *et al.*, 1989; Mergler and Baldwin, 1997; Racette *et al.*, 2017), although patients with manganism do not display severe

nigro-striatal dysfunction or resting tremors and are typically non-responsive to levodopa (L-DOPA) therapy (Guilarte *et al.*, 2006;Peres *et al.*, 2016). These differences are likely due to distinct patterns of neuropathology compared to idiopathic PD, causing toxicity primarily in more glial rich regions, such as the globus pallidus (Gp), subthalamic nucleus (Sth) and substantia nigra *pars reticulata* (SNpr) (Guilarte *et al.*, 2006; Peres *et al.*, 2016). In contrast, PD is characterized by preferential loss of dopamine (DA) neurons in the substantia nigra *pars compacta* (SN*pc*) and long axonal projections to the striatum (ST). Despite these findings, mechanisms by which Mn exposure could accelerate PD-like neuropathology have remained elusive.

We previously demonstrated that Mn-induced neurotoxicity results in marked activation astrocytes and microglia and expression of numerous neuroinflammatory genes that potentiate neuronal injury (Moreno *et al.*, 2011; Kirkley *et al.*, 2017). Furthermore, we reported that mice pre-exposed to Mn during juvenile development had higher levels of gliosis and neuronal dysfunction than mice exposed to Mn only as adults (Moreno, Yeomans, *et al.*, 2009). Neurotoxic levels of glial activation and neuroinflammation resulting from Mn exposure are modulated by the transcription factor, nuclear factor kappa B (NF-κB), a central regulator of innate immune responses in lymphoid and myeloid cells, as well as in microglia and astrocytes (Glass *et al.*, 2010; Kirkley *et al.*, 2017). NF-κB has distinct functions within different cell types of the CNS, including regulation of inflammatory gene expression in glia and induction of pro-survival genes in neurons including IAP's, Bcl2, Bcl-XL and surivin. (Glass *et al.*, 2010). *In vitro*, Mn directly activates microglia, stimulating NF-κB-dependent release of cytokines such as TNFα that subsequently stimulate a neurotoxic reactive phenotype in astrocytes(Kirkley *et al.*, 2017). NF-κB can be activated by numerous intra- and intercellular stressors, including reactive

oxygen species (ROS), inflammatory cytokines and chemokines, as well as Mn accumulation (Moreno *et al.* 2011).

To determine the role of NF-*κ*B in regulating the neuroinflammatory effects of Mn, we recently developed a novel transgenic mouse with astrocyte-specific deletion of the NF-*κ*B signaling pathway (Kirkley et al., 2019b). Mice expressing Cre recombinase under control of the human glial fibrillary acidic protein promoter (hGFAP) were crossed with I kappa B kinase 2 (Ikk2)-*l*ox*P* mice. Selective deletion of IKK2 in astrocytes provided almost complete protection against loss of DA neurons caused by the neurotoxin, 1-methyl-4-phenyl-1,2,3,6-tetrahydropyridine (MPTP) (Kirkley 2018). The active metabolite of MPTP, MPP^+, inhibits mitochondrial complex I and causes severe nigrostriatal dysfunction and behavioral deficits in mice similar to those in PD (Jackson-Lewis and Przedborski, 2007). Lack of functional NF-*κ*B in astrocytes also decreased reactive gliosis by suppressing the expression of NOS2 and TNFα resulting in prevention of MPTP-induced neuronal apoptosis and demonstrating that inflammatory activation of glial cells is an important determinant of MPTP neurotoxicity (Kirkley et al., 2019b). However, it is unknown whether exposure to Mn can exacerbate the effects of other dopaminergic neurotoxins such as MPTP by modulating glial reactivity and subsequent inflammatory neuronal injury.

In the present study, we postulated that Mn exposure during juvenile development would stimulate NF-κB-dependent activation of microglia and astrocytes, resulting in chronic neuroinflammation that increases susceptibility to neuronal injury from a secondary exposure to a dopaminergic neurotoxin. To test this hypothesis, we used a two-hit neurodegenerative model by administering Mn in drinking water to hGFAP-$cre^{+/-}$/$IKK2^{fl/fl}$ (astrocyte-specific knockout, KO) or hGFAP-$cre^{-/-}$/$IKK2^{fl/fl}$ (wildtype, WT) mice during juvenile development, followed by

exposure to MPTPp (MPTP + probenecid) four months later during adulthood. Neurobehavioral analysis was conducted during the two-week MPTPp dosing regimen to detect locomotor deficits associated with injury to the basal ganglia. Brain tissue from multiple regions was collected for determination of Mn, catecholamines, stereological assessment of neuronal numbers, glial activation and expression of proteins regulating DA function. Indeed, these studies indicate that early exposure to Mn exacerbates glial activation and neuronal loss following challenge with a second dopaminergic neurotoxicant through neuroinflammatory activation of NF-κB in astrocytes.

6.2.MATERIALS & METHODS

Animals and treatment regimen

All animals were housed on a 12 hr light/dark cycle in a temperature-controlled room (maintained at 22-24°C) and access to standard chow/water *ad libitum*. Procedures were approved by Colorado State University Institutional Animal Care and Use Committee (IACUC) and were conducted in compliance of National Institute of Health guidelines. Astrocyte-specific knockout mice for IKK2 were generated as previously described (Kirkley et al., 2019b). Briefly, *hGfap-cre*$^{+/-}$ (Cat#: 004600; Jackson Laboratories) mice were backcrossed on a C57/BlJ6 background for twelve generations before crossbreeding with *Ikk2-loxP*$^{+/+}$ mice (a kind gift from Professor Michael Karin, University of California San Diego). Four generations of crossbreeding were conducted to acquire *hGfap-cre*$^{+/-}$/*Ikk2-loxP*$^{+/+}$ (KO). Littermates lacking Cre recombinase (*hGfap-cre*$^{+/-}$/*Ikk2-loxP*$^{+/+}$) were used as genotype controls for the study. At day P21, mice were administered $MnCl_2$ (50mg/kg/day) by monitoring water intake and weight gain for thirty days. After P51, mice were placed back on normal drinking water for a period of four months for aging and susceptibility to MPTP-HCl solubilized in saline (0.9% $NaCl_2$) by subcutaneous injection

(s.c.; 20mg/kg; MedchemExpress; Monmouth Junction, NJ) and probenecid by intraperitoneal injection (i.p.; 100mg/kg; Sigma) every other day for one week (4 dosages total), per our previously published protocol (Hammond et al., 2018). Treated mice were aged an additional week before tissue collection.

Behavioral analysis

Two weeks before initial behavioral testing, all mice were acclimated to stress handling by methods closely adapted to previously established protocols (Gouveia and Hurst, 2013; Stuart and Robinson, 2015). Open field testing (OFT) was monitored with Versamax System (Omnitech Electronics, Inc; Columbus Ohio) as previously described by Hammond *et al.* 2018 (Hammond 2018). Gait measurements of stride length, rate and paw intensity were detected by our custom-made in house real-time video gait analysis system. Video recordings of mouse gait were conducted as previously reported (Hammond 2018). All behavioral testing was performed before mice were treated on days 0, 7 and 14 (no treatment) of the MPTPp dosing regimen. All parameter values were subtracted from day 0 for change from baseline measurements.

Tissue processing

For immunohistochemical analysis: mice were anaesthetized under deep isoflourane and transcardially perfused with 0.1M phosphate buffered saline (PBS)-cacodylate/heparin (10 U/ml) and 3% paraformaldehyde/PBS. Following decapitation, whole brains were dissected and stored in 3% paraformaldehyde/PBS overnight at 4°C. The next day, samples were transferred to a gradient of 15-30% sucrose/PBS prior to cryosectioning and storage in cryoprotectant at -20°C until processed for tissue staining. For neurochemical detection of Mn^{2+} and catecholamines: mice were similarly anaesthetized with isoflourane and then rapidly decapitated. Whole brains were dissected and placed on a 1 mm brain block for separation of ST, SN, hypothalamus (Hyp),

and cortex (Cx). Specific brain regions were frozen in liquid nitrogen and then stored at -80°C until processed for HPLC and ICP-MS. Blood was also collected and centrifuged at (1,500 rpm at 4°C /15 minutes) for plasma fractionation and stored at -80°C.

Western Blotting

Striatal tissue used for western blotting was homogenized and lysed in RIPA buffer in presence of protease inhibitors. Protein concentrations were determined by BCA protein assay (ThermoScientific, Pierce Rockford, Il). 23ug/well of protein was separated on 12% SDS-PAGE gel and transferred to PVDF membranes. Blots were incubated with Anti-TH (1:1000; Millipore AB152), anti-VMAT2 (1:750; a gift from Dr. Gary Miller's Laboratory, Emory University), anti-DARPP32 (1:1000; Millipore AB10518), anti-pDARPP32-Thr34 (1:1000; Millipore AB9206), anti-DARPP32-Thr75 (1:1000; Millipore AB9208), and anti-Beta Actin (1:2000; Sigma A1978) diluted into 5% milk/tris-buffered saline with tween (0.1%) blocking buffer. Secondary antibodies used were: anti-Rabbit (Cell signaling 7076S) or anti-Mouse (Cell Signaling 7074S) diluted in blocking buffer. Chemiluminescent imaging was conducted with on a BioRad ChemiDoc MP and raw TIFF files were analyzed for mean optical band density with ImageJ analysis software (Schneider *et al.*, 2012).

Immunostaining and automated stereological cell counting for fixed mouse brain tissue

For stereological determination of TH^+ neurons within the SN, the entire SNpc was serially cryosectioned from the subthalamic nucleus (rostral) to the retrorubal field (caudal) region. Every sixth free-floating section (8 total) was selected from each animal and immunostained for anti-TH (1:500; Millipore AB152) and anti-Neuronal Nuclei (NeuN; 1:250, Millipore; MAB377) by our previously reported protocol (Hammond et al. 2018) (Miller *et al.*, 2011). SNpc neurons were automatically quantitated from 10x-objective montage images of each

immunostained section using a Hammatsu ORCA-Flash4.0 digital CMOS camera, ProScan III stage controller (Prior, Rockland, MA USA) and CellSens Dimension software (version 1.12, Olympus, Center Valley, PA, USA). For automated relative counts of $GFAP^+$, $IBA\text{-}1^+$ and $NeuN^+$ cells, two sections/animal were selected from the same anatomical regions of SN and ST (4 animals were analyzed per group). Primary antibodies for glia labeling were anti-GFAP (1:500; DAKO Z0334), anti-IBA1 (1:250; WAKO 016-20001) and anti-TH (Abcam 76442) to demarcate the SNpc and SNr nuclei. Region of interest was highlighted based on Allen Brain Atlas for reference, following application of an adaptive threshold with shape factor and area (m^2) object filters for automatic cell detection, based on previously published algorythms (Tapias et al., 2013). Detected cell number was divided over the area (μm^2) of region. The investigator was blinded from all experimental groups during imaging and cell quantification.

Image analysis of microglia morphology and reactive astrocytes

For detection of microglia morphology, the same sections immunostained for anti-IBA1/TH for automated counting were re-imaged on a Zeiss Axiovert 200M inverted wide-field fluorescence microscope equipped and a Hammatsu ORCA-ER-cooled charge coupled device camera using a 10x and 40x Planapochromat air objectives with Slidebook imaging software (version 5.0, Intelligent Imaging Innovations, Denver CO). Optical fractionator method employed counting frame size (150 X 150 μm) and frame spacing (for SN; 250 X 250 μm, for ST; 550 X 550 μm). 40x z-stack images of IBA^+ cells from the SNpc, and Gp were acquired and converted to maximum projection, following a binary transformation and then rendered to a skeletonized image in ImageJ, as previously described (Schneider *et al.*, 2012; Morrison and Filosa, 2013). To detect expression of C3 in $S100\beta^+$ astrocytes, the same optical fractionator

method was applied for imaging. Cells were manually quantified based on z-stack images. The investigator was blinded from all experimental groups during cell counting.

High-performance liquid chromatography

Samples of striatum were processed for high performance liquid chromatography (HPLC) coupled with electrochemical detection to quantitate levels of dopamine (DA), 3, 4-dihydroxyphenylacetic acid (DOPAC), homovanillic acid (HVA), serotonin (5-HT) and metabolite 5-hydroxindoleacetic acid (5-HIAA). The Neurochemistry Core Laboratory at Vanderbilt University's Center for Molecular Neuroscience Research (Nashville, TN) processed all tissue samples from each experimental group with coded labeling for unbiased analysis.

Statistical Analysis

All data was presented as mean +/- SEM, unless otherwise noted. Experimental values from each mean were analyzed with a Grubb's (α=0.05) test for exclusion of significant outliers. Differences between each experimental group were analyzed by a one-way ANOVA following a Tukey *post hoc* multiple comparisons test. Significance was identified as $^{++}P < 0.01$, $^{*}P < 0.05$, $^{**}P < 0.01$, $^{***}P < 0.001$, $^{****}P < 0.0001$. All statistical analysis was conducted using Prism (version 6.0; Graph Pad Software, San Diego, CA).

6.3 RESULTS

Developmental weights and water consumption over $MnCl_2$ treatment

At post-natal day (PND) 7 mice were tail clipped for DNA purification and identification of KO and WT progeny per our previously published PCR genotyping protocol (Kirkley et al. 2018**)**. From PN 21 – 51, encompassing the period of juvenile development to early adulthood, mice were placed on drinking water containing $MnCl_2$ (50mg/kg/per day) prior to later exposure to MPTPp, as depicted in **Figure 1A**. Based on statistical analysis of $MnCl_2$ water consumption,

WT consumption increased 2.19 ± 0.44 (mL) and KO consumption increased 2.63 ± 0.78 (mL) from 21-51 PND (*n*=4-5; no significance difference between groups) (**Fig 1B**). For accurate dosing of $MnCl_2$ and detection in change of body weight, mice were weighed every day for the first week of treatment. From 21-27 PND, WT and KO animals significantly increased in weight by 10.65 ± 0.97 and 10.86 ± 0.83 (g), respectively (*n*=8/group; ****$P < 0.0001$). No significant difference in body weight was detected between WT and KO groups treated with $MnCl_2$ (**Fig 1C**).

Inhibition of NF-κB in astrocytes protects DA neurons from MPTP-induced toxicity in the SNpc

To determine the extent of neuronal loss in WT and KO mice following exposure to Mn and MPTP, the substantia nigra of each animal was serially cryosectioned and immunolabeled with anti-TH and anti-NeuN antibodies to label dopaminergic and total neurons, respectively (**Fig 2A-F**). The total number of TH^+ neurons within the SNpc was quantitated for each experimental animal group as follows: WT control (8,024 ± 637.1), WT with $MnCl_2$ (8,779 ± 777.0), WT with MPTPp (3,759 ± 503.7), WT with $MnCl_2$ + MPTPp (3,867 ± 222.1), KO with MPTPp (7,421 ± 537.2), KO with $MnCl_2$ + MPTPp (6,957 ± 1,049). Both WT with MPTPp and with $MnCl_2$ + MPTP displayed 51-53% loss of TH^+ neurons compared to control. KO with MPTPp and $MnCl_2$ + MPTPp had only 7.5-13.3% loss of TH^+ neurons (**Fig 2G**). The mean estimate of total NeuN+ neurons within the SNpc was quantitated as follows: WT control (14,034 ± 631.2), WT with $MnCl_2$ (15,162 ± 609.8), WT with MPTPp (9,778 ± 379.3), WT with $MnCl_2$ + MPTPp (9,636 ± 159.0), KO with MPTPp (12,932 ± 1,167), KO with $MnCl_2$ + MPTPp (11,695 ± 1,152). Comparably, WT with MPTPp and $MnCl_2$ + MPTPp each had a similar 30-

31% loss of total neurons neurons compared to control. KO with MPTPp and $MnCl_2$ + MPTPp only sustained a 7.8-16.7% loss of $NeuN^+$ cells which was not significantly different from control (**Fig 2H**) (*n*=6 animals/per group; $^{**}P < 0.01$, $^{***}P < 0.001$). $MnCl_2$ did not potentiate loss of dopaminergic neuronal soma following later exposure to MPTPp.

$MnCl_2$ potentiates MPTPp-induced neuronal cell death in the globus pallidus and striatum an NF-κB-dependent mechanism in astrocytes

In order to evaluate level of neuronal dysfunction in other basal ganglia nuclei affected by Mn, anatomically registered cyro-sections of the basal ganglia were selected for quantitation of total $NeuN^+$ neurons in the globus pallidus (Gp) and striatum (caudate-putamen, Cp). Representative montage images of sections immunolabeled with anti-NeuN (green) are depicted in **Figure 3 A-D**. The Gp (**Fig 3B**) and Cp (**Fig 3C**) were highlighted as regions of interest (ROI's, highlighted in blue) for automated quantitative detection of the total number of $NeuN^+$ neurons per area (um^2), with individual cell bodies visible in high magnification insets within each ROI. Based on quantitation of total $NeuN^+/um^2$, there was an apparent decrease the number of neurons in WT animals treated with MPTPp or $MnCl_2$ individually but this trend was not statistically different from control. In contrast, WT animals treated with $MnCl_2$ + MPTPp had a 44.1% loss of $NeuN^+$ neurons within the Gp. In contrast, KO animals with dual treatment were protected from loss of neurons, with no differences in neuronal numbers detected compared to WT control animals (**Fig 3E**). Quantitation of $NeuN^+$ cells/um^2 within the Cp showed a similar trend as the Gp, however no groups were statistically different (**Fig 3F**). To measure the integrity of TH^+ presynaptic terminals in the Cp, sections were also co-immunolabeled with anti-TH (red) as depicted in **Fig 3D**. An apparent decrease in TH+ terminal density in WT animals treated with

$MnCl_2$ or MPTPp individually was noted but was not significantly different from control. Dual treatment with both $MnCl_2$ and MPTPp in WT mice caused a decrease in DA terminal density to 62.5% of control animals, whereas KO animals with dual treatment only had a 20.7% loss of terminals compared to control WT mice (**Fig 3G**) (n=6-7 animals/group; *$P < 0.05$, **$P < 0.01$, ***$P < 0.001$).

IKK2 knockout mice are protected against behavioral and neurochemical deficits caused by exposure to Mn and MPTPp

Spontaneous locomotor activity was detected by open field test (OFT) for each experimental group. In adult WT mice treated only with $MnCl_2$ as juveniles, there was a decrease in the total distance traveled but other behavioral parameters were unchanged from baseline (**Fig 4A**). In contrast, dual-treated WT mice ($MnCl_2$/MPTPp) displayed hyperactive behavior in multiple parameters of OFT analysis. Dual treatment significantly increased levels of margin time (**Fig 4B**), center time (**Fig 4C**), horizontal movement (**Fig 4E**), stereotypy movement (**Fig 4F**), and ambulatory movement (**Fig 4G**) compared to MPTPp-only treatment. Interestingly, treated KO animals did not display hyperactive behavior and were not different from WT control animals, as depicted by the graphs in **Fig 4A-C** and **Fig 4EG**, as well as in representative traces and pseudocolored time plots of activity over a 5 min interval (**Fig 4D**) (n=7-10 animals/group; *$P < 0.05$, **$P < 0.01$, ***$P < 0.001$, ****$P < 0.0001$). Quantitative analysis of stride length from each experimental animal was conducted using a real-time video gait analysis system. WT animals treated with MPTPp and $MnCl_2$/MPTPp exhibited an apparent decrease of stride length compared to WT control that was not statistically significant. However, dual-treated KO animals

had a significantly longer stride length compared to treated WT animals during the course of the study (**Fig 4H**) (n=5-6 animals/group; *$P < 0.05$).

Levels of striatal catecholamines and metabolites were detected by HPLC analysis with electrochemical detection. All MPTPp-treated animals with or without $MnCl_2$ exhibited a drastic loss of DA and DOPAC. Additionally, a slight increase in DA levels was apparent in $MnCl_2$-only treated WT animals but was not statistically different from control (**Fig 4I, J**). Dual-treated WT animals also displayed a significantly higher ratio of DOPAC/DA compared to control (**Fig 4K**). The DA metabolite, HVA, was also decreased with MPTPp treatment, independent of $MnCl_2$ treatment and genotype (**Fig 4L**). Serotonin (5H-T) content showed no statistical difference between experimental groups (**Fig 4M**). However, analysis of the serotonin metabolite (5-HIAA) showed a significant increase in both WT and KO dual treated animals compared to MPTPp-only treatment (**Fig 4N**) (n=5-9 animals/group; *$P < 0.05$, **$P < 0.01$, ***$P < 0.001$).

Juvenile exposure to $MnCl_2$ intensifies activation of microglia in the globus pallidus after treatment with MPTPp and is suppressed in astrocyte-specific IKK2 knockout mice

The relative number of microglia within basal ganglia was detected by immunolabeling with anti-IBA1 as depicted in representative images of the Gp and Cp (**Fig 5A-C**). Both MPTPp and MPTPp/$MnCl_2$ treatments in WT animals increased the number of IBA-1^+ cells/$\square m^2$ within the Cp and treated KO animals displayed similar numbers as the control group, shown in **Fig 5D**. Dual-treated WT animals also exhibited the most IBA-1^+ cells/um^2 within the Gp, which was reduced in KO animals (**Fig 5E**) (n=5-6 animals/group; **$P < 0.01$, ***$P < 0.001$, ****$P < 0.0001$). There was a significant increase of IBA-1^+ cells/$\square m^2$ in the SNpc of MPTPp treated WT animals and slightly less in KO animals, that was not statically different from WT (**Fig 5F**).

A similar trend of IBA-1$^+$ cells/um^2 in the SNpr was noted, although not statically different between groups (**Fig 5F**). For assessment of microglia morphology, 40x-objective IBA-1 (greyscale) images of the Cp and Gp were skeletonized to detect for number of branches as depicted in representative images in **Fig 5H**. WT dual-treated animals exhibited significantly less branches/cell in the Cp (**Fig 5I**), Gp (**Fig 5J**), and less junctions/cell in the Cp (**Fig 5K**), and Gp (**Fig 5K**) compared to dual treated KO animals (n=7 animals/group; $*P < 0.05$).

Activation of astrocytes in the basal ganglia following dual treatment with $MnCl_2$ and MPTPp is regulated by NF-κB

Expression of IKK2 was determined in hGfap-cre$^{+/-}$/Ikk2$^{fl/fl}$ mice by co-immunolabeling with anti-GFAP (red) and anti-IKK2 (green), as depicted in representative 100x-objective images from the globus pallidus in WT control (**Fig 6A**), WT dual-treated (**Fig 6B**) and KO dual-treated (**Fig 6C**) mice. Expression of IKK2 protein was present in both control and dual-treated WT mice was not detected in any experimental group in KO mice. For assessment of the relative number of GFAP$^+$ cells present in multiple nuclei of each experimental group, anatomically consistent cyrosections of ST and SN were selected for automated counting of GFAP$^+$ cells/um^2. As depicted in representative 10x montage images of the Gp and Cp, dual-treated WT animals exhibited increased proliferation of GFAP$^+$ astrocytes in both nuclei (**Fig 6F**). Dual treatment significantly increased GFAP$^+$/um^2 over MPTPp-only treatment in WT animals in Gp and KO animals exhibited significantly less independent of treatment (**Fig 6 D-G)**. Similarly, increased GFAP$^+$ cells/um^2 was evident in dual-treated WT animals in the Cp but was not statistically different from WT animals treated only with MPTPp for this region (**Fig 6H**). Comparably, dual-treated WT animals exhibited the greatest amount of GFAP$^+$ immunoreactivity in the SNpc,

whereas KO animals had similar numbers of $GFAP^+$ cells/um^2 as control mice (**Fig 6I-L**) (n=6; *P < 0.05, **P < 0.01, ***P < 0.001, ****P < 0.001). We also observed an apparent trend of $GFAP^+$ cells/um^2 in the SNpr of each experimental group that was not statistically significant (**Fig 6M**).

Complement protein-C3 is highly expressed in reactive astrocytes following treatment with $MnCl_2$/MPTPp and down regulated in IKK2 KO mice

To quantitate number of neurotoxic astrocytes present throughout the basal ganglia, brain sections were stained for expression of the complement protein, C3 (**Figure 7**), which is uniquely expressed in reactive astrocytes in the CNS (Liddelow et al., 2017a). S100β was used to determine the total number of astrocytes. Each brain region was imaged using randomized sampling and the number of astrocytes co-expressing $C3^+$ and $S100\beta^+$ was compared to the total number of $S100\beta^+$cells. Wildtype animals treated with $MnCl_2$/MPTPp exhibited significantly higher numbers of neurotoxic astrocytes in the Gp (**Fig 7B, D, F**), Cp (**Fig 7B**, **F**, **H**), SNpc (**Fig 7J, L**, **N**) and SNpr (**Fig 7J**, **N**, **P**) than control mice. Inhibition of NF-κB signaling in astrocytes in KO mice suppressed the increase in C3+ astrocytes in each region following treatment with $MnCl_2$/MPTPp, as depicted in the representative images in **Figures 7C, G, K, O** (n=7 animals/group; *P < 0.05, **P < 0.01, ***P < 0.001).

6.4 DISCUSSION

Almost two hundred years ago, James Couper described the first case of manganism from inhalation of Mn oxide ore dusts in workers who developed gait disorders similar to Parkinson's disease (Couper, 1837). Today, the pathological mechanisms underlying irreversible neurological damage from Mn exposure are still not completely understood. However,

neuroinflammatory activation of glial cells is a common mechanism underpinning the neurotoxicity of Mn in both humans and in animal models of the disease, as we have previously reported (Kirkley et al. 2017; Moreno et al. 2011). Accordingly, we demonstrated that PND 20-34 juvenile mice were particularly susceptible to Mn-induced neuroinflammation (Moreno et al 2009), potentially due to a critical period of striatal development in rodents (Soiza-Reilly and Azcurra, 2009). Recently, we characterized a novel astrocyte-specific transgenic mouse deficient in IKK2, the upstream activating kinase for NF-κB, that prevented the production of the pro-inflammatory factors NOS2 and TNFα and was neuroprotective in the MPTPp animal model of PD (Kirkley et al. 2018). The present study expanded on this work and examined the role of IKK2/NF-κB activation in astrocytes following juvenile Mn exposure as a modulator of neuronal loss and glial reactivity in the basal ganglia afte a secondary exposure to the dopaminergic neurotoxicant, MPTP.

Combined developmental/adult exposure to Mn and MPTPp caused considerably different OFT performance compared to the other experimental groups. Spontaneous locomotor activity was increased in multiple parameters of total distance (**Fig 4A**), margin time (**Fig 4B**), center time (**Fig 4C**), horizontal count (**Fig 4E**), stereotypy count (**Fig 4F**), and ambulatory count (**Fig 4G**), representing an overall hyperactive phenotype. CNS activity aberrations such as abnormal neuromuscular function and fine motor deficits have been documented in rat models ranging from low (4.8mg/kg) subchronic to high (50mg/kg) chronic $MnCl_2$ administration (Witholt *et al.*, 2000) (Beaudin *et al.*, 2016). This suggests that pre-synaptic DA neurotransmission is not the major system effected, because dual treatment with $MnCl_2$/MPTPp did not exacerbate DA neuronal loss in the SNpc (**Fig 2G**) or striatal dopamine production (**Fig 4H**). However, MPTP is a potent and selective neurotoxicant and it is possible that loss of DA

neurons was already maximal and therefore not exacerbated by Mn. In contrast, Mn loss of TH+ terminals in the Cp in WT mice following dual treatment with MPTPp compared to control and MPTPp-only treatment (**Fig 3G**). Low subchronic dose of $MnCl_2$ for 5-weeks also demonstrated no further depletion of nigro-striatal DA depletion due to $MnCl_2$ treatment (Gwiazda *et al.*, 2002). In contrast, Beudin et al. showed chronic administration of 50mg/kg/day from PND 20-460 significantly depleted DA (Beaudin *et al.*, 2016). Extending $MnCl_2$ treatment more than 30 days prior to MPTPp treatment would therefore likely have produced more severe effects on DA neurons in the current study.

We also investigated $MnCl_2$ effects on neurons in the Gp, which primarily receive and relay inhibitory gamma butyric acid (GABA)-ergic innervation. Quantitation of total NeuN+ neurons in the Gp revealed a trend toward decreased numbers of $NeuN^+$ neurons/$\square m^2$ in mice treated only with $MnCl_2$ and in mice treated only with MPTPp but significant loss of $NeuN^+$ neurons/um^2 in the Gp was only detected in $MnCl_2$/MPTPp-treated WT animals compared to controls (**Fig 3E**). Astrocyte-specific deletion of IKK2 prevented neuronal loss in the Gp, indicating that prior exposure to Mn enhances neuronal injury after a secondary exposure to MPTP through a mechanism involving NF-κB-dependent inflammatory activation. The extent of Mn-induced glial reactivity may influence the dysregulation of neurotransmitters in the Gp, based in part on the model and dosing regimen. For example, chronic exposure to Mn (10 mg/kg) in non-human primates depleted expression of glutamine synthetase in the Gp but had no effect on GABAergic or glutamatergic systems (Burton *et al.*, 2009). Other studies in rats treated with 6 mg/kg/per day reported a significant increase in brain Mn levels and a decrease in GABA (Erikson and Aschner, 2003). Conversely, another study in rats demonstrated that 20 mg/kg/day

exposure to Mn led to a significant increase of both Mn and GABA concentrations in the brain (Lipe et al., 1999).

The hyperactive locomotor responses observed in Mn-treated mice might be associated with loss of neurons in the Gp, which would cause less GABAergic output to the subthalamic nucleus and therefore increased Glu excitation to the SNpc and increased firing of DA neurons to the ST (Erikson and Aschner, 2003). This theory of increased DA firing could explain the modest increases in the number of TH+ neurons observed in the SNpc (**Fig 2G**), as well as increases in DA content (**Fig 4G**). Serotonergic neurotransmission is also a possible target of Mn toxicity. Alterations in serotonin (5-HT) can cause abnormalities in motor activity and sleep, both of which are symptoms of manganism (Lesch *et al.*, 1996). There was significant increase of the 5-HT metabolite (5-HIAA) of the ST from both dual-treated animal groups, although no differences in levels of 5-HT were detected between groups (**Fig 4M**). This finding is consistent with previous data from our laboratory where we observed that juvenile mice treated with $MnCl_2$ exhibited high levels of 5-HIAA compared to mice treated with Mn only as adults (Moreno, Yeomans, *et al.*, 2009).

Neuronal cell death in response to $MnCl_2$/MPTPp treatment was significantly modulated by neurotoxic activation of astrocytes regulated by IKK2/ NF-κB. Inhibition of astrocyte- NF-κB protected DA neurons from both MPTPp and $MnCl_2$/MPTPp-induced toxicity by ~90% compared to control within the SNpc (**Fig 2G**). KO animals also did not sustain any loss of neurons in the Gp, terminals of the Cp and were protected from apoptotic mechanisms such as activation of cleaved-caspase 3 (**Fig 3E-G**). This is consistent with studies reporting that mice with constitutively active astrocyte-NF-κB had increased production of cytokines in the MPTP model of PD, as well as increased amyloid burden and gliosis in a mouse model of AD (Oeckl *et*

al., 2012; Lian *et al.*, 2016). Knock-out of IKK2 in all CNS cells demonstrated protection in a mouse model of auto-immune encephalitis (van Loo *et al.*, 2006). However, IKK2/NF-□B signaling in neurons is also necessary for protection against traumatic brain injury and synaptic plasticity for memory formation (Mettang *et al.*, 2017; Kaltschmidt *et al.*, 2006), suggesting that targeting NF-*κ*B pro-inflammatory signaling in glia may represent a better neuroprotective strategy. The current study is the first to report that inhibition of astrocyte-IKK2 protects against reactive gliosis and neuronal death induced by both $MnCl_2$ and MPTPp treatment.

Astrocyte-specific deletion of IKK2 also reduced microglial activation in the Gp (**Fig 5E, J, L**) and Cp (**Fig 5D, I, K**). Inhibition of microglia activation in the Gp of KO animals directly correlated with the preservation of $NeuN^+$ cells with dual treatment (**Fig 5E, 3E**). However, no significant suppression of microgliosis was observed in the SNpc or SNr, consistent with the initial characterization of hGFAP-$cre^{+/-}$/$IKK2^{fl/fl}$ treated with MPTPp (**Fig 5F-G**) (Kirkley 2018). Microglia stimulate phenotypic activation of neurotoxic A1 astrocytes through release of factors such as TNFα, C1q and IL1α (Liddelow et al., 2017a) that in turn further magnify microglial reactivity through NF-kB-dependent production of neuroinflammatory signaling molecules such as CCL2 (Popichak et al., 2018a). Thus, dampening innate immune inflammatory signaling in astrocytes through gene deletion of IKK2 likely prevented more severe neuroinflammatory activation of microglia in this model. These studies confirmed that immunopurified primary astrocytes isolated from KO mice exhibited 70% knockdown of IKK2, which we also observed here, as depicted in representative images of IKK2/GFAP co-localization in Figure **6A-C**. Quantitation of the number of $GFAP^+$ cells/um^2 confirmed that the most affected nucleus in WT mice exposed to Mn/MPTPp was the Gp (**Fig 6D, F**). KO animals exhibited significantly fewer $GFAP^+$ cells/um^2 in the Gp, Cp and SNpc, although no groups were different in the SNpr,

potentially due to constitutively high basal levels of astrocytes present in this brain region (**Fig 6D-M**).

Studies of MPTP neurotoxicity demonstrate that astrocytes remain chronically activated long after activation of microglia subsides subsequent to DA neuronal death (Hirsch and SP Hunot, 2009; Huang *et al.*, 2018). Therefore, we expected that $MnCl_2$ exposure would prime astrocytes to an activated state which was further enhanced to a neurotoxic state by MPTP administration months later through an NF-*κ*B dependent mechanism. To specifically detect neurotoxic astrocytes expressing a reactive A1 phenotype, we immunolabeled for complement protein-C3 in regions in which we saw induction of gliosis and neuronal death (**Fig 7**). C3 is an important component of the classical complement pathway that mediates a peripheral innate immune response in the presence of pathogens (Ricklin *et al.*, 2016). The expression of C3 in the CNS has more recently been identified in astrocytes from patients with PD, AD, ALS and even HIV infection and is uniquely expressed in reactive A1 astrocytes, not in resting A2 astrocytes (Liddelow *et al.*, 2017; Nitkiewicz *et al.*, 2017). Several of these studies demonstrate that astrocyte-C3 expression is regulated through NF-*κ*B (Lian *et al.*, 2016; Nitkiewicz *et al.*, 2017). Lian et al. reported that constitutively active NF-*κ*B driven by hGFAP in astrocytes promoted an increase of C3 expression in a mouse model of AD. Inversely, the present study, the KO animals had significantly fewer astrocytes expressing $C3^{+}$+$S100\beta^{+}$/$S100\beta^{+}$ in regions lesioned with dual $MnCl_2$/MPTPp treatment compared to the WT animals (**Fig 7D, H, L, P**). These data suggest that astrocyte- NF-*κ*B regulated C3 expression may be an important mechanism to attract reactive microglia and thereby maintain a chronic state of neurotoxic reactive A1 astrocytes that promotes neurodegeneration in affected brain regions, such as the Gp and Cp.

In conclusion, we report a novel neuroinflammatory mechanism in astrocytes associated with juvenile $MnCl_2$ exposure that exacerbated neurodegeneration from later adult exposure to MPTPp. These data demonstrate that astrocyte-specific gene deletion of NF-κB /IKK2 mitigates the numbers of reactive astrocytes and microglia and protects against neuronal loss in the basal ganglia induced by sequential exposure to Mn and MPTPp. Our results reveal that the Gp is the nucleus within the basal ganglia most affected by dual treatment with $MnCl_2$/MPTPp and that neurodegeneration can be blocked by inhibition of astrocyte- NF-κB. Additionally, we provide evidence that $MnCl_2$/MPTPp treatments in mice increase the presence of neurotoxic $C3^+$ A1 astrocytes that are highly regulated by NF-κB activation in astrocytes. Approaches that target NF-κB in astrocytes could therefore lead to novel therapeutic approaches for PD and PD-like disorders, such as manganism.

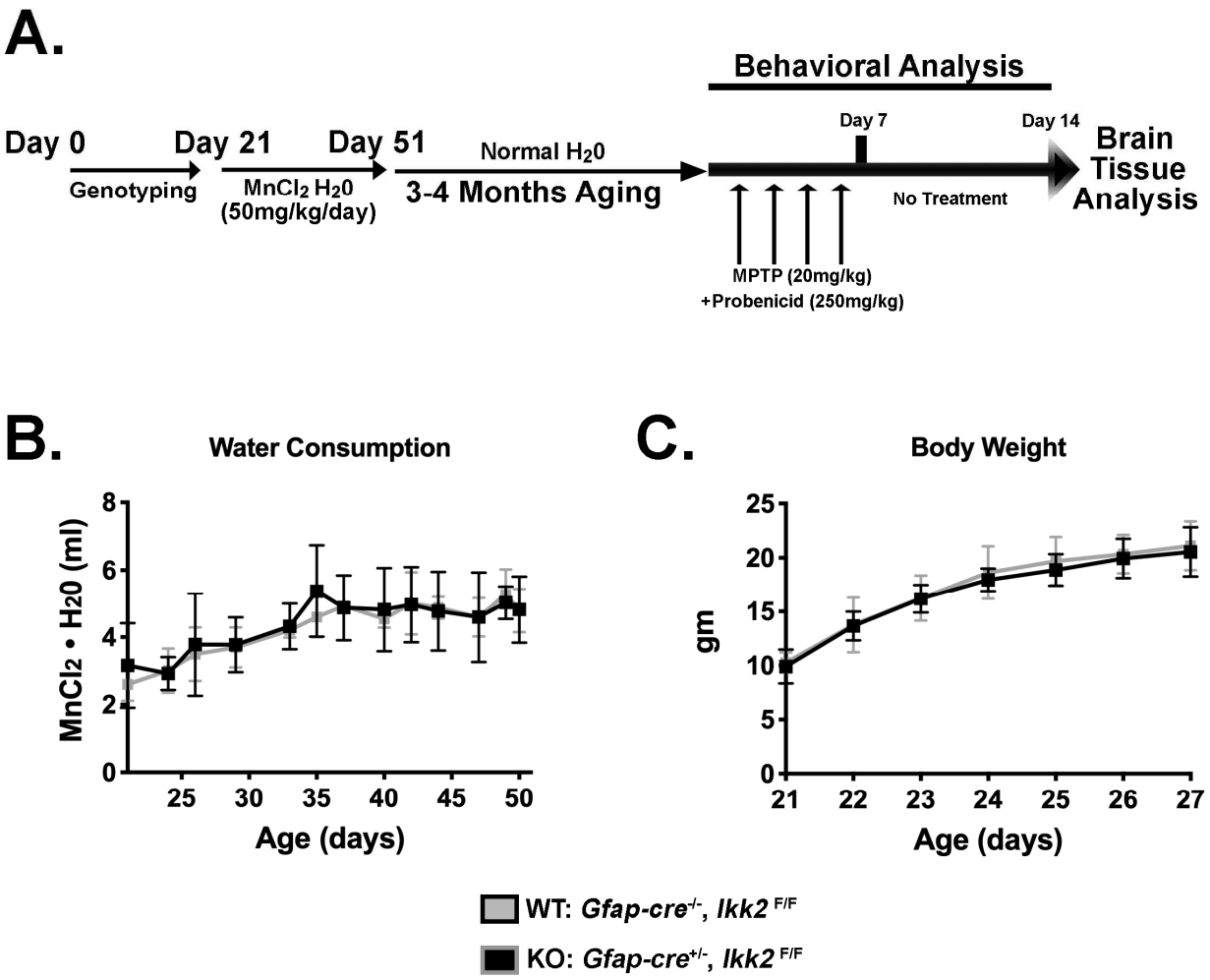

Figure 6.1. Treatment strategy for two-hit neurodegenerative model with manganese and MPTP. (**A**) Experimental design for two-hit neurodegenerative model. Wildtype (*Gfap-cre*$^{-/-}$, *Ikk2*$^{F/F}$) and astrocyte-specific knockout (*Gfap-cre*$^{-/-}$, *Ikk2*$^{F/F}$) mice were given either normal drinking water (18 Ω MilliQ) or $MnCl_2 \cdot 4H_2O$ in drinking water (50 mg/Kg/day Mn^{2+}) from PN21-51, followed by treatment with either vehicle or MPTP four months later. Behavioral analysis was conducted throughout the period of treatment with MPTP after collecting baseline data prior to dosing. All mice were terminated one week after the final dose of MPTP for analysis of neurochemical and immunohistochemical endpoints. (**B**) Consumption of water and (**C**) body weight was not different between wildtype and knockout mice exposed to $MnCl_2 \cdot 4H_2O$ in drinking water. Black bars - KO (*Gfap-cre*$^{+/-}$, *Ikbk2*$^{F/F}$), Gray bars – WT (*Gfap-cre*$^{-/-}$, *Ikbk2*$^{F/F}$). *N*=6-8 animals/genotype.

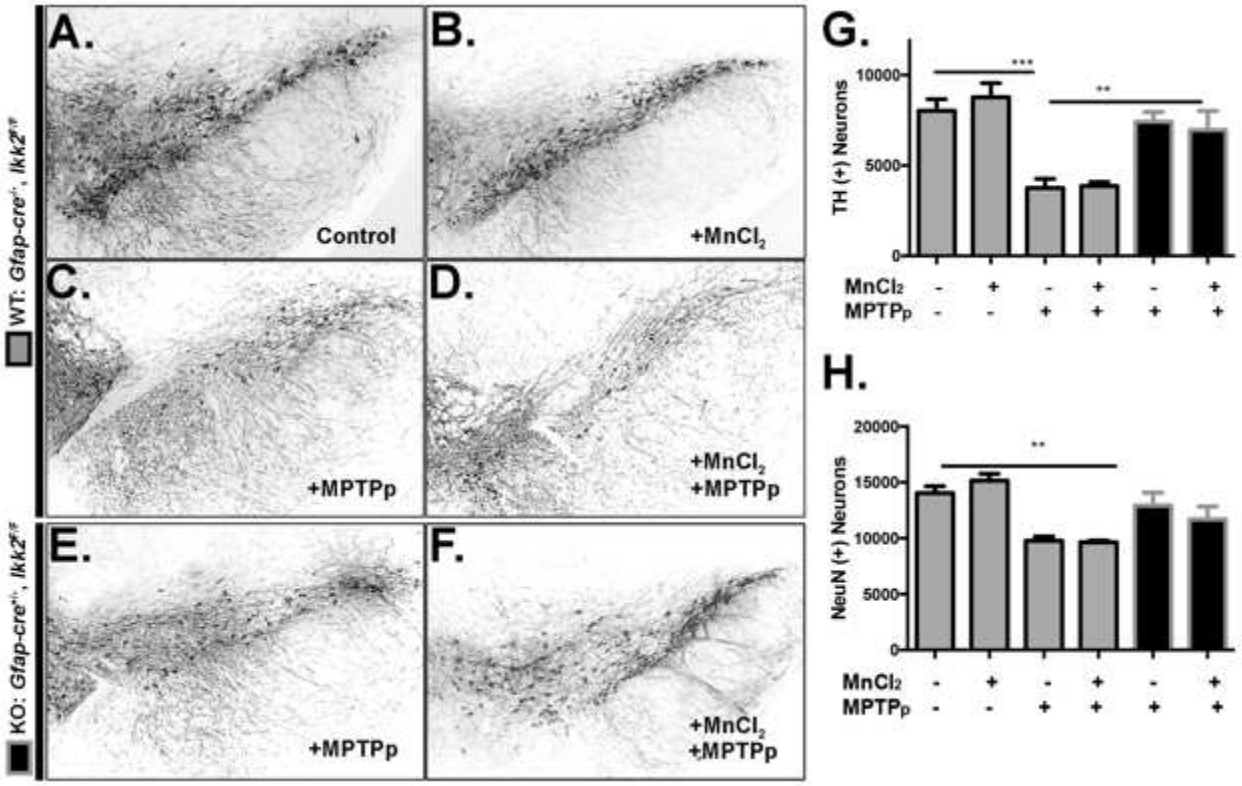

Figure 6.2. Astrocyte-specific knockout of IKK2 prevents loss of dopaminergic neurons following combined treatment with manganese and MPTP. The number of NeuN+ (total) and tyrosine hydroxylase+ (dopaminergic) neurons in the substantia nigra was determined by 3D designed-based stereology in frozen serial sections from WT (*Gfap-cre*$^{-/-}$*/Ikk2*$^{F/F}$) and KO (*Gfap-cre*$^{+/-}$*/Ikk2*$^{F/F}$ mice. Mice received either regular drinking water or drinking water containing 50 mg/Kg/day $MnCl_2$ from PN21-51 and were then treated with MPTP + probenecid (MPTPp) or vehicle at six months of age. Dual-labeled immunofluorescence montage images were collected using a 10X air Plan Apochromat objective, counterstained DAPI to identify cell nuclei. Grayscale images of TH labeling are presented for each treatment group as follows: (**A)** WT – Control, (**B**) WT - $MnCl_2$, (**C**) WT - MPTPp, (**D**) WT - $MnCl_2$/MPTPp, (**E**) KO - MPTPp (**F**) - $MnCl_2$/MPTPp. (**G**) Quantitative assessment of TH^+ neurons in the SNpc. (**H**) Quantitative assessment of total $NeuN^+$ neurons in the SNpc. $^{**}P < 0.01$, $^{***}P < 0.001$; N=6 animals/group.

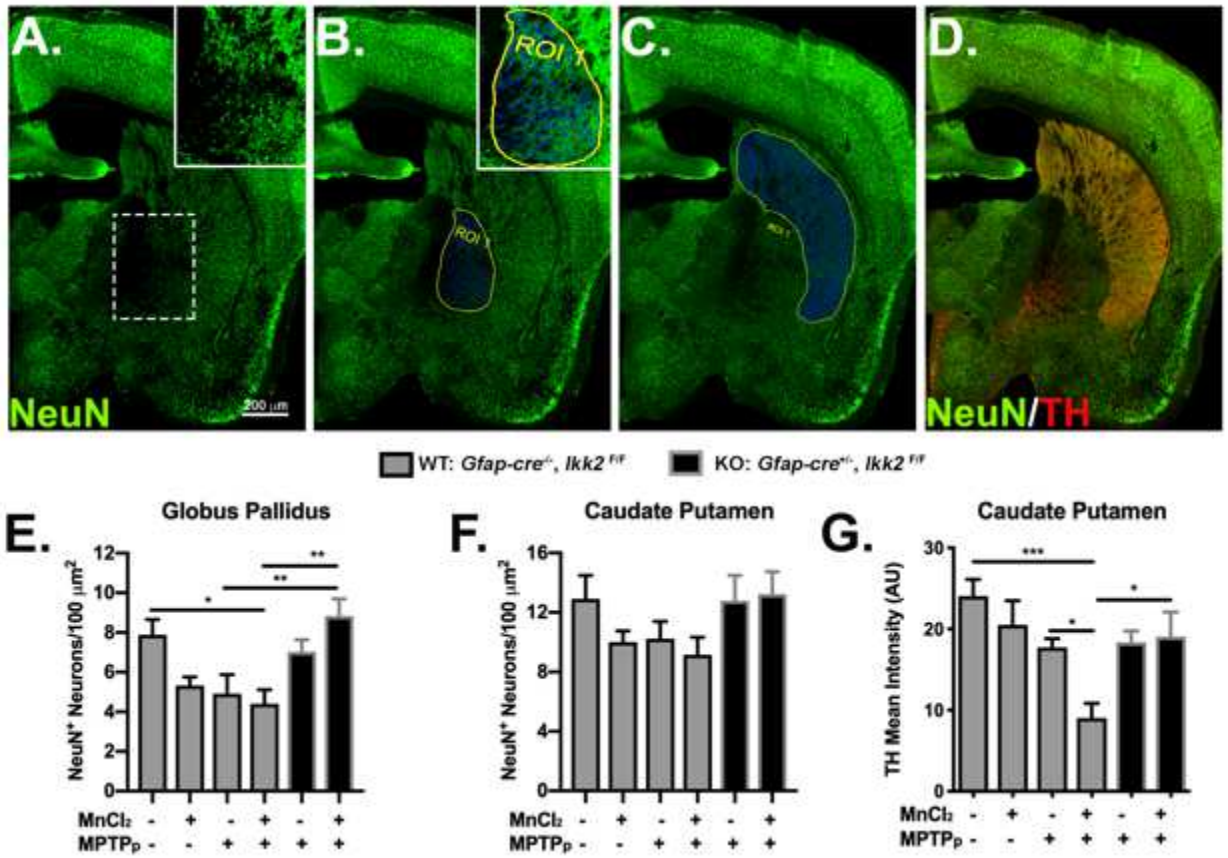

Figure 6.3. Sequential exposure to $MnCl_2$ and MPTP causes neuronal loss in the globus pallidus and enhances loss of dopaminergic fibers in the striatum through an astrocyte-dependent mechanism. Image analysis of NeuN+ neurons the globus pallidus (Gp) and caudate-putamen (Cp) in wildtype and astrocyte-specific IKK2 KO mice. (**A - D**) Total neurons were immunolabeled with NeuN+ (green) and sections were counterstained with TH (Red) to highlight dopaminergic terminals in the Cp (**D**). Regions of interest (ROI's) were drawn around each anatomically distinct nucleus for quantification of the total number of neurons. The Gp (**B**) and Cp (**C**) were identified as ROI's for automated cell detection (blue). Co-labeling with anti-TH (red) depicts DA pre-synaptic terminals in the Cp (**D**). Total number of $NeuN^+$ cells/100 um^2 was quantitated for the Gp (**E**) and Cp (**F**). (**G**) Mean intensity of TH+ immunoreactivity was measured for detection of DA innervation in the Cp. Juvenile exposure to Mn did not potentiate MPTP-induced neuronal loss in the Gp but did enhance MPTP-mediated loss of TH fibers in the Cp. $*P < 0.05$, $**P < 0.01$, $***P < 0.001$; N=6-7 animals/group.

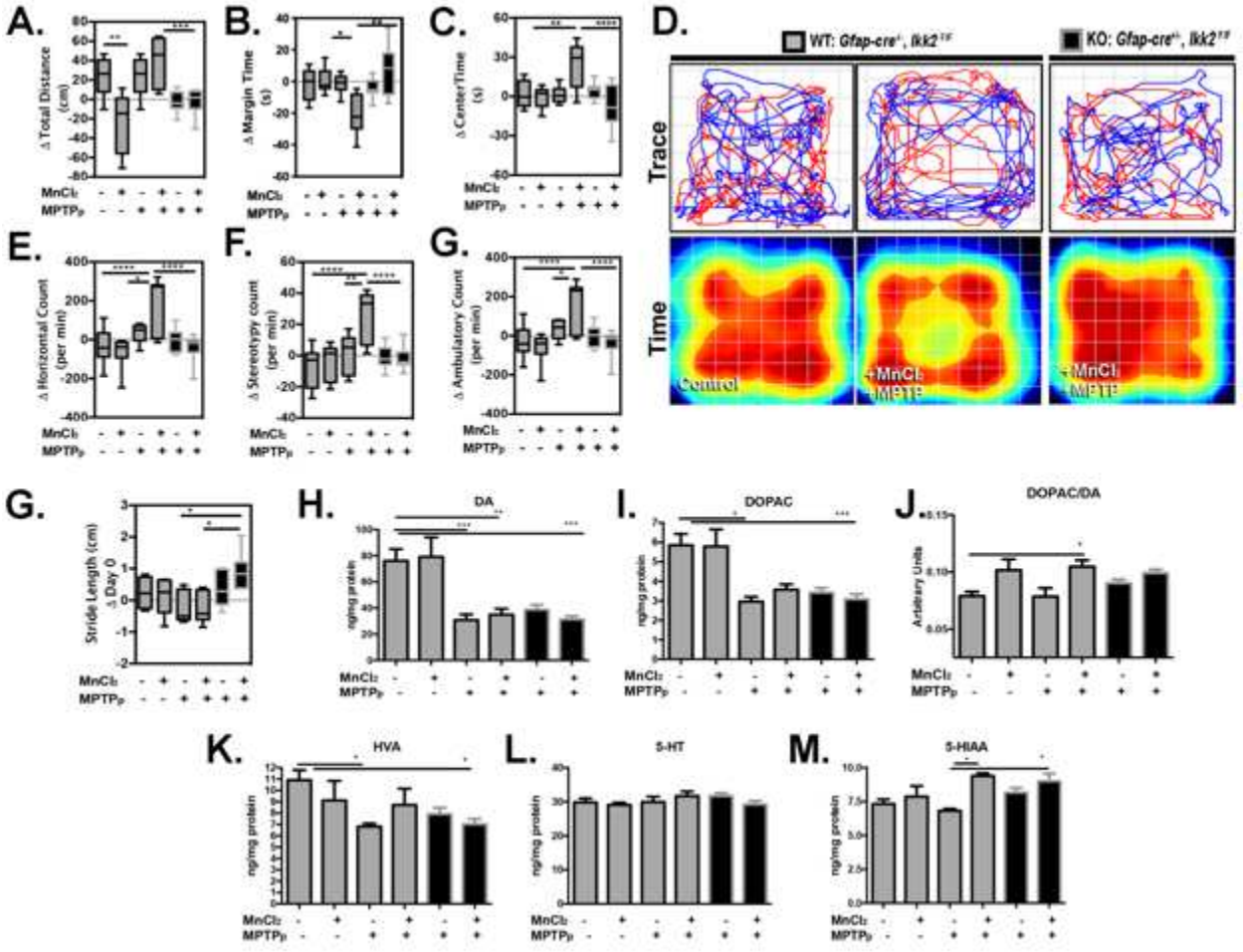

Figure 6.4. Juvenile exposure to manganese exacerbates MPTP-induced behavioral dysfunction through NF-κB signaling in astrocytes. Open field behavioral testing for locomotor function was conducted for total distance (**A**), margin time (**B**) and center time (**C**), compared to baseline values prior to dosing with MPTPp. (**D**) Representative trace plots (top) and pseudocolored heat maps of total time spent (bottom) in the position of the chamber for 5 min intervals are depicted for WT - control, WT - $MnCl_2$/MPTPp and KO - $MnCl_2$/MPTPp animals. (**E**) Change in horizontal count, (**F**) stereotypy count and (**G**) ambulatory count values were normalized to day 0 baseline values (*$P < 0.05$, **$P < 0.01$, ***$P < 0.001$, ****$P < 0.0001$; N=7-10 animals/group). (**H**) Real-time video gait analysis was utilized to quantitate change of stride length from day 0 (*$P < 0.05$; N=5-6 animals/group). HPLC analysis was used for detection of neurotransmitter content from striatal tissue for (**H**) DA, (**I**) DOPAC, (**J**) DOPAC/DA, (**K**) homovanillic acid (HVA), (**L**) serotonin (5-HT) and (**M**) 5-HIAA (*$P < 0.05$, **$P < 0.01$, ***$P < 0.001$; N=5-9 animals/group).

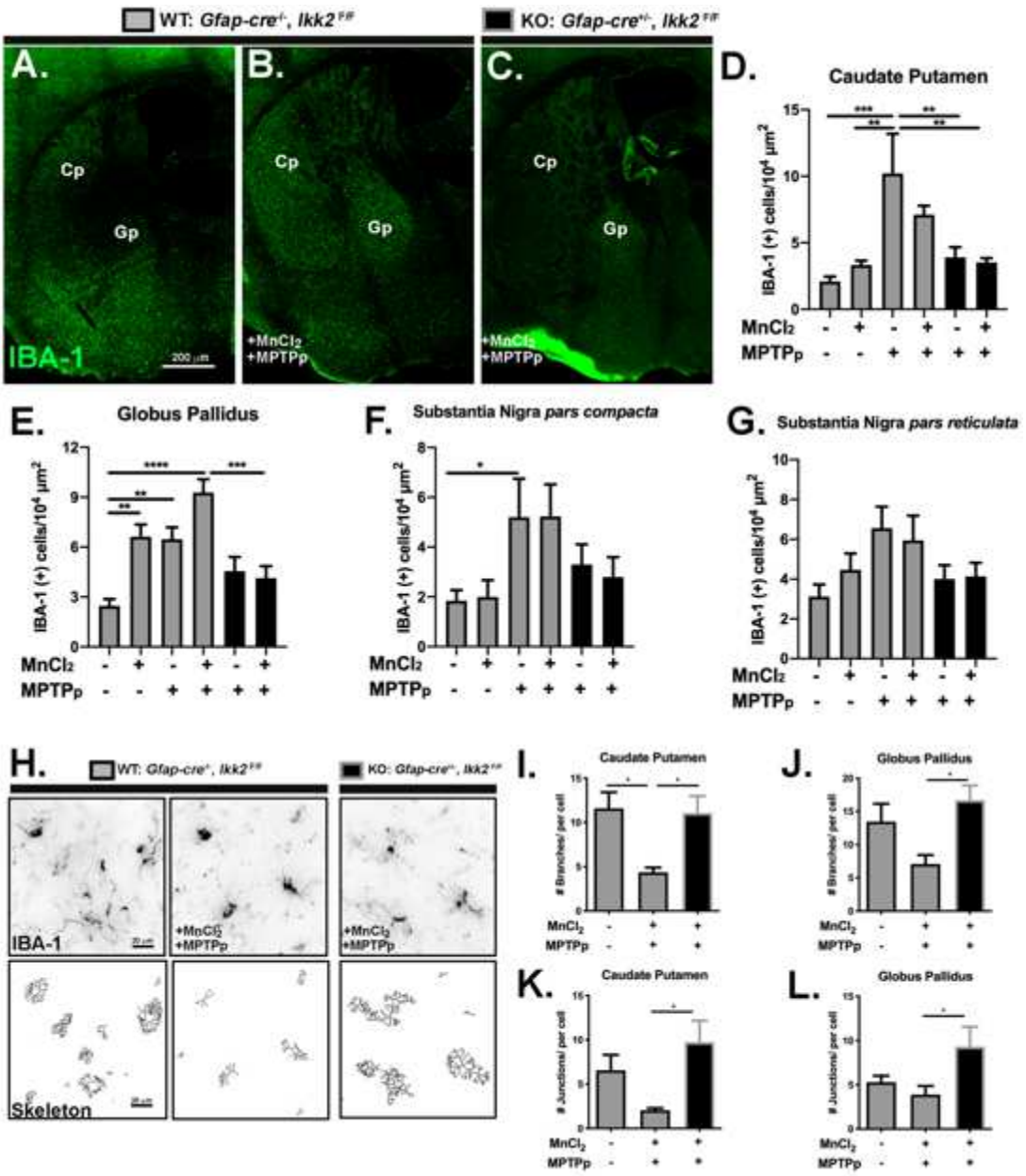

Figure 6.5. Inhibition of NF-κB signaling in astrocytes suppresses a reactive phenotype in microglia following sequential exposure to $MnCl_2$ and MPTP. Microglia were analyzed by automated quantitation of tissue sections immunolabeled with anti-IBA1 antibodies (green), as depicted in montage images of (**A**) WT - control, (**B**) WT - $MnCl_2$/MPTPp and (**C**) KO - $MnCl_2$/MPTPp treatment groups. The total number of $IBA1^+$ cells/100 um^2 for the Cp (**D**), Gp (**E**), SNpc (**F**) and SNpr (**G**) were quantitated for all experimental groups (**$P < 0.01$, ***$P < 0.001$, ****$P < 0.0001$; N=5-6 animals/group). (**H**) Image skeletonization of $IBA1^+$(black) cell morphology are depicted in representative images of WT-control, WT + $MnCl_2$/MPTPp, and KO + WT + $MnCl_2$/MPTPp. Three experimental groups were quantitated for #branches/cell in Cp/Gp (**I-J**), and #junctions/cell in Cp/Gp (**K-L**) (*$P < 0.05$; N=7 animals/group).

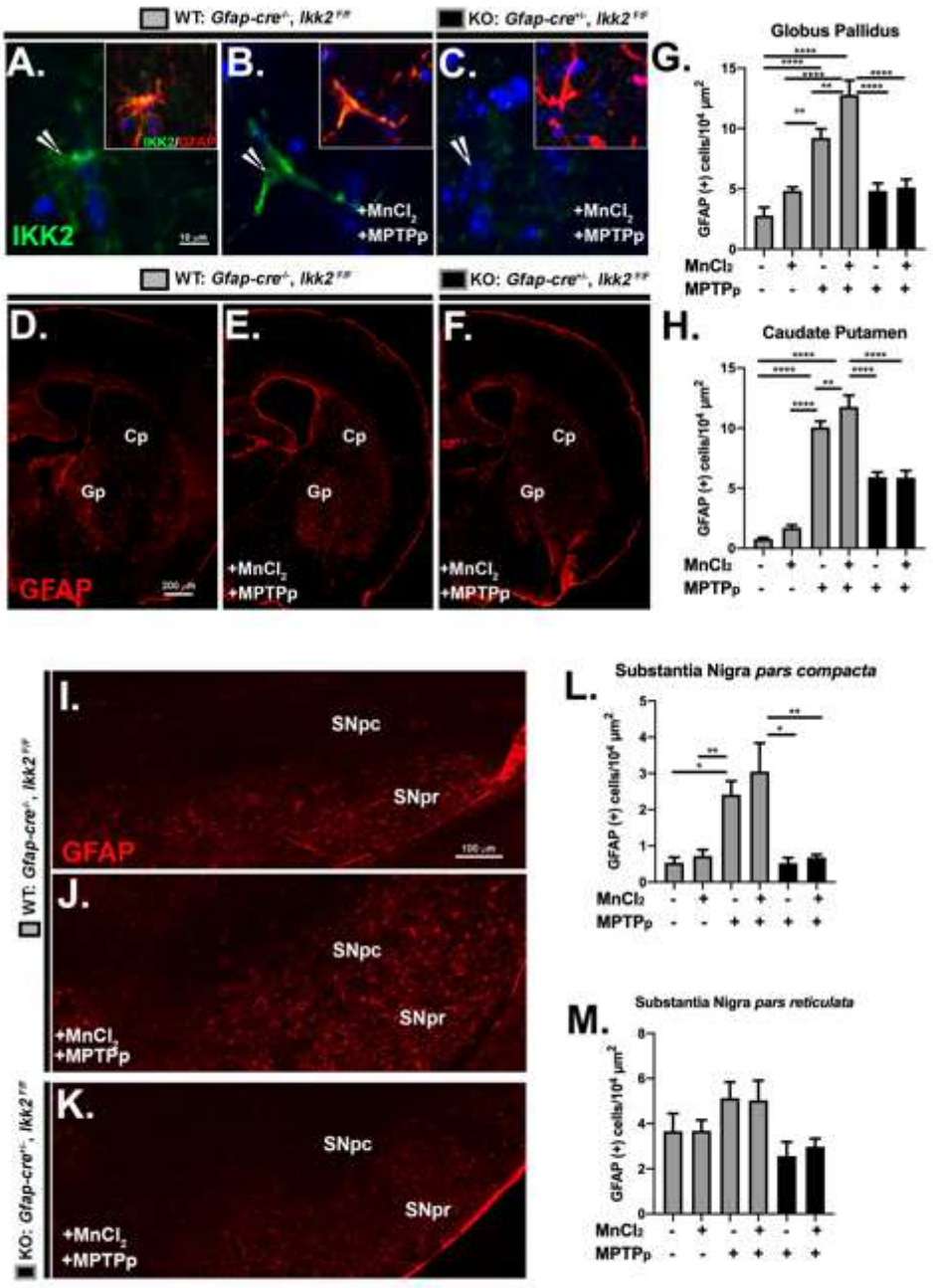

Figure 6.6. $MnCl_2$/MPTPp treatment increases astrocyte activation and by an astrocyte-NF-κB dependent mechanism 100x-objective representative images of anti-IKK2 (green), anti-GFAP (red) colocalizing cells (arrowheads) from WT-control (**A**), WT + $MnCl_2$/MPTPp (**B**), and KO + $MnCl_2$/MPTPp (**C**) treated animals. Total $GFAP^+/um^2$ were quantitated from the Gp (**D**) and Cp (**H**) in all experimental groups, as depicted in 10x-objective montage images of ST with anti-GFAP (red) in three groups (**E**-**G**). SNpc and SNr was also immunostained for GFAP as depicted in representative 10x-objective images in (**I**-**K**). Analysis of $GFAP^+/um^2$ in SNpc (**L**) and SNpr (**M**) (*$P < 0.05$, **$P < 0.01$, ***$P < 0.001$, ****$P < 0.001$; N=6).

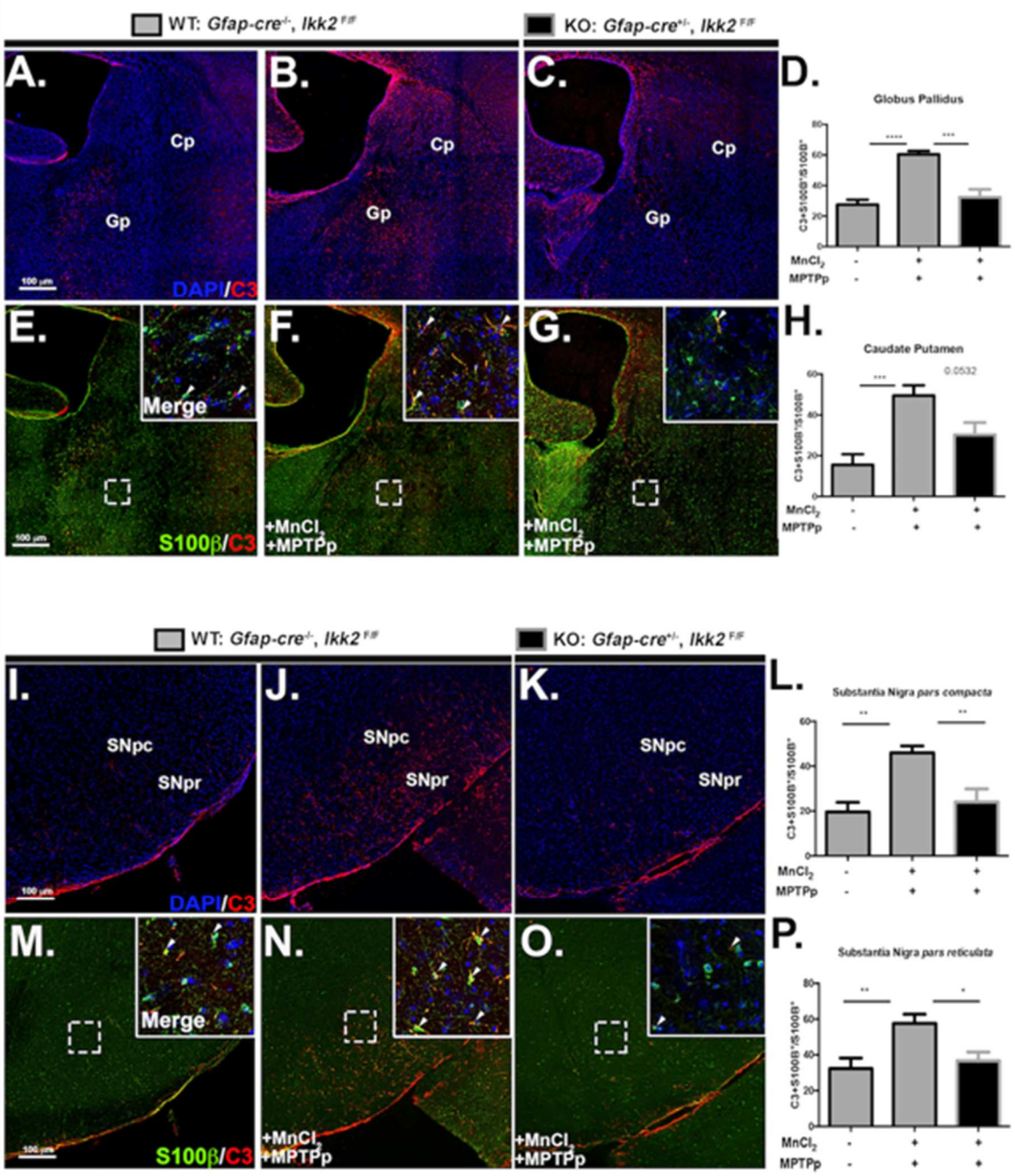

Figure 6.7. $MnCl_2$/MPTPp treatment induces neurotoxic astrocyte-C3 expression and is controlled by NF-κB Representative 10x-objective montage images of Gp/Cp co-immunostained for anti-C3 (red), dapi (blue) and S100β(green) from WT-control (**A**,**E**), WT + $MnCl_2$/MPTPp (**B**,**F**), and KO + $MnCl_2$/MPTPp (**C**,**G**) treated animals. Bottom inset displays 20x-magnification of outlined region with merged channels (**E**-**G**). Quantitation of $C3^+$ $S100\beta^+$/ $S100\beta^+$ in the Gp (**D**) and Cp (**E**), were conducted for three experimental groups. Similarly, SNpc/SNpr 10x-objective images of C3 with dapi (**I**-**K**) and S100β with C3 (**M**-**O**) and quantitation of $C3^+$ $S100\beta^+$/ $S100\beta^+$ in SNpc (**L**) and SNpr (**P**) (*$P < 0.05$, **$P < 0.01$, ***$P < 0.001$; N=7 animals/group).

CHAPTER 7

DISCUSSION & FINAL CONCLUSIONS

Parkinson's disease (PD) is a devastating degenerative disorder that affects more than 1 million Americans alive today. With an aging population, the burden of this disease is projected to rise steeply over the next 35 years. Research is beginning to shed light on common molecular pathways and networks of pathogenesis and pathophysiology but there are still no disease-modifying therapies, in part because the etiology of PD is not yet fully elucidated. Although multiple genetic mutations have been implicated in PD the majority of cases are sporadic, emphasizing the likelihood of environmental and exogenous factors playing a significant role in the development of the disease (Abou-Sleiman et al., 2006; Dauer and Przedborski, 2003). Irrespective of specific etiology, factors consistently associated with the neuropathology of PD include α-synuclein protein-aggregation, neuroinflammatory glial activation, mitochondrial dysfunction, oxidative stress and progressive neuronal loss.

Increasing evidence suggests a significant role of microglial-derived and astrocyte-derived neuroinflammation in progression of PD (Duffy et al., 2018; Gerhard et al., 2006; Lindqvist et al., 2013; Mogi et al., 1996). However, it is still unclear whether neuroinflammation plays a causal role in disease initiation or if neuroinflammation is a mere artifact of cell loss and protein aggregation associated with progression of the disease (Duffy et al., 2018; Gerhard et al., 2006; Lindqvist et al., 2013; Mogi et al., 1996). It was the central hypothesis of this work that chronic innate immune activation of glial cells initiates and promotes neuronal injury in single and two-hit models of postencephalitic and sporadic Parkinson's disease. Therefore, the studies described in Chapters 2-6 reflect the work performed to assess this hypothesis. Using novel viral

induced neuroinflammatory models of PD (Chapter 2) in transgenic animals (Chapter 3), and two-hit exposure models (Chapter 4-6) of neurodegeneration, we were able to elucidate how neuroinflammatory activation of glia likely plays a significant role in the initiation and progression of parkinsonism in models of postencephalitic and sporadic PD. We suggest that the results of these studies provide additional signaling pathways in glia for development of therapeutic interdictions designed to inhibit the damaging and neurotoxic effects of glial inflammatory responses in parkinsonian disorders.

We first characterized a novel virally-induced neuroinflammatory model of PD with the use of a mosquito-borne alphavirus, Western Equine Encephalitis Virus (WEEV) (Bantle et al., 2019). These studies sought to elucidate mechanisms underlying the capacity of this virus to cause parkinsonism in human patients and demonstrated that encephalitic infection with WEEV in outbred CD-1 mice targets multiple brain regions affected in neurodegenerative diseases such as PD (Schultz et al., 1977). To better model human cases of encephalitic infection with WEEV and to interrogate the long-term neurological consequences ensuing from such infections, immunotherapy treatment was used to establish a cohort of mice that consistently survive CNS infection with WEEV and completely clear virus. The onset, progression, and clearance of the infection was demonstrated by *in vivo* bioluminescence and fluorescent imaging of virally expressed firefly luciferase and dsRed. Examination of surviving mice revealed significant gait abnormalities, loss of dopaminergic neurons in the SNpc and VTA, loss of TH-positive terminals in the striatum, long-lasting activation of microglia and astrocytes, the formation of proteinase-K resistant α-synuclein inclusions and a gene expression profile consistent with neurodegeneration. The selective and rapid loss of TH+ dopamine neurons and development of proteinase K-resistant α-synuclein aggregates from a single inoculation with WEEV, coupled with high

specificity for the SNpc, may help to explain why encephalitic infections with mosquito-borne alphaviruses can cause parkinsonism in humans. Consistent with clinical cases of encephalitic infection with this virus, the experimental results presented indicated that the pattern of neuropathological injury and progression of neurodegeneration following infection with WEEV resembles certain features of parkinsonism. It was particularly striking that infection with WEEV caused the development of α–synuclein aggregates within eight weeks of infection in wild-type mice. This finding, combined with rapid progression, glial activation and selective loss of dopaminergic neurons within the SNpc suggested that recombinant WEEV, when used in conjunction with immunotherapy, could be a robust animal model for studying neurodegenerative mechanisms relevant to PD.

Collectively, the data in Chapter 2 reported that WEEV selectively induces degeneration of dopaminergic neurons in the SNpc with widespread gliosis and α-synuclein aggregate formation by 8WPI in outbred CD-1 mice, however, how neuroinflammatory activation of glial cells was linked to α-synuclein plaque formation and dopamine neuron loss remained to be determined (Bantle et al., 2019). In Chapter 3, we infected recombinant inbred C57BL/6J mice with WEEV and evaluated the progression of neurological injury over 8 weeks following immunotherapy to rescue animals from lethal infection. Following inoculation with WEEV, we observed a progressive loss of dopaminergic neurons, altered dopamine metabolism and neuromuscular gait abnormalities consistent with a parkinsonian phenotype. The overall loss of neurons in the SNpc, the histopathological acellularity of infected brain regions and the persistent neurobehavioral deficits observed at 8 WPI supported a progressive neurodegenerative lesion in the basal midbrain rather than merely decreased expression of tyrosine hydroxylase without overt neuronal loss (Alam et al., 2017). We also discovered that neuroinflammatory

activation of glia might be critical to the initiation and progression of neuronal loss and α-synuclein aggregation following infection with WEEV. Interestingly, microgliosis preceded α-synuclein aggregation in this model, and NFκB KO in astrocytes drastically ameliorated α-synuclein plaque formation and reduced the number of microglia in the SNpc. This data, along with others, supported chronic neuroinflammation from glia as a detrimental and possible initiating event in the development of parkinsonian deficits following encephalitic viral infection and may be more broadly applicable to the progression of other neurodegenerative diseases such as Alzheimer's disease (AD). This also highlighted the possibility of inhibiting neuroinflammatory activation of glia through NFκB as a potential therapy.

The results provided in Chapter 3, along with our previous studies, indicated that WEEV causes lasting neurodegenerative effects through inflammatory activation of glial cells, but whether an exaggerated neuroinflammatory response, in an environmentally relevant model, would potentiate the disease and worsen the PD-like pathology was unknown. To answer this question and to assess more specifically whether chronic astrocyte activation contributes to neuroinflammation and disease-like progression following infection with WEEV, we used a two-hit model of environmental neurodegeneration with juvenile exposure to $MnCl_2$ followed by adult infection with WEEV. These exposures were conducted in both wildtype mice and in astrocyte-specific knockout mice lacking nuclear factor Ikappa-B kinase subunit beta (IKK2) knockout (KO). Dual treated with $MnCl_2$ and WEEV in wild-type mice induced an exacerbated encephalitic infection, astrogliosis, and p129+ positive alpha-synuclein plaque formation in the SNpc, hippocampus, and cortex. Strikingly, KO mice pretreated with $MnCl_2$ during juvenile development prior to infection with WEEV were protected against this exacerbated encephalitic infection, astrogliosis and alpha-synuclein plaque development. This data highlighted that

excessive juvenile exposure to the environmental toxin $MnCl_2$ could increase neuronal susceptibility and injury follow a subsequent viral immune challenge with WEEV from chronic activation of NFκB in astrocytes. These observations could have significant implications in public health and in identifying critical signaling pathways in astrocytes that render individuals more susceptible to neurological disease following exposures to environmental neurotoxins and viral infections.

The data in Chapter 4 showed that juvenile environmental exposures with $MnCl_2$ may induce lasting neuroinflammatory effects in glia that could be a critical initiating and potentiating factor in post-encephalitic PD with the neurotropic virus WEEV, but it was unknown if these pathological effects were unique to WEEV. Previous work has shown that exposure to different classes of enveloped RNA viruses, experimental autoimmune encephalomyelitis (EAE) and H5N1 via intranasal infection can induce a parkinsonian pathology in the SNpc (Bantle et al., 2019; Jang et al., 2012). H5N1 avian influenza virus, WEEV and EAE likely induce neuronal loss through the activation of microglia and astrocytes and release of glial-derived neurotoxic mediators (Bantle et al., 2019; Jang et al., 2012; Ludlow et al., 2016). In Chapter 5, we questioned whether elevated levels of $MnCl_2$ during juvenile development could also modulate the neuroinflammatory response and neurodegeneration after infection with the more common and non-neurotropic virus H1N1 influenza virus. We found that exposure to 50 mg/Kg $MnCl_2$ from PN 21 – 51 did not result in loss of dopaminergic neurons in the SNpc or α-synuclein protein aggregation. However, a trend toward loss of DA neurons was noted in the dual treatment group, suggesting an increased susceptibility to injury following a systemic viral infection that would have likely been significant at a later time point. Juvenile exposure to Mn resulted in increased neuroinflammatory activation of microglia and astrocytes, and a pattern of

gene expression consistent with a neurodegenerative phenotype, particularly for genes related to oxidative stress, mitophagy, protein processing, and immune function. The unique expression of these genes only with combinatorial exposure to $MnCl_2$ and H1N1 could highlight how environmental exposures and microbial interactions may underlie the more severe neuroinflammatory pathology seen in some instances of sporadic and post-encephalitic PD. This data provides support to how individual environmental insults could act in concert to initiate neurodegenerative pathology during aging.

Lastly, to further elucidate the role of NFkB in astrocyte-derived neuroinflammatory responses during exposure to multiple environmental stressors, we used a two-hit neurodegenerative model by administering $MnCl_2$ in drinking water to astrocyte-specific knockout mice lacking nuclear factor IKK2 (KO) or wild-type mice during juvenile development, followed by exposure to the selective dopaminergic neurotoxin, MPTPp (MPTP + probenecid), four months later in adulthood. We were able to demonstrate that early exposure to $MnCl_2$ also exacerbated glial activation and neuronal loss following challenge with a second dopaminergic neurotoxicant through neuroinflammatory activation of NFκB in astrocytes, and that astrocyte-specific gene deletion of NFκB mitigated the numbers of reactive astrocytes and microglia and protected against neuronal loss in the basal ganglia induced by sequential exposure to Mn and MPTPp. Our results also reveal that the globus pallidus (Gp) is the nucleus within the basal ganglia most affected by dual treatment with $MnCl_2$+MPTPp and that neurodegeneration can be blocked by inhibition of astrocyte-NFκB. Additionally, we provided evidence that $MnCl_2$+MPTPp treatments in mice increase the presence of neurotoxic $C3^+$ A1 astrocytes that are highly regulated by NFκB activation in astrocytes. This study, along with our previous studies, provided valuable insight and support into how juvenile environmental exposure with

heavy metals can modulate neuroinflammatory activation in astrocytes and increase susceptibility to neurotoxic insult and PD-like pathology during aging.

Taken together, the identification of etiological factors and understanding how they may act in concert is crucial to understanding the pathogenesis and pathophysiology of PD. The majority of PD mechanistic research has been solely focused on the degeneration and malfunction of dopaminergic neurons in the SNpc. However, increasing clinical evidence has suggested a significant role of microglial-derived and astrocyte-derived neuroinflammation in PD, and this idea is supported by clinical observations of increased inflammatory cytokines in cerebral spinal fluid (CFS) and plasma and by longitudinal studies showing sustained neuroinflammatory activation of microglia in the midbrain with PET imaging (Nakano et al., 1998; Vermeulen et al., 2002) (Fernandes et al., 2007; Kim et al., 2006). The fact that glial activation may act in advance of dopaminergic neuronal cell death and α-synuclein protein aggregation may facilitate early diagnosis and drug targets that can prevent disease development. Accordingly, the data described in this dissertation using single exposure and dual-exposure neuroinflammatory models of PD showed that depending on the degree of glial activation and the severity of the toxic insults, glial NF-κB activation from inflammatory stressors can affect α-synuclein misfolding and dopaminergic neuronal dysfunction in the SNpc and other PD related brain regions. This data also suggests that a PD glial threshold may exist, that may be needed to initiate PD pathogenesis (Figure 1). This follows previous work showing that chronic inflammation within the CNS can sensitize neuronal tissue to secondary insults that would otherwise not induce significant neurological damage independently, and that glial activation precedes disease development (de Pablos et al., 2014; Kanaan et al., 2008; Koprich et al., 2008; Pintado et al., 2012; Tansey, 2010). This work partially elucidates that the long-term

neuroinflammatory effects in glia are most likely acting through NF-κB activation and epigenetic alterations, however, continued research exploring the specific signaling molecules and genetic locations of epigenetic modulations will help further elucidate critical molecular pathways and inflammatory signatures for therapeutic intervention.

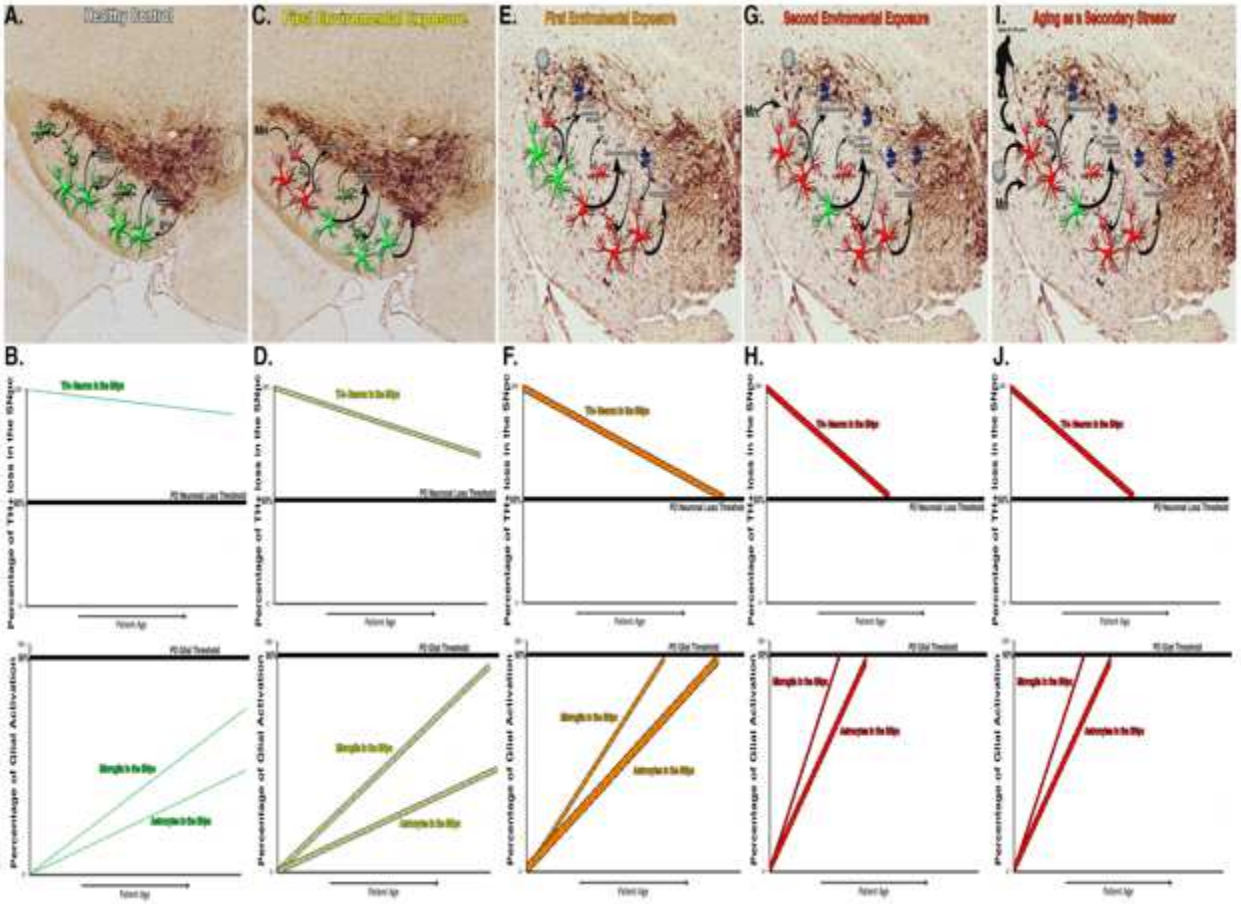

Figure 1. A PD glial threshold. Representative IHC images of the SNpc with TH+ dopaminergic neurons, animations of nonreactive (**Green**) and reactive (**Red**) astrocytes and microglia, and α-synuclein plaques following four different exposure models. (**A**) Healthy control. (**C**) First inflammatory exposure to $MnCl_2$. (**E**) First inflammatory exposure to an encephalitic infection. (**G**) Second inflammatory exposure to encephalitic infection or $MnCl_2$. (**I**) Second inflammatory exposure to encephalitic infection, $MnCl_2$, or Aging. The hypothetical neuronal loss and glial activation following each treatment group is illustrated below. The dopaminergic neuronal loss threshold for motor symptom development in PD (**Top**) with a hypothetical PD glial threshold on the bottom following four different exposure models. (**A**) Healthy control. (**C**) First inflammatory exposure to $MnCl_2$. (**E**) First inflammatory exposure to encephalitic infection. (**G**) Second inflammatory exposure to encephalitic infection or $MnCl_2$. (**I**) Second inflammatory exposure to encephalitic infection, $MnCl_2$, or aging.

REFERENCES

Abou-Sleiman, P.M., M.M. Muqit, and N.W. Wood. 2006. Expanding insights of mitochondrial dysfunction in Parkinson's disease. *Nat Rev Neurosci*. 7:207-219.

al, H.e.

2019. Juvenile exposure to manganese exacerbates astrocyte-dependent neuroinflammatory injury following adult challenge with MPTP.

.

Alam, G., M. Edler, S. Burchfield, and J.R. Richardson. 2017. Single low doses of MPTP decrease tyrosine hydroxylase expression in the absence of overt neuron loss. *Neurotoxicology*. 60:99-106.

Aloisi, F. 1999. The role of microglia and astrocytes in CNS immune surveillance and immunopathology. *Adv Exp Med Biol*. 468:123-133.

Amberger, J.S., C.A. Bocchini, F. Schiettecatte, A.F. Scott, and A. Hamosh. 2015. OMIM.org: Online Mendelian Inheritance in Man (OMIM(R)), an online catalog of human genes and genetic disorders. *Nucleic Acids Res*. 43:D789-798.

Amor, S., F. Puentes, D. Baker, and P. van der Valk. 2010. Inflammation in neurodegenerative diseases. *Immunology*. 129:154-169.

Anderson, J.P., D.E. Walker, J.M. Goldstein, R. de Laat, K. Banducci, R.J. Caccavello, R. Barbour, J. Huang, K. Kling, M. Lee, L. Diep, P.S. Keim, X. Shen, T. Chataway, M.G. Schlossmacher, P. Seubert, D. Schenk, S. Sinha, W.P. Gai, and T.J. Chilcote. 2006. Phosphorylation of Ser-129 is the dominant pathological modification of alpha-synuclein in familial and sporadic Lewy body disease. *J Biol Chem*. 281:29739-29752.

Antipova, D., and R. Bandopadhyay. 2017. Expression of DJ-1 in Neurodegenerative Disorders. *Adv Exp Med Biol*. 1037:25-43.

Aschner, M., K.M. Erikson, and D.C. Dorman. 2005. Manganese dosimetry: species differences and implications for neurotoxicity. *Crit Rev Toxicol*. 35:1-32.

Ashley, A.K., A.I. Hinds, W.H. Hanneman, R.B. Tjalkens, and M.E. Legare. 2016. DJ-1 mutation decreases astroglial release of inflammatory mediators. *Neurotoxicology*. 52:198-203.

Attems, J., and K.A. Jellinger. 2008. The dorsal motor nucleus of the vagus is not an obligatory trigger site of Parkinson's disease. *Neuropathol Appl Neurobiol*. 34:466-467.

Avelino, M.A., E.F. Fusao, J.L. Pedroso, J.H. Arita, R.T. Ribeiro, R.S. Pinho, K. Tuschl, O.G. Barsottini, and M.R. Masruha. 2014. Inherited manganism: the "cock-walk" gait and typical neuroimaging features. *J Neurol Sci*. 341:150-152.

Bae, E.J., N.Y. Yang, M. Song, C.S. Lee, J.S. Lee, B.C. Jung, H.J. Lee, S. Kim, E. Masliah, S.P. Sardi, and S.J. Lee. 2014. Glucocerebrosidase depletion enhances cell-to-cell transmission of alpha-synuclein. *Nat Commun*. 5:4755.

Bandopadhyay, R., A.E. Kingsbury, M.R. Cookson, A.R. Reid, I.M. Evans, A.D. Hope, A.M. Pittman, T. Lashley, R. Canet-Aviles, D.W. Miller, C. McLendon, C. Strand, A.J. Leonard, P.M. Abou-Sleiman, D.G. Healy, H. Ariga, N.W. Wood, R. de Silva, T. Revesz, J.A. Hardy, and A.J. Lees. 2004. The expression of DJ-1 (PARK7) in normal human CNS and idiopathic Parkinson's disease. *Brain*. 127:420-430.

Bantle, C.M., A.T. Phillips, R.J. Smeyne, S.M. Rocha, K.E. Olson, and R.B. Tjalkens. 2019. Infection with mosquito-borne alphavirus induces selective loss of dopaminergic neurons, neuroinflammation and widespread protein aggregation. *NPJ Parkinsons Dis*. 5:20.

Baquet, Z.C., D. Williams, J. Brody, and R.J. Smeyne. 2009. A comparison of model-based (2D) and design-based (3D) stereological methods for estimating cell number in the substantia nigra pars compacta (SNpc) of the C57BL/6J mouse. *Neuroscience*. 161:1082-1090.

Barcia, C. 2013. Glial-mediated inflammation underlying parkinsonism. *Scientifica (Cairo)*. 2013:357805.

Barhoumi, R., J. Faske, X. Liu, and R.B. Tjalkens. 2004. Manganese potentiates lipopolysaccharide-induced expression of NOS2 in C6 glioma cells through mitochondrial-dependent activation of nuclear factor kappaB. *Brain Res Mol Brain Res*. 122:167-179.

Beal, M.F. 2010. Parkinson's disease: a model dilemma. *Nature*. 466.

Beatman, E.L., A. Massey, K.D. Shives, K.S. Burrack, M. Chamanian, T.E. Morrison, and J.D. Beckham. 2015. Alpha-Synuclein Expression Restricts RNA Viral Infections in the Brain. *J Virol*. 90:2767-2782.

Beaudin, S.A., B.J. Strupp, S.M. Lasley, C.A. Fornal, S. Mandal, and D.R. Smith. 2015. Oral Methylphenidate Alleviates the Fine Motor Dysfunction Caused by Chronic Postnatal Manganese Exposure in Adult Rats. *Toxicol Sci*.

Bell, T.M., E.J. Field, and H.K. Narang. 1971. Zika virus infection of the central nervous system of mice. *Arch Gesamte Virusforsch*. 35:183-193.

Bendor, J.T., T.P. Logan, and R.H. Edwards. 2013. The function of alpha-synuclein. *Neuron*. 79:1044-1066.

Benskey, M.J., R.C. Sellnow, I.M. Sandoval, C.E. Sortwell, J.W. Lipton, and F.P. Manfredsson. 2018. Silencing Alpha Synuclein in Mature Nigral Neurons Results in Rapid Neuroinflammation and Subsequent Toxicity. *Front Mol Neurosci*. 11:36.

Berger, J.R., and G. Arendt. 2000. HIV dementia: the role of the basal ganglia and dopaminergic systems. *J Psychopharmacol*. 14:214-221.

Betarbet, R., T.B. Sherer, G. MacKenzie, M. Garcia-Osuna, A.V. Panov, and J.T. Greenamyre. 2000. Chronic systemic pesticide exposure reproduces features of Parkinson's disease. *Nat Neurosci*. 3:1301-1306.

Billingsley, K.J., S. Bandres-Ciga, S. Saez-Atienzar, and A.B. Singleton. 2018. Genetic risk factors in Parkinson's disease. *Cell Tissue Res*. 373:9-20.

Bjorkblom, B., A. Adilbayeva, J. Maple-Grodem, D. Piston, M. Okvist, X.M. Xu, C. Brede, J.P. Larsen, and S.G. Moller. 2013. Parkinson disease protein DJ-1 binds metals and protects against metal-induced cytotoxicity. *J Biol Chem*. 288:22809-22820.

Bjorklund, G., V. Stejskal, M.A. Urbina, M. Dadar, S. Chirumbolo, and J. Mutter. 2018. Metals and Parkinson's Disease: Mechanisms and Biochemical Processes. *Curr Med Chem*. 25:2198-2214.

Block, M.L., and J.S. Hong. 2005. Microglia and inflammation-mediated neurodegeneration: multiple triggers with a common mechanism. *Prog Neurobiol*. 76:77-98.

Bodea, L.G., Y. Wang, B. Linnartz-Gerlach, J. Kopatz, L. Sinkkonen, R. Musgrove, T. Kaoma, A. Muller, L. Vallar, D.A. Di Monte, R. Balling, and H. Neumann. 2014. Neurodegeneration by activation of the microglial complement-phagosome pathway. *J Neurosci*. 34:8546-8556.

Bonifati, V., P. Rizzu, F. Squitieri, E. Krieger, N. Vanacore, J.C. van Swieten, A. Brice, C.M. van Duijn, B. Oostra, G. Meco, and P. Heutink. 2003. DJ-1(PARK7), a novel gene for autosomal recessive, early onset parkinsonism. *Neurol Sci*. 24:159-160.

Booth, H.D.E., W.D. Hirst, and R. Wade-Martins. 2017. The Role of Astrocyte Dysfunction in Parkinson's Disease Pathogenesis. *Trends Neurosci*. 40:358-370.

Bouchard, M., F. Laforest, L. Vandelac, D. Bellinger, and D. Mergler. 2007a. Hair manganese and hyperactive behaviors: pilot study of school-age children exposed through tap water. *Environ Health Perspect*. 115:122-127.

Bouchard, M., D. Mergler, M. Baldwin, M. Panisset, and H.A. Roels. 2007b. Neuropsychiatric symptoms and past manganese exposure in a ferro-alloy plant. *Neurotoxicology*. 28:290-297.

Bozi, M., D. Papadimitriou, R. Antonellou, M. Moraitou, M. Maniati, D.K. Vassilatis, S.G. Papageorgiou, A. Leonardos, G. Tagaris, G. Malamis, D. Theofilopoulos, S. Kamakari, E. Stamboulis, G.M. Hadjigeorgiou, A. Athanassiadou, H. Michelakakis, A. Papadimitriou, T. Gasser, and L. Stefanis. 2014. Genetic assessment of familial and early-onset Parkinson's disease in a Greek population. *Eur J Neurol*. 21:963-968.

Braak, H., J. Brettschneider, A.C. Ludolph, V.M. Lee, J.Q. Trojanowski, and K. Del Tredici. 2013. Amyotrophic lateral sclerosis--a model of corticofugal axonal spread. *Nat Rev Neurol*. 9:708-714.

Braak, H., K. Del Tredici, U. Rub, R.A. de Vos, E.N. Jansen Steur, and E. Braak. 2003a. Staging of brain pathology related to sporadic Parkinson's disease. *Neurobiol Aging*. 24:197-211.

Braak, H., U. Rub, W.P. Gai, and K. Del Tredici. 2003b. Idiopathic Parkinson's disease: possible routes by which vulnerable neuronal types may be subject to neuroinvasion by an unknown pathogen. *J Neural Transm*. 110:517-536.

Braak, H., U. Rub, W.P. Gai, and K. Del Tredici. 2003c. Idiopathic Parkinson's disease: possible routes by which vulnerable neuronal types may be subject to neuroinvasion by an unknown pathogen. *J Neural Transm (Vienna)*. 110:517-536.

Brichta, L., and P. Greengard. 2014. Molecular determinants of selective dopaminergic vulnerability in Parkinson's disease: an update. *Front Neuroanat*. 8:152.

Brown, T.P., P.C. Rumsby, A.C. Capleton, L. Rushton, and L.S. Levy. 2006. Pesticides and Parkinson's disease--is there a link? *Environ Health Perspect*. 114:156-164.

Bruck, D., G.K. Wenning, N. Stefanova, and L. Fellner. 2016. Glia and alpha-synuclein in neurodegeneration: A complex interaction. *Neurobiol Dis*. 85:262-274.

Bu, X.L., X. Wang, Y. Xiang, L.L. Shen, Q.H. Wang, Y.H. Liu, S.S. Jiao, Y.R. Wang, H.Y. Cao, X. Yi, C.H. Liu, B. Deng, X.Q. Yao, Z.Q. Xu, H.D. Zhou, and Y.J. Wang. 2015. The association between infectious burden and Parkinson's disease: A case-control study. *Parkinsonism Relat Disord*. 21:877-881.

Cabezas, R., R.S. El-Bacha, J. Gonzalez, and G.E. Barreto. 2012. Mitochondrial functions in astrocytes: neuroprotective implications from oxidative damage by rotenone. *Neurosci Res*. 74:80-90.

Caboni, P., T.B. Sherer, N. Zhang, G. Taylor, H.M. Na, J.T. Greenamyre, and J.E. Casida. 2004. Rotenone, deguelin, their metabolites, and the rat model of Parkinson's disease. *Chem Res Toxicol*. 17:1540-1548.

Caggiu, E., G. Arru, S. Hosseini, M. Niegowska, G. Sechi, I.R. Zarbo, and L.A. Sechi. 2019. Inflammation, Infectious Triggers, and Parkinson's Disease. *Front Neurol*. 10:122.

Caggiu, E., K. Paulus, G. Arru, R. Piredda, G.P. Sechi, and L.A. Sechi. 2016. Humoral cross reactivity between alpha-synuclein and herpes simplex-1 epitope in Parkinson's disease, a triggering role in the disease? *J Neuroimmunol*. 291:110-114.

Caggiu, E., K. Paulus, G. Galleri, G. Arru, R. Manetti, G.P. Sechi, and L.A. Sechi. 2017. Homologous HSV1 and alpha-synuclein peptides stimulate a T cell response in Parkinson's disease. *J Neuroimmunol*. 310:26-31.

Campelo, C., and R.H. Silva. 2017. Genetic Variants in SNCA and the Risk of Sporadic Parkinson's Disease and Clinical Outcomes: A Review. *Parkinsons Dis*. 2017:4318416.

Cao, S., D.G. Standaert, and A.S. Harms. 2012. The gamma chain subunit of Fc receptors is required for alpha-synuclein-induced pro-inflammatory signaling in microglia. *J Neuroinflammation*. 9:259.

Cavaliere, F., L. Cerf, B. Dehay, P. Ramos-Gonzalez, F. De Giorgi, M. Bourdenx, A. Bessede, J.A. Obeso, C. Matute, F. Ichas, and E. Bezard. 2017. In vitro alpha-synuclein neurotoxicity and spreading among neurons and astrocytes using Lewy body extracts from Parkinson disease brains. *Neurobiol Dis*. 103:101-112.

Chartier-Harlin, M.C., J. Kachergus, C. Roumier, V. Mouroux, X. Douay, S. Lincoln, C. Levecque, L. Larvor, J. Andrieux, M. Hulihan, N. Waucquier, L. Defebvre, P. Amouyel, M. Farrer, and A. Destee. 2004. Alpha-synuclein locus duplication as a cause of familial Parkinson's disease. *Lancet*. 364:1167-1169.

Chen, J., P. Su, W. Luo, and J. Chen. 2018. Role of LRRK2 in manganese-induced neuroinflammation and microglial autophagy. *Biochem Biophys Res Commun*. 498:171-177.

Chen, L.W., H.J. Hu, H.L. Liu, K.K. Yung, and Y.S. Chan. 2004. Identification of brain-derived neurotrophic factor in nestin-expressing astroglial cells in the neostriatum of 1-methyl-4-phenyl-1,2,3,6-tetrahydropyridine-treated mice. *Neuroscience*. 126:941-953.

Chida, J., H. Hara, M. Yano, K. Uchiyama, N.R. Das, E. Takahashi, H. Miyata, Y. Tomioka, T. Ito, H. Kido, and S. Sakaguchi. 2018. Prion protein protects mice from lethal infection with influenza A viruses. *PLoS Pathog*. 14:e1007049.

Choi, D.J., J.K. Kwon, and E.H. Joe. 2018. A Parkinson's disease gene, DJ-1, regulates astrogliosis through STAT3. *Neurosci Lett*. 685:144-149.

Choi, I., D.J. Choi, H. Yang, J.H. Woo, M.Y. Chang, J.Y. Kim, W. Sun, S.M. Park, I. Jou, S.H. Lee, and E.H. Joe. 2016. PINK1 expression increases during brain development and stem cell differentiation, and affects the development of GFAP-positive astrocytes. *Mol Brain*. 9:5.

Choi, I., J. Kim, H.K. Jeong, B. Kim, I. Jou, S.M. Park, L. Chen, U.J. Kang, X. Zhuang, and E.H. Joe. 2013. PINK1 deficiency attenuates astrocyte proliferation through mitochondrial dysfunction, reduced AKT and increased p38 MAPK activation, and downregulation of EGFR. *Glia*. 61:800-812.

Chung, K., J. Wallace, S.Y. Kim, S. Kalyanasundaram, A.S. Andalman, T.J. Davidson, J.J. Mirzabekov, K.A. Zalocusky, J. Mattis, A.K. Denisin, S. Pak, H. Bernstein, C. Ramakrishnan, L. Grosenick, V. Gradinaru, and K. Deisseroth. 2013. Structural and molecular interrogation of intact biological systems. *Nature*. 497:332-337.

Clark, L.N., Y. Wang, E. Karlins, L. Saito, H. Mejia-Santana, J. Harris, E.D. Louis, L.J. Cote, H. Andrews, S. Fahn, C. Waters, B. Ford, S. Frucht, R. Ottman, and K. Marder. 2006. Frequency of LRRK2 mutations in early- and late-onset Parkinson disease. *Neurology*. 67:1786-1791.

Clarke, L.E., S.A. Liddelow, C. Chakraborty, A.E. Munch, M. Heiman, and B.A. Barres. 2018. Normal aging induces A1-like astrocyte reactivity. *Proc Natl Acad Sci U S A*. 115:E1896-E1905.

Clarke, P., J.S. Leser, E.D. Quick, K.R. Dionne, J.D. Beckham, and K.L. Tyler. 2014. Death receptor-mediated apoptotic signaling is activated in the brain following infection with West Nile virus in the absence of a peripheral immune response. *J Virol*. 88:1080-1089.

Clayton, D.F., and J.M. George. 1998. The synucleins: a family of proteins involved in synaptic function, plasticity, neurodegeneration and disease. *Trends Neurosci*. 21:249-254.

Cook, S.H., and D.E. Griffin. 2003. Luciferase Imaging of neurotropic viral infection in intact animals. *Journal of virology*. 77:5333-5338.

Couper, J. 1837. On the effects of black oxide of manganese when inhaled into the lungs. *Br Ann Med Pharm*. 1:41-45.

Cree, B.C., G.L. Bernardini, A.P. Hays, and G. Lowe. 2003. A fatal case of coxsackievirus B4 meningoencephalitis. *Arch Neurol*. 60:107-112.

Crossgrove, J., and W. Zheng. 2004. Manganese toxicity upon overexposure. *NMR Biomed*. 17:544-553.

Cummings, J.E., and R.A. Slayden. 2017. Transient In Vivo Resistance Mechanisms of Burkholderia pseudomallei to Ceftazidime and Molecular Markers for Monitoring Treatment Response. *PLoS Negl Trop Dis*. 11:e0005209.

Daher, J.P., H.A. Abdelmotilib, X. Hu, L.A. Volpicelli-Daley, M.S. Moehle, K.B. Fraser, E. Needle, Y. Chen, S.J. Steyn, P. Galatsis, W.D. Hirst, and A.B. West. 2015. Leucine-rich Repeat Kinase 2 (LRRK2) Pharmacological Inhibition Abates alpha-Synuclein Gene-induced Neurodegeneration. *J Biol Chem*. 290:19433-19444.

Dale, R.C., A.J. Church, R.A. Surtees, A.J. Lees, J.E. Adcock, B. Harding, B.G. Neville, and G. Giovannoni. 2004. Encephalitis lethargica syndrome: 20 new cases and evidence of basal ganglia autoimmunity. *Brain*. 127:21-33.

Darnell, J.C., and J.D. Richter. 2012. Cytoplasmic RNA-binding proteins and the control of complex brain function. *Cold Spring Harb Perspect Biol*. 4.

Das, K., M. Ghosh, C. Nag, S.P. Nandy, M. Banerjee, M. Datta, G. Devi, and G. Chaterjee. 2011. Role of familial, environmental and occupational factors in the development of Parkinson's disease. *Neurodegener Dis*. 8:345-351.

Dauer, W., and S. Przedborski. 2003. Parkinson's disease: mechanisms and models. *Neuron*. 39:889-909.

De Chiara, G., M.E. Marcocci, R. Sgarbanti, L. Civitelli, C. Ripoli, R. Piacentini, E. Garaci, C. Grassi, and A.T. Palamara. 2012. Infectious agents and neurodegeneration. *Molecular neurobiology*. 46:614-638.

De Jager, P.L., G. Srivastava, K. Lunnon, J. Burgess, L.C. Schalkwyk, L. Yu, M.L. Eaton, B.T. Keenan, J. Ernst, C. McCabe, A. Tang, T. Raj, J. Replogle, W. Brodeur, S. Gabriel, H.S. Chai, C. Younkin, S.G. Younkin, F. Zou, M. Szyf, C.B. Epstein, J.A. Schneider, B.E. Bernstein, A. Meissner, N. Ertekin-Taner, L.B. Chibnik, M. Kellis, J. Mill, and D.A. Bennett. 2014. Alzheimer's disease: early alterations in brain DNA methylation at ANK1, BIN1, RHBDF2 and other loci. *Nat Neurosci*. 17:1156-1163.

De Miranda, B.R., J.A. Miller, R.J. Hansen, P.J. Lunghofer, S. Safe, D.L. Gustafson, D. Colagiovanni, and R.B. Tjalkens. 2013. Neuroprotective efficacy and pharmacokinetic behavior of novel anti-inflammatory para-phenyl substituted diindolylmethanes in a mouse model of Parkinson's disease. *J Pharmacol Exp Ther*. 345:125-138.

De Miranda, B.R., K.A. Popichak, S.L. Hammond, J.A. Miller, S. Safe, and R.B. Tjalkens. 2015. Novel para-phenyl substituted diindolylmethanes protect against MPTP neurotoxicity and suppress glial activation in a mouse model of Parkinson's disease. *Toxicol Sci*. 143:360-373.

De Miranda, B.R., E.M. Rocha, Q. Bai, A. El Ayadi, D. Hinkle, E.A. Burton, and J. Timothy Greenamyre. 2018. Astrocyte-specific DJ-1 overexpression protects against rotenone-induced neurotoxicity in a rat model of Parkinson's disease. *Neurobiol Dis*. 115:101-114.

de Pablos, R.M., A.J. Herrera, A.M. Espinosa-Oliva, M. Sarmiento, M.F. Munoz, A. Machado, and J.L. Venero. 2014. Chronic stress enhances microglia activation and exacerbates death of nigral dopaminergic neurons under conditions of inflammation. *J Neuroinflammation*. 11:34.

Deleidi, M., and O. Isacson. 2012. Viral and inflammatory triggers of neurodegenerative diseases. *Science translational medicine*. 4:121ps123.

di Domenico, A., G. Carola, C. Calatayud, M. Pons-Espinal, J.P. Munoz, Y. Richaud-Patin, I. Fernandez-Carasa, M. Gut, A. Faella, J. Parameswaran, J. Soriano, I. Ferrer, E. Tolosa, A. Zorzano, A.M. Cuervo, A. Raya, and A. Consiglio. 2019. Patient-Specific iPSC-Derived Astrocytes Contribute to Non-Cell-Autonomous Neurodegeneration in Parkinson's Disease. *Stem Cell Reports*. 12:213-229.

Di Malta, C., J.D. Fryer, C. Settembre, and A. Ballabio. 2012. Astrocyte dysfunction triggers neurodegeneration in a lysosomal storage disorder. *Proc Natl Acad Sci U S A*. 109:E2334-2342.

Di Monte, D.A., E.Y. Wu, and J.W. Langston. 1992. Role of astrocytes in MPTP metabolism and toxicity. *Ann N Y Acad Sci*. 648:219-228.

Di Rocco, A., S.P. Molinari, B. Kollmeier, and M.D. Yahr. 1996. Parkinson's disease: progression and mortality in the L-DOPA era. *Adv Neurol*. 69:3-11.

Di Virgilio, F., S. Ceruti, P. Bramanti, and M.P. Abbracchio. 2009. Purinergic signalling in inflammation of the central nervous system. *Trends Neurosci*. 32:79-87.

Dimova, P.S., V. Bojinova, D. Georgiev, and I. Milanov. 2006. Acute reversible parkinsonism in Epstein-Barr virus-related encephalitis lethargica-like illness. *Mov Disord*. 21:564-566.

Doan, L., B. Handa, N.A. Roberts, and K. Klumpp. 1999. Metal ion catalysis of RNA cleavage by the influenza virus endonuclease. *Biochemistry*. 38:5612-5619.

Dobbs, R.J., A. Charlett, A.G. Purkiss, S.M. Dobbs, C. Weller, and D.W. Peterson. 1999. Association of circulating TNF-alpha and IL-6 with ageing and parkinsonism. *Acta Neurol Scand*. 100:34-41.

Dorsey, E.R., T. Sherer, M.S. Okun, and B.R. Bloem. 2018. The Emerging Evidence of the Parkinson Pandemic. *J Parkinsons Dis*. 8:S3-S8.

Dourmashkin, R.R. 1997. What caused the 1918-30 epidemic of encephalitis lethargica? *J R Soc Med*. 90:515-520.

Du, L., and J.D. Richter. 2005. Activity-dependent polyadenylation in neurons. *RNA*. 11:1340-1347.

Du, R.H., H.B. Sun, Z.L. Hu, M. Lu, J.H. Ding, and G. Hu. 2018. Kir6.1/K-ATP channel modulates microglia phenotypes: implication in Parkinson's disease. *Cell Death Dis*. 9:404.

Duffy, M.F., T.J. Collier, J.R. Patterson, C.J. Kemp, K.C. Luk, M.G. Tansey, K.L. Paumier, N.M. Kanaan, D.L. Fischer, N.K. Polinski, O.L. Barth, J.W. Howe, N.N. Vaikath, N.K. Majbour, O.M.A. El-Agnaf, and C.E. Sortwell. 2018. Lewy body-like alpha-synuclein

inclusions trigger reactive microgliosis prior to nigral degeneration. *J Neuroinflammation*. 15:129.
Eimer, W.A., D.K. Vijaya Kumar, N.K. Navalpur Shanmugam, A.S. Rodriguez, T. Mitchell, K.J. Washicosky, B. Gyorgy, X.O. Breakefield, R.E. Tanzi, and R.D. Moir. 2018. Alzheimer's Disease-Associated beta-Amyloid Is Rapidly Seeded by Herpesviridae to Protect against Brain Infection. *Neuron*. 99:56-63 e53.
Eisbach, S.E., and T.F. Outeiro. 2013. Alpha-synuclein and intracellular trafficking: impact on the spreading of Parkinson's disease pathology. *J Mol Med (Berl)*. 91:693-703.
Elizan, T.S., and J. Casals. 1991. Astrogliosis in von Economo's and postencephalitic Parkinson's diseases supports probable viral etiology. *Journal of the neurological sciences*. 105:131-134.
Elizan, T.S., J. Schwartz, M.D. Yahr, and J. Casals. 1978. Antibodies against arboviruses in postencephalitic and idiopathic Parkinson's disease. *Arch Neurol*. 35:257-260.
Episcopo, F.L., C. Tirolo, N. Testa, S. Caniglia, M.C. Morale, and B. Marchetti. 2013. Reactive astrocytes are key players in nigrostriatal dopaminergic neurorepair in the MPTP mouse model of Parkinson's disease: focus on endogenous neurorestoration. *Curr Aging Sci*. 6:45-55.
Erikson, K.M., and M. Aschner. 2003. Manganese neurotoxicity and glutamate-GABA interaction. *Neurochemistry International*. 43:475-480.
Fazekas, T., P. Wiesbauer, B. Schroth, U. Potschger, H. Gadner, and A. Heitger. 2005. Selective IgA deficiency in children with recurrent parotitis of childhood. *Pediatr Infect Dis J*. 24:461-462.
Fekete, R., C. Cserep, N. Lenart, K. Toth, B. Orsolits, B. Martinecz, E. Mehes, B. Szabo, V. Nemeth, B. Gonci, B. Sperlagh, Z. Boldogkoi, A. Kittel, M. Baranyi, S. Ferenczi, K. Kovacs, G. Szalay, B. Rozsa, C. Webb, G.G. Kovacs, T. Hortobagyi, B.L. West, Z. Kornyei, and A. Denes. 2018. Microglia control the spread of neurotropic virus infection via P2Y12 signalling and recruit monocytes through P2Y12-independent mechanisms. *Acta Neuropathol*. 136:461-482.
Fell, J.M., A.P. Reynolds, N. Meadows, K. Khan, S.G. Long, G. Quaghebeur, W.J. Taylor, and P.J. Milla. 1996. Manganese toxicity in children receiving long-term parenteral nutrition. *Lancet*. 347:1218-1221.
Fernandes, A., A.S. Falcao, R.F. Silva, M.A. Brito, and D. Brites. 2007. MAPKs are key players in mediating cytokine release and cell death induced by unconjugated bilirubin in cultured rat cortical astrocytes. *Eur J Neurosci*. 25:1058-1068.
Fernandes, H.J., E.M. Hartfield, H.C. Christian, E. Emmanoulidou, Y. Zheng, H. Booth, H. Bogetofte, C. Lang, B.J. Ryan, S.P. Sardi, J. Badger, J. Vowles, S. Evetts, G.K. Tofaris, K. Vekrellis, K. Talbot, M.T. Hu, W. James, S.A. Cowley, and R. Wade-Martins. 2016. ER Stress and Autophagic Perturbations Lead to Elevated Extracellular alpha-Synuclein in GBA-N370S Parkinson's iPSC-Derived Dopamine Neurons. *Stem Cell Reports*. 6:342-356.
Filippini, A., M. Gennarelli, and I. Russo. 2019. alpha-Synuclein and Glia in Parkinson's Disease: A Beneficial or a Detrimental Duet for the Endo-Lysosomal System? *Cell Mol Neurobiol*. 39:161-168.
Finley, K.H., W.A. Longshore, R.J. Palmer, R.E. Cook, and N. Riggs. 1955. WESTERN EQUINE AND ST LOUIS ENCEPHALITIS - PRELIMINARY REPORT OF A CLINICAL FOLLOW-UP STUDY IN CALIFORNIA. *Neurology*. 5:223-235.

Flagmeier, P., G. Meisl, M. Vendruscolo, T.P. Knowles, C.M. Dobson, A.K. Buell, and C. Galvagnion. 2016. Mutations associated with familial Parkinson's disease alter the initiation and amplification steps of alpha-synuclein aggregation. *Proc Natl Acad Sci U S A*. 113:10328-10333.

Frank-Cannon, T.C., L.T. Alto, F.E. McAlpine, and M.G. Tansey. 2009. Does neuroinflammation fan the flame in neurodegenerative diseases? *Mol Neurodegener*. 4:47.

Fricke, I.B., T. Viel, M.M. Worlitzer, F.M. Collmann, A. Vrachimis, A. Faust, L. Wachsmuth, C. Faber, F. Dolle, M.T. Kuhlmann, K. Schafers, S. Hermann, J.C. Schwamborn, and A.H. Jacobs. 2016. 6-hydroxydopamine-induced Parkinson's disease-like degeneration generates acute microgliosis and astrogliosis in the nigrostriatal system but no bioluminescence imaging-detectable alteration in adult neurogenesis. *Eur J Neurosci*. 43:1352-1365.

Gao, F., D. Chen, Q. Hu, and G. Wang. 2013. Rotenone directly induces BV2 cell activation via the p38 MAPK pathway. *PLoS One*. 8:e72046.

Gao, H.M., J.S. Hong, W. Zhang, and B. Liu. 2002. Distinct role for microglia in rotenone-induced degeneration of dopaminergic neurons. *J Neurosci*. 22:782-790.

Gao, H.M., P.T. Kotzbauer, K. Uryu, S. Leight, J.Q. Trojanowski, and V.M. Lee. 2008. Neuroinflammation and oxidation/nitration of alpha-synuclein linked to dopaminergic neurodegeneration. *J Neurosci*. 28:7687-7698.

Garcia, S.J., K. Gellein, T. Syversen, and M. Aschner. 2007. Iron deficient and manganese supplemented diets alter metals and transporters in the developing rat brain. *Toxicol Sci*. 95:205-214.

Gardet, A., Y. Benita, C. Li, B.E. Sands, I. Ballester, C. Stevens, J.R. Korzenik, J.D. Rioux, M.J. Daly, R.J. Xavier, and D.K. Podolsky. 2010. LRRK2 is involved in the IFN-gamma response and host response to pathogens. *J Immunol*. 185:5577-5585.

Gavin, C.E., K.K. Gunter, and T.E. Gunter. 1999. Manganese and calcium transport in mitochondria: implications for manganese toxicity. *Neurotoxicology*. 20:445-453.

Gegg, M.E., and A.H.V. Schapira. 2018. The role of glucocerebrosidase in Parkinson disease pathogenesis. *FEBS J*. 285:3591-3603.

Gelb, D.J., E. Oliver, and S. Gilman. 1999. Diagnostic criteria for Parkinson disease. *Arch Neurol*. 56:33-39.

Gerhard, A., N. Pavese, G. Hotton, F. Turkheimer, M. Es, A. Hammers, K. Eggert, W. Oertel, R.B. Banati, and D.J. Brooks. 2006. In vivo imaging of microglial activation with [11C](R)-PK11195 PET in idiopathic Parkinson's disease. *Neurobiol Dis*. 21:404-412.

German, D.C., K. Manaye, W.K. Smith, D.J. Woodward, and C.B. Saper. 1989. Midbrain dopaminergic cell loss in Parkinson's disease: computer visualization. *Ann Neurol*. 26:507-514.

Gillardon, F., R. Schmid, and H. Draheim. 2012. Parkinson's disease-linked leucine-rich repeat kinase 2(R1441G) mutation increases proinflammatory cytokine release from activated primary microglial cells and resultant neurotoxicity. *Neuroscience*. 208:41-48.

Gingras, S., L.R. Earls, S. Howell, R.J. Smeyne, S.S. Zakharenko, and S. Pelletier. 2015. SCYL2 Protects CA3 Pyramidal Neurons from Excitotoxicity during Functional Maturation of the Mouse Hippocampus. *J Neurosci*. 35:10510-10522.

Ginns, E.I., S.K. Mak, N. Ko, J. Karlgren, S. Akbarian, V.P. Chou, Y. Guo, A. Lim, S. Samuelsson, M.L. LaMarca, J. Vazquez-DeRose, and A.B. Manning-Bog. 2014.

Neuroinflammation and alpha-synuclein accumulation in response to glucocerebrosidase deficiency are accompanied by synaptic dysfunction. *Mol Genet Metab*. 111:152-162.
Glass, C.K., K. Saijo, B. Winner, M.C. Marchetto, and F.H. Gage. 2010a. Mechanisms underlying inflammation in neurodegeneration. *Cell*. 140:918-934.
Glass, C.K., K. Saijo, B. Winner, M.C. Marchetto, and F.H. Gage. 2010b. Mechanisms underlying inflammation in neurodegeneration. *Cell*. 140:918-934.
Gonzalez-Cuyar, L.F., G. Nelson, S.R. Criswell, P. Ho, J.A. Lonzanida, H. Checkoway, N. Seixas, B.B. Gelman, B.A. Evanoff, J. Murray, J. Zhang, and B.A. Racette. 2014. Quantitative neuropathology associated with chronic manganese exposure in South African mine workers. *Neurotoxicology*. 45:260-266.
Gouveia, K., and J.L. Hurst. 2013. Reducing mouse anxiety during handling: effect of experience with handling tunnels. *PLoS One*. 8:e66401.
Graeber, M.B., and W.J. Streit. 2010. Microglia: biology and pathology. *Acta Neuropathol*. 119:89-105.
Grubaugh, N.D., J. Weger-Lucarelli, R.A. Murrieta, J.R. Fauver, S.M. Garcia-Luna, A.N. Prasad, W.C.t. Black, and G.D. Ebel. 2016. Genetic Drift during Systemic Arbovirus Infection of Mosquito Vectors Leads to Decreased Relative Fitness during Host Switching. *Cell Host Microbe*. 19:481-492.
Gu, X.L., C.X. Long, L. Sun, C. Xie, X. Lin, and H. Cai. 2010. Astrocytic expression of Parkinson's disease-related A53T alpha-synuclein causes neurodegeneration in mice. *Mol Brain*. 3:12.
Guilarte, T.R., N.C. Burton, J.L. McGlothan, T. Verina, Y. Zhou, M. Alexander, L. Pham, M. Griswold, D.F. Wong, T. Syversen, and J.S. Schneider. 2008a. Impairment of nigrostriatal dopamine neurotransmission by manganese is mediated by pre-synaptic mechanism(s): implications to manganese-induced parkinsonism. *Journal of neurochemistry*. 107:1236-1247.
Guilarte, T.R., N.C. Burton, T. Verina, V.V. Prabhu, K.G. Becker, T. Syversen, and J.S. Schneider. 2008b. Increased APLP1 expression and neurodegeneration in the frontal cortex of manganese-exposed non-human primates. *Journal of neurochemistry*. 105:1948-1959.
Gullberg, R.C., J. Jordan Steel, S.L. Moon, E. Soltani, and B.J. Geiss. 2015. Oxidative stress influences positive strand RNA virus genome synthesis and capping. *Virology*. 475:219-229.
Gunter, T.E., C.E. Gavin, M. Aschner, and K.K. Gunter. 2006. Speciation of manganese in cells and mitochondria: a search for the proximal cause of manganese neurotoxicity. *Neurotoxicology*. 27:765-776.
Guo, C.H., P.C. Chen, K.P. Lin, M.Y. Shih, and W.S. Ko. 2012. Trace metal imbalance associated with oxidative stress and inflammatory status in anti-hepatitis C virus antibody positive subjects. *Environmental toxicology and pharmacology*. 33:288-296.
Guo, Z., Z. Zhang, Q. Wang, J. Zhang, L. Wang, Q. Zhang, H. Li, and S. Wu. 2018. Manganese chloride induces histone acetylation changes in neuronal cells: Its role in manganese-induced damage. *Neurotoxicology*. 65:255-263.
Gutzmer, R., B. Kother, J. Zwirner, D. Dijkstra, R. Purwar, M. Wittmann, and T. Werfel. 2006. Human plasmacytoid dendritic cells express receptors for anaphylatoxins C3a and C5a and are chemoattracted to C3a and C5a. *J Invest Dermatol*. 126:2422-2429.

Hahn, C.S., S. Lustig, E.G. Strauss, and J.H. Strauss. 1988. Western equine encephalitis virus is a recombinant virus. *Proc Natl Acad Sci U S A*. 85:5997-6001.

Hall, G.L., J. Girdlestone, D.A. Compston, and M.G. Wing. 1999. Recall antigen presentation by gamma-interferon-activated microglia results in T cell activation and propagation of the immune response. *J Neuroimmunol*. 98:105-111.

Halliday, G.M., and C.H. Stevens. 2011. Glia: initiators and progressors of pathology in Parkinson's disease. *Mov Disord*. 26:6-17.

Hamaue, N., A. Ogata, M. Terado, K. Ohno, S. Kikuchi, H. Sasaki, K. Tashiro, M. Hirafuji, and M. Minami. 2006. Brain catecholamine alterations and pathological features with aging in Parkinson disease model rat induced by Japanese encephalitis virus. *Neurochem Res*. 31:1451-1455.

Hammond, S.L., A.N. Leek, E.H. Richman, and R.B. Tjalkens. 2017. Cellular selectivity of AAV serotypes for gene delivery in neurons and astrocytes by neonatal intracerebroventricular injection. *PLoS One*. 12:e0188830.

Hammond, S.L., K.A. Popichak, X. Li, L.G. Hunt, E.H. Richman, P.U. Damale, E.K.P. Chong, D.S. Backos, S. Safe, and R.B. Tjalkens. 2018. The Nurr1 Ligand,1,1-bis(3'-Indolyl)-1-(p-Chlorophenyl)Methane, Modulates Glial Reactivity and Is Neuroprotective in MPTP-Induced Parkinsonism. *J Pharmacol Exp Ther*. 365:636-651.

Harischandra, D.S., D. Rokad, M.L. Neal, S. Ghaisas, S. Manne, S. Sarkar, N. Panicker, G. Zenitsky, H. Jin, M. Lewis, X. Huang, V. Anantharam, A. Kanthasamy, and A.G. Kanthasamy. 2019. Manganese promotes the aggregation and prion-like cell-to-cell exosomal transmission of alpha-synuclein. *Sci Signal*. 12.

Harris, M.A., J.K. Tsui, S.A. Marion, H. Shen, and K. Teschke. 2012. Association of Parkinson's disease with infections and occupational exposure to possible vectors. *Mov Disord*. 27:1111-1117.

Harrison, I.F., A.D. Smith, and D.T. Dexter. 2018. Pathological histone acetylation in Parkinson's disease: Neuroprotection and inhibition of microglial activation through SIRT 2 inhibition. *Neurosci Lett*. 666:48-57.

Hartlova, A., S. Herbst, J. Peltier, A. Rodgers, O. Bilkei-Gorzo, A. Fearns, B.D. Dill, H. Lee, R. Flynn, S.A. Cowley, P. Davies, P.A. Lewis, I.G. Ganley, J. Martinez, D.R. Alessi, A.D. Reith, M. Trost, and M.G. Gutierrez. 2018. LRRK2 is a negative regulator of Mycobacterium tuberculosis phagosome maturation in macrophages. *EMBO J*. 37.

Hawkes, C.H., K. Del Tredici, and H. Braak. 2007. Parkinson's disease: a dual-hit hypothesis. *Neuropathol Appl Neurobiol*. 33:599-614.

Hayase, Y., and K. Tobita. 1997. Influenza virus and neurological diseases. *Psychiatry Clin Neurosci*. 51:181-184.

Hayashi, S., K. Wakabayashi, A. Ishikawa, H. Nagai, M. Saito, M. Maruyama, T. Takahashi, T. Ozawa, S. Tsuji, and H. Takahashi. 2000. An autopsy case of autosomal-recessive juvenile parkinsonism with a homozygous exon 4 deletion in the parkin gene. *Mov Disord*. 15:884-888.

He, S., C. Wang, H. Dong, F. Xia, H. Zhou, X. Jiang, C. Pei, H. Ren, H. Li, R. Li, and H. Xu. 2012. Immune-related GTPase M (IRGM1) regulates neuronal autophagy in a mouse model of stroke. *Autophagy*. 8:1621-1627.

Hedrich, K., A. Djarmati, N. Schafer, R. Hering, C. Wellenbrock, P.H. Weiss, R. Hilker, P. Vieregge, L.J. Ozelius, P. Heutink, V. Bonifati, E. Schwinger, A.E. Lang, J. Noth, S.B. Bressman, P.P. Pramstaller, O. Riess, and C. Klein. 2004. DJ-1 (PARK7) mutations are

less frequent than Parkin (PARK2) mutations in early-onset Parkinson disease. *Neurology*. 62:389-394.
Henry, J., R.J. Smeyne, H. Jang, B. Miller, and M.S. Okun. 2010a. Parkinsonism and neurological manifestations of influenza throughout the 20th and 21st centuries. *Parkinsonism Relat. Disord.* 16:566-571.
Henry, J., R.J. Smeyne, H. Jang, B. Miller, and M.S. Okun. 2010b. Parkinsonism and neurological manifestations of influenza throughout the 20th and 21st centuries. *Parkinsonism Relat Disord*. 16:566-571.
Herbst, S., and M.G. Gutierrez. 2019. LRRK2 in Infection: Friend or Foe? *ACS Infect Dis*. 5:809-815.
Herrero Hernandez, E., G. Discalzi, P. Dassi, L. Jarre, and E. Pira. 2003. Manganese intoxication: the cause of an inexplicable epileptic syndrome in a 3 year old child. *Neurotoxicology*. 24:633-639.
Hersh, B.P., P.R. Rajendran, and D. Battinelli. 2001. Parkinsonism as the presenting manifestation of HIV infection: improvement on HAART. *Neurology*. 56:278-279.
Hirsch, E.C., and S. Hunot. 2009. Neuroinflammation in Parkinson's disease: a target for neuroprotection? *Lancet Neurol*. 8:382-397.
Hirsch, E.C., S. Hunot, and A. Hartmann. 2005. Neuroinflammatory processes in Parkinson's disease. *Parkinsonism Relat Disord*. 11 Suppl 1:S9-S15.
Ho, D.H., H. Lee, I. Son, and W. Seol. 2019. G2019s LRRK2 promotes mitochondrial fission and increases TNFalpha-mediated neuroinflammation responses. *Anim Cells Syst (Seoul)*. 23:106-111.
Hsieh, J.C., K.H. Lue, and Y.L. Lee. 2002. Parkinson-like syndrome as the major presenting symptom of Epstein-Barr virus encephalitis. *Arch Dis Child*. 87:358.
Huang, C.C., N.S. Chu, C.S. Lu, J.D. Wang, J.L. Tsai, J.L. Tzeng, E.C. Wolters, and D.B. Calne. 1989. Chronic manganese intoxication. *Arch Neurol*. 46:1104-1106.
Huang, Y.S., J.H. Carson, E. Barbarese, and J.D. Richter. 2003. Facilitation of dendritic mRNA transport by CPEB. *Genes Dev.* 17:638-653.
Hyman, C., M. Hofer, Y.A. Barde, M. Juhasz, G.D. Yancopoulos, S.P. Squinto, and R.M. Lindsay. 1991. BDNF is a neurotrophic factor for dopaminergic neurons of the substantia nigra. *Nature*. 350:230-232.
Ibanez, P., A.M. Bonnet, B. Debarges, E. Lohmann, F. Tison, P. Pollak, Y. Agid, A. Durr, and A. Brice. 2004. Causal relation between alpha-synuclein gene duplication and familial Parkinson's disease. *Lancet*. 364:1169-1171.
Ihle, N.T., and R.T. Abraham. 2017. The Pten-Parkin Axis: At the Nexus of Cancer and Neurodegeneration. *Mol Cell*. 65:959-960.
Jackson-Lewis, V., and S. Przedborski. 2007. Protocol for the MPTP mouse model of Parkinson's disease. *Nat Protoc*. 2:141-151.
Jang, H., D. Boltz, J. McClaren, A.K. Pani, M. Smeyne, A. Korff, R. Webster, and R.J. Smeyne. 2012. Inflammatory effects of highly pathogenic H5N1 influenza virus infection in the CNS of mice. *J Neurosci*. 32:1545-1559.
Jang, H., D. Boltz, K. Sturm-Ramirez, K.R. Shepherd, Y. Jiao, R. Webster, and R.J. Smeyne. 2009a. Highly pathogenic H5N1 influenza virus can enter the central nervous system and induce neuroinflammation and neurodegeneration. *Proc Natl Acad Sci U S A*. 106:14063-14068.

Jang, H., D.A. Boltz, R.G. Webster, and R.J. Smeyne. 2009b. Viral parkinsonism. *Biochim Biophys Acta*. 7:714-721.
Jang, H., D.A. Boltz, R.G. Webster, and R.J. Smeyne. 2009c. Viral parkinsonism. *Biochim Biophys Acta*. 1792:714-721.
Jellinger, K.A. 2008. Neuropathological aspects of Alzheimer disease, Parkinson disease and frontotemporal dementia. *Neurodegener Dis*. 5:118-121.
Jiang, T., J. Hoekstra, X. Heng, W. Kang, J. Ding, J. Liu, S. Chen, and J. Zhang. 2015. P2X7 receptor is critical in alpha-synuclein--mediated microglial NADPH oxidase activation. *Neurobiol Aging*. 36:2304-2318.
Joers, V., M.G. Tansey, G. Mulas, and A.R. Carta. 2017. Microglial phenotypes in Parkinson's disease and animal models of the disease. *Prog Neurobiol*. 155:57-75.
Kalaitzakis, M.E., M.B. Graeber, S.M. Gentleman, and R.K. Pearce. 2008. Controversies over the staging of alpha-synuclein pathology in Parkinson's disease. *Acta Neuropathol*. 116:125-128; author reply 129-131.
Kanaan, N.M., J.H. Kordower, and T.J. Collier. 2008. Age and region-specific responses of microglia, but not astrocytes, suggest a role in selective vulnerability of dopamine neurons after 1-methyl-4-phenyl-1,2,3,6-tetrahydropyridine exposure in monkeys. *Glia*. 56:1199-1214.
Karin, M. 2005. Inflammation-activated protein kinases as targets for drug development. *Proc Am Thorac Soc*. 2:386-390; discussion 394-385.
Keatinge, M., H. Bui, A. Menke, Y.C. Chen, A.M. Sokol, Q. Bai, F. Ellett, M. Da Costa, D. Burke, M. Gegg, L. Trollope, T. Payne, A. McTighe, H. Mortiboys, S. de Jager, H. Nuthall, M.S. Kuo, A. Fleming, A.H. Schapira, S.A. Renshaw, J.R. Highley, A. Chacinska, P. Panula, E.A. Burton, M.J. O'Neill, and O. Bandmann. 2015. Glucocerebrosidase 1 deficient Danio rerio mirror key pathological aspects of human Gaucher disease and provide evidence of early microglial activation preceding alpha-synuclein-independent neuronal cell death. *Hum Mol Genet*. 24:6640-6652.
Kessler, K.R., G. Wunderlich, H. Hefter, and R.J. Seitz. 2003. Secondary progressive chronic manganism associated with markedly decreased striatal D2 receptor density. *Mov Disord*. 18:217-218.
Khasnavis, S., and K. Pahan. 2014. Cinnamon treatment upregulates neuroprotective proteins Parkin and DJ-1 and protects dopaminergic neurons in a mouse model of Parkinson's disease. *J Neuroimmune Pharmacol*. 9:569-581.
Kim, B., M.S. Yang, D. Choi, J.H. Kim, H.S. Kim, W. Seol, S. Choi, I. Jou, E.Y. Kim, and E.H. Joe. 2012. Impaired inflammatory responses in murine Lrrk2-knockdown brain microglia. *PLoS One*. 7:e34693.
Kim, C., D.H. Ho, J.E. Suk, S. You, S. Michael, J. Kang, S. Joong Lee, E. Masliah, D. Hwang, H.J. Lee, and S.J. Lee. 2013a. Neuron-released oligomeric alpha-synuclein is an endogenous agonist of TLR2 for paracrine activation of microglia. *Nat Commun*. 4:1562.
Kim, J., E. Pajarillo, A. Rizor, D.S. Son, J. Lee, M. Aschner, and E. Lee. 2019. LRRK2 kinase plays a critical role in manganese-induced inflammation and apoptosis in microglia. *PLoS One*. 14:e0210248.
Kim, J.M., S.H. Cha, Y.R. Choi, I. Jou, E.H. Joe, and S.M. Park. 2016. DJ-1 deficiency impairs glutamate uptake into astrocytes via the regulation of flotillin-1 and caveolin-1 expression. *Sci Rep*. 6:28823.

Kim, K.S., J.S. Kim, J.Y. Park, Y.H. Suh, I. Jou, E.H. Joe, and S.M. Park. 2013b. DJ-1 associates with lipid rafts by palmitoylation and regulates lipid rafts-dependent endocytosis in astrocytes. *Hum Mol Genet*. 22:4805-4817.

Kim, Y. 2006. Neuroimaging in manganism. *Neurotoxicology*. 27:369-372.

Kim, Y., J.K. Park, Y. Choi, C.I. Yoo, C.R. Lee, H. Lee, J.H. Lee, S.R. Kim, T.H. Jeong, C.S. Yoon, and J.H. Park. 2005. Blood manganese concentration is elevated in iron deficiency anemia patients, whereas globus pallidus signal intensity is minimally affected. *Neurotoxicology*. 26:107-111.

Kim, Y.J., S.Y. Hwang, E.S. Oh, S. Oh, and I.O. Han. 2006. IL-1beta, an immediate early protein secreted by activated microglia, induces iNOS/NO in C6 astrocytoma cells through p38 MAPK and NF-kappaB pathways. *J Neurosci Res*. 84:1037-1046.

Kirkley, K.S., K.A. Popichak, M.F. Afzali, M.E. Legare, and R.B. Tjalkens. 2017a. Microglia amplify inflammatory activation of astrocytes in manganese neurotoxicity.1-18.

Kirkley, K.S., K.A. Popichak, S.L. Hammond, C. Davies, L. Hunt, and R.B. Tjalkens. 2019a. Genetic suppression of IKK2/NF-kappaB in astrocytes inhibits neuroinflammation and reduces neuronal loss in the MPTP-Probenecid model of Parkinson's disease. *Neurobiol Dis*. 127:193-209.

Kirkley, K.S., K.A. Popichak, S.L. Hammond, C. Davies, L. Hunt, and R.B. Tjalkens. 2019b. Genetic suppression of IKK2/NF-κB in astrocytes inhibits neuroinflammation and reduces neuronal loss in the MPTP-Probenecid model of Parkinson's disease. *Neurobiology of Disease*.

Kirkley, K.S., K.D. Walton, C. Duncan, and R.B. Tjalkens. 2017b. Spontaneous Development of Cutaneous Squamous Cell Carcinoma in Mice with Cell-specific Deletion of Inhibitor of kappaB Kinase 2. *Comp Med*. 67:407-415.

Kitada, T., S. Asakawa, N. Hattori, H. Matsumine, Y. Yamamura, S. Minoshima, M. Yokochi, Y. Mizuno, and N. Shimizu. 1998. Mutations in the parkin gene cause autosomal recessive juvenile parkinsonism. *Nature*. 392:605-608.

Kobayashi, N., T. Nagata, S. Shinagawa, N. Oka, K. Shimada, A. Shimizu, Y. Tatebayashi, H. Yamada, K. Nakayama, and K. Kondo. 2013. Increase in the IgG avidity index due to herpes simplex virus type 1 reactivation and its relationship with cognitive function in amnestic mild cognitive impairment and Alzheimer's disease. *Biochem Biophys Res Commun*. 430:907-911.

Kohutnicka, M., E. Lewandowska, I. Kurkowska-Jastrzebska, A. Czlonkowski, and A. Czlonkowska. 1998. Microglial and astrocytic involvement in a murine model of Parkinson's disease induced by 1-methyl-4-phenyl-1,2,3,6-tetrahydropyridine (MPTP). *Immunopharmacology*. 39:167-180.

Koprich, J.B., C. Reske-Nielsen, P. Mithal, and O. Isacson. 2008. Neuroinflammation mediated by IL-1beta increases susceptibility of dopamine neurons to degeneration in an animal model of Parkinson's disease. *J Neuroinflammation*. 5:8.

Koschinski, A., G. Wengler, G. Wengler, and H. Repp. 2005. Rare earth ions block the ion pores generated by the class II fusion proteins of alphaviruses and allow analysis of the biological functions of these pores. *J Gen Virol*. 86:3311-3320.

Kostuk, E.W., J. Cai, and L. Iacovitti. 2019. Subregional differences in astrocytes underlie selective neurodegeneration or protection in Parkinson's disease models in culture. *Glia*.

Koyano, F., and N. Matsuda. 2015. Molecular mechanisms underlying PINK1 and Parkin catalyzed ubiquitylation of substrates on damaged mitochondria. *Biochim Biophys Acta*. 1853:2791-2796.

Kozina, E., S. Sadasivan, Y. Jiao, Y. Dou, Z. Ma, H. Tan, K. Kodali, T. Shaw, J. Peng, and R.J. Smeyne. 2018. Mutant LRRK2 mediates peripheral and central immune responses leading to neurodegeneration in vivo. *Brain*. 141:1753-1769.

Kruger, R., W. Kuhn, T. Muller, D. Woitalla, M. Graeber, S. Kosel, H. Przuntek, J.T. Epplen, L. Schols, and O. Riess. 1998. Ala30Pro mutation in the gene encoding alpha-synuclein in Parkinson's disease. *Nat Genet*. 18:106-108.

Kuno, R., Y. Yoshida, A. Nitta, T. Nabeshima, J. Wang, Y. Sonobe, J. Kawanokuchi, H. Takeuchi, T. Mizuno, and A. Suzumura. 2006. The role of TNF-alpha and its receptors in the production of NGF and GDNF by astrocytes. *Brain Res*. 1116:12-18.

Lai, J.C., M.J. Minski, A.W. Chan, T.K. Leung, and L. Lim. 1999. Manganese mineral interactions in brain. *Neurotoxicology*. 20:433-444.

Landrigan, P.J., B. Sonawane, R.N. Butler, L. Trasande, R. Callan, and D. Droller. 2005. Early environmental origins of neurodegenerative disease in later life. *Environ Health Perspect*. 113:1230-1233.

Lashuel, H.A., C.R. Overk, A. Oueslati, and E. Masliah. 2013. The many faces of alpha-synuclein: from structure and toxicity to therapeutic target. *Nat Rev Neurosci*. 14:38-48.

Lee, H.J., J.E. Suk, E.J. Bae, and S.J. Lee. 2008. Clearance and deposition of extracellular alpha-synuclein aggregates in microglia. *Biochem Biophys Res Commun*. 372:423-428.

Lee, H.J., J.E. Suk, C. Patrick, E.J. Bae, J.H. Cho, S. Rho, D. Hwang, E. Masliah, and S.J. Lee. 2010. Direct transfer of alpha-synuclein from neuron to astroglia causes inflammatory responses in synucleinopathies. *J Biol Chem*. 285:9262-9272.

Lee, J.H., J.H. Han, H. Kim, S.M. Park, E.H. Joe, and I. Jou. 2019. Parkinson's disease-associated LRRK2-G2019S mutant acts through regulation of SERCA activity to control ER stress in astrocytes. *Acta Neuropathol Commun*. 7:68.

Lesage, S., and A. Brice. 2009. Parkinson's disease: from monogenic forms to genetic susceptibility factors. *Hum Mol Genet*. 18:R48-59.

Lesteberg, K.E., and J.D. Beckham. 2019. Immunology of West Nile Virus Infection and the Role of Alpha-Synuclein as a Viral Restriction Factor. *Viral Immunol*. 32:38-47.

Levine, B., and D.E. Griffin. 1992. Persistence of viral RNA in mouse brains after recovery from acute alphavirus encephalitis. *J Virol*. 66:6429-6435.

Lewy, F.H. 1932. Die Entstehung der Einschlußkörper und ihre Bedeutung für die systematische Einordnung der sogenannten Viruskrankheiten. *Deutsche Zeitschrift für Nervenheilkunde*. 124:93-100.

Li, Q., and B.A. Barres. 2018. Microglia and macrophages in brain homeostasis and disease. *Nat Rev Immunol*. 18:225-242.

Lian, H., A. Litvinchuk, A.C. Chiang, N. Aithmitti, J.L. Jankowsky, and H. Zheng. 2016. Astrocyte-Microglia Cross Talk through Complement Activation Modulates Amyloid Pathology in Mouse Models of Alzheimer's Disease. *J Neurosci*. 36:577-589.

Lian, H., L. Yang, A. Cole, L. Sun, A.C. Chiang, S.W. Fowler, D.J. Shim, J. Rodriguez-Rivera, G. Taglialatela, J.L. Jankowsky, H.C. Lu, and H. Zheng. 2015. NFkappaB-activated astroglial release of complement C3 compromises neuronal morphology and function associated with Alzheimer's disease. *Neuron*. 85:101-115.

Liang, Y., T. Zhou, Y. Chen, D. Lin, X. Jing, S. Peng, D. Zheng, Z. Zeng, M. Lei, X. Wu, K. Huang, L. Yang, S. Xiao, J. Liu, and E. Tao. 2017. Rifampicin inhibits rotenone-induced microglial inflammation via enhancement of autophagy. *Neurotoxicology*. 63:137-145.
Liberto, C.M., P.J. Albrecht, L.M. Herx, V.W. Yong, and S.W. Levison. 2004. Pro-regenerative properties of cytokine-activated astrocytes. *J Neurochem*. 89:1092-1100.
Liccione, J.J., and M.D. Maines. 1988. Selective vulnerability of glutathione metabolism and cellular defense mechanisms in rat striatum to manganese. *J Pharmacol Exp Ther*. 247:156-161.
Liddelow, S.A., and B.A. Barres. 2017. Reactive Astrocytes: Production, Function, and Therapeutic Potential. *Immunity*. 46:957-967.
Liddelow, S.A., K.A. Guttenplan, L.E. Clarke, F.C. Bennett, C.J. Bohlen, L. Schirmer, M.L. Bennett, A.E. Münch, W.-S. Chung, T.C. Peterson, D.K. Wilton, A. Frouin, B.A. Napier, N. Panicker, M. Kumar, M.S. Buckwalter, D.H. Rowitch, V.L. Dawson, T.M. Dawson, B. Stevens, and B.A. Barres. 2017a. Neurotoxic reactive astrocytes are induced by activated microglia. *Nature Publishing Group*. 541:481-487.
Liddelow, S.A., K.A. Guttenplan, L.E. Clarke, F.C. Bennett, C.J. Bohlen, L. Schirmer, M.L. Bennett, A.E. Munch, W.S. Chung, T.C. Peterson, D.K. Wilton, A. Frouin, B.A. Napier, N. Panicker, M. Kumar, M.S. Buckwalter, D.H. Rowitch, V.L. Dawson, T.M. Dawson, B. Stevens, and B.A. Barres. 2017b. Neurotoxic reactive astrocytes are induced by activated microglia. *Nature*. 541:481-487.
Lill, C.M. 2016. Genetics of Parkinson's disease. *Mol Cell Probes*. 30:386-396.
Lill, C.M., and L. Bertram. 2015. Probing the epigenome by EWAS: a new era in brain disease research. *Mov Disord*. 30:197.
Limongi, D., and S. Baldelli. 2016. Redox Imbalance and Viral Infections in Neurodegenerative Diseases. *Oxidative medicine and cellular longevity*. 2016:6547248.
Limphaibool, N., P. Iwanowski, M.J.V. Holstad, D. Kobylarek, and W. Kozubski. 2019. Infectious Etiologies of Parkinsonism: Pathomechanisms and Clinical Implications. *Front Neurol*. 10:652.
Lin, K.I., S.H. Lee, R. Narayanan, J.M. Baraban, J.M. Hardwick, and R.R. Ratan. 1995. Thiol agents and Bcl-2 identify an alphavirus-induced apoptotic pathway that requires activation of the transcription factor NF-kappa B. *The Journal of cell biology*. 131:1149-1161.
Lindqvist, D., S. Hall, Y. Surova, H.M. Nielsen, S. Janelidze, L. Brundin, and O. Hansson. 2013. Cerebrospinal fluid inflammatory markers in Parkinson's disease--associations with depression, fatigue, and cognitive impairment. *Brain Behav Immun*. 33:183-189.
Linnartz, B., and H. Neumann. 2013. Microglial activatory (immunoreceptor tyrosine-based activation motif)- and inhibitory (immunoreceptor tyrosine-based inhibition motif)-signaling receptors for recognition of the neuronal glycocalyx. *Glia*. 61:37-46.
Lipe, G.W., H. Duhart, G.D. Newport, W. Slikker, Jr., and S.F. Ali. 1999. Effect of manganese on the concentration of amino acids in different regions of the rat brain. *J Environ Sci Health B*. 34:119-132.
Liu, C., D.W. Voth, P. Rodina, L.R. Shauf, and G. Gonzalez. 1970. A comparative study of the pathogenesis of western equine and eastern equine encephalomyelitis viral infections in mice by intracerebral and subcutaneous inoculations. *J Infect Dis*. 122:53-63.

Liu, X., J.A. Buffington, and R.B. Tjalkens. 2005. NF-kappaB-dependent production of nitric oxide by astrocytes mediates apoptosis in differentiated PC12 neurons following exposure to manganese and cytokines. *Brain Res Mol Brain Res*. 141:39-47.

Loeffler, D.A., D.M. Camp, and S.B. Conant. 2006. Complement activation in the Parkinson's disease substantia nigra: an immunocytochemical study. *J Neuroinflammation*. 3:29.

Logue, C.H., C.F. Bosio, T. Welte, K.M. Keene, J.P. Ledermann, A. Phillips, B.J. Sheahan, D.J. Pierro, N. Marlenee, A.C. Brault, C.M. Bosio, A.J. Singh, A.M. Powers, and K.E. Olson. 2009. Virulence variation among isolates of western equine encephalitis virus in an outbred mouse model. *J Gen Virol*. 90:1848-1858.

Logue, C.H., A.T. Phillips, E.C. Mossel, J.P. Ledermann, T. Welte, S.W. Dow, K.E. Olson, and A.M. Powers. 2010a. Treatment with cationic liposome-DNA complexes (CLDCs) protects mice from lethal Western equine encephalitis virus (WEEV) challenge. *Antiviral Res*. 87:195-203.

Logue, C.H., A.T. Phillips, E.C. Mossel, J.P. Ledermann, T. Welte, S.W. Dow, K.E. Olson, and A.M. Powers. 2010b. Treatment with cationic liposome-DNA complexes (CLDCs) protects mice from lethal Western equine encephalitis virus (WEEV) challenge. *Antiviral Res*. 87:195-203.

Lopez de Maturana, R., J.C. Aguila, A. Sousa, N. Vazquez, P. Del Rio, A. Aiastui, A. Gorostidi, A. Lopez de Munain, and R. Sanchez-Pernaute. 2014. Leucine-rich repeat kinase 2 modulates cyclooxygenase 2 and the inflammatory response in idiopathic and genetic Parkinson's disease. *Neurobiol Aging*. 35:1116-1124.

Loria, F., J.Y. Vargas, L. Bousset, S. Syan, A. Salles, R. Melki, and C. Zurzolo. 2017. alpha-Synuclein transfer between neurons and astrocytes indicates that astrocytes play a role in degradation rather than in spreading. *Acta neuropathologica*. 134:789-808.

Ludlow, M., J. Kortekaas, C. Herden, B. Hoffmann, D. Tappe, C. Trebst, D.E. Griffin, H.E. Brindle, T. Solomon, A.S. Brown, D. van Riel, K.C. Wolthers, D. Pajkrt, P. Wohlsein, B.E.E. Martina, W. Baumgartner, G.M. Verjans, and A. Osterhaus. 2016. Neurotropic virus infections as the cause of immediate and delayed neuropathology. *Acta Neuropathol*. 131:159-184.

Lunnon, K., R. Smith, E. Hannon, P.L. De Jager, G. Srivastava, M. Volta, C. Troakes, S. Al-Sarraj, J. Burrage, R. Macdonald, D. Condliffe, L.W. Harries, P. Katsel, V. Haroutunian, Z. Kaminsky, C. Joachim, J. Powell, S. Lovestone, D.A. Bennett, L.C. Schalkwyk, and J. Mill. 2014. Methylomic profiling implicates cortical deregulation of ANK1 in Alzheimer's disease. *Nat Neurosci*. 17:1164-1170.

Machado, V., T. Zoller, A. Attaai, and B. Spittau. 2016. Microglia-Mediated Neuroinflammation and Neurotrophic Factor-Induced Protection in the MPTP Mouse Model of Parkinson's Disease-Lessons from Transgenic Mice. *Int J Mol Sci*. 17.

Magalhaes, J., M.E. Gegg, A. Migdalska-Richards, M.K. Doherty, P.D. Whitfield, and A.H. Schapira. 2016. Autophagic lysosome reformation dysfunction in glucocerebrosidase deficient cells: relevance to Parkinson disease. *Hum Mol Genet*. 25:3432-3445.

Marker, D.F., J.M. Puccini, T.E. Mockus, J. Barbieri, S.M. Lu, and H.A. Gelbard. 2012. LRRK2 kinase inhibition prevents pathological microglial phagocytosis in response to HIV-1 Tat protein. *J Neuroinflammation*. 9:261.

Martinez, E.M., A.L. Young, Y.R. Patankar, B.L. Berwin, L. Wang, K.M. von Herrmann, J.M. Weier, and M.C. Havrda. 2017. Editor's Highlight: Nlrp3 Is Required for Inflammatory

Changes and Nigral Cell Loss Resulting From Chronic Intragastric Rotenone Exposure in Mice. *Toxicol Sci*. 159:64-75.
Marttila, R.J., U.K. Rinne, P. Halonen, D.L. Madden, and J.L. Sever. 1981. Herpesviruses and parkinsonism. Herpes simplex virus types 1 and 2, and cytomegalovirus antibodies in serum and CSF. *Arch Neurol*. 38:19-21.
Matthews, K.A., W. Xu, A.H. Gaglioti, J.B. Holt, J.B. Croft, D. Mack, and L.C. McGuire. 2019. Racial and ethnic estimates of Alzheimer's disease and related dementias in the United States (2015-2060) in adults aged >/=65 years. *Alzheimers Dement*. 15:17-24.
Mattos, J.P., A.L. Rosso, R.B. Correa, and S.A. Novis. 2002. Movement disorders in 28 HIV-infected patients. *Arq Neuropsiquiatr*. 60:525-530.
Mattson, M.P. 2004. Infectious agents and age-related neurodegenerative disorders. *Ageing Res Rev*. 3:105-120.
Mayeux, R. 2003. Epidemiology of neurodegeneration. *Annu Rev Neurosci*. 26:81-104.
McCabe, K., R.M. Concannon, D.P. McKernan, and E. Dowd. 2017. Time-course of striatal Toll-like receptor expression in neurotoxic, environmental and inflammatory rat models of Parkinson's disease. *J Neuroimmunol*. 310:103-106.
McCarthy, M.M., B.M. Nugent, and K.M. Lenz. 2017. Neuroimmunology and neuroepigenetics in the establishment of sex differences in the brain. *Nat Rev Neurosci*. 18:471-484.
Miller, J.A., K.A. Kirkley, R. Padmanabhan, L.P. Liang, Y.H. Raol, M. Patel, R.A. Bialecki, and R.B. Tjalkens. 2014. Repeated exposure to low doses of kainic acid activates nuclear factor kappa B (NF-kappaB) prior to seizure in transgenic NF-kappaB/EGFP reporter mice. *Neurotoxicology*. 44:39-47.
Miller, J.A., S.A. Runkle, R.B. Tjalkens, and M.A. Philbert. 2011. 1,3-Dinitrobenzene-induced metabolic impairment through selective inactivation of the pyruvate dehydrogenase complex. *Toxicol Sci*. 122:502-511.
Miner, J.J., A. Sene, J.M. Richner, A.M. Smith, A. Santeford, N. Ban, J. Weger-Lucarelli, F. Manzella, C. Ruckert, J. Govero, K.K. Noguchi, G.D. Ebel, M.S. Diamond, and R.S. Apte. 2016. Zika Virus Infection in Mice Causes Panuveitis with Shedding of Virus in Tears. *Cell Rep*. 16:3208-3218.
Minghetti, L., M.A. Ajmone-Cat, M.A. De Berardinis, and R. De Simone. 2005. Microglial activation in chronic neurodegenerative diseases: roles of apoptotic neurons and chronic stimulation. *Brain Res Brain Res Rev*. 48:251-256.
Mittelbronn, M., K. Dietz, H.J. Schluesener, and R. Meyermann. 2001. Local distribution of microglia in the normal adult human central nervous system differs by up to one order of magnitude. *Acta neuropathologica*. 101:249-255.
Moehle, M.S., P.J. Webber, T. Tse, N. Sukar, D.G. Standaert, T.M. DeSilva, R.M. Cowell, and A.B. West. 2012. LRRK2 inhibition attenuates microglial inflammatory responses. *J Neurosci*. 32:1602-1611.
Mogi, M., M. Harada, H. Narabayashi, H. Inagaki, M. Minami, and T. Nagatsu. 1996. Interleukin (IL)-1 beta, IL-2, IL-4, IL-6 and transforming growth factor-alpha levels are elevated in ventricular cerebrospinal fluid in juvenile parkinsonism and Parkinson's disease. *Neurosci Lett*. 211:13-16.
Mogi, M., T. Kondo, Y. Mizuno, and T. Nagatsu. 2007. p53 protein, interferon-gamma, and NF-kappaB levels are elevated in the parkinsonian brain. *Neurosci Lett*. 414:94-97.
Moon, H.E., and S.H. Paek. 2015. Mitochondrial Dysfunction in Parkinson's Disease. *Exp Neurobiol*. 24:103-116.

Morello, M., A. Canini, P. Mattioli, R.P. Sorge, A. Alimonti, B. Bocca, G. Forte, A. Martorana, G. Bernardi, and G. Sancesario. 2008. Sub-cellular localization of manganese in the basal ganglia of normal and manganese-treated rats An electron spectroscopy imaging and electron energy-loss spectroscopy study. *Neurotoxicology*. 29:60-72.

Moreno, J.A., K.M. Streifel, K.A. Sullivan, W.H. Hanneman, and R.B. Tjalkens. 2011a. Manganese-induced NF-kappaB activation and nitrosative stress is decreased by estrogen in juvenile mice. *Toxicol Sci*. 122:121-133.

Moreno, J.A., K.M. Streifel, K.A. Sullivan, W.H. Hanneman, and R.B. Tjalkens. 2011b. Manganese-induced NF-kappaB activation and nitrosative stress is decreased by estrogen in juvenile mice. *Toxicological sciences : an official journal of the Society of Toxicology*. 122:121-133.

Moreno, J.A., K.M. Streifel, K.A. Sullivan, M.E. Legare, and R.B. Tjalkens. 2009a. Developmental exposure to manganese increases adult susceptibility to inflammatory activation of glia and neuronal protein nitration. *Toxicol Sci*. 112:405-415.

Moreno, J.A., K.A. Sullivan, D.L. Carbone, W.H. Hanneman, and R.B. Tjalkens. 2008. Manganese potentiates nuclear factor-kappaB-dependent expression of nitric oxide synthase 2 in astrocytes by activating soluble guanylate cyclase and extracellular responsive kinase signaling pathways. *J Neurosci Res*. 86:2028-2038.

Moreno, J.A., E.C. Yeomans, K.M. Streifel, B.L. Brattin, R.J. Taylor, and R.B. Tjalkens. 2009b. Age-Dependent Susceptibility to Manganese-Induced Neurological Dysfunction. *Toxicological Sciences*. 112:394-404.

Moreno, J.A., E.C. Yeomans, K.M. Streifel, B.L. Brattin, R.J. Taylor, and R.B. Tjalkens. 2009c. Age-dependent susceptibility to manganese-induced neurological dysfunction. *Toxicol Sci*. 112:394-404.

Mosley, R.L., E.J. Benner, I. Kadiu, M. Thomas, M.D. Boska, K. Hasan, C. Laurie, and H.E. Gendelman. 2006. Neuroinflammation, Oxidative Stress and the Pathogenesis of Parkinson's Disease. *Clin Neurosci Res*. 6:261-281.

Mossel, E.C., J.P. Ledermann, A.T. Phillips, E.M. Borland, A.M. Powers, and K.E. Olson. 2013a. Molecular determinants of mouse neurovirulence and mosquito infection for Western equine encephalitis virus. *PLoS One*. 8:27.

Mossel, E.C., J.P. Ledermann, A.T. Phillips, E.M. Borland, A.M. Powers, and K.E. Olson. 2013b. Molecular determinants of mouse neurovirulence and mosquito infection for Western equine encephalitis virus. *PLoS One*. 8:e60427.

Mucci, J.M., and P. Rozenfeld. 2015. Pathogenesis of Bone Alterations in Gaucher Disease: The Role of Immune System. *J Immunol Res*. 2015:192761.

Mulder, D.W., M. Parrott, and M. Thaler. 1951. Sequelae of western equine encephalitis. *Neurology*. 1:318-327.

Murgod, U.A., U.B. Muthane, V. Ravi, S. Radhesh, and A. Desai. 2001. Persistent movement disorders following Japanese encephalitis. *Neurology*. 57:2313-2315.

Nakano, H., M. Shindo, S. Sakon, S. Nishinaka, M. Mihara, H. Yagita, and K. Okumura. 1998. Differential regulation of IkappaB kinase alpha and beta by two upstream kinases, NF-kappaB-inducing kinase and mitogen-activated protein kinase/ERK kinase kinase-1. *Proc Natl Acad Sci U S A*. 95:3537-3542.

Netolitzky, D.J., F.L. Schmaltz, M.D. Parker, G.A. Rayner, G.R. Fisher, D.W. Trent, D.E. Bader, and L.P. Nagata. 2000. Complete genomic RNA sequence of western equine encephalitis virus and expression of the structural genes. *J Gen Virol*. 81:151-159.

Neumann, H., M.R. Kotter, and R.J. Franklin. 2009. Debris clearance by microglia: an essential link between degeneration and regeneration. *Brain*. 132:288-295.
Neumann, M., V. Muller, K. Gorner, H.A. Kretzschmar, C. Haass, and P.J. Kahle. 2004. Pathological properties of the Parkinson's disease-associated protein DJ-1 in alpha-synucleinopathies and tauopathies: relevance for multiple system atrophy and Pick's disease. *Acta neuropathologica*. 107:489-496.
Nimmerjahn, A., F. Kirchhoff, and F. Helmchen. 2005. Resting microglial cells are highly dynamic surveillants of brain parenchyma in vivo. *Science*. 308:1314-1318.
Ogata, A., K. Tashiro, S. Nukuzuma, K. Nagashima, and W.W. Hall. 1997. A rat model of Parkinson's disease induced by Japanese encephalitis virus. *J Neurovirol*. 3:141-147.
Oliveira, T.G., and G. Di Paolo. 2010. Phospholipase D in brain function and Alzheimer's disease. *Biochim Biophys Acta*. 1801:799-805.
Olsen, A.L., and M.B. Feany. 2019. Glial alpha-synuclein promotes neurodegeneration characterized by a distinct transcriptional program in vivo. *Glia*. 67:1933-1957.
Osellame, L.D., and M.R. Duchen. 2013. Defective quality control mechanisms and accumulation of damaged mitochondria link Gaucher and Parkinson diseases. *Autophagy*. 9:1633-1635.
Paisan-Ruiz, C., S. Jain, E.W. Evans, W.P. Gilks, J. Simon, M. van der Brug, A. Lopez de Munain, S. Aparicio, A.M. Gil, N. Khan, J. Johnson, J.R. Martinez, D. Nicholl, I. Marti Carrera, A.S. Pena, R. de Silva, A. Lees, J.F. Marti-Masso, J. Perez-Tur, N.W. Wood, and A.B. Singleton. 2004. Cloning of the gene containing mutations that cause PARK8-linked Parkinson's disease. *Neuron*. 44:595-600.
Palmer, R.J., and K.H. Finley. 1956. Sequelae of encephalitis; report of a study after the California epidemic. *Calif Med*. 84:98-100.
Pang, S.Y., P.W. Ho, H.F. Liu, C.T. Leung, L. Li, E.E.S. Chang, D.B. Ramsden, and S.L. Ho. 2019. The interplay of aging, genetics and environmental factors in the pathogenesis of Parkinson's disease. *Transl Neurodegener*. 8:23.
Peres, T.V., M.R. Schettinger, P. Chen, F. Carvalho, D.S. Avila, A.B. Bowman, and M. Aschner. 2016. "Manganese-induced neurotoxicity: a review of its behavioral consequences and neuroprotective strategies". *BMC Pharmacol Toxicol*. 17:57.
Perl, D.P., and C.W. Olanow. 2007. The neuropathology of manganese-induced Parkinsonism. *J Neuropathol Exp Neurol*. 66:675-682.
Phillips, A.T., A.B. Rico, C.B. Stauft, S.L. Hammond, T.A. Aboellail, R.B. Tjalkens, and K.E. Olson. 2016. Entry Sites of Venezuelan and Western Equine Encephalitis Viruses in the Mouse Central Nervous System following Peripheral Infection. *J Virol*. 90:5785-5796.
Phillips, A.T., T. Schountz, A.M. Toth, A.B. Rico, D.L. Jarvis, A.M. Powers, and K.E. Olson. 2014. Liposome-antigen-nucleic Acid complexes protect mice from lethal challenge with Western and eastern equine encephalitis viruses. *J Virol*. 88:1771-1780.
Phillips, A.T., C.B. Stauft, T.A. Aboellail, A.M. Toth, D.L. Jarvis, A.M. Powers, and K.E. Olson. 2013. Bioluminescent imaging and histopathologic characterization of WEEV neuroinvasion in outbred CD-1 mice. *PLoS One*. 8:2.
Pintado, C., M.P. Gavilan, E. Gavilan, L. Garcia-Cuervo, A. Gutierrez, J. Vitorica, A. Castano, R.M. Rios, and D. Ruano. 2012. Lipopolysaccharide-induced neuroinflammation leads to the accumulation of ubiquitinated proteins and increases susceptibility to neurodegeneration induced by proteasome inhibition in rat hippocampus. *J Neuroinflammation*. 9:87.

Pistollato, F., D. Canovas-Jorda, D. Zagoura, and A. Bal-Price. 2017. Nrf2 pathway activation upon rotenone treatment in human iPSC-derived neural stem cells undergoing differentiation towards neurons and astrocytes. *Neurochem Int*. 108:457-471.

Polymeropoulos, M.H., C. Lavedan, E. Leroy, S.E. Ide, A. Dehejia, A. Dutra, B. Pike, H. Root, J. Rubenstein, R. Boyer, E.S. Stenroos, S. Chandrasekharappa, A. Athanassiadou, T. Papapetropoulos, W.G. Johnson, A.M. Lazzarini, R.C. Duvoisin, G. Di Iorio, L.I. Golbe, and R.L. Nussbaum. 1997. Mutation in the alpha-synuclein gene identified in families with Parkinson's disease. *Science*. 276:2045-2047.

Pontikis, C.C., C.V. Cella, N. Parihar, M.J. Lim, S. Chakrabarti, H.M. Mitchison, W.C. Mobley, P. Rezaie, D.A. Pearce, and J.D. Cooper. 2004. Late onset neurodegeneration in the Cln3-/- mouse model of juvenile neuronal ceroid lipofuscinosis is preceded by low level glial activation. *Brain Res*. 1023:231-242.

Popichak, K.A., M.F. Afzali, K.S. Kirkley, and R.B. Tjalkens. 2018a. Glial-neuronal signaling mechanisms underlying the neuroinflammatory effects of manganese. *J Neuroinflammation*. 15:324.

Popichak, K.A., S.L. Hammond, J.A. Moreno, M.F. Afzali, D.S. Backos, R.D. Slayden, S. Safe, and R.B. Tjalkens. 2018b. Compensatory expression of Nur77 and Nurr1 regulates NF-kappaB-dependent inflammatory signaling in astrocytes. *Mol Pharmacol*.

Qin, H., J.A. Buckley, X. Li, Y. Liu, T.H. Fox, 3rd, G.P. Meares, H. Yu, Z. Yan, A.S. Harms, Y. Li, D.G. Standaert, and E.N. Benveniste. 2016. Inhibition of the JAK/STAT Pathway Protects Against alpha-Synuclein-Induced Neuroinflammation and Dopaminergic Neurodegeneration. *J Neurosci*. 36:5144-5159.

Racette, B.A., M. Aschner, T.R. Guilarte, U. Dydak, S.R. Criswell, and W. Zheng. 2012. Pathophysiology of manganese-associated neurotoxicity. *Neurotoxicology*. 33:881-886.

Ramakrishnan, M.A. 2016. Determination of 50% endpoint titer using a simple formula. *World J Virol*. 5:85-86.

Ranger, A., S. Ray, S. Szak, A. Dearth, N. Allaire, R. Murray, R. Gardner, D. Cadavid, and S. Mi. 2018. Anti-LINGO-1 has no detectable immunomodulatory effects in preclinical and phase 1 studies. *Neurol Neuroimmunol Neuroinflamm*. 5:e417.

Rannikko, E.H., S.S. Weber, and P.J. Kahle. 2015. Exogenous alpha-synuclein induces toll-like receptor 4 dependent inflammatory responses in astrocytes. *BMC Neurosci*. 16:57.

Reale, M., C. Iarlori, A. Thomas, D. Gambi, B. Perfetti, M. Di Nicola, and M. Onofrj. 2009. Peripheral cytokines profile in Parkinson's disease. *Brain Behav Immun*. 23:55-63.

Refolo, V., and N. Stefanova. 2019. Neuroinflammation and Glial Phenotypic Changes in Alpha-Synucleinopathies. *Front Cell Neurosci*. 13:263.

Reid, A.H., S. McCall, J.M. Henry, and J.K. Taubenberger. 2001. Experimenting on the past: the enigma of von Economo's encephalitis lethargica. *J Neuropathol Exp Neurol*. 60:663-670.

Rey, N.L., S. George, J.A. Steiner, Z. Madaj, K.C. Luk, J.Q. Trojanowski, V.M. Lee, and P. Brundin. 2018. Spread of aggregates after olfactory bulb injection of alpha-synuclein fibrils is associated with early neuronal loss and is reduced long term. *Acta Neuropathol*. 135:65-83.

Rey, N.L., J.A. Steiner, N. Maroof, K.C. Luk, Z. Madaj, J.Q. Trojanowski, V.M. Lee, and P. Brundin. 2016. Widespread transneuronal propagation of alpha-synucleinopathy triggered in olfactory bulb mimics prodromal Parkinson's disease. *J Exp Med*. 213:1759-1778.

Richter, J.D. 2007. CPEB: a life in translation. *Trends Biochem.Sci.* 32:279-285.
Rico, A.B., A.T. Phillips, T. Schountz, D.L. Jarvis, R.B. Tjalkens, A.M. Powers, and K.E. Olson. 2016. Venezuelan and western equine encephalitis virus E1 liposome antigen nucleic acid complexes protect mice from lethal challenge with multiple alphaviruses. *Virology*. 499:30-39.
Rijnboutt, S., H.M. Aerts, H.J. Geuze, J.M. Tager, and G.J. Strous. 1991. Mannose 6-phosphate-independent membrane association of cathepsin D, glucocerebrosidase, and sphingolipid-activating protein in HepG2 cells. *J Biol Chem*. 266:4862-4868.
Rodier, J. 1955. Manganese poisoning in Moroccan miners. *Br J Ind Med*. 12:21-35.
Rohn, T.T., and L.W. Catlin. 2011. Immunolocalization of influenza A virus and markers of inflammation in the human Parkinson's disease brain. *PLoS One*. 6:e20495.
Ronca, S.E., J. Smith, T. Koma, M.M. Miller, N. Yun, K.T. Dineley, and S. Paessler. 2017. Mouse Model of Neurological Complications Resulting from Encephalitic Alphavirus Infection. *Front Microbiol*. 8:188.
Roselli, F., I. Russo, A. Fraddosio, M.S. Aniello, M. De Mari, P. Lamberti, P. Livrea, and G. Defazio. 2006. Reversible Parkinsonian syndrome associated with anti-neuronal antibodies in acute EBV encephalitis: a case report. *Parkinsonism Relat Disord*. 12:257-260.
Rothhammer, V., D.M. Borucki, E.C. Tjon, M.C. Takenaka, C.C. Chao, A. Ardura-Fabregat, K.A. de Lima, C. Gutierrez-Vazquez, P. Hewson, O. Staszewski, M. Blain, L. Healy, T. Neziraj, M. Borio, M. Wheeler, L.L. Dragin, D.A. Laplaud, J. Antel, J.I. Alvarez, M. Prinz, and F.J. Quintana. 2018. Microglial control of astrocytes in response to microbial metabolites. *Nature*. 557:724-728.
Rudyk, C., Z. Dwyer, S. Hayley, and C. membership. 2019. Leucine-rich repeat kinase-2 (LRRK2) modulates paraquat-induced inflammatory sickness and stress phenotype. *J Neuroinflammation*. 16:120.
Rugless, F., A. Bhattacharya, P. Succop, K.N. Dietrich, C. Cox, J. Alden, P. Kuhnell, M. Barnas, R. Wright, P.J. Parsons, M.L. Praamsma, C.D. Palmer, C. Beidler, R. Wittberg, and E.N. Haynes. 2014. Childhood exposure to manganese and postural instability in children living near a ferromanganese refinery in Southeastern Ohio. *Neurotoxicol Teratol*. 41:71-79.
Russo, I., G. Berti, N. Plotegher, G. Bernardo, R. Filograna, L. Bubacco, and E. Greggio. 2015. Leucine-rich repeat kinase 2 positively regulates inflammation and down-regulates NF-kappaB p50 signaling in cultured microglia cells. *J Neuroinflammation*. 12:230.
Russo, I., A. Kaganovich, J. Ding, N. Landeck, A. Mamais, T. Varanita, A. Biosa, I. Tessari, L. Bubacco, E. Greggio, and M.R. Cookson. 2019. Transcriptome analysis of LRRK2 knock-out microglia cells reveals alterations of inflammatory- and oxidative stress-related pathways upon treatment with alpha-synuclein fibrils. *Neurobiol Dis*. 129:67-78.
Sadasivan, S., B.B. Pond, A.K. Pani, C. Qu, Y. Jiao, and R.J. Smeyne. 2012. Methylphenidate exposure induces dopamine neuron loss and activation of microglia in the basal ganglia of mice. *PLoS One*. 7:e33693.
Sadasivan, S., B. Sharp, S. Schultz-Cherry, and R.J. Smeyne. 2017. Synergistic effects of influenza and 1-methyl-4-phenyl-1,2,3,6-tetrahydropyridine (MPTP) can be eliminated by the use of influenza therapeutics: experimental evidence for the multi-hit hypothesis. *NPJ Parkinsons Dis*. 3:18.

Sadasivan, S., M. Zanin, K. O'Brien, S. Schultz-Cherry, and R.J. Smeyne. 2015. Induction of microglia activation after infection with the non-neurotropic A/CA/04/2009 H1N1 influenza virus. *PLoS One*. 10:e0124047.

Saijo, K., B. Winner, C.T. Carson, J.G. Collier, L. Boyer, M.G. Rosenfeld, F.H. Gage, and C.K. Glass. 2009. A Nurr1/CoREST pathway in microglia and astrocytes protects dopaminergic neurons from inflammation-induced death. *Cell*. 137:47-59.

Sanchez-Guajardo, V., C.J. Barnum, M.G. Tansey, and M. Romero-Ramos. 2013. Neuroimmunological processes in Parkinson's disease and their relation to alpha-synuclein: microglia as the referee between neuronal processes and peripheral immunity. *ASN Neuro*. 5:113-139.

Schafer, D.P., E.K. Lehrman, A.G. Kautzman, R. Koyama, A.R. Mardinly, R. Yamasaki, R.M. Ransohoff, M.E. Greenberg, B.A. Barres, and B. Stevens. 2012. Microglia sculpt postnatal neural circuits in an activity and complement-dependent manner. *Neuron*. 74:691-705.

Schapansky, J., J.D. Nardozzi, F. Felizia, and M.J. LaVoie. 2014. Membrane recruitment of endogenous LRRK2 precedes its potent regulation of autophagy. *Hum Mol Genet*. 23:4201-4214.

Schultz, D.R., J.S. Barthal, and C. Garrett. 1977. WESTERN EQUINE ENCEPHALITIS WITH RAPID ONSET OF PARKINSONISM. *Neurology*. 27:1095-1096.

Sedelis, M., K. Hofele, G.W. Auburger, S. Morgan, J.P. Huston, and R.K. Schwarting. 2000. MPTP susceptibility in the mouse: behavioral, neurochemical, and histological analysis of gender and strain differences. *Behav Genet*. 30:171-182.

Seirafi, M., G. Kozlov, and K. Gehring. 2015. Parkin structure and function. *FEBS J*. 282:2076-2088.

Seth, P., M.M. Husain, P. Gupta, A. Schoneboom, B.F. Grieder, H. Mani, and R.K. Maheshwari. 2003. Early onset of virus infection and up-regulation of cytokines in mice treated with cadmium and manganese. *Biometals : an international journal on the role of metal ions in biology, biochemistry, and medicine*. 16:359-368.

Shendelman, S., A. Jonason, C. Martinat, T. Leete, and A. Abeliovich. 2004. DJ-1 is a redox-dependent molecular chaperone that inhibits alpha-synuclein aggregate formation. *PLoS Biol*. 2:e362.

Sherer, T.B., J.R. Richardson, C.M. Testa, B.B. Seo, A.V. Panov, T. Yagi, A. Matsuno-Yagi, G.W. Miller, and J.T. Greenamyre. 2007. Mechanism of toxicity of pesticides acting at complex I: relevance to environmental etiologies of Parkinson's disease. *Journal of neurochemistry*. 100:1469-1479.

Shi, Q., S. Chowdhury, R. Ma, K.X. Le, S. Hong, B.J. Caldarone, B. Stevens, and C.A. Lemere. 2017. Complement C3 deficiency protects against neurodegeneration in aged plaque-rich APP/PS1 mice. *Sci Transl Med*. 9.

Sidoryk-Wegrzynowicz, M., and M. Aschner. 2013. Role of astrocytes in manganese mediated neurotoxicity. *BMC Pharmacol Toxicol*. 14:23.

Silva da Costa, L., A.P. Pereira da Silva, A.T. Da Poian, and T. El-Bacha. 2012. Mitochondrial bioenergetic alterations in mouse neuroblastoma cells infected with Sindbis virus: implications to viral replication and neuronal death. *PLoS One*. 7:2.

Simons, K., and R. Ehehalt. 2002. Cholesterol, lipid rafts, and disease. *J Clin Invest*. 110:597-603.

Skaper, S.D. 2012. The neurotrophin family of neurotrophic factors: an overview. *Methods Mol Biol*. 846:1-12.
Skaper, S.D., L. Facci, M. Zusso, and P. Giusti. 2018. An Inflammation-Centric View of Neurological Disease: Beyond the Neuron. *Front Cell Neurosci*. 12:72.
Sliter, D.A., J. Martinez, L. Hao, X. Chen, N. Sun, T.D. Fischer, J.L. Burman, Y. Li, Z. Zhang, D.P. Narendra, H. Cai, M. Borsche, C. Klein, and R.J. Youle. 2018. Parkin and PINK1 mitigate STING-induced inflammation. *Nature*. 561:258-262.
Smeyne, R.J., C.B. Breckenridge, M. Beck, Y. Jiao, M.T. Butt, J.C. Wolf, D. Zadory, D.J. Minnema, N.C. Sturgess, K.Z. Travis, A.R. Cook, L.L. Smith, and P.A. Botham. 2016. Assessment of the Effects of MPTP and Paraquat on Dopaminergic Neurons and Microglia in the Substantia Nigra Pars Compacta of C57BL/6 Mice. *PLoS One*. 11:e0164094.
Sofroniew, M.V., and H.V. Vinters. 2010. Astrocytes: biology and pathology. *Acta neuropathologica*. 119:7-35.
Solano, R.M., M.J. Casarejos, J. Menendez-Cuervo, J.A. Rodriguez-Navarro, J. Garcia de Yebenes, and M.A. Mena. 2008. Glial dysfunction in parkin null mice: effects of aging. *J Neurosci*. 28:598-611.
Song, C., A. Kanthasamy, V. Anantharam, F. Sun, and A.G. Kanthasamy. 2010. Environmental neurotoxic pesticide increases histone acetylation to promote apoptosis in dopaminergic neuronal cells: relevance to epigenetic mechanisms of neurodegeneration. *Mol Pharmacol*. 77:621-632.
Song, C., A. Kanthasamy, H. Jin, V. Anantharam, and A.G. Kanthasamy. 2011. Paraquat induces epigenetic changes by promoting histone acetylation in cell culture models of dopaminergic degeneration. *Neurotoxicology*. 32:586-595.
Spatola, M., and C. Wider. 2014. Genetics of Parkinson's disease: the yield. *Parkinsonism Relat Disord*. 20 Suppl 1:S35-38.
Sperlagh, B., and P. Illes. 2007. Purinergic modulation of microglial cell activation. *Purinergic Signal*. 3:117-127.
Stirnemann, J., N. Belmatoug, F. Camou, C. Serratrice, R. Froissart, C. Caillaud, T. Levade, L. Astudillo, J. Serratrice, A. Brassier, C. Rose, T. Billette de Villemeur, and M.G. Berger. 2017. A Review of Gaucher Disease Pathophysiology, Clinical Presentation and Treatments. *Int J Mol Sci*. 18.
Stolzenberg, E., D. Berry, Yang, E.Y. Lee, A. Kroemer, S. Kaufman, G.C.L. Wong, J.J. Oppenheim, S. Sen, T. Fishbein, A. Bax, B. Harris, D. Barbut, and M.A. Zasloff. 2017. A Role for Neuronal Alpha-Synuclein in Gastrointestinal Immunity. *J Innate Immun*. 9:456-463.
Streifel, K.M., A.L. Gonzales, B. De Miranda, R. Mouneimne, S. Earley, and R. Tjalkens. 2014. Dopaminergic neurotoxicants cause biphasic inhibition of purinergic calcium signaling in astrocytes. *PLoS One*. 9:e110996.
Streifel, K.M., J. Miller, R. Mouneimne, and R.B. Tjalkens. 2013. Manganese inhibits ATP-induced calcium entry through the transient receptor potential channel TRPC3 in astrocytes. *Neurotoxicology*. 34:160-166.
Streifel, K.M., J.A. Moreno, W.H. Hanneman, M.E. Legare, and R.B. Tjalkens. 2012. Gene deletion of nos2 protects against manganese-induced neurological dysfunction in juvenile mice. *Toxicol Sci*. 126:183-192.

Streit, W.J., N.W. Sammons, A.J. Kuhns, and D.L. Sparks. 2004. Dystrophic microglia in the aging human brain. *Glia*. 45:208-212.
Stuart, S.A., and E.S. Robinson. 2015. Reducing the stress of drug administration: implications for the 3Rs. *Sci Rep*. 5:14288.
Sulzer, D. 2007. Multiple hit hypotheses for dopamine neuron loss in Parkinson's disease. *Trends Neurosci*. 30:244-250.
Sulzer, D., R.N. Alcalay, F. Garretti, L. Cote, E. Kanter, J. Agin-Liebes, C. Liong, C. McMurtrey, W.H. Hildebrand, X. Mao, V.L. Dawson, T.M. Dawson, C. Oseroff, J. Pham, J. Sidney, M.B. Dillon, C. Carpenter, D. Weiskopf, E. Phillips, S. Mallal, B. Peters, A. Frazier, C.S. Lindestam Arlehamn, and A. Sette. 2017. T cells from patients with Parkinson's disease recognize alpha-synuclein peptides. *Nature*. 546:656-661.
Sun, G., C. Ota, S. Kitaoka, Y. Chiba, M. Takayanagi, T. Kitamura, K. Yamamoto, H. Fujie, H. Mikami, M. Uematsu, N. Hino-Fukuyo, M. Munakata, S. Kure, and K. Haginoya. 2015. Elevated serum levels of neutrophil elastase in patients with influenza virus-associated encephalopathy. *Journal of the neurological sciences*. 349:190-195.
Sun, L., R. Shen, S.K. Agnihotri, Y. Chen, Z. Huang, and H. Bueler. 2018. Lack of PINK1 alters glia innate immune responses and enhances inflammation-induced, nitric oxide-mediated neuron death. *Sci Rep*. 8:383.
Szklarczyk, D., A.L. Gable, D. Lyon, A. Junge, S. Wyder, J. Huerta-Cepas, M. Simonovic, N.T. Doncheva, J.H. Morris, P. Bork, L.J. Jensen, and C.V. Mering. 2019. STRING v11: protein-protein association networks with increased coverage, supporting functional discovery in genome-wide experimental datasets. *Nucleic Acids Res*. 47:D607-D613.
Szklarczyk, D., J.H. Morris, H. Cook, M. Kuhn, S. Wyder, M. Simonovic, A. Santos, N.T. Doncheva, A. Roth, P. Bork, L.J. Jensen, and C. von Mering. 2017. The STRING database in 2017: quality-controlled protein-protein association networks, made broadly accessible. *Nucleic Acids Res*. 45:D362-D368.
Tanaka, T., S. Kai, T. Matsuyama, T. Adachi, K. Fukuda, and K. Hirota. 2013. General anesthetics inhibit LPS-induced IL-1beta expression in glial cells. *PLoS One*. 8:e82930.
Tang, Y., and W. Le. 2016. Differential Roles of M1 and M2 Microglia in Neurodegenerative Diseases. *Mol Neurobiol*. 53:1181-1194.
Tanner, C.M., F. Kamel, G.W. Ross, J.A. Hoppin, S.M. Goldman, M. Korell, C. Marras, G.S. Bhudhikanok, M. Kasten, A.R. Chade, K. Comyns, M.B. Richards, C. Meng, B. Priestley, H.H. Fernandez, F. Cambi, D.M. Umbach, A. Blair, D.P. Sandler, and J.W. Langston. 2011. Rotenone, paraquat, and Parkinson's disease. *Environ Health Perspect*. 119:866-872.
Tansey, M.G. 2010. Inflammation in neuropsychiatric disease. *Neurobiol Dis*. 37:491-492.
Tansey, M.G., and M.S. Goldberg. 2010. Neuroinflammation in Parkinson's disease: its role in neuronal death and implications for therapeutic intervention. *Neurobiol Dis*. 37:510-518.
Tanuma, N., H. Sakuma, A. Sasaki, and Y. Matsumoto. 2006. Chemokine expression by astrocytes plays a role in microglia/macrophage activation and subsequent neurodegeneration in secondary progressive multiple sclerosis. *Acta Neuropathol*. 112:195-204.
Tapias, V., J.T. Greenamyre, and S.C. Watkins. 2013. Automated imaging system for fast quantitation of neurons, cell morphology and neurite morphometry in vivo and in vitro. *Neurobiol Dis*. 54:158-168.

Thakur, P., and B. Nehru. 2015. Inhibition of neuroinflammation and mitochondrial dysfunctions by carbenoxolone in the rotenone model of Parkinson's disease. *Mol Neurobiol*. 51:209-219.

Tjalkens, R.B., X. Liu, B. Mohl, T. Wright, J.A. Moreno, D.L. Carbone, and S. Safe. 2008. The peroxisome proliferator-activated receptor-gamma agonist 1,1-bis(3'-indolyl)-1-(p-trifluoromethylphenyl)methane suppresses manganese-induced production of nitric oxide in astrocytes and inhibits apoptosis in cocultured PC12 cells. *J Neurosci Res*. 86:618-629.

Tjalkens, R.B., K.A. Popichak, and K.A. Kirkley. 2017. Inflammatory Activation of Microglia and Astrocytes in Manganese Neurotoxicity. *Adv Neurobiol*. 18:159-181.

Torres-Odio, S., J. Key, H.H. Hoepken, J. Canet-Pons, L. Valek, B. Roller, M. Walter, B. Morales-Gordo, D. Meierhofer, P.N. Harter, M. Mittelbronn, I. Tegeder, S. Gispert, and G. Auburger. 2017. Progression of pathology in PINK1-deficient mouse brain from splicing via ubiquitination, ER stress, and mitophagy changes to neuroinflammation. *J Neuroinflammation*. 14:154.

Tran, T.A., A.D. Nguyen, J. Chang, M.S. Goldberg, J.K. Lee, and M.G. Tansey. 2011. Lipopolysaccharide and tumor necrosis factor regulate Parkin expression via nuclear factor-kappa B. *PLoS One*. 6:e23660.

Troncoso-Escudero, P., A. Parra, M. Nassif, and R.L. Vidal. 2018. Outside in: Unraveling the Role of Neuroinflammation in the Progression of Parkinson's Disease. *Front Neurol*. 9:860.

Truban, D., X. Hou, T.R. Caulfield, F.C. Fiesel, and W. Springer. 2017. PINK1, Parkin, and Mitochondrial Quality Control: What can we Learn about Parkinson's Disease Pathobiology? *J Parkinsons Dis*. 7:13-29.

Trudler, D., O. Weinreb, S.A. Mandel, M.B. Youdim, and D. Frenkel. 2014. DJ-1 deficiency triggers microglia sensitivity to dopamine toward a pro-inflammatory phenotype that is attenuated by rasagiline. *J Neurochem*. 129:434-447.

Ueda, K., H. Fukushima, E. Masliah, Y. Xia, A. Iwai, M. Yoshimoto, D.A. Otero, J. Kondo, Y. Ihara, and T. Saitoh. 1993. Molecular cloning of cDNA encoding an unrecognized component of amyloid in Alzheimer disease. *Proc Natl Acad Sci U S A*. 90:11282-11286.

van Horssen, J., J.A. Drexhage, T. Flor, W. Gerritsen, P. van der Valk, and H.E. de Vries. 2010. Nrf2 and DJ1 are consistently upregulated in inflammatory multiple sclerosis lesions. *Free Radic Biol Med*. 49:1283-1289.

van Rossum, D., and U.K. Hanisch. 2004. Microglia. *Metab Brain Dis*. 19:393-411.

Vasek, M.J., C. Garber, D. Dorsey, D.M. Durrant, B. Bollman, A. Soung, J. Yu, C. Perez-Torres, A. Frouin, D.K. Wilton, K. Funk, B.K. DeMasters, X. Jiang, J.R. Bowen, S. Mennerick, J.K. Robinson, J.R. Garbow, K.L. Tyler, M.S. Suthar, R.E. Schmidt, B. Stevens, and R.S. Klein. 2016. A complement-microglial axis drives synapse loss during virus-induced memory impairment. *Nature*. 534:538-543.

Verina, T., S.F. Kiihl, J.S. Schneider, and T.R. Guilarte. 2011. Manganese exposure induces microglia activation and dystrophy in the substantia nigra of non-human primates. *Neurotoxicology*. 32:215-226.

Vermeulen, L., G. De Wilde, S. Notebaert, W. Vanden Berghe, and G. Haegeman. 2002. Regulation of the transcriptional activity of the nuclear factor-kappaB p65 subunit. *Biochem Pharmacol*. 64:963-970.

Vielhaber, G., S. Pfeiffer, L. Brade, B. Lindner, T. Goldmann, E. Vollmer, U. Hintze, K.P. Wittern, and R. Wepf. 2001. Localization of ceramide and glucosylceramide in human epidermis by immunogold electron microscopy. *J Invest Dermatol*. 117:1126-1136.

Vilarino-Guell, C., C. Wider, O.A. Ross, B. Jasinska-Myga, J. Kachergus, S.A. Cobb, A.I. Soto-Ortolaza, B. Behrouz, M.G. Heckman, N.N. Diehl, C.M. Testa, Z.K. Wszolek, R.J. Uitti, J. Jankovic, E.D. Louis, L.N. Clark, A. Rajput, and M.J. Farrer. 2010. LINGO1 and LINGO2 variants are associated with essential tremor and Parkinson disease. *Neurogenetics*. 11:401-408.

Vitner, E.B., T. Farfel-Becker, N.S. Ferreira, D. Leshkowitz, P. Sharma, K.S. Lang, and A.H. Futerman. 2016. Induction of the type I interferon response in neurological forms of Gaucher disease. *J Neuroinflammation*. 13:104.

Wang, L.M., J.M. Dragich, T. Kudo, I.H. Odom, D.K. Welsh, T.J. O'Dell, and C.S. Colwell. 2009. Expression of the circadian clock gene Period2 in the hippocampus: possible implications for synaptic plasticity and learned behaviour. *ASN Neuro*. 1.

Wang, L.M., N.A. Suthana, D. Chaudhury, D.R. Weaver, and C.S. Colwell. 2005. Melatonin inhibits hippocampal long-term potentiation. *Eur J Neurosci*. 22:2231-2237.

Wang, X.H., G. Lu, X. Hu, K.S. Tsang, W.H. Kwong, F.X. Wu, H.W. Meng, S. Jiang, S.W. Liu, H.K. Ng, and W.S. Poon. 2012. Quantitative assessment of gait and neurochemical correlation in a classical murine model of Parkinson's disease. *BMC Neurosci*. 13:142.

Wasserman, G.A., X. Liu, F. Parvez, H. Ahsan, D. Levy, P. Factor-Litvak, J. Kline, A. van Geen, V. Slavkovich, N.J. LoIacono, Z. Cheng, Y. Zheng, and J.H. Graziano. 2006. Water manganese exposure and children's intellectual function in Araihazar, Bangladesh. *Environ Health Perspect*. 114:124-129.

Wendeln, A.C., K. Degenhardt, L. Kaurani, M. Gertig, T. Ulas, G. Jain, J. Wagner, L.M. Hasler, K. Wild, A. Skodras, T. Blank, O. Staszewski, M. Datta, T.P. Centeno, V. Capece, M.R. Islam, C. Kerimoglu, M. Staufenbiel, J.L. Schultze, M. Beyer, M. Prinz, M. Jucker, A. Fischer, and J.J. Neher. 2018. Innate immune memory in the brain shapes neurological disease hallmarks. *Nature*. 556:332-338.

West, M.J., L. Slomianka, and H.J. Gundersen. 1991. Unbiased stereological estimation of the total number of neurons in thesubdivisions of the rat hippocampus using the optical fractionator. *Anat Rec*. 231:482-497.

Wilde, G.J., A.K. Pringle, P. Wright, and F. Iannotti. 1997. Differential vulnerability of the CA1 and CA3 subfields of the hippocampus to superoxide and hydroxyl radicals in vitro. *J Neurochem*. 69:883-886.

Wilhelmus, M.M., S.M. van der Pol, Q. Jansen, M.E. Witte, P. van der Valk, A.J. Rozemuller, B. Drukarch, H.E. de Vries, and J. Van Horssen. 2011. Association of Parkinson disease-related protein PINK1 with Alzheimer disease and multiple sclerosis brain lesions. *Free Radic Biol Med*. 50:469-476.

Wirdefeldt, K., M. Gatz, M. Schalling, and N.L. Pedersen. 2004. No evidence for heritability of Parkinson disease in Swedish twins. *Neurology*. 63:305-311.

Witte, M.E., J.G. Bol, W.H. Gerritsen, P. van der Valk, B. Drukarch, J. van Horssen, and M.M. Wilhelmus. 2009. Parkinson's disease-associated parkin colocalizes with Alzheimer's disease and multiple sclerosis brain lesions. *Neurobiol Dis*. 36:445-452.

Wong, T.P., J.G. Howland, J.M. Robillard, Y. Ge, W. Yu, A.K. Titterness, K. Brebner, L. Liu, J. Weinberg, B.R. Christie, A.G. Phillips, and Y.T. Wang. 2007. Hippocampal long-term

depression mediates acute stress-induced spatial memory retrieval impairment. *Proc Natl Acad Sci U S A*. 104:11471-11476.
Woolf, A., R. Wright, C. Amarasiriwardena, and D. Bellinger. 2002. A child with chronic manganese exposure from drinking water. *Environ Health Perspect*. 110:613-616.
Wozniak, M.A., and R.F. Itzhaki. 2013. Intravenous immunoglobulin reduces beta amyloid and abnormal tau formation caused by herpes simplex virus type 1. *J Neuroimmunol*. 257:7-12.
Wu, L., D. Wells, J. Tay, D. Mendis, M.A. Abbott, A. Barnitt, E. Quinlan, A. Heynen, J.R. Fallon, and J.D. Richter. 1998. CPEB-mediated cytoplasmic polyadenylation and the regulation of experience-dependent translation of alpha-CaMKII mRNA at synapses. *Neuron.* 21:1129-1139.
Wu, Y.W., K.M. Prakash, T.Y. Rong, H.H. Li, Q. Xiao, L.C. Tan, W.L. Au, J.Q. Ding, S.D. Chen, and E.K. Tan. 2011. Lingo2 variants associated with essential tremor and Parkinson's disease. *Hum Genet*. 129:611-615.
Wyrsch, P., C. Blenn, J. Bader, and F.R. Althaus. 2012. Cell death and autophagy under oxidative stress: roles of poly(ADP-Ribose) polymerases and Ca(2+). *Mol Cell Biol*. 32:3541-3553.
Yahalom, G., L. Greenbaum, S. Israeli-Korn, T. Fay-Karmon, V. Livneh, J.A. Ruskey, L. Ronciere, A. Alam, Z. Gan-Or, and S. Hassin-Baer. 2019. Carriers of both GBA and LRRK2 mutations, compared to carriers of either, in Parkinson's disease: Risk estimates and genotype-phenotype correlations. *Parkinsonism Relat Disord*. 62:179-184.
Yamada, M., S. Ohno, I. Okayasu, R. Okeda, S. Hatakeyama, H. Watanabe, K. Ushio, and H. Tsukagoshi. 1986. Chronic manganese poisoning: a neuropathological study with determination of manganese distribution in the brain. *Acta Neuropathol*. 70:273-278.
Yamamoto, H., E. Yamauchi, H. Taniguchi, T. Ono, and E. Miyamoto. 2002. Phosphorylation of microtubule-associated protein tau by Ca2+/calmodulin-dependent protein kinase II in its tubulin binding sites. *Arch Biochem Biophys*. 408:255-262.
Yamanaka, G., H. Kawashima, Y. Suganami, C. Watanabe, Y. Watanabe, T. Miyajima, K. Takekuma, S. Oguchi, and A. Hoshika. 2006. Diagnostic and predictive value of CSF d-ROM level in influenza virus-associated encephalopathy. *Journal of the neurological sciences*. 243:71-75.
Yang, X., H. Ren, K. Wood, M. Li, S. Qiu, F.D. Shi, C. Ma, and Q. Liu. 2018. Depletion of microglia augments the dopaminergic neurotoxicity of MPTP. *FASEB J*. 32:3336-3345.
Yang, Y., J. Ye, X. Yang, R. Jiang, H. Chen, and S. Cao. 2011. Japanese encephalitis virus infection induces changes of mRNA profile of mouse spleen and brain. *Virol J*. 8:80.
Yasuda, Y., T. Shimoda, K. Uno, N. Tateishi, S. Furuya, K. Yagi, K. Suzuki, and S. Fujita. 2008. The effects of MPTP on the activation of microglia/astrocytes and cytokine/chemokine levels in different mice strains. *J Neuroimmunol*. 204:43-51.
Yuan, Y.H., J.D. Sun, M.M. Wu, J.F. Hu, S.Y. Peng, and N.H. Chen. 2013. Rotenone could activate microglia through NFkappaB associated pathway. *Neurochem Res*. 38:1553-1560.
Zanon, A., P.P. Pramstaller, A.A. Hicks, and I. Pichler. 2018. Environmental and Genetic Variables Influencing Mitochondrial Health and Parkinson's Disease Penetrance. *Parkinsons Dis*. 2018:8684906.
Zarranz, J.J., J. Alegre, J.C. Gomez-Esteban, E. Lezcano, R. Ros, I. Ampuero, L. Vidal, J. Hoenicka, O. Rodriguez, B. Atares, V. Llorens, E. Gomez Tortosa, T. del Ser, D.G.

Munoz, and J.G. de Yebenes. 2004. The new mutation, E46K, of alpha-synuclein causes Parkinson and Lewy body dementia. *Ann Neurol*. 55:164-173.
Zhang, P., T.A. Wong, K.M. Lokuta, D.E. Turner, K. Vujisic, and B. Liu. 2009. Microglia enhance manganese chloride-induced dopaminergic neurodegeneration: role of free radical generation. *Exp Neurol*. 217:219-230.
Zhang, S., Z. Zhou, and J. Fu. 2003. Effect of manganese chloride exposure on liver and brain mitochondria function in rats. *Environ Res*. 93:149-157.
Zhang, Y., K. Chen, S.A. Sloan, M.L. Bennett, A.R. Scholze, S. O'Keeffe, H.P. Phatnani, P. Guarnieri, C. Caneda, N. Ruderisch, S. Deng, S.A. Liddelow, C. Zhang, R. Daneman, T. Maniatis, B.A. Barres, and J.Q. Wu. 2014. An RNA-sequencing transcriptome and splicing database of glia, neurons, and vascular cells of the cerebral cortex. *J Neurosci*. 34:11929-11947.
Zhang, Y., A.D. Hoppe, and J.A. Swanson. 2010. Coordination of Fc receptor signaling regulates cellular commitment to phagocytosis. *Proc Natl Acad Sci U S A*. 107:19332-19337.
Zhao, F., T. Cai, M. Liu, G. Zheng, W. Luo, and J. Chen. 2009. Manganese induces dopaminergic neurodegeneration via microglial activation in a rat model of manganism. *Toxicol Sci*. 107:156-164.
Zhou, W., M. Zhu, M.A. Wilson, G.A. Petsko, and A.L. Fink. 2006. The oxidation state of DJ-1 regulates its chaperone activity toward alpha-synuclein. *J Mol Biol*. 356:1036-1048.
Zhou, Y., T.K. Frey, and J.J. Yang. 2009. Viral calciomics: Interplays between Ca(2+) and virus. *Cell calcium*. 46:1-17.
Zimprich, A., S. Biskup, P. Leitner, P. Lichtner, M. Farrer, S. Lincoln, J. Kachergus, M. Hulihan, R.J. Uitti, D.B. Calne, A.J. Stoessl, R.F. Pfeiffer, N. Patenge, I.C. Carbajal, P. Vieregge, F. Asmus, B. Muller-Myhsok, D.W. Dickson, T. Meitinger, T.M. Strom, Z.K. Wszolek, and T. Gasser. 2004. Mutations in LRRK2 cause autosomal-dominant parkinsonism with pleomorphic pathology. *Neuron*. 44:601-607.
Zwirner, J., T. Werfel, H.C. Wilken, E. Theile, and O. Gotze. 1998. Anaphylatoxin C3a but not C3a(desArg) is a chemotaxin for the mouse macrophage cell line J774. *Eur J Immunol*. 28:1570-1577.